NPS ARCHIVE
1961
WHIPPLE, C.

THE DYNAMIC RESPONSE OF SHALLOW-BURIED ARCHES SUBJECTED TO BLAST LOADING

CARYLL ROBBINS WHIPPLE

DUDLEY KNOX LIBRARY
NAVAL POSTGRADUATE SCHOOL
MONTEREY CA 93943-5101

LIBRARY
U.S. NAVAL POSTGRADUATE SCHOOL
MONTEREY, CALIFORNIA

THE DYNAMIC RESPONSE OF SHALLOW-BURIED ARCHES SUBJECTED TO BLAST LOADING

BY

CARYLL ROBBINS WHIPPLE

B.S., United States Naval Academy, 1950
B.C.E., Rensselaer Polytechnic Institute, 1953
M.S., University of Illinois, 1957

THESIS

SUBMITTED IN PARTIAL FULFILLMENT OF THE REQUIREMENTS
FOR THE DEGREE OF DOCTOR OF PHILOSOPHY IN CIVIL ENGINEERING
IN THE GRADUATE COLLEGE OF THE
UNIVERSITY OF ILLINOIS, 1961

URBANA, ILLINOIS

NPS Archive
[illegible]
Whipple, C.

Library
U. S. Naval Postgraduate School
Monterey, California

ACKNOWLEDGMENT

This thesis was prepared under a postgraduate program sponsored at the University of Illinois by the United States Navy and administered by the Superintendent, U.S. Naval Postgraduate School, for the education of Civil Engineer Corps Officers. The author is deeply grateful for the opportunity of participating in this program. The report is sponsored as a part of the investigation conducted in the Civil Engineering Department of the University of Illinois under contract AF 29(601)-2591 with the United States Air Force Special Weapons Center, Albuquerque, New Mexico.

The author is particularly indebted to Dr. N. M. Newmark, Professor and Head of the Department of Civil Engineering at the University of Illinois, for his kind encouragement and thoughtful guidance during preparation of this thesis.

The author wishes to acknowledge and thank Dr. R. B. Peck, Professor of Foundation Engineering, for his advice and suggestions on those portions of the thesis dealing with soil behavior.

Appreciation is expressed to Mr. J. W. Melin, Research Associate in Civil Engineering, for his valuable assistance in coding the problem for the ILLIAC, the University of Illinois Automatic Digital Computer, and to the personnel of the Digital Computer Laboratory for their fine cooperation in the performance of the numerical studies on the ILLIAC. In addition the author would like to extend his appreciation to Dr. J. L. Merritt and Dr. A. R. Robinson, Associate Professors of Civil Engineering, and to Mr. J. W. Melin and Mr. W. C. Schnobrich, Research Associates in Civil Engineering, for frequent and stimulating exchanges of ideas.

TABLE OF CONTENTS

Page

LIST OF TABLES vi
LIST OF FIGURES vii

I. INTRODUCTION 2

- 1.1 Object and Scope 2
- 1.2 Method of Approach 2
- 1.3 Notation 5

II. GENERAL DISCUSSION OF THE VARIABLES 11

- 2.1 Arch Resistance 11
- 2.2 Soil Resistance 13
- 2.3 Mass Effects 17
- 2.4 Blast Pressure Loading 18

III. ARCH RESISTANCE 22

- 3.1 Development of Model 22
- 3.2 Constraint Relationships 24
  - 3.2.1 Load Relationships 24
  - 3.2.2 Deflection Relationships 26
  - 3.2.3 Joint Rotation Relationships 28
- 3.3 Moment-Rotation Relationships for Joints 29
- 3.4 Development of Equivalent Arch Resistance 31
- 3.5 Rib Shortening 33

IV. SOIL RESISTANCE 45

- 4.1 Interior Haunch 46
- 4.2 Exterior Haunch 52
- 4.3 Crown 56
- 4.4 Development of Equivalent Soil Resistance 57

V. MASS EFFECTS 73

- 5.1 Mass Concentrations on the Model 73
- 5.2 Development of Equivalent Mass 79

VI. BLAST PRESSURE LOADING 86

- 6.1 Definition of Loading Regions 87
  - 6.1.1 Case I - Vertical Shock Front in Soil 89
  - 6.1.2 Case II - Shock Front in Soil Inclined at Angle Less than Inclination of Upper Bars of Model 92
  - 6.1.3 Case III - Shock Front in Soil Inclined at Angle Intermediate Between Inclinations of Upper and Lower Bars of Model 95

TABLE OF CONTENTS (Continued)

Page

VI. BLAST PRESSURE LOADING (Continued)

- 6.2 Load Concentrations On Model 97
- 6.3 Development of Equivalent Load 100

VII. EQUATIONS OF MOTION 105

- 7.1 Development of Equations 105
- 7.2 Natural Periods of Vibration 107

VIII. NUMERICAL STUDIES 112

- 8.1 Range of Variables Studied 112
- 8.2 Shock Wave Properties 114
- 8.3 Description of Numerical Examples 116
- 8.4 Sample Calculations 117
  - 8.4.1 Calculation of Parameters and Coefficients 118
  - 8.4.2 Investigation of General Yielding and Buckling of Arch Rib 135
  - 8.4.3 Integration 140
  - 8.4.4 Rib Shortening 146
  - 8.4.5 Calculation of Natural Periods of Vibration 150

IX. SUMMARY 159

- 9.1 Discussion 159
- 9.2 Conclusions 165
- 9.3 Recommendations 166

LIST OF REFERENCES 169

APPENDIX A. HYDROSTATIC PRESSURE RATIOS IN SOIL SUBJECTED TO NUCLEAR BLAST LOADING 172

APPENDIX B. SHAPE OF SHOCK FRONT IN SOIL 179

APPENDIX C. TABULAR COMPARISONS OF NUMERICAL RESULTS 186

APPENDIX D. GRAPHICAL PRESENTATION OF NUMERICAL RESULTS 194

LIST OF TABLES

Table No.	Title	Page No.
3.1	Constraint Loadings	38
8.1	Shock Wave Properties	154
8.2	Overpressure-Time Coordinates for 50-psi Shock Wave	154
8.3	Overpressure-Time Coordinates for 100-psi Shock Wave	154
8.4	Overpressure-Time Coordinates for 1000-psi Shock Wave	154
8.5	Summary of Numerical Examples	155
8.6	Overpressure-Time Relationships	156
A.1	Hydrostatic Pressure Ratios in Soil as Computed by "Trial Wedge" Method and Coulomb Formulas	177
A.2	Inclination with Respect to Horizontal of Failure Surfaces in Soil	177
C.1	Natural Periods of Vibration with No Overpressure Acting on Soil Failure Wedges	187
C.2	Natural Periods of Vibration at First Maximum Response of Leeward Haunch	188
C.3	First Maximum Response at Windward Haunch	189
C.4	First Maximum Response at Crown	190
C.5	First Maximum Response at Leeward Haunch	191
C.6	Effect of Horizontal-to-Vertical Overpressure Ratio on Lateral Response	192
C.7	Effect of Inclination of Shock Front in Soil on Lateral Response	193

LIST OF FIGURES

Figure No.	Title	Page No.
2.1	Model Considered in Analysis	21
2.2	Effect of Movement of a Wall on the Lateral Thrust	21
3.1	Constraint Loadings	39
3.2	Load Concentrations on Model	40
3.3	Diagram Used in Determining Joint Rotation Relationships	40
3.4	Diagram Used in Determining Moment-Rotation Relationships for Joints	41
3.5	Idealized Moment-Rotation Diagram for Joints	41
3.6	Free-Body Diagram of Typical Bars and Joint	42
3.7	Free-Body Diagram of Typical Joint	42
3.8	Uniform Radial Load on Arch	43
3.9	Deformation of Model Due to Rib Shortening	43
3.10	Diagram Used in Determining Rib-Shortening Correction at Haunch	44
3.11	Diagram Used in Determining Rib-Shortening Correction at Crown	44
4.1	Forces Acting on Pressure Surface for "Interior" Haunch	66
4.2	Load-Displacement Diagram for "Interior" Haunch	66
4.3	Soil Resistance-Displacement Diagram for "Interior" Haunch	67
4.4	Effective Soil Resistance for "Interior" Haunch	67
4.5	Diagram Used in Determining K_{OA}	68
4.6	Forces Acting on Pressure Surface for "Exterior" Haunch	68
4.7	Load-Displacement Diagram for "Exterior" Haunch	69
4.8	Effective Soil Resistance for "Exterior" Haunch	69

LIST OF FIGURES (Continued)

Figure No.	Title	Page No.
4.9	Diagram Used in Determining K_{OP}	70
4.10	Partial, Idealized, Soil Resistance-Displacement Diagram	70
4.11	Partial, Idealized, Soil Resistance-Displacement Diagram Showing Effect of Overpressure	71
4.12	Complete, Idealized, Soil Resistance-Displacement Diagram	71
4.13	Assumed Variation in Soil Resistance During Rebound	72
5.1	Masses of Soil Associated with Horizontal Components of Inertial Forces at Joints	83
5.2	Masses of Soil Associated with Vertical Components of Inertial Forces at Joints	84
5.3	Motions of Model	85
6.1	Loading Regions for Case I	102
6.2	Loading Regions for Case II	102
6.3	Loading Regions for Case III	103
6.4	Generalized Overpressure-Time Diagram for Typical Loading Region	104
7.1	Forces Acting on Typical Equivalent Mass	111
8.1	Reinforced Concrete Arch, $d_c = B/4$	157
8.2	Moment-Rotation Diagram for Joints of Model	157
8.3	Arch Rib Cross Section	158
8.4	Equivalent Soil Resistance-Displacement Diagram	158
A.1	Semicircular Arch, B = 16'8", $d_c = B/4$	178
B.1	Shock Front in Soil: $p_{so} = 100$ psi, $C_s = 1{,}000$ fps	182
B.2	Shock Front in Soil: $p_{so} = 100$ psi, $C_s = 2{,}000$ fps	182
B.3	Shock Front in Soil: $p_{so} = 100$ psi, $C_s = 3{,}000$ fps	183

LIST OF FIGURES (Continued)

Figure No.	Title	Page No.
B.4	Shock Front in Soil: p_{so} = 100 psi, C_s = 6,000 fps	184
B.5	Inclination of Shock Front in Soil	185
D.1	Response Curves for Reinforced Concrete Arch: p_{so} = 100 psi, d_c = 0	195
D.2	Response Curves for Reinforced Concrete Arch: p_{so} = 100 psi, d_c = B/8	196
D.3	Response Curves for Reinforced Concrete Arch: p_{so} = 100 psi, d_c = B/4, C_s = 3,000 fps	197
D.4	Response Curves for Reinforced Concrete Arch: p_{so} = 100 psi, d_c = B/4, C_s = 2,400 fps	198
D.5	Response Curves for Reinforced Concrete Arch: p_{so} = 100 psi, d_c = B/4, C_s = 1,000 fps	199
D.6	Response Curves for Reinforced Concrete Arch: p_{so} = 100 psi, d_c = B/2	200
D.7	Response Curves for Reinforced Concrete Arch: p_{so} = 1,000 psi, d_c = 0	201
D.8	Response Curves for Reinforced Concrete Arch: p_{so} = 1,000 psi, d_c = B/8	202
D.9	Response Curves for Reinforced Concrete Arch: p_{so} = 1,000 psi, d_c = B/4	203
D.10	Response Curves for Reinforced Concrete Arch: p_{so} = 1,000 psi, d_c = B/2	204
D.11	Response Curves for Corrugated Metal Arch: p_{so} = 50 psi, d_c = 0	205
D.12	Response Curves for Corrugated Metal Arch: p_{so} = 50 psi, d_c = B/8	206
D.13	Response Curves for Corrugated Metal Arch: p_{so} = 50 psi, d_c = B/4	207
D.14	Response Curves for Corrugated Metal Arch: p_{so} = 50 psi, d_c = B/2	208
D.15	Response Curves for Corrugated Metal Arch: p_{so} = 100 psi, d_c = 0	209

LIST OF FIGURES (Continued)

Figure No.	Title	Page No.
D.16	Response Curves for Corrugated Metal Arch: $p_{so} = 100$ psi, $d_c = B/8$	210
D.17	Response Curves for Corrugated Metal Arch: $p_{so} = 100$ psi, $d_c = B/4$, $K_{pr} = 1/4$	211
D.18	Response Curves for Corrugated Metal Arch: $p_{so} = 100$ psi, $d_c = B/4$, $K_{pr} = 1/2$	212
D.19	Response Curves for Corrugated Metal Arch: $p_{so} = 100$ psi, $d_c = B/4$, $K_{pr} = 3/4$	213
D.20	Response Curves for Corrugated Metal Arch: $p_{so} = 100$ psi, $d_c = B/4$, $K_{pr} = 1$	214
D.21	Response Curves for Corrugated Metal Arch: $p_{so} = 100$ psi, $d_c = B/2$	215
D.22	Response Curves for Corrugated Metal Arch: $p_{so} = 1{,}000$ psi, $d_c = 0$	216
D.23	Response Curves for Corrugated Metal Arch: $p_{so} = 1{,}000$ psi, $d_c = B/4$	217
D.24	Configuration Diagram for Reinforced Concrete Arch: $p_{so} = 100$ psi, $d_c = B/4$, $t = 0.0173$ sec., $(+h_3)_{max}$	218
D.25	Configuration Diagram for Reinforced Concrete Arch: $p_{so} = 100$ psi, $d_c = B/4$, $t = 0.0198$ sec., $(-h_5)_{max}$	219
D.26	Configuration Diagram for Reinforced Concrete Arch: $p_{so} = 100$ psi, $d_c = B/4$, $t = 0.0229$ sec., $(-h_1)_{max}$	220
D.27	Configuration Diagram for Corrugated Metal Arch: $p_{so} = 50$ psi, $d_c = B/4$, $t = 0.0337$ sec., $(+h_3)_{max}$	221
D.28	Configuration Diagram for Corrugated Metal Arch: $p_{so} = 50$ psi, $d_c = B/4$, $t = 0.0388$ sec., $(-h_5)_{max}$	222
D.29	Configuration Diagram for Corrugated Metal Arch: $p_{so} = 50$ psi, $d_c = B/4$, $t = 0.0450$ sec., $(-h_1)_{max}$	223
D.30	Configuration Diagram for Corrugated Metal Arch: $p_{so} = 50$ psi, $d_c = B/4$, $t = 0.0750$ sec., $(+h_1)_{max}$	224

CHAPTER I

INTRODUCTION

1.1 Object and Scope

This thesis is a study of the effectiveness of the surrounding soil in restraining the lateral movement of shallow-buried arches subjected to blast overpressures from a nuclear explosion. An understanding of this effect is important in the safe and economical proportioning of such structures.

The theory is developed for parabolic arches with circular or barrel arches included as a special case. It can be applied equally well to arches oriented with their longitudinal axes perpendicular to or parallel to the direction of travel of the blast wave.

The arch is considered to be buried near the surface of a semi-infinite soil mass. The term "shallow-buried" as used herein refers to a configuration and amount of earth cover such that reflected pressures and dynamic pressures need not be considered in the loading of the arch and yet not so great as to provide significant free-field attenuation of air-blast-induced overpressures in the soil. This is a convenient and meaningful area of investigation. It is convenient because it eliminates the dynamic and reflected pressure loading components at one extreme and the free-field attenuation of overpressure in soil at the other. Consideration of either of these extremes would serve further to complicate the problem while contributing little to the significance of the results. It is meaningful in that an economical balance may be reached in practical installations by locating structures near the ground surface in order to minimize excavation requirements and facilitate access while at the same time using earth cover to eliminate dynamic and reflected pressure loading components from the blast

loading which the structural system must withstand. In this study the depth of cover over the crown is limited to one-half of the arch span. This restricts the location of the structure to a region adjacent to the earth's surface in which there appears to be no measurable attenuation of free-field overpressure in the soil and in which the restraint offered to soil movement by the overpressure acting on the ground surface is significant.

The two-hinged rather than the fixed arch is selected as representing more closely the shallow-buried arch structures used in full-scale nuclear tests to date.(1,2,3) While these structures were not actually pinned at the arch abutments, their behavior under blast loading appears to the writer to resemble more closely the pinned than the fixed case. Further, such techniques as separating the arch footings from the floor slab in order to reduce accelerations imposed on the floor slab, and keeping the arch footings small to encourage downward movement under blast loading in order to reduce direct compression stresses in the arch, tend to produce a more nearly pinned than fixed condition at the abutments. The greater structural flexibility of the two-hinged arch is an additional favorable feature in enabling underground structures to adjust to imposed loading systems.

The principal variables studied in the numerical examples include:

1. Depth of cover
2. Overpressure loading
3. Arch material
4. Arch span

1.2 Method of Approach

The arch is replaced by a model consisting of four inextensible bars connected at moment-resistant joints.(4) This model is developed

---

(1) Numbers in parenthesis refer to the List of References.

herein in Section 3.1. The arch is thus reduced to a two-degree-of-freedom system. This greatly facilitates the dynamic analysis while at the same time permitting meaningful assumptions to be made regarding the loading and resistance parameters at the two haunches and at the crown.

The two independent variables chosen to describe the system are the horizontal displacement components at the haunches. While any two independent displacements could have been chosen, these are most convenient since they provide a direct picture of the primary mode of response of the model and are used directly in the determination of the state of stress within the soil mass at each side of the arch.

The two independent modes of response of the model are referred to herein as the symmetric mode, in which the haunches move simultaneously in opposite directions, i.e. both inward or both outward, and the asymmetric mode, in which the haunches move simultaneously in the same direction, i.e. both toward the right or both toward the left.

Solutions for the response of this system are obtained using the Newmark β-methods.(4,5,6,7) These are step-by-step numerical integration techniques in which the accelerations, velocities and displacements of the dynamic system are determined at each time interval from the time of arrival of the shock wave until the significant response of the system has occurred. These techniques are readily adaptable for use in digital computers. One of the University of Illinois Structural Research Laboratory Codes was modified and used for the solution of the numerical examples presented in this thesis.

The blast overpressure loading is concentrated as discussed in Section 2.4 and Chapter VI and is placed directly on the arch. Modification of the blast loading due to its transmission through the soil mass from the ground surface to the arch rib is handled separately as "soil resistance". This is discussed further in the following sections.

In general, the resistance of the arch-soil "structure" is handled by:

1. Considering the bending resistance of the arch as it deforms,
2. Considering the frictional and shearing stresses developed within the soil as the arch moves into or away from it,
3. Combining these arch and soil resistances vectorially as they act upon the model, and
4. Considering the mass effects of the arch and soil.

While these resistances are closely interrelated and act in combination during the response of the system, it is convenient and admissible to handle them separately in developing the equations of motion for the system.

The soil resistance is developed by considering the states of stress which exist within the soil surrounding the arch as the arch-soil "structure" deforms laterally.

Direct compression in the arch is handled separately. This is an approximation but a necessary one with this model, since to include it directly would violate one of the assumptions upon which the model is based, i.e. the bars are inextensible. Note that it would also change the model from a two-degree-of-freedom system to a six-degree-of-freedom system. However, the response studies presented remain valid with respect to lateral movements as long as the arch section is sufficient to withstand direct compression and buckling. A separate "rib-shortening correction" (cf. Section 3.5) is applied to certain of the results to give an approximate picture of its significance. This is discussed further in Chapter IX.

The arch supports are considered to be unyielding. While this is a common assumption in structural problems, it is an approximation. Again, the assumption is necessary in order to limit the system to two degrees of

freedom; however, this does offer an interesting possibility for further study as stated in Chapter IX.

Throughout this thesis displacements, velocities and accelerations to the right and upward are considered positive, and conversely. Loads are considered positive when they act on the structure to the right or upward. Resistances are considered as negative loads.

The method of approach described above is approximate. The necessity of approximating actual conditions is discussed in Chapter II and is also pointed out as occasions arise in the development of the loading and resistance expressions for the system. The approach used gives calculated magnitudes of response which differ from values measured in field tests. However, as will be seen, the results do describe the behavior of the actual structure and permit meaningful comparisons to be made of arch behavior under varying combinations of structure geometry and loading conditions (cf. Chapter IX).

1.3 Notation

Each symbol used in the text is fully explained when it is first introduced. A summary of the most important notation is presented here for the convenience of the reader.

a = vertical projection of a lower bar of the dynamic model (cf. Figure 2.1)

A = cross-sectional area of the arch rib

A_1, A_2, A_3 = influence coefficients for total joint rotation (cf. Equation (3.2.11))

b = horizontal projection of a lower bar of the dynamic model (cf. Figure 2.1)

B = span of the arch (cf. Figure 2.1)

c = vertical projection of an upper bar of the dynamic model (cf. Figure 2.1)

C_s = seismic velocity of the soil

C'_s = apparent vertical component of the velocity of the shock wave in the soil

d = horizontal projection of an upper bar of the dynamic model (cf. Figure 2.1)

d_c = depth of soil cover over the crown of the arch

d_{mj} = vertical dimensions of the soil prisms used in the mass calculations (cf. Figures 5.1 and 5.2)

d_o = total depth of soil cover from the ground surface to the arch abutments

E = modulus of elasticity of the arch material

$F_{j,m}$ = equivalent mass factor (cf. Equations (7.1.4))

g = acceleration of gravity, 32.2 ft/sec^2

$G_{j,m}$ = equivalent mass factor (cf. Equations (7.1.4))

h_a = thickness of the arch rib

h_j = displacement

$\dot{h}_j$ = velocity

$\ddot{h}_j$ = acceleration

H_j = effective external load

$\bar{H}_j$ = equivalent external load

I = effective moment of inertia of the arch rib cross section

j = as a subscript, unless otherwise specified, refers to the horizontal component at joint j

$j+3$ = as a subscript, unless otherwise specified, refers to the vertical component at joint j

J_1, J_2, J_3 = influence coefficients for the equivalent load on the dynamic model (cf. Equations (6.3.2))

k', k'' = influence coefficients for equivalent soil stiffness (cf. Equation (4.4.10))

k_o = observed value of the ratio between the horizontal and vertical soil pressures for the condition of earth pressure at rest

K_A = hydrostatic pressure ratio for the "active" state of stress in the soil

K_B = bending stiffness of the arch rib as concentrated at a joint of the dynamic model

K_{OA} = ratio of the soil pressure in the direction of P'_A to the vertical soil pressure for the condition of earth pressure at rest

K_{OP} = ratio of the soil pressure in the direction of P'_P to the vertical soil pressure for the condition of earth pressure at rest

K_P = hydrostatic pressure ratio for the "passive" state of stress in the soil

K_{pr} = ratio of the horizontal to the vertical overpressure induced in the soil by the shock wave in air

$\bar{K}_{sj}$ = soil stiffness during the development of an "active" state of stress in the soil adjacent to haunch j

$\bar{K}'_{sj}$ = soil stiffness during the development of a "passive" state of stress in the soil adjacent to haunch j

L_j = length of bar j of the dynamic model (cf. Figure 2.1)

m_j = concentrated mass at a joint of the dynamic model

m_{aj} = arch contribution to m_j

m_{sj} = soil contribution to m_j

$\bar{m}_{j,m}$ = equivalent mass

M_j = moment resistance of the arch-rib cross section

M_y = maximum moment-resisting capacity of the arch rib cross section

n = as a subscript, refers to time $t = t_n$

n+1 = as a subscript, refers to time $t = t_{n+1}$

p = overpressure in the shock wave in air

p_{so} = peak value of the overpressure in the shock wave in air

$\bar{p}_a$ = vertical component of the average overpressure acting on the arch

$\bar{p}'_a$ = uniform radial component of the average overpressure acting on the arch

$\bar{p}_j$ = average overpressure acting at the ground surface on loading region j

$\bar{p}_{sj}$ = average overpressure acting at the ground surface on the potential "active" failure wedge in the soil adjacent to haunch j

$\bar{p}'_{sj}$ = average overpressure acting at the ground surface on the potential "passive" failure wedge in the soil adjacent to haunch j

P' = force on the side of the arch due to the weight of the soil

P'' = force on the side of the arch due to the "surcharge" of the blast overpressure acting on the ground surface

P'_A = force acting on the side of the arch due to the weight of the soil and corresponding to a fully developed "active" state of stress in the soil mass

P''_A = force acting on the side of the arch due to the blast overpressure and corresponding to a fully developed "active" state of stress in the soil mass

P'_{OA} = component in the direction of P'_A of the force acting on the side of the arch due to the weight of the soil and corresponding to the condition of earth pressure at rest

P''_{OA} = component in the direction of P'_A of the force acting on the side of the arch due to the blast overpressure and corresponding to the condition of earth pressure at rest

P'_{OP} = component in the direction of P'_P of the force acting on the side of the arch due to the weight of the soil and corresponding to the condition of earth pressure at rest

P''_{OP} = component in the direction of P'_P of the force acting on the side of the arch due to the blast overpressure and corresponding to the condition of earth pressure at rest

P'_P = force acting on the side of the arch due to the weight of the soil and corresponding to a fully developed "passive" state of stress in the soil mass

P''_P = force acting on the side of the arch due to the blast overpressure and corresponding to a fully developed "passive" state of stress in the soil mass

q_a, q_b, q_c, q_d = influence coefficients for equivalent arch resistance (cf. Equation (3.4.7))

Q_j = equivalent resistance due to deformation of the arch rib

Q_{sj} = effective resistance at an "interior" haunch due to deformation in the soil mass

Q'_{sj} = effective resistance at an "exterior" haunch due to deformation in the soil mass

$\bar{Q}_{sj}$ = equivalent resistance due to deformation in the soil mass

R = radius of a circular arch

R'_A = maximum value of soil resistance (based upon a consideration of gravity forces) for a fully developed "active" state of stress in the soil

R''_A = maximum value of soil resistance (based upon a consideration of overpressure forces) for a fully developed "active" state of stress in the soil

R'_P = maximum value of soil resistance (based upon a consideration of gravity forces) for a fully developed "passive" state of stress in the soil.

R''_P = maximum value of soil resistance (based upon a consideration of overpressure forces) for a fully developed "passive" state of stress in the soil

S_j = shear in bar j

t = time

t' = elapsed time following passage of the shock front at a point of interest

t_d = duration of the positive phase of the shock wave

t_{ja} = time of arrival of the shock front at the windward boundary of loading region j

t_{jb} = time of arrival of the shock front at the leeward boundary of loading region j

T = thrust in the arch rib

T_m = natural period of vibration of the system

U = velocity of the shock wave in air

Z_j = effective inertial force

$\bar{Z}_j$ = equivalent inertial force

$\alpha_{j,m}$ = element of the constraint loadings

β = one-half the angle of opening of a circular arch

γ_a = weight per unit volume of the arch material

γ_s = weight per unit volume of the soil

δ = friction angle corresponding to the friction developed between the surface of the arch and the soil

δh_j = "rib-shortening" correction

δL_j = change in length of bar j due to thrust in the arch rib

$\delta \theta_j$ = rotation of bar j

Δt = time interval used for numerical integration

η = inclination with respect to the horizontal of the shock front in soil

θ_j = inclination of bar j with respect to the horizontal

λ_m = multiplying factor for the constraint loadings

$\mu_{j,m}$ = influence coefficient for equivalent mass (cf. Equation (5.2.6))

$\nu_{j,m}$ = influence coefficient for equivalent mass (cf. Equation (5.2.6))

ξ_{ℓ} = rotation of the lower bar of the model at haunch ℓ

$\xi_{\ell y}$ = rotation of the lower bar of the model corresponding to full development of an "active" state of stress in the soil adjacent to haunch ℓ

$\xi'_{\ell y}$ = rotation of the lower bar of the model corresponding to full development of a "passive" state of stress in the soil adjacent to haunch ℓ

τ_j = influence coefficient for equivalent arch resistance (cf. Equation (7.2.3))

φ = angle of internal friction of the soil

ψ_j = rotation of joint j

ψ_y = joint rotation required to produce yielding of the joint

ω = inclination of the lower bar of the model with respect to the vertical

ω_m = circular natural frequency of the system

CHAPTER II

GENERAL DISCUSSION OF THE VARIABLES

2.1 Arch Resistance

The inertial resistance of the arch is discussed separately in Section 2.3. The discussion here considers the arch resistance in terms of the forces required to pull a massless, deformable structure into the deflection configuration defined by the two independent displacements.

For the purpose of the dynamic analysis the arch, which has an infinite number of degrees of freedom as it responds to dynamic loading, is replaced by a mathematical model. This model consists of four rigid, inextensible bars connected together at three moment-resistant joints and connected to the arch abutments at two frictionless hinges as shown in Figure 2.1. This model has two degrees of freedom. Note that it permits assumptions to be made regarding conditions at the two haunches and at the crown. It has been demonstrated(8) that these are the critical sections of arch behavior, and thus the model provides a relatively simple though useful tool for the study of the dynamic response of the arch itself.

In this thesis, an arch of unit width is considered. Also it is assumed that the arch section under consideration is sufficiently far removed from endwalls or intermediate stiffeners that they have no effect on its dynamic response. This, in effect, reduces the problem of one of two dimensions.

The flexural resistance of the arch is determined herein by first finding the moment-resisting capacity of the arch cross section and then concentrating this moment resistance at the three moment-resistant joints of the model. The joint resistance is then represented by an idealized moment-rotation relationship. This is believed to be a reasonable

representation of the flexural resistance of the arch, since it will be shown (cf. Chapter IX) that the flexural resistance of the arch contributes relatively little of the total resistance of the soil-arch "structure" to lateral deformation under blast loading. Thus, modification of the flexural resistance to allow for dead and live loads acting on the arch prior to the arrival of the shock wave or for thrust in the arch due to the blast loading does not appear warranted and no modification is made herein.

Since the model used to represent the arch is composed of inextensible bars, it is necessary to handle the direct compression resistance of the arch separately. This is an approximation; however, its effect upon the lateral deformation response of the soil-arch "structure" is not considered serious as long as the arch section is sufficient to resist the maximum thrust imposed on the arch by the blast overpressure without general yielding or buckling inward. Well compacted soil surrounding the arch should restrain any tendency of the arch to buckle outward into the soil mass. It is important to note at this point also that the arch section must be sufficient to withstand imposed dead and live loadings during construction and by normal service conditions prior to the nuclear explosion. Also worthy of note is the probable loading condition on the arch after the nuclear blast wave has passed and dynamic response has ceased. The importance of attention to these conditions in the design of any buried structure is obvious.

An approximate "rib-shortening correction" is applied to certain of the numerical results obtained in this study. While this is not directly a part of a study of lateral deformation, it does give some indication of the total deformation which may be expected under the given conditions. It also serves to indicate the effect of direct compression in the arch rib on arch response.

2.2 Soil Resistance

The present state of knowledge regarding the interaction of soil and underground structures contains many uncertainties. This is true for "static" behavior and is even more true for "dynamic" behavior such as that now under consideration. The development in this thesis is considered reasonable but is necessarily approximate, consequently a high degree of refinement is not attempted.

As with the arch discussion in the preceding section, the inertial effects of the soil are covered separately in Section 2.3. The discussion here considers the shear and frictional forces developed within the soil surrounding the arch as the soil-arch "structure" deforms under blast loading. It is assumed throughout that prior to the arrival of the blast wave the soil surrounding the arch is in the "at rest" state described below.

The concept of soil resistance used in this thesis derives from a consideration of the states of stress which are developed within the soil mass surrounding the arch as the arch undergoes lateral deformation. The confining action of the blast overpressure on the soil is also considered.

The states of equilibrium within the soil mass which have been used in developing this concept are:(9)

1. Active State of Plastic Equilibrium - the state of stress within a soil mass which has undergone a "stretching," i.e. the soil mass has been permitted to expand laterally, until the ratio of the horizontal to the vertical pressure within the soil mass has reached a minimum value, called the "coefficient of active earth pressure."

2. Passive State of Plastic Equilibrium - the state of stress within a soil mass which has undergone a lateral compression until the ratio

of horizontal to vertical pressure has reached a maximum value, called the "coefficient of passive earth pressure."

3. Earth Pressure at Rest - this is a state of stress which is intermediate between the two states of plastic equilibrium described above for the soil mass and exists after the soil has been deposited by natural and artificial processes in the vicinity of the arch. It is a state of elastic equilibrium. Since this definition includes "artificial" processes for deposit of soil, it will be restricted herein to require careful compaction for optimum density of all fill materials used during construction and backfilling of the arch.

The hydrostatic pressure ratios, or ratios of horizontal to vertical soil pressure, referred to in the foregoing definitions differ because of the differences in magnitude and direction of the shear and frictional forces in the soil mass. In general, these stresses are developed within the surrounding soil as the arch-soil "structure" deforms under blast loading. The extent of development of these stresses at any particular time depends upon:

1. The state of stress within the soil mass, and
2. The restraint imposed upon the deformation of the soil mass by the confining action of the blast overpressure.

Since the blast loading is applied to the arch rib through the soil, these stresses will assist the arch in "resisting" the loading.

The degree of restraint imposed upon the deformation of the soil mass by the blast overpressure will, of course, vary with time as the blast overpressure varies.

The primary variables determining the state of stress within the soil mass are the direction and amount of deformation to which the soil mass

has been subjected. These will, of course, vary with time, but, at any given time, will also vary from one region to another around the arch. In this thesis, three regions are considered, viz. the regions adjacent to each of the haunches and the region adjacent to the crown.

As noted above, prior to any deformation it is assumed that the "at rest" stress state exists in the soil surrounding the arch. As a haunch moves inward, an "active state of plastic equilibrium" tends to develop. This does not develop fully immediately but requires a certain amount of deformation within the soil mass as discussed below. As a haunch moves outward into the soil mass, a "passive state of plastic equilibrium" tends to develop. This, too, does not develop fully until sufficient deformation has occurred.

The amount of deformation required for the full development of an active state of plastic equilibrium within the soil mass was studied by Dr. Karl Terzaghi.(10) In a series of tests on a large-scale retaining wall Dr. Terzaghi demonstrated that the lateral force on a wall varies as the wall undergoes lateral movement. The relationship between the force and the movement is shown qualitatively in Figure 2.2.(11) The resistance-displacement functions developed in this thesis are essentially idealizations of this figure.

While Figure 2.2 is qualitative only, Dr. Terzaghi and others(10,11,12) have estimated the amount of wall movement required to reduce the earth pressure to the active state for retaining walls and specific soil conditions. These recommendations form the basis for the quantitative assumptions of deformation required to develop fully the active state of stress which are used in this thesis. There is little guidance in the literature regarding the amount of deformation required to develop fully the passive state of

stress within the soil mass. Limited investigation (10,13) has indicated, however, that it is greater than that required to develop the active state of stress. Accordingly, in this study it is assumed to be such that the idealized resistance-displacement function for the soil has a constant slope in the active and passive "elastic" regions for a given value of overpressure restraint (cf. Section 4.4).

In determining numerical values of the hydrostatic pressure ratios corresponding to the limiting states of stress described above the classical Coulomb assumptions have been used. (14) It is assumed that:

1. The soil slides along a solid pressure surface, i.e. the soil failure wedge is bounded on one side by the pressure surface and on the other side by the surface of rupture.

2. The obliquity of the resultant pressure on the pressure surface has a value less than or equal to the friction angle of the soil.

3. Sufficient movement has occurred within the soil mass to develop the state of stress being considered, i.e. active or passive. These assumptions yield directly the pressure acting on the pressure surface. A comparison between results obtained from the Coulomb Equation and those obtained by the Trial Wedge Method is given in Appendix A. The equation gives results which are considered sufficiently accurate for this study.

An additional assumption required to define the soil failure wedge is the character of the surface of rupture within the soil mass. A plane surface of rupture is assumed throughout.

The pressure surface is taken as the lower bar of the model on each side and is considered to continue upward in the same direction from the haunch to the ground surface. This facilitates the development of the soil resistance concept used in this study and, for the relatively shallow depths of burial considered, does not appear unreasonable.

The soil resistance at the crown is limited primarily to the inertial resistance of the soil at and adjacent to the crown. While there must obviously be shearing forces developed in this soil mass as the arch-soil "structure" deforms, the relatively small volume of this region for the shallow depths of burial considered, as compared with the volumes of the soil wedges influenced by lateral movements of the haunches, indicates that these shearing forces will be relatively small. Also, it is possible that they will act, at least in part, only to carry the load to another portion of the arch. The extension upward to the ground surface of the pressure surfaces at the sides of the arch as described in the preceding paragraph is an attempt to include that portion of these shearing forces which will be effective in reducing the load brought to the arch. No load reduction is made, i.e. no "deformation resistance" is developed, for the remainder of the soil in this region. While this approach is somewhat arbitrary, it is not considered to have a significant influence on the response of the system as a whole.

2.3 Mass Effects

The inertial resistance of the arch-soil "structure" has an important effect on both the magnitude and time history of its dynamic response. As noted previously in Section 2.1, the model used in this study for the dynamic analysis permits appreciable latitude in the choice of the masses which are considered to move with the system at any given time. This property of the model will be used to advantage in adapting the model to fit changing conditions during the response history of the actual structure.

The mass of the arch is concentrated at the joints connecting the inextensible, massless bars, except for the mass of the lower portion of the

arch on each side. This portion of the mass of the arch is concentrated at the abutments, i.e. is not considered to have a significant effect upon the response of the system. This technique is commonly used in dynamic analyses and gives reasonable results.

The mass of soil which is assumed to move with the arch is selected according to:

1. The location of the joint,
2. The direction of movement of the joint, and
3. The depth of burial of the arch.

Varying the mass assumption with the direction of movement of the joint has the effect of giving the dynamic system a variable mass. While this increases the complexity of the analysis somewhat, it may be handled readily by the numerical integration procedure, and it appears to give a better approximation to the actual field condition than the use of a constant mass assumption. Logic indicates, for example, that the quantity of soil influenced by the inward movement of a haunch is different from the quantity influenced by the outward movement of the haunch into the soil.

Limits are placed on the dimensions of the soil masses considered. In no case is a dimension considered which is greater than the corresponding span of the arch.(15)

2.4 Blast Pressure Loading

Since the object of this study is to investigate the response of a shallow-buried arch to blast loading from a nuclear explosion, the blast overpressure is the primary weapon effect considered. In applying the results of this study to any field situation, other weapon effects obviously must be considered as well. Further, the fact that the limiting cases of

the numerical examples studied herein would not prove feasible in the field because of other-than-blast effects should not detract from their value in developing an understanding of structural response to the blast overpressure itself.

The results of this study are considered applicable to structures located outside of the crater, i.e. outside both the zone of rupture and the zone of plastic deformation.(16) It is doubtful that structures can be built to withstand weapons effects levels at closer ranges.

Direct ground shock is not considered. For structures located near the ground surface and outside the crater this omission appears reasonable.(17) Much of the energy of the direct ground shock is dissipated in disruptive effects in and immediately adjacent to the crater. Further, as the direct ground shock wave travels outward from the point of the explosion, its rise time increases so that it becomes even less effective in causing damage.

Thus, the air-induced ground shock is considered the major structural damaging effect. It is assumed that if the structure can withstand the air-induced ground shock it can resist both the direct ground shock and differential soil movements. This latter consideration may become more important with larger structures than those considered herein. However, no truly "large" underground arch structures have been tested to date, and the possible importance of differential soil movements in this case has not been established.(15)

The shock wave in air is assumed to have a single front, i.e. the structure is assumed to be in the region of Mach reflection. This assumption is not necessary but is convenient when defining the load on the structure. The study may be extended readily to cover other types of blast waves if desired.

No attenuation of free-field overpressures with depth is assumed. For the relatively shallow depths considered in this study, this is entirely reasonable (cf. Section 1.1).(18)

The decay of free-field overpressure with time in the soil mass is assumed to be the same as that of the shock wave in air. Again, for the relatively shallow depths considered in this study, this is a reasonable assumption.(18)

The free-field horizontal-to-vertical overpressure ratio in the soil is assumed as 1/4. This is the lowest of the values normally recommended(15,17,19) and was chosen to accentuate any tendency of the arch to move laterally. A low value of this ratio acts, of course, to decrease the horizontal component of the pressure acting on the arch during passage of the blast wave and thus to decrease the restraint which the load itself offers to lateral movement.

A plane shock front is assumed for the shock wave in soil. A study of the inclination of this shock front is presented in Appendix B. The rise time of the overpressure at this shock front is assumed instantaneous. The fact that studies and field measurements do indicate a finite and increasing rise time as the shock wave travels downward from the ground surface(18) is partially allowed for in developing the loading on the arch by considering the average overpressure over a region of interest(16) rather than the instantaneous overpressure at any particular point.

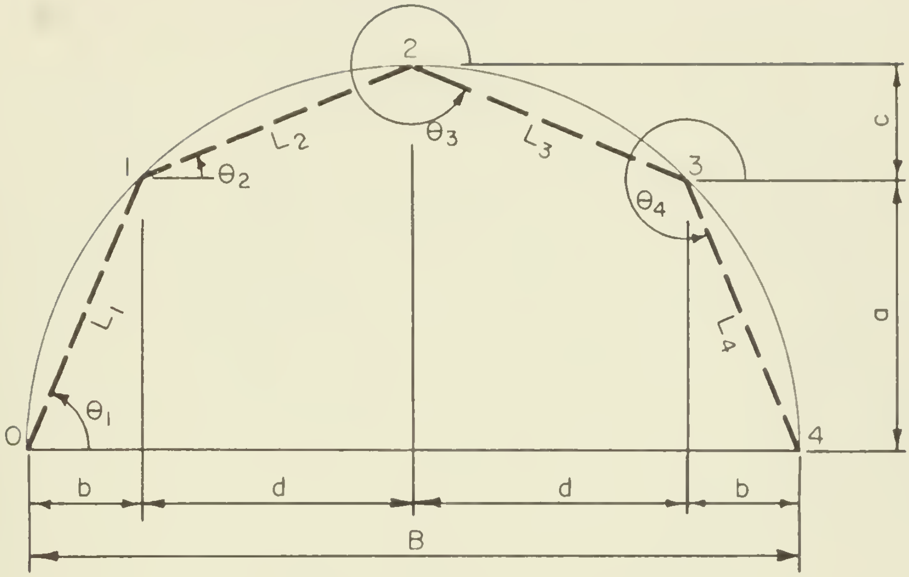

Figure 2.1. Model Considered in Analysis

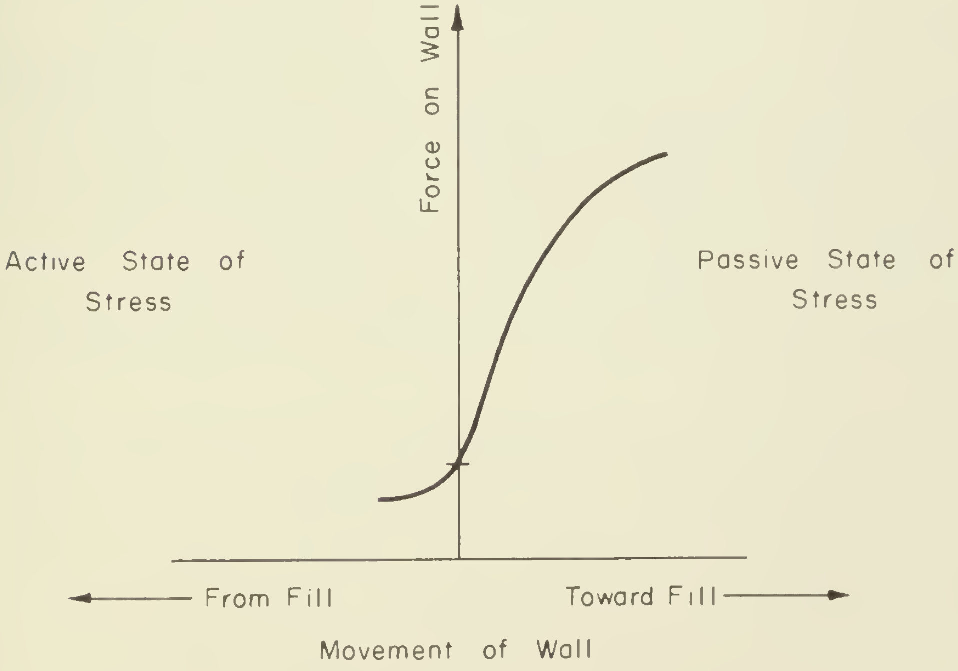

Figure 2.2. Effect of Movement of a Wall on the Lateral Thrust$^{(11)}$

CHAPTER III

ARCH RESISTANCE

In developing an expression for the resistance offered by the arch to lateral deformation under nuclear blast loading one must consider the manner in which the arch will respond and the relative importance of the various resistance parameters. In general, as the arch responds to a dynamic loading, the arch will mobilize both inertial and deformation resistance. This chapter is limited to a discussion of resistance due to the deformation of the arch rib. Inertial effects are discussed separately in Chapter V.

As the arch moves laterally in response to a dynamic, unsymmetrical loading, significant deformations occur at the haunches and at the crown. It has been shown(8) that these are also the critical sections for bending moment and that the thrust is nearly uniform throughout the arch.

3.1 Development of Model

Since the arch itself is continuous, it has an infinite number of degrees of freedom as it responds to a dynamic loading. Thus, it is inconvenient to analyze the arch directly. In this study, for the purpose of the dynamic analysis, the arch is replaced by the four-bar model shown in Figure 2.1.(4)

The model consists of four inextensible bars connected at three interior joints. At the interior joints are concentrated both the moment resistance of the arch rib and the mass of the arch. These joints also act as node points. The model permits the introduction of load and soil resistances into the analysis at each joint location. As mentioned in Section 2.1, the four-bar model is connected to the arch abutments by frictionless hinges. This is permissible for the two-hinged arches studied in this thesis.

If the bars were capable of deformation, the model would be a six-degree-of-freedom system. Since the bars are inextensible, one can write four "constraint" relationships among the joint displacements, one "constraint" relationship for each bar. This reduces the number of degrees of freedom to two. These "constraint" relationships are based upon the condition that the deformations of the model at the joints correspond to no change in the length of the members. These relationships are developed for the model in Section 3.2.

In this study the constraint relations will be derived using four loading patterns which produce only axial stresses in the bars. They thus cause no movement of the model and, of course, do no work when applied to the model. The principle of virtual work and the fact that these force patterns cause no movement are then used in deriving relationships among the displacements and among any general set of loading components. These relationships are then consistent with the two-degree-of-freedom system.

A limitation in the use of this model is that direct compression in the arch cannot be handled directly. This follows from the inextensible nature of the bars. This limitation would be serious if this study were of the total stability of the arch, since the arch rib must be able to withstand the thrust loading imposed upon it without failing by general yielding or buckling. However, if the arch section is sufficient to carry the imposed thrusts, it may then be studied from the standpoint of lateral deformation response without simultaneous consideration of direct compression load components.

The prime reason for accepting this limitation in the model is, of course, to retain the convenience of the two-degree-of-freedom system. If the bars were extensible, the model would have not two but six degrees of freedom and the analysis would become correspondingly more involved. The nature of the behavioral assumptions upon which this study is based is approximate

enough that a more refined analysis is not considered justified at the present time.

The independent displacement components chosen to define the configuration of the model at any instant are the horizontal displacements of the haunches. While other pairs of independent displacements could be used, those chosen are particularly convenient in that they: (1) indicate directly the primary mode of response of the system (cf. Article 2.1) and (2) simplify the expression of the soil resistance (cf. Chapter IV).

3.2 Constraint Relationships

The constraint relationships relate the various arch parameters and serve to reduce the continuous arch to a two-degree-of-freedom system. These relationships are developed herein by considering four independent loading patterns, each of which produces only axial forces in the bars of the model. Thus, since the bars are inextensible, no deformation of the arch can take place under any of these loading patterns.

The four loading patterns chosen are shown in Figure 3.1. For convenience these loading patterns will be referred to herein as the "constraint loadings". Other loading patterns could be developed by combining these; however, these possess certain orthogonal properties which are convenient in deriving the following relationships. The constraint loadings may be tabulated conveniently as shown in Table 3.1.

3.2.1 Loading Relationships

The load concentrations which will be applied to the model are shown in Figure 3.2. Relationships among these load components are now derived using the constraint loadings shown in Figure 3.1 and the fact that these constraint loadings, when applied to the model, produce no movement of the model.

Now any general system of loads can be replaced by a set of loading patterns consisting of some proportion of each of the four constraint loadings plus a loading pattern which does produce movement of the model. This latter pattern is that portion of the original system of loads which is effective in producing dynamic response of the system. This concept is expressed in Equation (3.2.1).

$$H_j = \sum_{m=1}^{4} \lambda_m \alpha_{j,m} + \bar{H}_j \tag{3.2.1}$$

where H_j = any system of loads on the model (cf. Figure 3.2)

λ_m = multiplying factors for the constraint loadings

$\alpha_{j,m}$ = elements of the constraint loadings

$\bar{H}_j$ = that portion of the loading system which is effective in producing motion of the model

j = load component index; $j = 1,2,\ldots 6$

m = constraint loading index; $m = 1,2,3,4$.

In developing the load relationships from Equation (3.2.1) the constraint loadings serve to reduce the number of equations from six to two. This is accomplished algebraically by seeking four values of the multiplying factor, λ_m, such that four of the quantities $\bar{H}_j$ are zero. Since the horizontal displacements at the haunches have been chosen as the independent variables, the corresponding load components $\bar{H}_1$ and $\bar{H}_3$ will be retained here. Thus, in the following derivation multiplying factors are sought such that $\bar{H}_2 = \bar{H}_4 = \bar{H}_5 = \bar{H}_6 = 0$.

Using either Figure 3.1 or Table 3.1 and Equation (3.2.1), one may write:

$$\begin{aligned}
&H_4 && - a\,\lambda_2 && && + a\,\lambda_4 = 0 \\
&H_2 && && - 2\left(\frac{d}{c}\right)\lambda_3 && = 0 \\
&H_5 + 2\lambda_1 && && && = 0 \\
&H_6 && - a\,\lambda_2 && && - a\,\lambda_4 = 0
\end{aligned} \tag{3.2.2}$$

Note that the constraint loadings were chosen so that Equations (3.2.2) are orthogonal, i.e. $\sum_j \alpha_{j,m}\,\alpha_{j,n} = 0$, for $m \neq n$ and $j = 2,4,5,6$. Thus, the multiplying factors, λ_m, may be obtained from:

$$\lambda_m = \frac{\sum_j \alpha_{j,n} H_j}{\sum_j (\alpha_{j,m})^2}, \quad j = 2,4,5,6 \qquad (3.2.3)$$

Equation (3.2.3) gives directly:

$$\begin{aligned}
\lambda_1 &= -\tfrac{1}{2}(H_5) \\
\lambda_2 &= +\tfrac{1}{2a}(H_4 + H_6) \\
\lambda_3 &= +\tfrac{c}{2d}(H_2) \\
\lambda_4 &= -\tfrac{1}{2a}(H_4 - H_6)
\end{aligned} \qquad (3.2.4)$$

Substituting Equations (3.2.4) into Equation (3.2.1) and solving for $\bar{H}_1$ and $\bar{H}_3$ yield the load relationships for the two-degree-of-freedom system. They express the "equivalent" load on the system, i.e. that portion of the total load which is effective in causing movement of the structure in the horizontal direction at the haunches.

$$\begin{aligned}
\bar{H}_1 &= H_1 + \tfrac{1}{2}(1 - \tfrac{bc}{ad})H_2 - (\tfrac{b}{a})H_4 + \tfrac{1}{2}(\tfrac{d}{c} - \tfrac{b}{a})H_5 \\
\bar{H}_3 &= +\tfrac{1}{2}(1 - \tfrac{bc}{ad})H_2 + H_3 - \tfrac{1}{2}(\tfrac{d}{c} - \tfrac{b}{a})H_5 + (\tfrac{b}{a})H_6
\end{aligned} \qquad (3.2.5)$$

These load relationships will be used later in developing the equations of motion for the model (cf. Chapter VII).

3.2.2 Deflection Relationships

In deriving relationships among the displacement components of the model use is again made of the constraint loadings of Figure 3.1 together with

the principle of virtual work. Since none of the loading patterns produces any displacement of the model, the product of the loadings in the pattern times the displacements in any consistent set of displacements of the structure in the direction of the loadings in the pattern must be zero. This is expressed algebraically in Equation (3.2.6).

$$\sum_{j=1}^{6} h_j \alpha_{j,m} = 0 \qquad (3.2.6)$$

where h_j = displacement components

$\alpha_{j,m}$ = elements of the constraint loadings

j = displacement component index; $j = 1,2,\ldots 6$

m = constraint loading index; $m = 1,2,3,4$.

Again referring to the choice of the horizontal displacement components of the haunches as the independent variables, the other displacement components may be written in terms of them using Equation (3.2.6).

Solving Equation (3.2.6) explicitly for each of the deflection components yields:

$$\begin{aligned} h_2 &= \tfrac{1}{2}(1 - bc/ad)(h_1 + h_3) \\ h_4 &= -(b/a)h_1 \\ h_5 &= \tfrac{1}{2}\left(\frac{d}{c} - \frac{b}{a}\right)(h_1 - h_3) \\ h_6 &= (b/a)h_3 \end{aligned} \qquad (3.2.7)$$

where a,b,c,d = generalized arch dimensions (cf. Figure 2.1)

h_1 = horizontal displacement component of joint 1

h_2 = horizontal displacement component of joint 2

h_3 = horizontal displacement component of joint 3

h_4 = vertical displacement component of joint 1

h_5 = vertical displacement component of joint 2

h_6 = vertical displacement component of joint 3

3.2.3 Joint Rotation Relationships

It is necessary to know the relationships between the rotations of the joints and the independent displacement variables in order to determine the moment resistance developed in the joints of the model for any particular deflected shape. Since the horizontal displacement components of the haunches have already been chosen as the independent variables, they will be used as such in this derivation also.

Referring to Figure 3.3, it can be seen that for small displacements the rotations of the bars may be expressed as:

$$\delta\theta_j \approx \frac{(h_{j-1} - h_j) \csc \theta_j}{L_j} \qquad (3.2.8)$$

where $\delta\theta_j$ = rotation of bar j

h_j, h_{j-1} = horizontal displacement components at the ends of bar j

L_j = length of bar j

θ_j = inclination of bar j

Substituting into Equation (3.2.8) and rearranging terms give the following expressions for the bar rotations of the model in terms of the independent displacement coordinates and the geometry of the arch:

$$\begin{aligned}
\delta\theta_1 &\simeq - h_1/a \\
\delta\theta_2 &\simeq + \tfrac{1}{2}(1/c + b/ad)h_1 - \tfrac{1}{2}(1/c - b/ad)h_3 \\
\delta\theta_3 &\simeq - \tfrac{1}{2}(1/c - b/ad)h_1 + \tfrac{1}{2}(1/c + b/ad)h_3 \\
\delta\theta_4 &\simeq - h_3/a
\end{aligned} \qquad (3.2.9)$$

The total rotation at each of the joints is simply the algebraic difference of the rotations of the bars connecting at the joint. This may be expressed as:

$$\psi_j = \delta\theta_{j+1} - \delta\theta_j \qquad (3.2.10)$$

where ψ_j = total rotation of joint j

$\delta\theta_j$ = rotation of bar j.

Substituting Equations (3.2.9) into Equation (3.2.10) and introducing simplified notation give the desired joint rotation relationships.

$$\begin{aligned}\psi_1 &= A_1h_1 - A_3h_3\\ \psi_2 &= -A_2h_1 + A_2h_3\\ \psi_3 &= A_3h_1 - A_1h_3\end{aligned} \qquad (3.2.11)$$

where $A_1 = \frac{1}{2}(2/a + 1/c + b/ad)$

$A_2 = 1/c$

$A_3 = \frac{1}{2}(1/c - b/ad)$

3.3 Moment-Rotation Relationships for Joints

As the arch displaces laterally under load, bending moments are developed in the arch which act to resist the displacement. Likewise in the model, as a change occurs in the angle between the bars meeting at a joint, a resisting moment is developed in the joint. In Section 3.2.3 expressions are derived relating joint rotations and model displacements. It is the purpose of this section to derive relationships between these joint rotations and the corresponding moment resistance developed by the joints.

If bending in the arch is assumed to be uniform over a region such as that shown in Figure 3.4, the moment-rotation relationship for the joint may be derived as follows:

Let M_j = moment resistance of the arch rib cross section

E_j = modulus of elasticity of the material from which the arch rib is made

I_j = moment of inertia of the arch rib cross section

L_j = length of bar (assumed of equal length on either side of joint)

ψ_j = joint rotation

Then, from Figure 3.4:

$$\frac{\psi_j}{2} = \frac{M_j}{E_j I_j} \times \frac{L_j}{2}$$

Hence:

$$M_j = \frac{E_j I_j}{L_j} \psi_j$$

For an arch of constant cross section, E_j and I_j may be considered constant. L_j may be chosen as a constant when setting up the model. For these conditions it is convenient to simplify the notation as:

$$M_j = K_{B_j} \psi_j \qquad (3.3.1)$$

where $K_{B_j} = E_j I_j / L_j$ = bending stiffness of the arch rib as concentrated at joint j of the model.

Strictly speaking, Equation (3.3.1) is valid only in the elastic range. Since it is intended to permit plastic deformation of the arch rib, the moment-rotation relationship is extended as shown in idealized form in Figure 3.5. This follows directly from Equation (3.3.1) and the requirement that the arch rib possess sufficient ductility to continue to rotate without rupture or decreasing moment resistance once the maximum moment resistance is developed. This can be achieved readily in the design of the arch rib.

The limits of this moment-rotation diagram for any particular case will thus be determined by the strength, ductility and geometry of the arch rib cross section as well as by the geometry of the arch itself. As mentioned previously (cf. Section 2.1), no modification of bending resistance is made for thrust in the arch caused by the blast loading, or for dead and live loads existing on the arch prior to the arrival of the shock wave. In general, these effects will tend to reduce the stiffness of the arch. Again, while the arch must be capable of withstanding these loads, their net effect on the total resistance of the arch-soil "structure" to lateral deformation is

relatively small and such modification is not considered warranted for this study.

3.4 Development of Equivalent Arch Resistance

In order that the moment resistance of the joints may be inserted conveniently into the equations of motion for the model, relationships are needed expressing the resistance of the arch to lateral deformation. These are derived in this section first in general terms and then specialized for the choice of independent displacement variables used in this thesis, viz. the horizontal displacements of the haunches.

In the sign convention used for this derivation clockwise shears are considered positive. Bending moments are considered positive when they tend to produce compression in the outer fibers of the arch rib. Bar rotations are measured at the left ends of bars, counterclockwise from a horizontal axis directed toward the right. As stated in Section 1.2, loads and displacements are taken as positive horizontally to the right and vertically upward.

Referring to Figure 3.6 and considering the equilibrium of either one of the bars, it can be seen that:

$$S_j = \frac{M_j - M_{j-1}}{L_j} \tag{3.4.1}$$

where S_j = shear in bar j

M_j = resisting moment in joint j

L_j = length of bar j

Summing horizontal forces acting on the free body shown in Figure 3.7 gives:

$$Q_j = S_j \sin(\theta_j + \delta\theta_j) - S_{j+1} \sin(\theta_{j+1} + \delta\theta_{j+1}) \tag{3.4.2}$$

where Q_j = horizontal component of arch resistance at joint j

S_j = shear in bar j

θ_j = inclination of bar j

$\delta\theta_j$ = rotation of bar j under nuclear blast loading.

Summing vertical forces acting on the free body shown in Figure 3.7 gives:

$$Q_{j+3} = - S_j \cos(\theta_j + \delta\theta_j) + S_{j+1} \cos(\theta_{j+1} + \delta\theta_{j+1}) \qquad (3.4.3)$$

where Q_{j+3} = vertical component of the arch resistance of joint j.

In deriving the equivalent arch resistance at the haunches, it is convenient to express the inclination of the shearing forces in the bars in terms of the arch geometry. This is readily accomplished using the familiar trigonometric identity stated in Equation (3.4.4).

$$\sin(\theta_j + \delta\theta_j) = \sin\theta_j \cos\delta\theta_j + \cos\theta_j \sin\delta\theta_j \qquad (3.4.4)$$

Using the notation of Figure 2.1, and limiting consideration to small rotations, one can write:

$$\begin{aligned}
\sin(\theta_1 + \delta\theta_1) &= \frac{1}{L_1} [a - (\tfrac{b}{a})h_1] \\
\sin(\theta_2 + \delta\theta_2) &= \frac{1}{L_2} [c + \tfrac{1}{2}(d/c + b/a)h_1 - \tfrac{1}{2}(d/c - b/a)h_3] \\
\sin(\theta_3 + \delta\theta_3) &= \frac{1}{L_3} [-c - \tfrac{1}{2}(d/c - b/a)h_1 + \tfrac{1}{2}(d/c + b/a)h_3] \\
\sin(\theta_4 + \delta\theta_4) &= \frac{1}{L_4} [-a - (b/a)h_3]
\end{aligned} \qquad (3.4.5)$$

It is now possible to write expressions for the equivalent arch resistance in the horizontal direction at the haunches by substituting Equations (3.4.1) and (3.4.5) into Equation (3.4.2). Thus:

$$Q_1 = \frac{M_1}{L_1^2}\left[a - (\frac{b}{a})h_1\right] - \left[\frac{M_2 - M_1}{L_2^2}\right]\left[c + \frac{1}{2}(\frac{d}{c} + \frac{b}{a})h_1 - \frac{1}{2}(\frac{d}{c} - \frac{b}{a})h_3\right]$$

$$Q_3 = \left[\frac{M_3 - M_2}{L_3^2}\right]\left[-c - \frac{1}{2}(\frac{d}{c} - \frac{b}{a})h_1 + \frac{1}{2}(\frac{d}{c} + \frac{b}{a})h_3\right] + \frac{M_3}{L_4^2}\left[-a - (\frac{b}{a})h_3\right] \qquad (3.4.6)$$

where Q_1 and Q_3 = horizontal components of arch resistance at joints 1 and 3 respectively

M_1, M_2, M_3 = resisting moments developed in joints 1, 2 and 3 respectively

a,b,c,d = generalized arch dimensions as given in Figure 2.1

h_1, h_3 = horizontal components of displacement at joints 1 and 3 respectively.

By limiting consideration to equal bar lengths, rearranging terms and simplifying notation, one can write the equivalent arch resistances as:

$$Q_1 = M_1(q_a + q_b h_1 - q_b h_3) - M_2(q_c + q_d h_1 - q_b h_3)$$

$$Q_3 = -M_3(q_a + q_b h_1 - q_b h_3) + M_2(q_c + q_b h_1 - q_d h_3) \qquad (3.4.7)$$

where $q_a = (1/L^2)(a + c)$

$q_b = (1/2L^2)(d/c - b/a)$

$q_c = (c/L^2)$

$q_d = (1/2L^2)(d/c + b/a)$

3.5 Rib Shortening

The results of the dynamic analysis developed elsewhere in this thesis may be modified using the "rib-shortening" correction derived in this section in order to give an indication of the significance of the effect of direct compression in the arch rib on the total displacement of the arch. The necessity of considering direct compression effects separately was discussed earlier (cf. Sections 2.1 and 3.1). Essentially, the model cannot accept axial

changes in the length of the bars and retain its characteristics as a two-degree-of-freedom system. While this is a definite limitation, it is not serious in a study of lateral deformations as long as the arch rib has sufficient capacity to withstand the thrust in the arch without general yielding or buckling.

The approach used in this section is to consider the response of the arch to a uniform compression loading. This response is then superimposed on the lateral response in order to approximate the total response of the arch. This is an approximation in that these effects are in fact interrelated and cannot be entirely separated, although if one considers the relative compressibilities of the arch and the soil, direct compression effects are not as important as might otherwise be expected (cf. Chapter IX).

Note that the soil provides a high degree of damping to the response of the arch in this mode. This effect cannot be neglected as it tends to produce an over-critically damped response. Further, the extremely short natural period of vibration of the arch-soil "structure" in this mode makes the rise time of the shock wave in soil significant. This also tends to reduce the magnitude of the response. Therefore, for the purpose of the approximate correction derived in this section, a dynamic magnification factor of unity is assumed for this motion.

The arch loading does contain a significant "uniform compression" component because of the rapid envelopement of the arch by the shock wave and the relatively slow decay of overpressure with time behind the shock front. Therefore, it appears reasonable to consider this component of the loading in computing the thrust in the arch rib. In this study, the uniform compression loading on the arch is taken as a proportion of the average vertical overpressure acting on the arch (cf. Chapter VI). This proportion depends

principally upon the ratio of the horizontal to the vertical overpressure in the soil, although the fact that the crown is subjected to a higher value of overpressure than the average radial overpressure on the arch must also be considered.

Two additional assumptions are made in order to simplify the computation of the rib shortening itself. First, the average thrust in the arch is assumed to be equal to that in a circular ring under uniform compression. Second, the arch is assumed to maintain its same general shape as it deforms under the uniform compressive loading. This is approximate, but then the nature of the correction derived in this section does not warrant a rigorous solution for rib shortening in the arch. As will be seen, these assumptions lead to simple expressions which give reasonable results and are therefore justified on this basis.

Consider the arch to be loaded as shown in Figure 3.8. The thrust in the arch, T, may then be determined by equating the sum of the vertical forces acting on the arch to zero.

$$2T\sin\beta = 2R\sin\beta\, \bar{p}'_a$$

$$T = \bar{p}'_a\, R$$

$$T \approx \frac{1}{2}\, \bar{p}'_a\, B \qquad (3.5.1)$$

where $\bar{p}'_a$ = "uniform compression" component of the average overpressure loading the arch (cf. Chapter VI).

The change in length of any one of the bars of the model caused by the thrust is given by Equation (3.5.2).

$$\delta L_j = TL_j/AE$$

$$\delta L_j = \frac{1}{2}\, \bar{p}'_a\, BL_j/AE \qquad (3.5.2)$$

where δL_j = change in length of bar j due to thrust

L_j = length of bar j

A = cross-sectional area of the arch rib (assumed constant)

E = modulus of elasticity of the arch material.

The model is shown in its undeformed and deformed configurations in Figure 3.9. The arch abutments are considered immovable (cf. Section 1.2); therefore, joint 0 remains stationary. For the model to maintain the same general shape as the bars shorten, let bar 2 rotate about point 0' such that joint 1 moves in a direction perpendicular to the original direction of bar 2. This is shown in Figure 3.10. Now, from symmetry joint 2 must move vertically downward. Therefore, joint 2 may be considered first to perform the same motion as joint 1 and then to rotate and shorten until it is vertically below its original position. This is illustrated in Figure 3.11.

The displacement coordinates of joint 1, i.e. the "rib-shortening" correction for joint 1, may be written directly from Figure 3.10.

$$\begin{aligned}\delta_1 &= \delta L_1/\sin(\theta_1-\theta_2)\\ &= \delta L_1/\sin\theta_1\cos\theta_2-\cos\theta_1\sin\theta_2\\ &= \delta L_1(L)^2/ad-bc \qquad (3.5.3)\end{aligned}$$

$$\begin{aligned}\delta h_1 &= -\delta_1\sin\theta_2\\ &= -(\delta L_1)Lc/ad-bc \qquad (3.5.4)\end{aligned}$$

$$\begin{aligned}\delta h_4 &= +\delta_1\cos\theta_2\\ &= +(\delta L_1)Ld/ad-bc \qquad (3.5.5)\end{aligned}$$

The displacement coordinates for the crown may be written directly from Figure 3.11.

$$\delta h_2 = 0 \qquad (3.5.6)$$

$$\begin{aligned}\delta h_5 &= \delta L_2/\sin\theta_2\\ &= (\delta L_2)L/c \qquad (3.5.7)\end{aligned}$$

The "rib-shortening" corrections for the model in terms of the arch geometry and the uniform overpressure which is effective on the arch

may now be obtained by substituting Equation (3.5.2) into Equations (3.5.4) through (3.5.7) and considering symmetry.

$$
\begin{aligned}
\delta h_1 &= -\frac{1}{2}\,\bar{p}_a' \left[\frac{BL^2c}{AE(ad-bc)}\right] \\
\delta h_2 &= 0 \\
\delta h_3 &= -\,\delta h_1 \\
\delta h_4 &= +\frac{1}{2}\,\bar{p}_a' \left[\frac{BL^2d}{AE(ad-bc)}\right] \\
\delta h_5 &= +\frac{1}{2}\,\bar{p}_a' \left[\frac{BL^2}{cAE}\right] \\
\delta h_6 &= \delta h_4
\end{aligned}
\qquad (3.5.8)
$$

Note that if the overpressure, $\bar{p}_a'$, is expressed in units of force/(length)^2, the cross-sectional area of the arch rib, A, must be expressed in units of (length)^2/length.

An alternate approach to the derivation of the "rib-shortening" corrections is to allow the haunches and the crown to move such that, if the elevation of the abutments is used as a reference, the ratio of the elevation of the haunches to the elevation of the crown remains constant. Expressions were derived on this basis and found to give results, for the numerical examples studied herein (cf. Chapter VIII), which do not differ significantly from those given by Equations (3.5.8). Since the alternate expressions are somewhat more involved, they were discarded in favor of Equations (3.5.8).

TABLE 3.1

CONSTRAINT LOADINGS

m	$\alpha_{1,m}$	$\alpha_{2,m}$	$\alpha_{3,m}$	$\alpha_{4,m}$	$\alpha_{5,m}$	$\alpha_{6,m}$
1	$+(\frac{d}{c} - \frac{b}{a})$	0	$-(\frac{d}{c} - \frac{b}{a})$	0	-2	0
2	+b	0	-b	+a	0	+a
3	$-(\frac{d}{c} - \frac{b}{a})$	$+2(\frac{d}{c})$	$-(\frac{d}{c} - \frac{b}{a})$	0	0	0
4	-b	0	-b	-a	0	+a

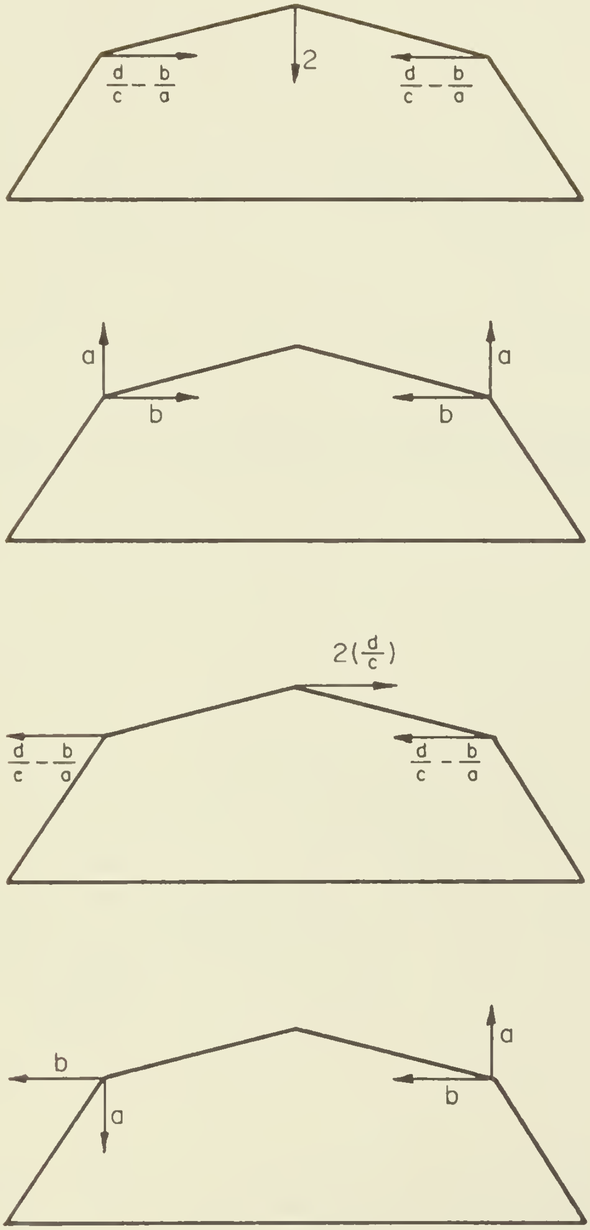
$\frac{d}{c} - \frac{b}{a}$
2
$\frac{d}{c} - \frac{b}{a}$
a
a
b
b
$2(\frac{d}{c})$
$\frac{d}{c} - \frac{b}{a}$
$\frac{d}{c} - \frac{b}{a}$
b
a
a
b

Figure 3.1. Constraint Loadings

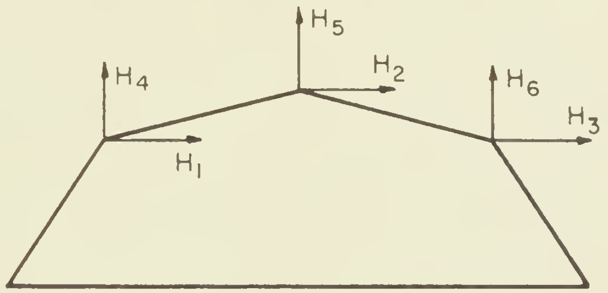

Figure 3.2. Load Concentrations on Model

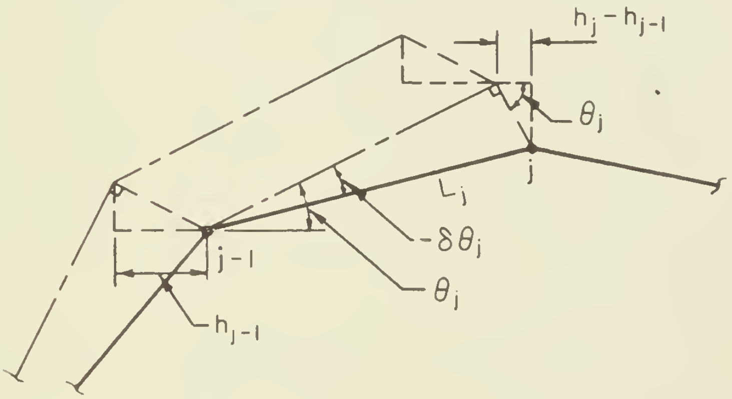

Figure 3.3. Diagram Used in Determining Joint Rotation Relationships

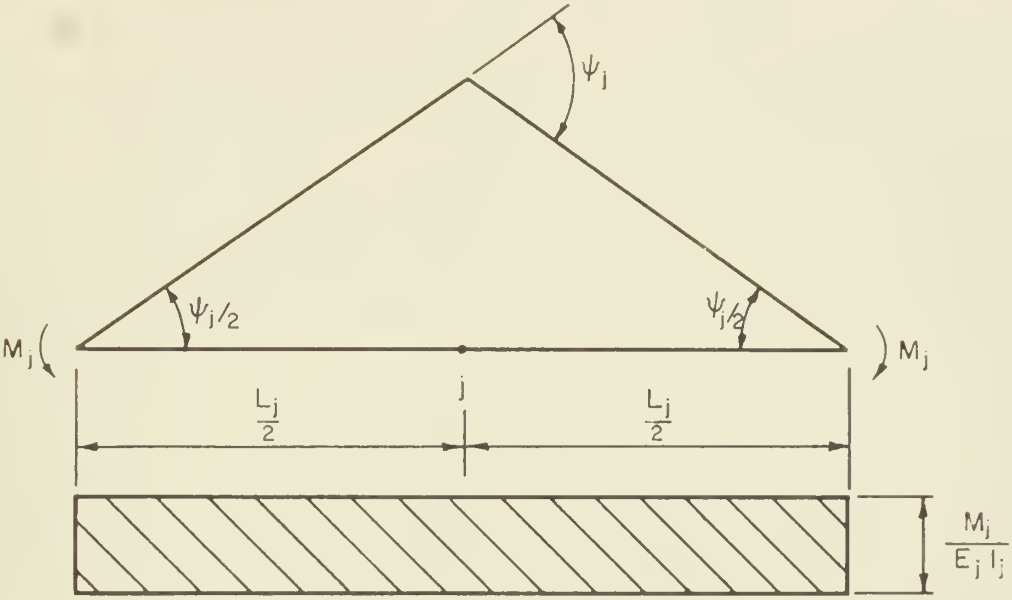

Figure 3.4. Diagram Used in Determining Moment-Rotation Relationships for Joints

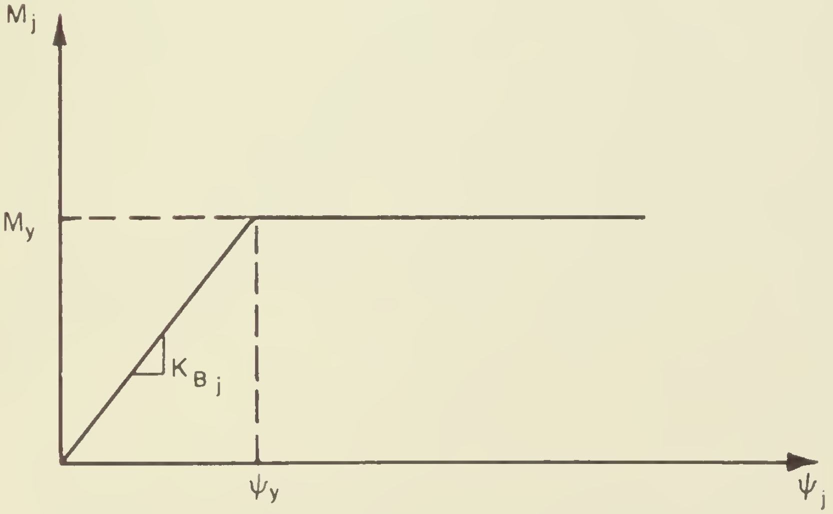

Figure 3.5. Idealized Moment-Rotation Diagram for Joints

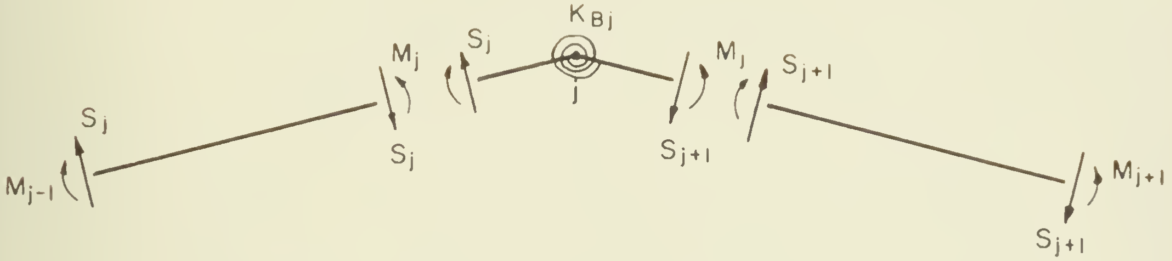

Figure 3.6. Free-Body Diagram of Typical Bars and Joint

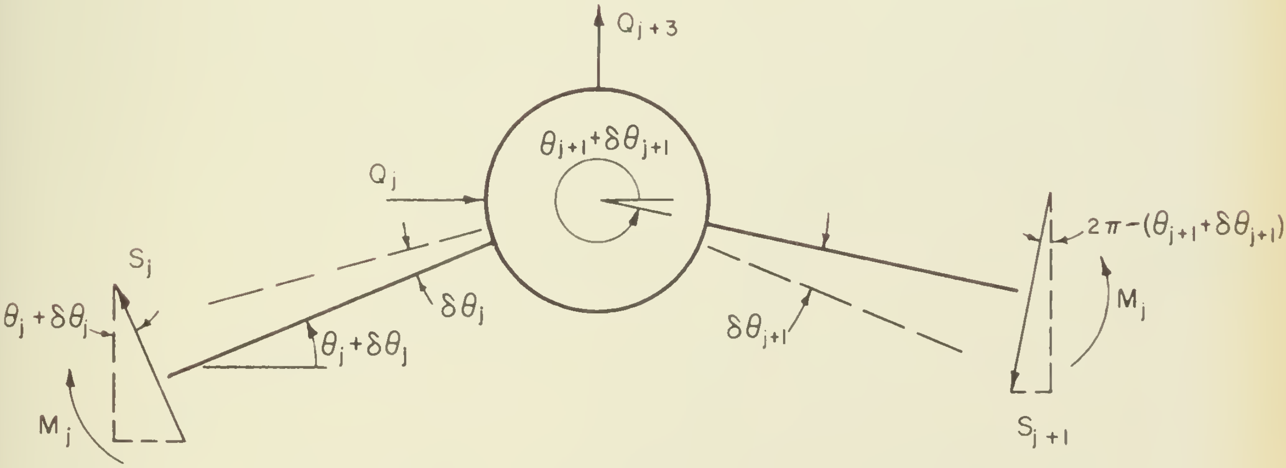
Q_{j+3}
$\theta_{j+1}+\delta\theta_{j+1}$
Q_j
S_j
$2\pi-(\theta_{j+1}+\delta\theta_{j+1})$
$\theta_j+\delta\theta_j$
$\delta\theta_j$
M_j
$\delta\theta_{j+1}$
$\theta_j+\delta\theta_j$
M_j
S_{j+1}

Figure 3.7. Free-Body Diagram of Typical Joint

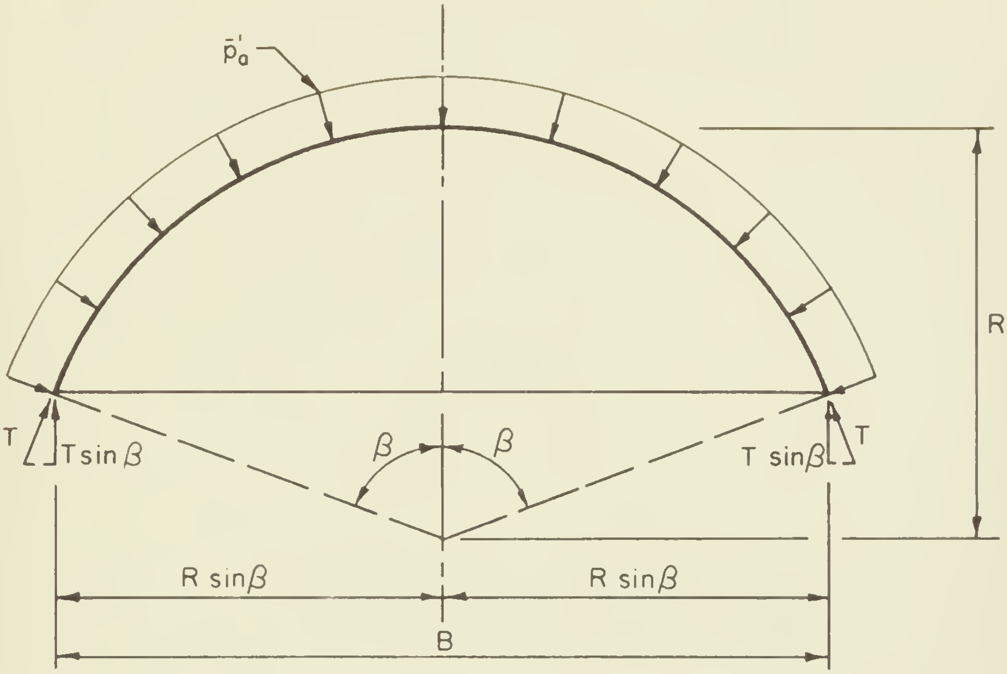

Figure 3.8. Uniform Radial Load on Arch

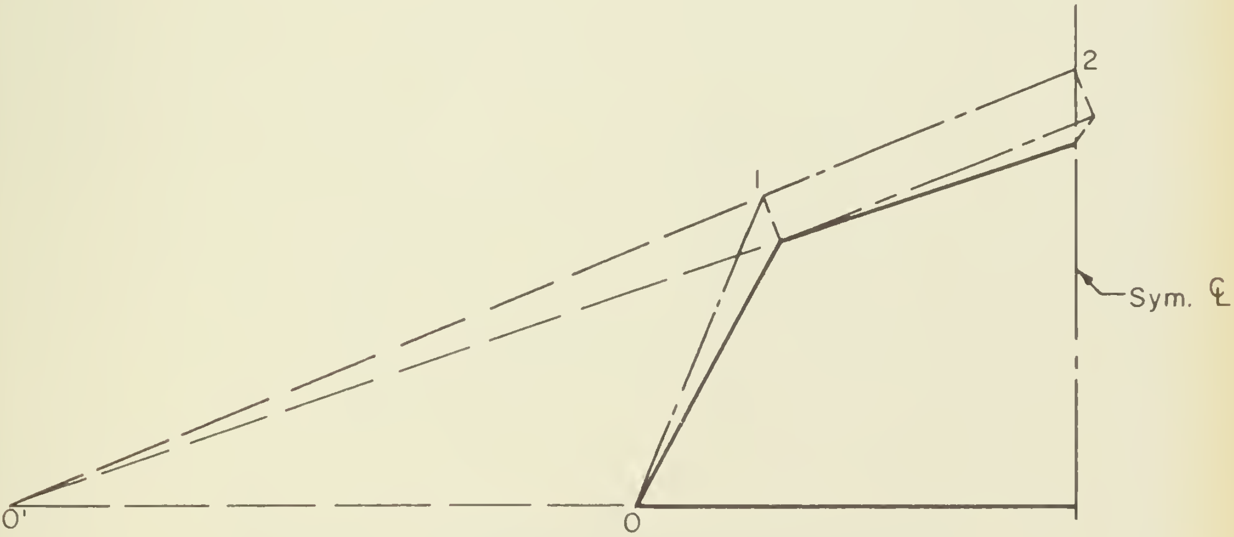

Figure 3.9. Deformation of Model Due to Rib Shortening

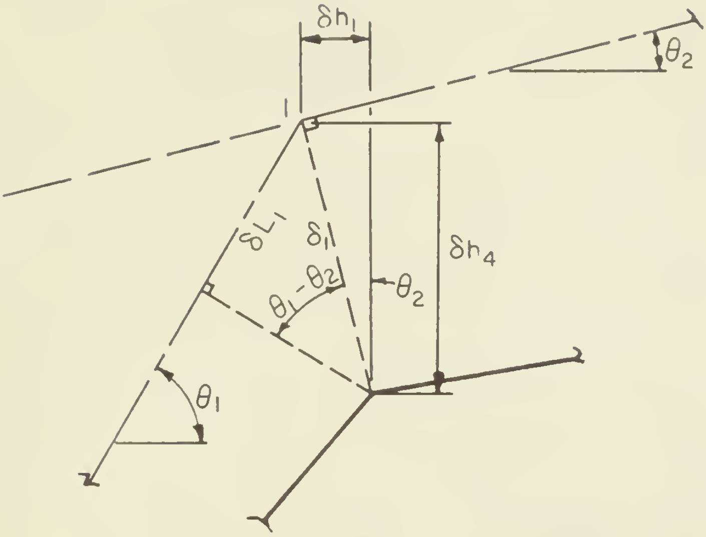

Figure 3.10. Diagram Used in Determining Rib-Shortening Correction at Haunch

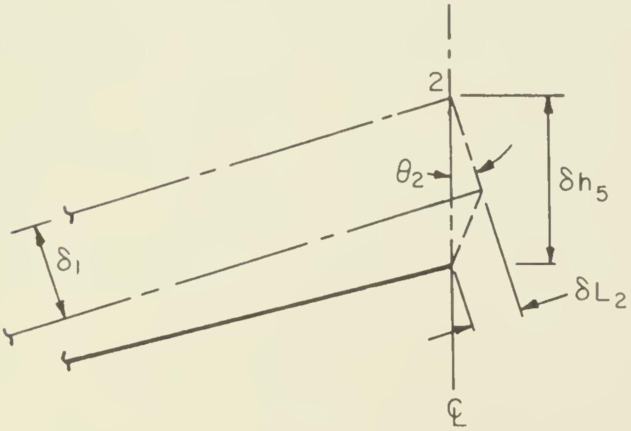

Figure 3.11. Diagram Used in Determining Rib-Shortening Correction at Crown

CHAPTER IV

SOIL RESISTANCE

In the case of an underground arch the soil contributes significantly to the total resistance to nuclear blast loading of the arch-soil "structure". As with the arch, this resistance can be conveniently considered in two parts, viz. inertial resistance, or that due to the mass of the soil which moves with the arch, and deformation resistance, or that due to the presence of shear and frictional forces within that portion of the soil which deforms with the arch under blast loading. Deformation resistance is discussed here. Inertial or mass effects are considered separately in Chapter V.

As discussed in Section 2.2, the concept developed in this study regarding soil resistance due to frictional and shearing forces in the soil is based upon consideration of the state of stress existing in the soil at any particular instant during the response of the structure. Specifically, in the derivations which follow, the limiting stress conditions of the "Active State of Plastic Equilibrium" and the "Passive State of Plastic Equilibrium," as defined in Section 2.2, are considered as well as the intermediate condition of "Earth Pressure at Rest." In general, differences in the gravity forces acting on the arch for different states of stress in the soil, together with the difference between the blast loading exerted on the ground surface and that transmitted to the arch by the soil, are considered as due to "soil resistance." A linear interpolation is used between the "at rest" and the "plastic equilibrium" states, and an unchanging soil resistance assumed for deformations greater than those required for "plastic equilibrium." This in effect assumes an elasto-plastic resistance function for the soil which is consistent with the present state of knowledge of soil-structure behavior.

Since the model developed for the dynamic analysis (cf. Section 3.1), contains three interior hinges, three regions, one adjacent to each hinge, are considered separately from the standpoint of soil deformation and resistance. Conditions are different at the haunches from those at the crown. Further, since conditions at a haunch are different depending upon whether the haunch has moved inward into the arch or outward into the soil, these cases are treated separately. For convenience, a haunch which has moved inward into the arch with respect to its original position prior to the arrival of the shock wave, or with respect to its original position as modified by any "permanent set" in the soil adjacent to the arch, is referred to herein as an "interior" haunch. A haunch which has moved outward into the soil with respect to the same reference position is referred to as an "exterior" haunch. This classification is particularly useful when studying "rebound," or response of the system after the first maximum response has occurred (cf. Section 4.4).

4.1 Interior Haunch

As a haunch moves inward into the arch, the soil tends to follow it under the influence of the overpressure acting on the ground surface. This tends to create an "active" state of stress within the soil surrounding the haunch. Further, since the blast loading is applied to the arch through the soil, the shearing and frictional stresses developed within the soil mass will assist the structure in resisting the load.

To illustrate how this "soil resistance" is developed, consider the loading "sensed" by the arch as the arch deforms. As mentioned in Section 2.2, the pressure surface, or surface on which the soil pressure acts, at the side of the arch is assumed to coincide with the lower bar of the model and in addition to extend upward in the same direction from the haunch to the ground surface. In Figure 4.1 P' represents the force on the side of the arch due to

the weight of the soil. It is assumed to act at the lower third point of the pressure surface. P" represents the force on the side of the arch due to the "surcharge" of the blast overpressure acting on the ground surface. It is assumed to act at the midheight of the pressure surface. Since classical earth pressure theory (Coulomb assumptions, cf. Section 2.2)is being used to define the limiting stress conditions for the calculation of hydrostatic pressure ratios for the soil stresses, P' and P" are assumed to act at an angle to the direction of the pressure surface. This angle, δ, is the friction angle corresponding to the friction developed between the surface of the arch and the soil.

Now consider the hinges of the model to be "locked" so that when the blast loading is applied, no deformation can take place. If no movement takes place, the state of stress in the soil cannot change, and it therefore remains in the "at rest" condition. For this condition of "no deformation" one can write expressions for the forces acting on the sides of the arch as:

$$P'_{OA} = \frac{1}{2} \gamma_s d_o^2 K_{OA} \qquad (4.1.1)$$

where P'_{OA} = component in the direction of P'_A of the force acting on the side of the arch due to the weight of the soil and corresponding to the condition of earth pressure at rest

γ_s = weight of soil per unit volume

d_o = total depth from the ground surface to the arch abutment

K_{OA} = ratio of the soil pressure in the direction of P'_A to the vertical soil pressure for the condition of earth pressure at rest,

and:

$$P''_{OA} = - \bar{p}_{sj} d_o K_{OA} \qquad (4.1.2)$$

where P''_{OA} = component in the direction of P'_A of the force acting on the side of the arch due to the blast overpressure and corresponding to the condition of earth pressure at rest

$\bar{p}_{sj}$ = average overpressure acting at the ground surface on the potential "active" failure wedge in the soil (defined below). Note that since $\bar{p}_{sj}$ acts downward, it is considered negative in accordance with the sign convention used herein (cf. Section 1.2).

Now consider the hinges of the model to be "unlocked" and the model permitted to deform until a fully developed "Active State of Plastic Equilibrium" is reached. At this point frictional and shearing forces exist within the soil mass and the expressions for the forces acting on the side of the arch are:

$$P'_A = \frac{1}{2} \gamma_s d_o^2 K_A \tag{4.1.3}$$

where P'_A = force acting on the side of the arch due to the weight of the soil and corresponding to a fully developed "active" state of stress within the soil mass.

K_A = hydrostatic pressure ratio for the "active" state of stress in the soil,

and:

$$P''_A = - \bar{p}_{sj} d_o K_A \tag{4.1.4}$$

where P''_A = force acting on the side of the arch due to blast overpressure and corresponding to a fully developed "active" state of stress within the soil mass.

The results of the preceding discussion are presented graphically in Figure 4.2. The "no deformation" load components, Equations (4.1.1) and (4.1.2), are plotted along the vertical axis, i.e. corresponding to no rotation of the pressure surface. The "fully active" load components, Equations (4.1.3) and (4.1.4), are plotted at a deformation $\xi_{\ell y}$ corresponding to that amount of rotation of the pressure surface required to reach the "Active State of Plastic Equilibrium" within the soil mass. A discussion of the amount of deformation required is contained in Sections 2.2 and 4.4.

Because of the forces developed within the soil during deformation, $P'_A + P''_A$ is less than $P'_{OA} + P''_{OA}$. This difference is defined herein as the "soil resistance" corresponding to an inward movement of a haunch sufficient

to develop fully an "active" state of stress in the adjacent soil. An expression for the soil resistance corresponding to this "fully active" condition can now be derived by taking the difference of each of the load components considered, i.e.:

Let: R'_A and R''_A = maximum values of soil resistance corresponding to a fully developed "active" state of stress in the soil.

Then, using Equations (4.1.1) and (4.1.3):

$$R'_A = P'_{OA} - P'_A$$

$$= \frac{1}{2}\gamma_s d_o^2 K_{OA} - \frac{1}{2}\gamma_s d_o^2 K_A$$

$$R'_A = \frac{1}{2}\gamma_s d_o^2 (K_{OA} - K_A) \tag{4.1.5}$$

and, using Equations (4.1.2) and (4.1.4):

$$R''_A = P''_{OA} - P''_A$$

$$= -\bar{p}_{sj} d_o K_{OA} + \bar{p}_{sj} d_o K_A$$

$$R''_A = -\bar{p}_{sj} d_o (K_{OA} - K_A) \tag{4.1.6}$$

The nature of the variation of the soil resistance between the "at rest" and the "fully active" states can only be inferred from field observations of test structures, laboratory model studies and a general consideration of the nature of stresses in masses of soil. No exact relationship is known to the writer. One possible relationship is shown qualitatively in Figure 4.3. This corresponds, in general, to Figure 2.2. For the purposes of this study the relationships between deformation and soil resistance will be approximated using linear functions. This is discussed in detail in Section 4.4.

While Figures 4.2 and 4.3 are helpful in visualizing the development of the soil resistance concept used in this study, they are somewhat misleading in that the two components of soil resistance as expressed by Equations (4.1.5) and (4.1.6) cannot be added directly to one another for insertion in the equations of motion for the model because they act at different points. In

order to combine these quantities into what will be termed herein the "effective" soil resistance at the haunch, the lower bar is considered as a beam simply supported at the haunch and at the abutment and "loaded" with the two soil resistances R'_A and R''_A. The "reaction" at the haunch is then taken as the soil resistance which is "effective" at the haunch. This concept is illustrated in Figure 4.4. While this neglects moments at the haunch, it is sufficiently accurate for this study.

Also shown in Figure 4.4 is the soil wedge corresponding to the development of the "active" state of stress in the soil. This wedge is bounded by the ground surface, the pressure surface and a plane passing upward through the arch abutment at an angle of $(\frac{\pi}{4} + \frac{\varphi}{2})$ with respect to the horizontal, where φ is the angle of internal friction of the soil. This concept follows directly from the use of classical earth pressure theory to define the "active" state of stress in the soil plus the assumption of a plane failure surface for the determination of K_A. As with the arch itself, this wedge is considered herein to have a unit thickness in the direction of the longitudinal arch axis. The overpressure term, $\bar{p}_{sj}$, in Equations (4.1.2), (4.1.4) and (4.1.6) is taken as the average overpressure acting at the ground surface on this failure wedge.

Keeping in mind that R'_A and R''_A as given by Equations (4.1.5) and (4.1.6) are maximum values, the maximum effective soil resistance for an interior haunch may be obtained directly from Figure 4.4 as:

$$\hat{Q}_{sj} = \frac{1}{a} \cos(\omega + \delta)\ [R'_A(d_o/3) + R''_A(d_o/2)]$$

$$\hat{Q}_{sj} = \frac{d_o}{6a} (2R'_A + 3R''_A) \cos\ (\omega + \delta) \qquad (4.1.7)$$

and:

$$\hat{Q}_{sj+3} = - \frac{1}{b} \sin(\omega + \delta) \left[R'_A \left(\frac{bd_o}{3a}\right) + R''_A \left(\frac{bd_o}{2a}\right) \right]$$

$$\hat{Q}_{sj+3} = - \frac{d_o}{6a} (2R'_A + 3R''_A) \sin(\omega + \delta) \qquad (4.1.8)$$

where $\hat{Q}_{sj}$ = maximum value of the horizontal component of the soil resistance which may be considered effective at an interior haunch

$\hat{Q}_{sj+3}$ = maximum value of the vertical component of the soil resistance which may be considered effective at an interior haunch

a,b,c,d = generalized arch dimensions (cf. Figure 2.1)

ω = inclination of the lower bar of the model with respect to the vertical

δ = friction angle corresponding to the friction developed between the surface of the arch and the soil.

d_o = depth from the ground surface to the arch abutment

R'_A, R''_A = maximum values of soil resistance components as defined by Equations (4.1.5) and (4.1.6)

Substituting Equations (4.1.5) and (4.1.6) into Equations (4.1.7) and (4.1.8):

$$\hat{Q}_{sj} = \frac{d_o^2}{6a}(K_{OA} - K_A)(\gamma_s d_o - 3\bar{p}_{sj})\cos(\omega + \delta) \tag{4.1.9}$$

$$\hat{Q}_{sj+3} = -\frac{d_o^2}{6a}(K_{OA} - K_A)(\gamma_s d_o - 3\bar{p}_{sj})\sin(\omega + \delta) \tag{4.1.10}$$

These equations will be used in Section 4.4 in developing expressions for the total soil resistance of the system.

One further point to be considered here involves the hydrostatic pressure ratios for this case. Methods for determining K_A are compared in Appendix A. Values for K_{OA} cannot be calculated using classical earth pressure theory, although values have been measured in tests.(10) In the numerical solutions of this study an observed value of the ratio of horizontal to vertical soil pressures corresponding to the "at rest" condition is assumed. It is then necessary to "resolve" this ratio from that corresponding to horizontal pressures to that corresponding to pressures parallel to the line of action of P'_A. A diagram of the relationships involved is given in Figure 4.5.

Referring to this figure, one may write:

$$\frac{\frac{1}{2}\gamma_s d_o^2 K_A}{\frac{1}{2}\gamma_s d_o^2 \sqrt{1 + k_o^2}} = \cos \left[(\omega + \delta) - \arctan \frac{1}{k_o} \right]$$

From which:

$$K_{OA} = \sqrt{1 + k_o^2} \cos \left[(\omega + \delta) - \arctan \frac{1}{k_o} \right] \qquad (4.1.11)$$

where k_o = observed value of the ratio between the horizontal and vertical soil pressures for the condition of earth pressure at rest.

4.2 Exterior Haunch

The soil resistance developed at an exterior haunch may be derived in a manner analogous to that used in the previous section for the interior haunch. The essential difference is that movement of the arch outward against the soil tends to produce a "Passive State of Plastic Equilibrium" (cf. Section 2.2) within the soil. As in the previous case, the "soil resistance" will be taken as the differences in the loads transmitted to the arch by the soil in the "locked" and "unlocked" conditions. The forces acting on the arch for this case are shown in Figure 4.6.

If the arch is now considered to be "locked" so that no deformation can take place, hence no frictional forces develop in the soil, and the blast loading applied, one can write:

$$P'_{OP} = \frac{1}{2}\gamma_s d_o^2 K_{OP} \qquad (4.2.1)$$

where P'_{OP} = component in the direction of P'_P of the force acting on the side of the arch due to the weight of the soil and corresponding to the condition of earth pressure at rest,

K_{OP} = ratio of the soil pressure in the direction of P'_P to the vertical soil pressure for the condition of earth pressure at rest,

and:

$$P''_{OP} = - \bar{p}'_{sj} d_o K_{OP} \qquad (4.2.2)$$

where P''_{OP} = component in the direction of P'_P of the force acting on the side of the arch due to the blast overpressure and corresponding to the condition of earth pressure at rest,

$\bar{p}'_{sj}$ = average overpressure acting at the ground surface on the potential "passive" soil failure wedge (defined below). Note that since $\bar{p}'_{sj}$ acts downward, it is considered negative in accordance with the sign convention used herein (cf. Section 1.2).

If the structure is now "unlocked" and permitted to deform until the "Passive State of Plastic Equilibrium" is reached, frictional forces will develop within the soil mass and the forces acting directly on the side of the arch will be:

$$P'_P = \frac{1}{2} \gamma_s d_o^2 K_P \qquad (4.2.3)$$

where P'_P = force acting on the side of the arch due to the weight of the soil and corresponding to a fully developed "passive" state of stress within the soil,

K_P = hydrostatic pressure ratio for the "passive" state of stress in in the soil,

and:

$$P''_P = - \bar{p}'_{sj} d_o K_P \qquad (4.2.4)$$

where P''_P = force acting on the side of the arch due to the blast overpressure and corresponding to a fully developed "passive" state of stress within the soil.

These load components are plotted in Figure 4.7. The "locked" condition is represented by $\xi_\ell = 0$, i.e. no rotation of the pressure surface. The "unlocked" condition is represented by $\xi'_{\ell y}$, i.e. sufficient rotation of the pressure surface to develop fully the "Passive State of Plastic Equilibrium" within the soil (cf. Section 2.2).

As in the case of the interior haunch, the differences between the "locked" and "unlocked" conditions are taken as the "soil resistance." Referring to Figure 4.7, these differences may be expressed by subtracting Equations (4.2.1) and (4.2.2) from Equations (4.2.3) and (4.2.4).

Thus, if: R_P' and R_P'' = maximum values of soil resistance corresponding to a fully developed "passive" state of stress in the soil,

Then:
$$R_P' = P_P' - P_{OP}'$$
$$= \frac{1}{2}\gamma_s d_o^2 K_P - \frac{1}{2}\gamma_s d_o^2 K_{OP}$$
$$R_P' = \frac{1}{2}\gamma_s d_o^2 (K_P - K_{OP}) \qquad (4.2.5)$$

And:
$$R_P'' = P_P'' - P_{OP}''$$
$$= -\bar{p}_{sj}' d_o K_P + \bar{p}_{sj}' d_o K_{OP}$$
$$R_P'' = -\bar{p}_{sj}' d_o (K_P - K_{OP}) \qquad (4.2.6)$$

Since the load components P' and P" are assumed to act at different points on the pressure surface (cf. Figure 4.6), the corresponding soil resistances R_P' and R_P'' must be combined in a similar manner to that used in the case of the interior haunch. Again considering the lower bar of the model as a simply supported beam acted upon by the soil resistances R_P' and R_P'', the effective soil resistance components at the haunch are (cf. Figure 4.8):

$$\hat{Q}_{sj}' = \frac{1}{a}\cos(\delta - \omega)\left[R_P' \left(\frac{d_o}{3}\right) + R_P'' \left(\frac{d_o}{2}\right)\right]$$
$$= \frac{d_o}{6a}(2R_P' + 3R_P'')\cos(\delta - \omega) \qquad (4.2.7)$$

And:
$$\hat{Q}_{sj+3}' = -\frac{1}{b}\sin(\delta - \omega)\left[R_P' \left(\frac{bd_o}{3a}\right) + R_P'' \left(\frac{bd_o}{2a}\right)\right]$$
$$= -\frac{d_o}{6a}(2R_P' + 3R_P'')\sin(\delta - \omega) \qquad (4.2.8)$$

where $\hat{Q}_{sj}'$ = maximum value of the horizontal component of the soil resistance which may be considered effective at an exterior haunch,

$\hat{Q}_{sj+3}'$ = maximum value of the vertical component of the soil resistance which may be considered effective at an exterior haunch,

a,b,c,d = generalized arch dimensions (cf. Figure 2.1),

ω = inclination of the lower bar of the model with respect to the vertical,

δ = friction angle corresponding to the friction developed between the surface of the arch and the soil.

Substituting Equations (4.2.5) and (4.2.6) into Equations (4.2.7) and (4.2.8):

$$\hat{Q}'_{sj} = \frac{d_o^2}{6a}(K_P - K_{OP})(\gamma_s d_o - 3\bar{p}'_{sj})\cos(\delta - \omega) \qquad (4.2.9)$$

$$\hat{Q}'_{sj+3} = -\frac{d_o^2}{6a}(K_P - K_{OP})(\gamma_s d_o - 3\bar{p}'_{sj})\sin(\delta - \omega) \qquad (4.2.10)$$

Note that the soil failure wedge now considered (cf. Figure 4.8) is bounded by the ground surface, the pressure surface and a plane through the arch abutment inclined at an angle of $(\frac{\pi}{4} - \frac{\varphi}{2})$ with respect to the horizontal, where φ is the angle of internal friction of the soil. A unit thickness of wedge parallel to the horizontal arch axis is considered in this thesis. The assumptions leading to this wedge are the same as those leading to the definition of the "active" soil failure wedge described in Section 4.1, i.e. the use of classical earth pressure theory (Coulomb's assumptions) and the assumption of a plane failure surface in the determination of the hydrostatic pressure ratio corresponding to full development of the "passive" state of stress within the soil (cf. Appendix A).

Equations (4.2.9) and (4.2.10) are used in Section 4.4 in deriving expressions for the total soil resistance of the system. In order to use these equations, one must be able to calculate the hydrostatic pressure ratios for the soil pressures corresponding to the "at rest" and "passive" states of stress. Methods of finding K_P are compared in Appendix A. K_{OP} is found by "resolving" observed hydrostatic pressure ratios relating horizontal to vertical soil pressures to a ratio relating soil pressures acting parallel to the line of action of P'_P to vertical soil pressures. The technique used is

analogous to that described in Section 4.1 for finding K_{OA}. A diagram of the relationships involved is given in Figure 4.9. Referring to this figure, one may write:

$$\frac{\frac{1}{2}\gamma_s d_o^2 K_{OP}}{\frac{1}{2}\gamma_s d_o^2 \sqrt{1 + k_o^2}} = \cos\left[\arctan\frac{1}{k_o} + (\delta - \omega)\right]$$

From which: $$K_{OP} = \sqrt{1 + k_o^2}\ \cos\left[\arctan\frac{1}{k_o} + (\delta - \omega)\right] \qquad (4.2.11)$$

where k_o = observed value of the ratio between the horizontal and vertical soil pressures for the condition of earth pressure at rest.

4.3 Crown

As the soil-arch "structure" deforms in response to a blast loading, shear and frictional forces are developed in the soil near the crown. The definition of these forces is not an easy matter. In evaluating the relative importance of these forces, consider that for the shallow depths of cover included in this study (cf. Section 1.1) the volume of soil at and adjacent to the crown is relatively much smaller than the volume of the soil wedges defined in the preceding sections, affected by lateral displacements of the sides of the arch. Thus, the maximum resultant value of these soil forces will necessarily be relatively smaller at the crown than at the sides of the arch because of the smaller volume of soil involved. Further, some of these resisting forces serve only to distribute the applied load away from the crown to other regions of the arch, thus contributing no net resistance to the system. A portion of these forces can, however, be assumed logically to act to transmit some of the applied load away from the arch. This latter portion of the soil forces does assist the arch in resisting an applied load but is not readily defined explicitly.

An attempt to include at least part of this "effective" portion of the soil resistance near the crown in the total soil resistance of the system is made by continuing upward the pressure surfaces at the sides of the arch, in the same direction as the lower bars of the model, until they intersect the ground surface. This is not a rigorous approach, but it is believed to be sufficiently accurate for the present. Since the forces involved are relatively small, it would seem to follow that their influence on the response of the system as a whole should be relatively small as well.

The effect of the inertial resistance of the soil near the crown is discussed in Chapter V.

As a result of the foregoing discussion, the effective soil resistance to be placed on the model at the crown is zero. Thus, the following expressions may be written:

$$Q_{s2} = 0 \tag{4.3.1}$$

where Q_{s2} = horizontal component of the effective soil resistance at the crown,

and:

$$Q_{s5} = 0 \tag{4.3.2}$$

where Q_{s5} = vertical component of the effective soil resistance at the crown.

4.4 Development of Equivalent Soil Resistance

Since the model is a two-degree-of-freedom system (cf. Section 3.1), the effective soil resistances derived in the preceding sections must be combined such that their net, or "equivalent," effect on the model is defined in the direction of the independent displacement coordinates. This is done in this section for the set of independent coordinates already selected, viz. the horizontal displacements of the haunches. Thus, the object here is to

define the resultant resistance offered by the soil to horizontal movements of the haunches. Note that this is not the same as the soil resistance components derived in Sections 4.1 and 4.2 since now the entire system is considered simultaneously.

The technique used herein is simply to apply the effective soil resistance components to the model as a system of loads. Then, by applying the "Load Relationships" derived in Section 3.2.1 (Equations (3.2.5)), the equivalent soil resistances in the horizontal direction at the haunches are determined. This may be expressed algebraically by substituting the effective soil resistance components, Q_{sj}, for the load components, H_j, in Equations (3.2.5). Thus:

$$\begin{aligned} \overline{Q}_{s1} &= Q_{s1} + \frac{1}{2}\left(1 - \frac{bc}{ad}\right) Q_{s2} - \left(\frac{b}{a}\right) Q_{s4} + \frac{1}{2}\left(\frac{d}{c} - \frac{b}{a}\right) Q_{s5} \\ \overline{Q}_{s3} &= \frac{1}{2}\left(1 - \frac{bc}{ad}\right) Q_{s2} + Q_{s3} - \frac{1}{2}\left(\frac{d}{c} - \frac{b}{a}\right) Q_{s5} + \left(\frac{b}{a}\right) Q_{s6} \end{aligned} \tag{4.4.1}$$

where $\overline{Q}_{s1}$ = equivalent soil resistance at the windward haunch,

$\overline{Q}_{s3}$ = equivalent soil resistance at the leeward haunch.

Since the expressions for the components of the effective soil resistance at the joints were derived in the preceding sections in terms of the limiting or maximum values, it is convenient here to write maximum values for the equivalent soil resistance. Further, since the haunches may be displaced either inward or outward, it will be convenient to have two sets of equations, one for interior haunches and one for exterior haunches. These equations may then be used in various combinations for dynamic analysis as the configuration of the system dictates.

For the case of both haunches displaced inward, the maximum equivalent soil resistance may be found by substituting Equations (4.1.9), (4.1.10), (4.3.1) and (4.3.2) into Equations (4.4.1). This gives:

$$\hat{\overline{Q}}_{s1} = \frac{d_o^2}{6a}(K_{OA} - K_A)(\gamma_s d_o - 3\overline{p}_{s1})\left[\cos(\omega + \delta) + (\frac{b}{a})\sin(\omega + \delta)\right]$$

$$\hat{\overline{Q}}_{s3} = \frac{d_o^2}{6a}(K_{OA} - K_A)(\gamma_s d_o - 3\overline{p}_{s3})\left[\cos(\omega + \delta) + (\frac{b}{a})\sin(\omega + \delta)\right]$$

Note that the preceding expressions differ only in the overpressure term. Thus, one may write, in general:

$$\hat{\overline{Q}}_{sj} = \frac{d_o^2}{6a}(K_{OA} - K_A)(\gamma_s d_o - 3\overline{p}_{sj})\left[\cos(\omega + \delta) + (\frac{b}{a})\sin(\omega + \delta)\right] \tag{4.4.2}$$

where $\hat{\overline{Q}}_{sj}$ = maximum value of the horizontal component of the equivalent soil resistance at haunch j when the haunch is displaced inward,

$\overline{p}_{sj}$ = average overpressure acting at the ground surface on the "active" soil failure wedge adjacent to joint j (cf. Figure 4.4).

Similar expressions may be written in the case where both haunches are displaced outward. Substituting Equations (4.2.9), (4.2.10), (4.3.1) and (4.3.[illegible]) into Equations (4.4.1):

$$\hat{\overline{Q}}'_{s1} = \frac{d_o^2}{6a}(K_P - K_{OP})(\gamma_s d_o - 3\overline{p}'_{s1})\left[\cos(\omega - \delta) + (\frac{b}{a})\sin(\omega - \delta)\right]$$

$$\hat{\overline{Q}}'_{s3} = \frac{d_o^2}{6a}(K_P - K_{OP})(\gamma_s d_o - 3\overline{p}'_{s3})\left[\cos(\omega - \delta) + (\frac{b}{a})\sin(\omega - \delta)\right]$$

Note that these expressions also differ only in the overpressure term. Thus, in general:

$$\hat{\overline{Q}}'_{sj} = \frac{d_o^2}{6a}(K_P - K_{OP})(\gamma_s d_o - 3\overline{p}'_{sj})\left[\cos(\omega - \delta) + (\frac{b}{a})\sin(\omega - \delta)\right] \tag{4.4.3}$$

where $\hat{\overline{Q}}'_{sj}$ = maximum value of the horizontal component of the equivalent soil resistance at haunch j when the haunch is displaced outward,

$\overline{p}'_{sj}$ = average overpressure acting at the ground surface on the "passive" soil failure wedge adjacent to joint j (cf. Figure 4.8).

Note that both Equation (4.4.2) and Equation (4.4.3) express the equivalent soil resistance at a haunch solely in terms of the components of the effective soil resistance acting at that haunch. This permits the haunches to be considered separately and reduces the number of cases which must be considered in the remainder of this discussion to two, viz. the interior haunch and the exterior haunch. The resulting expressions can then be applied to any conceivable configuration of the system.

An important aspect of the soil resistance developed as the system responds to a dynamic load involves the amounts of deformation required to develop fully the "active" and "passive" states of plastic equilibrium. In Section 2.2 reference was made to a number of estimates(10,11,12,13) of these parameters. There is general agreement that in the case of retaining walls backfilled with cohesionless soil, a rotation of the wall about its base corresponding to a movement away from the backfill at the top on the order of 0.1% of the wall height is sufficient to reduce the state of stress in the soil behind the wall from the "at rest" to the "fully active" state. In the case of the development of the "passive" state of stress, quantitative estimates are generally lacking, although it appears certain that the required movements are greater than for the "active" case (cf. Figure 2.2). A technique for estimating this required movement is outlined below. Note that the pressure surfaces assumed in deriving the effective soil resistances (cf. Section 4.1 and 4.2) are similar to the pressure surfaces behind retaining walls. Therefore, the significant deformations of the model for the development of soil resistance are the rotations of the lower bars, since these define the positions of the pressure surfaces.

In this study the idealized soil resistance-displacement function is obtained by assuming a linear buildup of soil resistance with increasing displacement until a maximum value is reached. The soil resistance is then

assumed to remain at this maximum value for further displacements in the same direction. This results in a so-called "elasto-plastic" resistance diagram as illustrated in Figure 4.10.

Thus, the soil resistance-displacement function for an interior haunch may be defined by using Equation (4.4.2) to find the maximum value of the soil resistance, and the assumption that this value of soil resistance corresponds to an inward rotation of the lower bar, ξ_l, of 0.001. This is illustrated in Figure 4.11. The range of possible values for the soil resistance corresponding to each value of displacement results from the overpressure term, $\bar{p}_{sj}$, in Equation (4.4.2).

The maximum value of soil resistance for an exterior haunch is given by Equation (4.4.3). Since quantitative estimates of the corresponding deformations are lacking, the assumption is made that the slope of the idealized soil resistance-displacement function in the elastic range is constant for any given value of overpressure acting on the soil failure wedges. For the specific examples studied herein, this deformation corresponds to a rotation of the pressure surface on the order of 0.005, which appears to be in reasonable agreement with existing theory and experimental evidence.(10,13) Note, however, that this value has not yet been determined definitely. An experimental investigation of the deformation corresponding to full development of the "passive" state of stress in the soil is certainly needed (cf. Chapter IX). A complete, idealized soil resistance-displacement diagram is shown in Figure 4.12.

Expressions for the "yield" deformations of the soil may be derived as follows:

Let: ξ_l = rotation of the lower bar of the model as the structure responds to a blast loading,

$\xi_{\ell y}$ = rotation of the lower bar of the model corresponding to full development of the "active" state of stress within the soil adjacent to the haunch,

$\xi'_{\ell y}$ = rotation of the lower bar of the model corresponding to full development of the "passive" state of stress within the soil adjacent to the haunch.

Then, from Figure 4.12:

$$\xi'_{\ell y} = \xi_{\ell y} \left(\frac{\hat{\bar{Q}}'_{sj}}{\hat{\bar{Q}}_{sj}}\right) \tag{4.4.4}$$

Substituting Equations (4.4.2) and (4.4.3) into Equation (4.4.4):

$$\xi'_{\ell y} = \xi_{\ell y} \left\{ \frac{\frac{d_o^2}{6a}(K_P - K_{OP})(\gamma_s d_o - 3\bar{p}'_{sj}) \left[\cos(\omega - \delta) + (\frac{b}{a})\sin(\omega - \delta)\right]}{\frac{d_o^2}{6a}(K_{OA} - K_A)(\gamma_s d_o - 3\bar{p}_{sj}) \left[\cos(\omega + \delta) + (\frac{b}{a})\sin(\omega + \delta)\right]} \right\} \tag{4.4.5}$$

Now, the difference between $\bar{p}_{sj}$ and $\bar{p}'_{sj}$ is very small except for the brief interval during which the shock front traverses the structure and the adjacent soil wedges. This is due to the relatively small dimensions of the structure as compared with the spatial dimensions and slow decay with time of the nuclear blast wave. Further, the large differences which do exist between $\bar{p}_{sj}$ and $\bar{p}'_{sj}$ during the shock front transit, when pressure buildup occurs, are not significant here because during this interval the structure does not have time to respond sufficiently to develop significant soil resistances. Thus, Equation (4.4.5) may be reduced to:

$$\xi'_{\ell y} = \xi_{\ell y} \left[\frac{K_P - K_{OP}}{K_{OA} - K_A}\right] \left[\frac{\cos(\omega - \delta) + (b/a)\sin(\omega - \delta)}{\cos(\omega + \delta) + (b/a)\sin(\omega + \delta)}\right] \tag{4.4.6}$$

Now, note that:

$$\left[\frac{\cos(\omega - \delta) + (b/a)\ \sin(\omega - \delta)}{\cos(\omega + \delta) + (b/a)\ \sin(\omega + \delta)}\right] = \frac{\cos\ (\omega - \delta) + \tan\ \omega\ \sin(\omega - \delta)}{\cos\ (\omega + \delta) + \tan\ \omega\ \sin(\omega + \delta)} = 1 \tag{4.4.7}$$

Therefore:

$$\xi'_{\ell y} = \xi_{\ell y} \left(\frac{K_P - K_{OP}}{K_{OA} - K_A}\right) \tag{4.4.8}$$

Alternatively, the idealized soil resistance-displacement function, Figure 4.12, may be defined using either the maximum soil resistances or the "yield" displacements for the soil masses as derived above, and the slope of the "elastic" line, or "soil stiffness." For an interior haunch the "soil stiffness" may be expressed as:

$$\bar{K}_{sj} = \frac{\hat{Q}_{sj}}{\xi_{\ell y}} \tag{4.4.9}$$

where $\bar{K}_{sj}$ = "stiffness" of the soil during the development of the "active" state of stress.

Substituting Equation (4.4.2) into Equation (4.4.9):

$$\bar{K}_{sj} = \frac{d_o^2}{6a\ \xi_{\ell y}} (K_{OA} - K_A)(\gamma_s d_o - 3\bar{p}_{sj}) \left[\cos(\omega + \delta) + (\frac{b}{a})\sin(\omega + \delta)\right]$$

or:

$$\bar{K}_{sj} = k' - k''\bar{p}_{sj} \tag{4.4.10}$$

where $k' = \frac{\gamma_s d_o^3}{6a\ \xi_{\ell y}} (K_{OA} - K_A) \left[\cos(\omega + \delta) + (\frac{b}{a})\sin(\omega + \delta)\right]$

$k'' = (\frac{3}{\gamma_s d_o})\ k'$

While for an exterior haunch, the "soil resistance" may be expressed as:

$$\bar{K}'_{sj} = \frac{\hat{Q}'_{sj}}{\xi'_{\ell y}} \tag{4.4.11}$$

where $\bar{K}'_{sj}$ = "stiffness" of the soil during development of the "passive" state of stress.

Substituting Equations (4.4.3), (4.4.7) and (4.4.8) into Equation (4.4.10) gives:

$$\bar{K}'_{sj} = \frac{\frac{d_o^2}{6a}(K_P - K_{OP})(\gamma_s d_o - 3\bar{p}'_{sj})\,[\cos(\omega - \delta) + (\frac{b}{a})\sin(\omega - \delta)]}{\xi_{ly}\,(\frac{K_P - K_{OP}}{K_{OA} - K_A})\left[\frac{\cos(\omega - \delta) + (b/a)\sin(\omega - \delta)}{\cos(\omega + \delta) + (b/a)\sin(\omega + \delta)}\right]}$$

or:

$$\bar{K}'_{sj} = k' - k''\,\bar{p}'_{sj} \qquad (4.4.12)$$

Note that the development of the two expressions for "soil stiffness," $\bar{K}_{sj}$ and $\bar{K}'_{sj}$ (Equations (4.4.10) and (4.4.12)), is consistent with the assumption of a constant slope for the "elastic" line of the soil resistance-displacement function for a given value of average overpressure, i.e. for $\bar{p}_{sj} = \bar{p}'_{sj}$.

Equations (4.4.10) and (4.4.12) express the soil stiffness in terms of a " $\bar{Q}_{sj}$ vs ξ_l " diagram (cf. Figure 4.12). It is sometimes more convenient to deal directly in terms of the horizontal displacements of the haunches rather than with the rotations of the lower bars. Now, from Equations (3.2.9):

$$\delta\theta_1 = \delta\theta_4 = -\,\xi_l = -\,h_j/a. \qquad (4.4.13)$$

Therefore, the soil stiffnesses may be expressed as:

$$(\frac{1}{a})\,\bar{K}_{sj} = \frac{1}{a}\,(k' - k''\,\bar{p}_{sj}) \qquad (4.4.14)$$

and:

$$(\frac{1}{a})\,\bar{K}'_{sj} = \frac{1}{a}\,(k' - k''\,\bar{p}'_{sj}) \qquad (4.4.15)$$

At this point one should consider the resistance offered by the soil as the structure "rebounds," or reverses its direction of motion, during response to a blast load. Keeping in mind the fact that the overpressure tends to force the soil into intimate contact with the arch, the variation in soil resistance during rebound is assumed to be as shown in Figure 4.13.

It is now possible to examine more closely the classification of haunches according to their displacement into "interior" and "exterior" haunches as was done at the beginning of this chapter. Referring to Figure 4.13, the original position of the haunch is represented by the origin of the coordinate system. The effect of the "permanent set" is to transfer the origin of the coordinate system to allow for any "plastic" deformation which may take place in the soil during the response. This is, of course, an approximation of the behavior of the soil, but it is consistent with the behavioral assumptions made previously in this chapter. Note that a reversal in the direction of haunch movement does not cause an immediate reversal in the direction of the soil resistance. There is some evidence to indicate(10,13) that the reversal of the direction of the soil resistance will occur more rapidly with reversal of the direction of movement than Figure 4.13 indicates; however, further investigation of this behavior was not included in this study (cf. Chapter IX).

Consistent with the sign conventions used elsewhere in this thesis, soil resistances acting to the left are positive, and conversely.

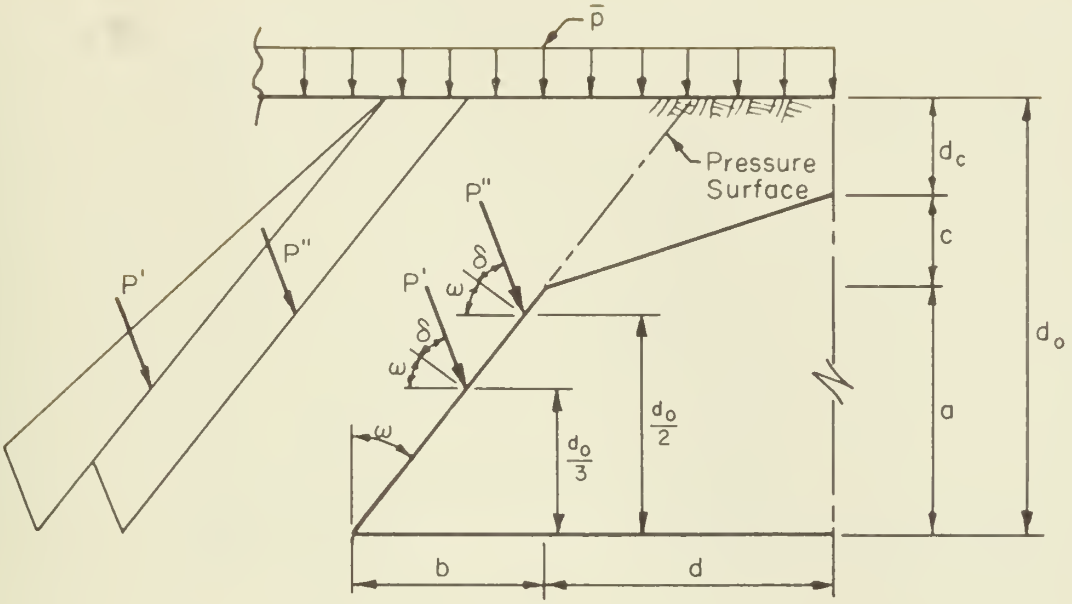

Figure 4.1. Forces Acting on Pressure Surface for "Interior" Haunch

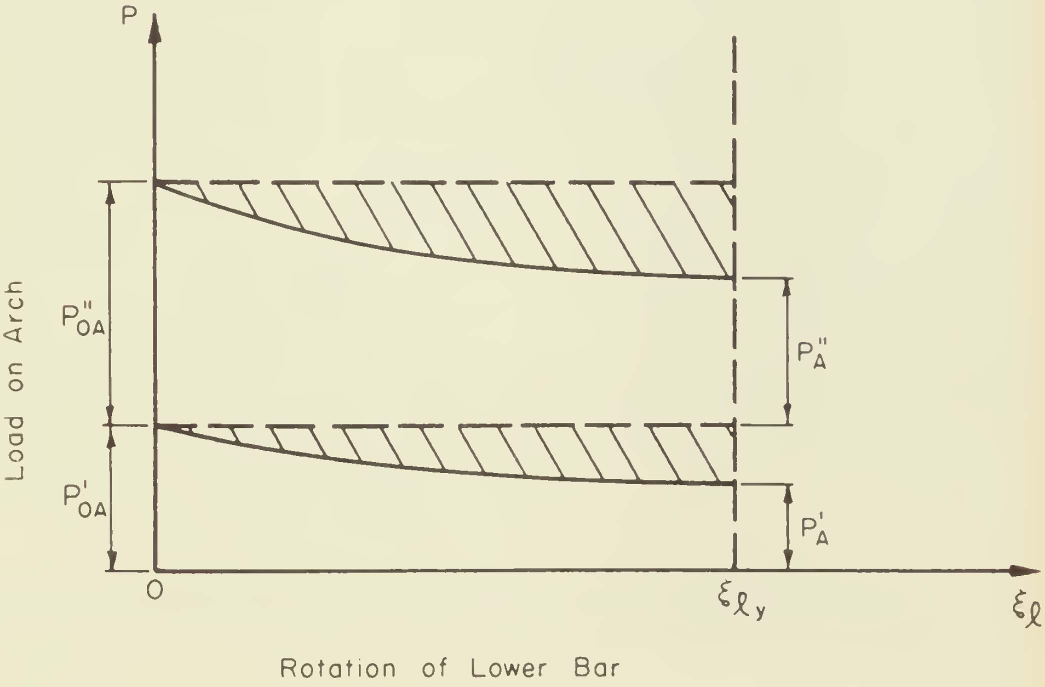

Figure 4.2. Load-Displacement Diagram for "Interior" Haunch

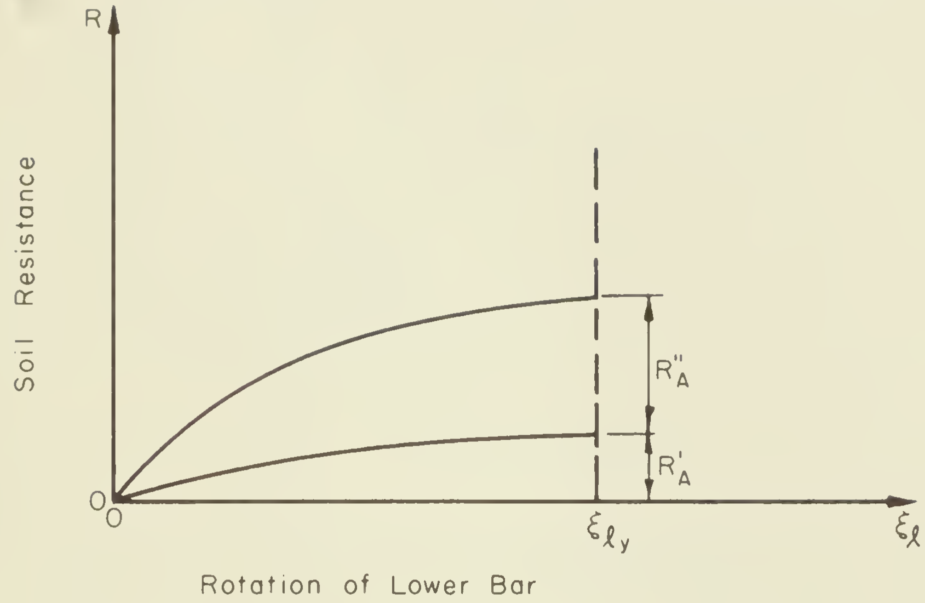

Figure 4.3. Soil Resistance-Displacement Diagram for "Interior" Haunch

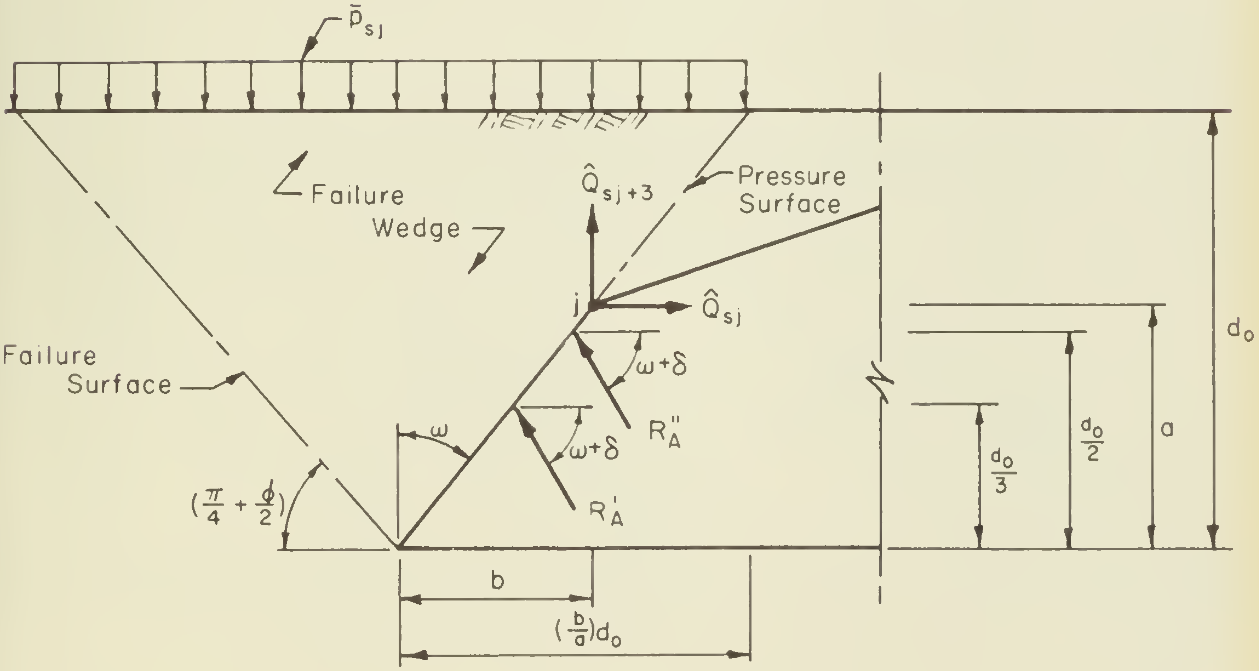

Figure 4.4. Effective Soil Resistance for "Interior" Haunch

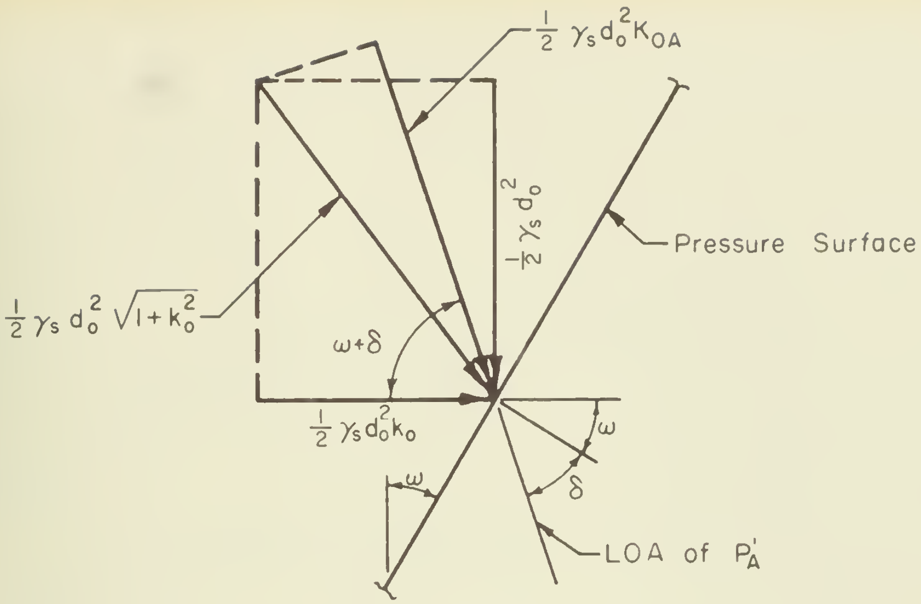
$\frac{1}{2}\gamma_s d_o^2 K_{OA}$
$\frac{1}{2}\gamma_s d_o^2$
Pressure Surface
$\frac{1}{2}\gamma_s d_o^2\sqrt{1+k_o^2}$
$\omega+\delta$
$\frac{1}{2}\gamma_s d_o^2 k_o$
ω
δ
ω
LOA of P_A'

Figure 4.5. Diagram Used in Determining K_{OA}

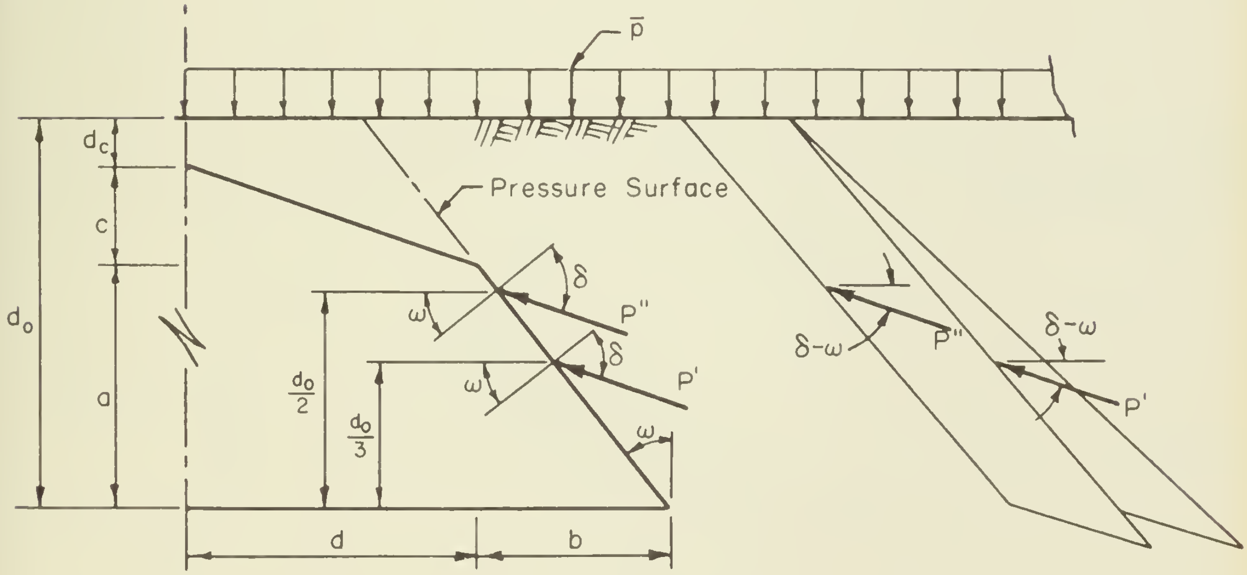

Figure 4.6. Forces Acting on Pressure Surface for "Exterior" Haunch

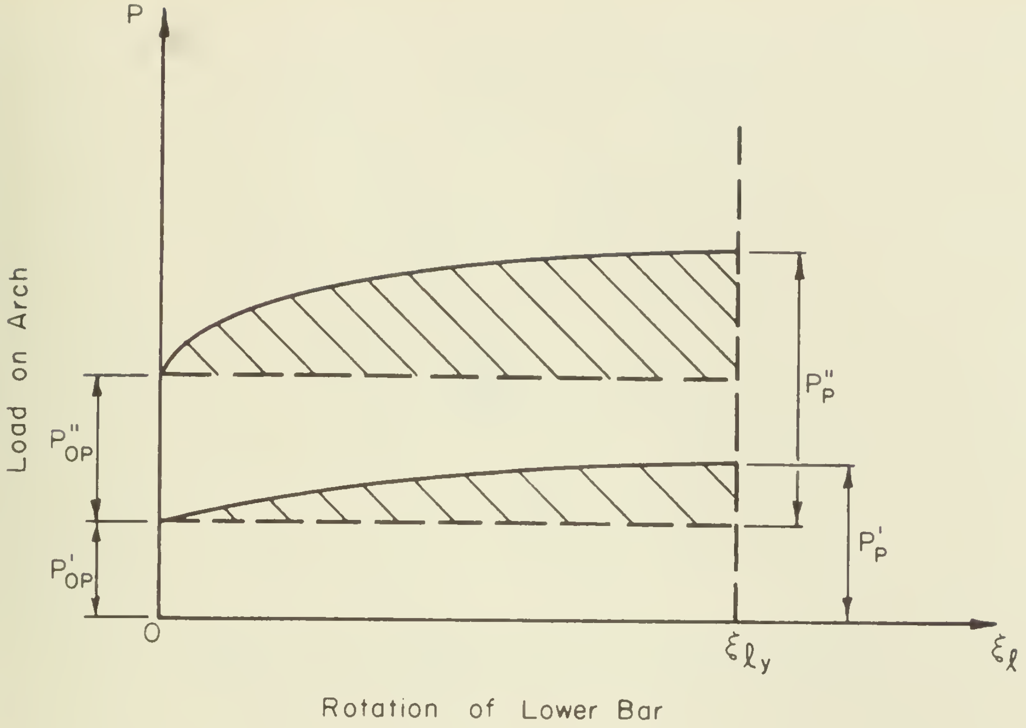

Figure 4.7. Load-Displacement Diagram for "Exterior" Haunch

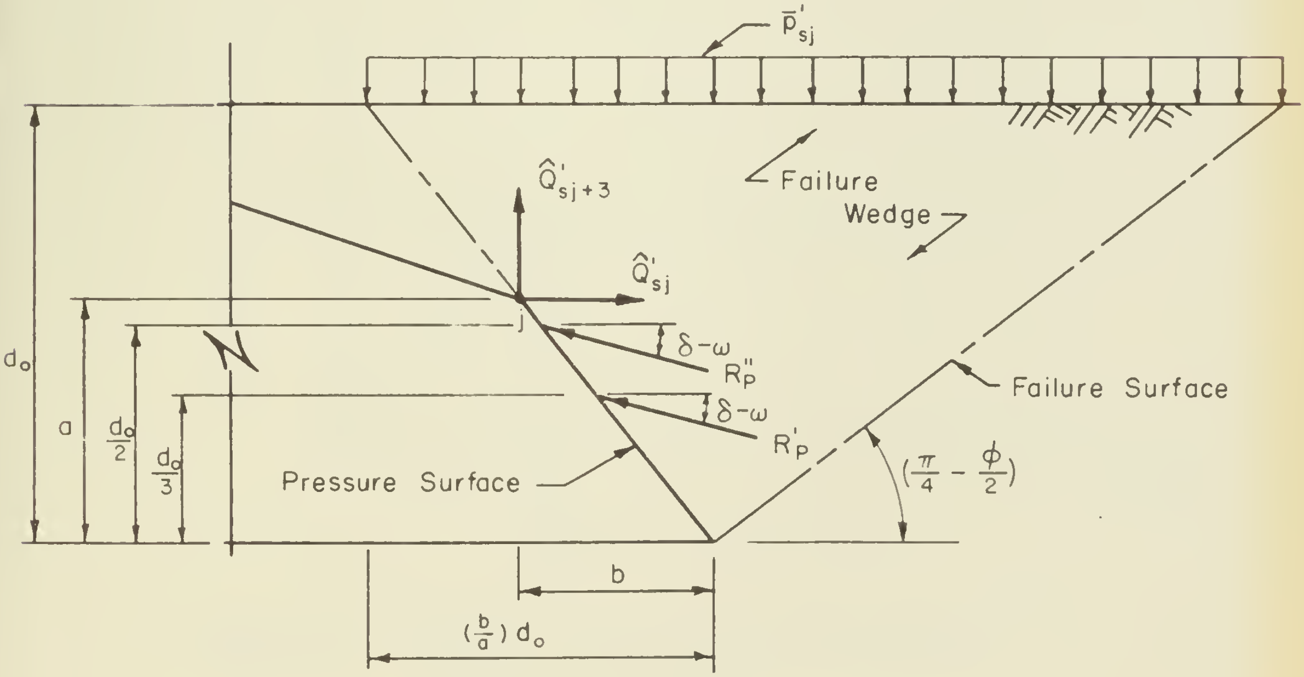

Figure 4.8. Effective Soil Resistance for "Exterior" Haunch

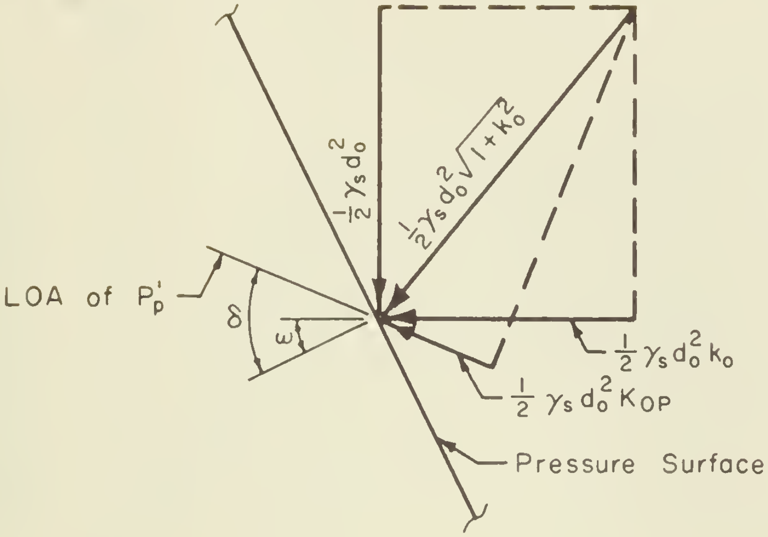

$\frac{1}{2}\gamma_s d_o^2$
$\frac{1}{2}\gamma_s d_o^2\sqrt{1+k_o^2}$
LOA of P_p'
δ
ω
$\frac{1}{2}\gamma_s d_o^2 k_o$
$\frac{1}{2}\gamma_s d_o^2 K_{OP}$
Pressure Surface

Figure 4.9. Diagram Used in Determining K_{OP}

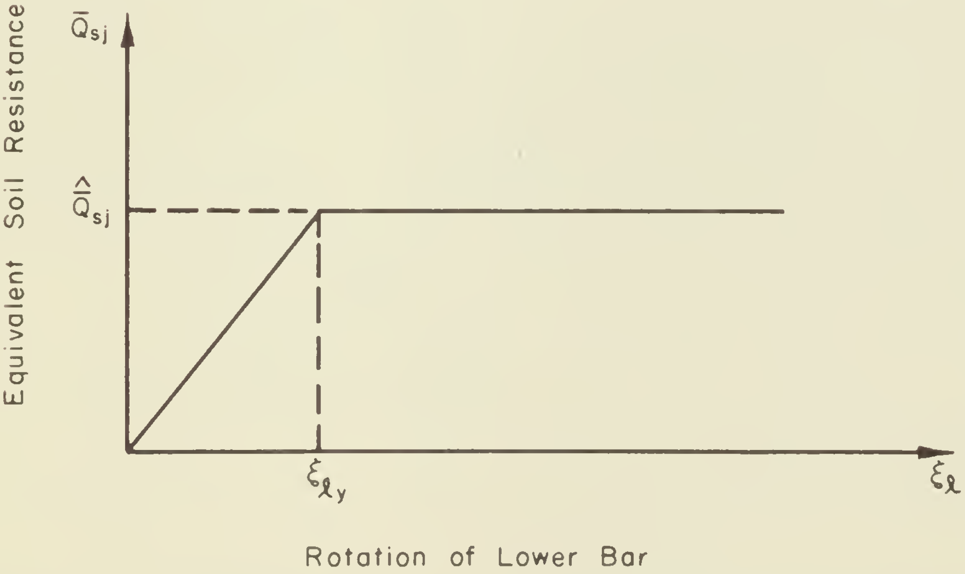

Figure 4.10. Partial, Idealized, Soil Resistance-Displacement Diagram

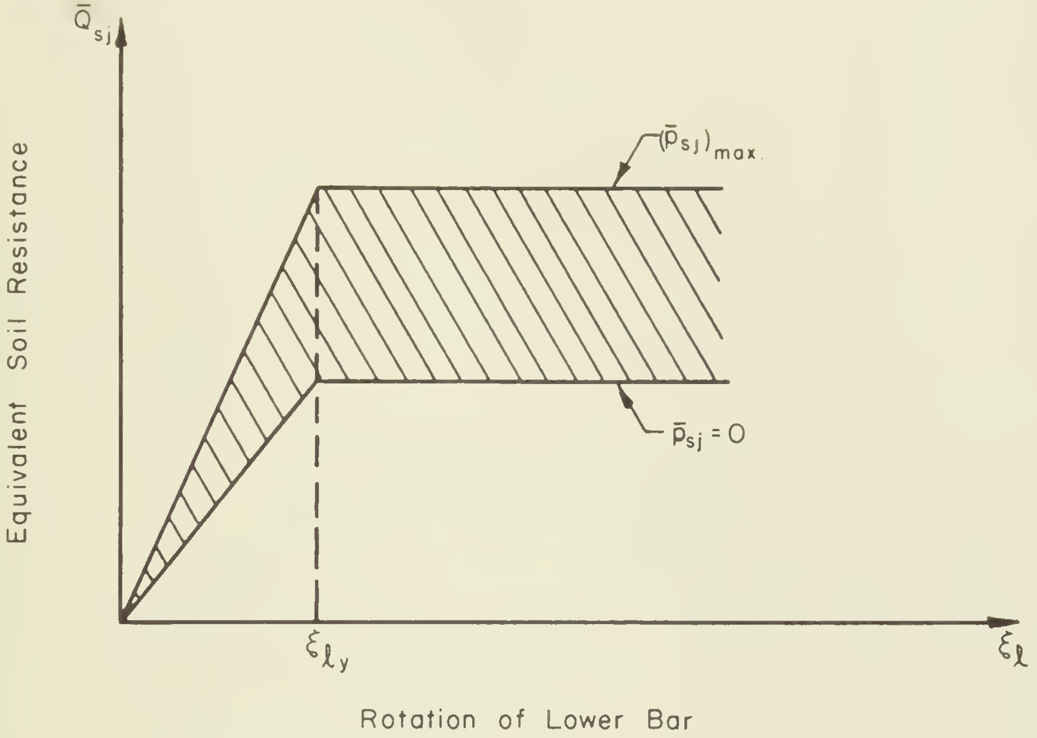

Figure 4.11. Partial, Idealized, Soil Resistance-Displacement Diagram Showing Effect of Overpressure

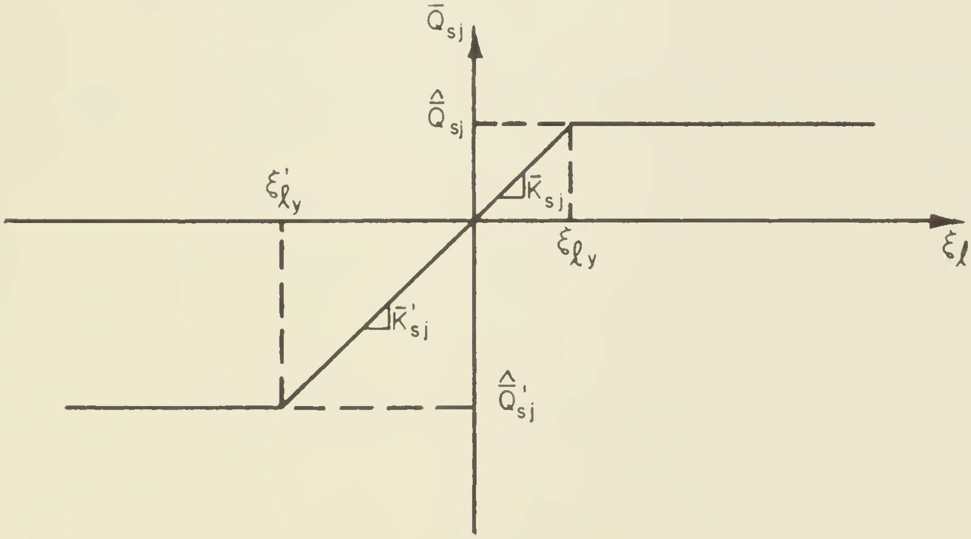

Figure 4.12. Complete, Idealized, Soil Resistance-Displacement Diagram

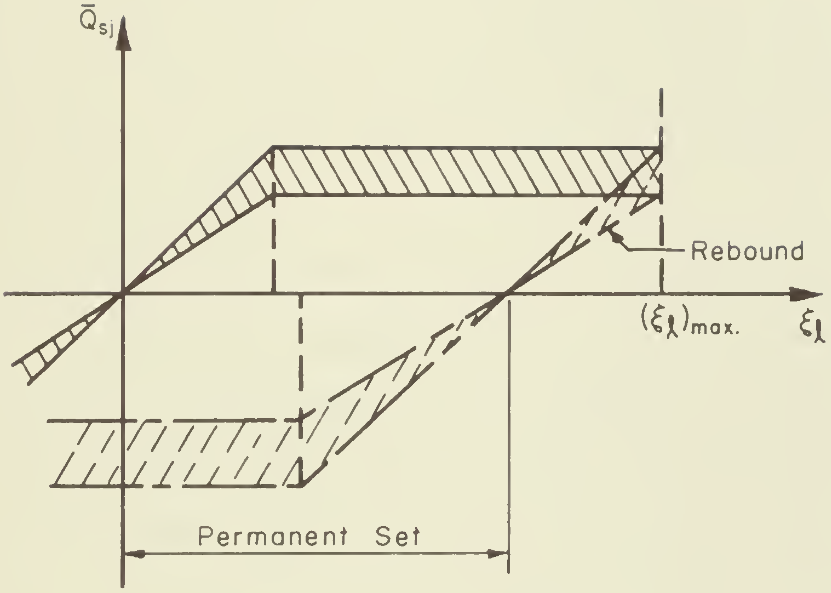

Figure 4.13. Assumed Variation in Soil Resistance During Rebound

CHAPTER V

MASS EFFECTS

The mass of a system subjected to dynamic loading directly affects the inertial resistance of the system and thus has an important effect on both the magnitude and the time history of the response of the system. It is the purpose of this chapter to list and discuss the assumptions made regarding the mass of the arch-soil "structure" and to derive the relationships necessary to incorporate inertial resistance into the equations of motion of the system (cf. Chapter VII).

In general, the approach used here is to consider the masses of arch and soil which may logically be assumed to move as the system responds. The inertial resistances of these masses are then calculated and applied to the model as a system of loads. The resultant effect of these inertial forces is taken as the equivalent inertial resistance of the model. As in the case of the equivalent deformation resistances determined earlier, the equivalent inertial resistance is determined in agreement with the choice of independent displacements for the model.

5.1 Mass Concentrations on the Model

Since the model has three interior joints, masses may be placed at each joint in such a manner as to approximate in the most realistic possible fashion the inertial resistance of the actual system in the region adjacent to that joint. The model itself imposes no inherent restrictions on the choice of the masses which may be placed at the joints. The mass of the arch may be handled quite readily by concentrating at each joint the mass of the arch rib for a one-half bar length to either side of the joint. Note that this results in the concentration of the mass of the lower half of each of the lower bars

at the arch abutments. Since the abutments are assumed immovable (cf. Section 1.2), this portion of the mass of the arch is thus assumed to have no significant effect upon the response of the system. As pointed out in Section 2.3, such assumptions are not uncommon in dynamic analyses and give reasonable results.

The mass of soil which may logically be assumed to move with the arch is more difficult to define. In general, the mass of soil moving with a joint depends upon:

1. The location of the joint, e.g. the mass of soil moving with the crown will be different from the mass of soil moving with one of the haunches.

2. The direction of movement of the joint, e.g. the mass of soil affected by the inward movement of a haunch is different from that affected by its outward movement.

3. The depth of burial of the arch, e.g. the mass of soil moving with the crown will tend to increase as the depth of cover increases.

Further discussion of the latter two considerations is warranted here. With regard to the direction of movement of the joint, note that this approach is somewhat different from that used in Chapter IV in developing the soil resistance due to deformation. The effect of both approaches is the same during initial response. However, once rebound occurs, the "deformation" resistance of the soil is assumed to decrease linearly to zero before building up in the opposite direction (cf. Section 4.4). On the other hand, by considering only the direction of movement when choosing the effective soil mass, the start of rebound causes an immediate change in the magnitude of the mass of soil considered to move with the system. This apparent contradiction is not as serious as it might first appear, since the start of rebound corresponds

to a maximum displacement, hence zero velocity, of one of the two independent motions of the system, so that there is actually no momentum when the mass assumption is changed. The expressions derived below permit the mass assumptions to be changed independently for each degree of freedom of the system, since in general the independent motions will not reverse their direction of movement, i.e. "rebound," at the same time.

With regard to the depth of burial of the arch, it has been suggested in the case of rectangular, buried structures that a depth of cover greater than the span length should not be used in estimating the mass of soil moving with the structure.(15) This is a logical restriction and is incorporated into the derivations in this chapter.

In deriving the mass concentrations on the model consider first that these concentrated masses will affect the inertial forces developed at each of the joints as the system responds to a blast loading. Second, the magnitude and direction of these inertial forces is variable but can be determined at any time during the response. Now, instead of dealing with the resultant inertial forces at the joints, consider instead the horizontal and vertical components of these forces. The mass concentrations on the model which are derived in the remainder of this section correspond to these horizontal and vertical components. This approach is more convenient than dealing with the masses corresponding to the resultant inertial forces at the joints. Note that this concept is not based upon horizontal and vertical "components" of the masses themselves.

The masses at each joint corresponding to the horizontal and vertical components of the inertial forces at the joint may be expressed as:

$$m_j = m_{sj} + m_{aj} \tag{5.1.1}$$

where m_j = mass concentration at joint j corresponding to the horizontal, or the vertical, component of the inertial force at joint j.

m_{sj} = soil contribution to m_j.

m_{aj} = arch contribution to m_j.

As mentioned previously, the mass contribution of the arch at each joint is the mass of the arch rib for half a bar length to either side of the joint. This may be expressed as:

$$m_{aj} = \frac{\gamma_a h_a}{2g} (L_{j-1} + L_j) \tag{5.1.2}$$

where m_{aj} = mass contribution of the arch at joint j

γ_a = weight per unit volume of the material from which the arch is made

h_a = thickness of the arch rib

g = acceleration due to gravity

L_{j-1} = length of the bar to the left of joint j

L_j = length of the bar to the right of joint j.

The masses of soil associated with the horizontal components of the inertial forces at the joints are shown in Figure 5.1. While both of the haunches are free to move either inward or outward, Figure 5.1 is presented, for convenience, as though the left-hand haunch, joint 1, were moving inward and the right-hand haunch, joint 3, moving outward. Note that in order for the dimensions of the soil blocks not to exceed the "corresponding span" of the model, restrictions have been placed on two of the dimensions as follows:

$$d_{m1} = (\frac{a}{2} + c + d_c) \leq (b + d) \tag{5.1.3}$$

$$d_{m2} = (\frac{c}{2} + d_c) \leq 2d \tag{5.1.4}$$

where the dimensions are defined in Figure 5.1.

Referring to Figure 5.1, one may write:

$$(m_{s1})_{in} = \frac{\gamma_s}{2g}\Big[d_{m1}(\frac{b}{2}) + (d_{m1} - \frac{a}{2})(\frac{b + d}{2})$$

$$+ (d_{m1} - \frac{a+c}{2})(\frac{d}{2}) + d_{m1}^2 \cot(\frac{\pi}{4} + \frac{\varphi}{2})\Big] \qquad (5.1.5)$$

where $(m_{s1})_{in}$ = mass contribution of the soil at joint 1 corresponding to the horizontal component of the inertial force acting at joint 1 when the joint is moving inward

$$m_{s2} = \frac{\gamma_s d}{g}(d_{m2} - \frac{c}{4}) \qquad (5.1.6)$$

where m_{s2} = mass contribution of the soil at joint 2 corresponding to the horizontal component of the inertial force acting at the crown for both inward and outward movement of the crown

$$(m_{s3})_{out} = \frac{\gamma_s}{2g}\Big[d_{m1}(\frac{b}{2}) + (d_{m1} - \frac{a}{2})(\frac{b+d}{2})$$

$$+ (d_{m1} - \frac{a+c}{2})(\frac{d}{2}) + d_{m1}^2 \cot(\frac{\pi}{4} - \frac{\varphi}{2})\Big] \qquad (5.1.7)$$

where $(m_{s3})_{out}$ = mass contribution of the soil at joint 3 corresponding to the horizontal component of the inertial force at joint 3 when the joint is moving outward.

Note also that:

$$(m_{s3})_{in} = (m_{s1})_{in} \qquad (5.1.8)$$

where $(m_{s3})_{in}$ = mass contribution of the soil at joint 3 corresponding to the horizontal component of the inertial force at joint 3 when the joint is moving inward

$$(m_{s1})_{out} = (m_{s3})_{out} \qquad (5.1.9)$$

where $(m_{s1})_{out}$ = mass contribution of the soil at joint 1 corresponding to the horizontal component of the inertial force at joint 1 when the joint is moving outward.

The masses of soil associated with the vertical components of the inertial forces at the joints are shown in Figure 5.2. Note that the restrictions stated by Equations (5.1.3) and (5.1.4) also apply here.

Referring now to the figure:

$$m_{s4} = \frac{\gamma_s}{2g}\left[d_{m1}\left(\frac{b}{2}\right) + \left(d_{m1} - \frac{a}{2}\right)\left(\frac{b+d}{2}\right) + \left(d_{m1} - \frac{a+c}{2}\right)\left(\frac{d}{2}\right)\right] \quad (5.1.10)$$

where m_{s4} = mass contribution of the soil at joint 1 corresponding to the vertical component of the inertial force at joint 1 for both inward and outward movement of the joint

$$m_{s5} = \frac{\gamma_s d}{g}\left(d_{m2} - c/4\right) \quad (5.1.11)$$

where m_{s5} = mass contribution of the soil at joint 2 corresponding to the vertical component of the inertial force at joint 2 for both inward and outward movement of the joint

$$m_{s6} = \frac{\gamma_s}{2g}\left[d_{m1}(b/2) + \left(d_{m1} - \frac{a}{2}\right)\left(\frac{b+d}{2}\right) + \left(d_{m1} - \frac{a+c}{2}\right)\left(\frac{d}{2}\right)\right] \quad (5.1.12)$$

where m_{s6} = mass contribution of the soil at joint 3 corresponding to the vertical component of the inertial force at joint 3 for both inward and outward movement of the joint.

Now substituting Equations (5.1.2) and (5.1.5) through (5.1.12) into Equation (5.1.1):

$$\begin{aligned}
(m_1)_{in} &= \frac{\gamma_s}{2g}\left[d_{m1}\left(\frac{b}{2}\right) + \left(d_{m1} - \frac{a}{2}\right)\left(\frac{b+d}{2}\right) + \left(d_{m1} - \frac{a+c}{2}\right)\left(\frac{d}{2}\right)\right. \\
&\qquad \left. + d_{m1}^2 \cot\left(\frac{\pi}{4} + \frac{\varphi}{2}\right)\right] + \gamma_a h_a L/g \\
(m_1)_{out} &= \frac{\gamma_s}{2g}\left[d_{m1}\left(\frac{b}{2}\right) + \left(d_{m1} - \frac{a}{2}\right)\left(\frac{b+d}{2}\right) + \left(d_{m1} - \frac{a+c}{2}\right)\left(\frac{d}{2}\right)\right. \\
&\qquad \left. + d_{m1}^2 \cot\left(\frac{\pi}{4} - \frac{\varphi}{2}\right)\right] + \gamma_a h_a L/g \\
m_2 &= \frac{\gamma_s d}{g}\left(d_{m2} - \frac{c}{4}\right) + \gamma_a h_a L/g \\
(m_3)_{in} &= (m_1)_{in} \\
(m_3)_{out} &= (m_1)_{out} \\
m_4 &= \frac{\gamma_s}{2g}\left[d_{m1}\left(\frac{b}{2}\right) + \left(d_{m1} - \frac{a}{2}\right)\left(\frac{b+d}{2}\right) + \left(d_{m1} - \frac{a+c}{2}\right)\left(\frac{d}{2}\right)\right] + \gamma_a h_a L/g \qquad (5.1.13) \\
m_5 &= m_2 \\
m_6 &= m_4
\end{aligned}$$

Equations (5.1.13) are expressions for the effective mass concentrations at the joints of the model. They are used in the next section in deriving expressions for the equivalent masses of the two-degree-of-freedom system.

5.2 Development of Equivalent Mass

It is now necessary to combine the inertial resistances of the arch-soil "structure" in such a manner as to obtain their resultant effect on the response of the model. Again, the expressions which follow are developed considering the horizontal displacement components of the haunches as the independent variables.

The technique followed here consists of using the mass concentration expressions derived in the preceding section to write the horizontal and vertical components of the inertial forces acting on the model at each of the joints. From the fact that in the response of any one of the masses the component of its acceleration in a given direction is proportional to the corresponding displacement component, the accelerations are related to one another using the "Displacement Relationships" derived for the model in Section 3.2.2. The inertial forces are then applied to the model and their resultant effect in the horizontal direction at the haunches found using the "Load Relationships" derived in Section 3.2.1.

Thus, using Equations (3.2.7) and the principle stated above, one may relate the acceleration components of the masses, $\ddot{h}_j$ as:

$$\begin{aligned}
\ddot{h}_2 &= + \tfrac{1}{2}\,(1 - bc/ad)(\ddot{h}_1 + \ddot{h}_3) \\
\ddot{h}_4 &= - (b/a)\ddot{h}_1 \\
\ddot{h}_5 &= + \tfrac{1}{2}\,(d/c - b/a)(\ddot{h}_1 - \ddot{h}_3) \qquad (5.2.1) \\
\ddot{h}_6 &= + (b/a)\ddot{h}_3
\end{aligned}$$

where $\ddot{h}_1$ = horizontal component of the acceleration at joint 1

$\ddot{h}_2$ = horizontal component of the acceleration at joint 2

$\ddot{h}_3$ = horizontal component of the acceleration at joint 3

$\ddot{h}_4$ = vertical component of the acceleration at joint 1

$\ddot{h}_5$ = vertical component of the acceleration at joint 2

$\ddot{h}_6$ = vertical component of the acceleration at joint 3.

Note that the acceleration components chosen for reference, i.e. $\ddot{h}_1$ and $\ddot{h}_3$, correspond to the horizontal displacement components of the haunches, which have already been chosen as the independent displacement coordinates for the dynamic analysis.

Using Equations (5.1.13) and (5.2.1) it is now possible to write the horizontal and vertical components of the inertial forces acting on each joint of the model. Since there is nothing to be gained by rewriting here the mass concentration expressions given in Equations (5.1.13), the notation will be simplified by merely indicating the proper mass concentration, m_j, to use for each inertial force component. Thus, the inertial force components, Z_j, are:

$$\begin{aligned} Z_1 &= m_1\ddot{h}_1 \\ Z_2 &= (m_2/2)(1 - bc/ad)(\ddot{h}_1 + \ddot{h}_3) \\ Z_3 &= m_3\ddot{h}_3 \\ Z_4 &= - m_4(b/a)\ddot{h}_1 \\ Z_5 &= (m_5/2)(d/c - b/a)(\ddot{h}_1 - \ddot{h}_3) \\ Z_6 &= m_6(b/a)\ddot{h}_3 \end{aligned} \qquad (5.2.2)$$

By applying the inertial force components, Z_j, to the model as a system of loads, the equivalent inertial force in the horizontal direction at the haunches, $\overline{Z}_j$, may be found, using Equations (3.2.5), as:

$$\begin{aligned}\bar{Z}_1 &= Z_1 + \frac{1}{2}\left(1 - \frac{bc}{ad}\right)Z_2 - \left(\frac{b}{a}\right)Z_4 + \frac{1}{2}\left(\frac{d}{c} - \frac{b}{a}\right)Z_5 \\ \bar{Z}_3 &= \frac{1}{2}\left(1 - \frac{bc}{ad}\right)Z_2 + Z_3 - \frac{1}{2}\left(\frac{d}{c} - \frac{b}{a}\right)Z_5 + \left(\frac{b}{a}\right)Z_6\end{aligned} \qquad (5.2.3)$$

Now let $\bar{m}_{j,m}$ = equivalent mass of the system in the horizontal direction at haunch j. Then:

$$\bar{Z}_j = \bar{m}_{j,m}\, \ddot{h}_j \qquad (5.2.4)$$

Substituting Equations (5.2.2) and (5.2.4) into Equations (5.2.3):

$$\begin{aligned}\bar{m}_{1,m}\ddot{h}_1 &= m_1\ddot{h}_1 + (m_2/4)(1 - bc/ad)^2(\ddot{h}_1 + \ddot{h}_3) \\ &\quad + m_4(b/a)^2\ddot{h}_1 + (m_5/4)(d/c - b/a)^2(\ddot{h}_1 - \ddot{h}_3) \\ \bar{m}_{3,m}\ddot{h}_3 &= (m_2/4)(1 - bc/ad)^2(\ddot{h}_1 + \ddot{h}_3) + m_3\ddot{h}_3 \\ &\quad - (m_5/4)(d/c - b/a)^2(\ddot{h}_1 - \ddot{h}_3) + m_6(b/a)^2\ddot{h}_3\end{aligned}$$

Rearranging terms gives:

$$\begin{aligned}\bar{m}_{1,m} &= \left[m_1 + (m_2/4)(1 - bc/ad)^2 + m_4(b/a)^2 + (m_5/4)\left(\frac{d}{c} - \frac{b}{a}\right)^2\right] \\ &\quad - \frac{\ddot{h}_3}{\ddot{h}_1}\left[-(m_2/4)(1 - bc/ad)^2 + (m_5/4)(d/c - b/a)^2\right] \\ \bar{m}_{3,m} &= \left[(m_2/4)(1 - bc/ad)^2 + m_3 + (m_5/4)\left(\frac{d}{c} - \frac{b}{a}\right)^2 + m_6(b/a)^2\right] \\ &\quad - \frac{\ddot{h}_1}{\ddot{h}_3}\left[-(m_2/4)(1 - bc/ad)^2 + (m_5/4)(d/c - b/a)^2\right]\end{aligned} \qquad (5.2.5)$$

Note that either $(m_j)_{in}$ or $(m_j)_{out}$ may be used for a particular joint in Equations (5.2.5) as the motion of the system dictates.

Since the mass effects at the haunches are not separated in Equations (5.2.5), it is not possible to treat them separately here as was done in the derivation of expressions for equivalent soil resistance in

Section 4.4. This, together with the fact that each of Equations (5.2.5) can have either of two possible values, one for inward and one for outward movement of the corresponding haunch, makes it necessary at this point to consider the possible motions of the model (cf. Section 1.2). There are four of these motions as illustrated in Figure 5.3. For convenience, they are designated as follows:

#1 = Asymmetric-Right. This motion is characterized by the simultaneous movement of both haunches to the right.

#2 = Symmetric-In. This motion is characterized by the simultaneous inward movement of both haunches.

#3 = Symmetric-Out. This motion is characterized by the simultaneous outward movement of both haunches.

#4 = Asymmetric-Left. This motion is characterized by the simultaneous movement of both haunches to the left.

Note that in the case of each of the four motions defined above the crown may move either upward or downward depending upon the relative velocities and displacements of the haunches.

The notation of Equations (5.2.5) may now be simplified as:

$$\bar{m}_{1,m} = \mu_{1,m} - \frac{\ddot{h}_3}{\ddot{h}_1} \nu_{1,m}$$

$$\bar{m}_{3,m} = \mu_{3,m} - \frac{\ddot{h}_1}{\ddot{h}_3} \nu_{3,m} \qquad (5.2.6)$$

where $\mu_{1,m} = m_1 + (m_2/4)(1-bc/ad)^2 + m_4(b/a)^2 + (m_5/4)(d/c-b/a)^2$

$\nu_{1,m} = -(m_2/4)(1-bc/ad)^2 + (m_5/4)(d/c - b/a)^2$

$\mu_{3,m} = (m_2/4)(1-bc/ad)^2 + m_3 + (m_5/4)(d/c-b/a)^2 + m_6(b/a)^2$

$\nu_{3,m} = -(m_2/4)(1-bc/ad)^2 + (m_5/4)(d/c-b/a)^2$

m = index denoting the motion of the system as defined above. $m = 1,2,3,4$.

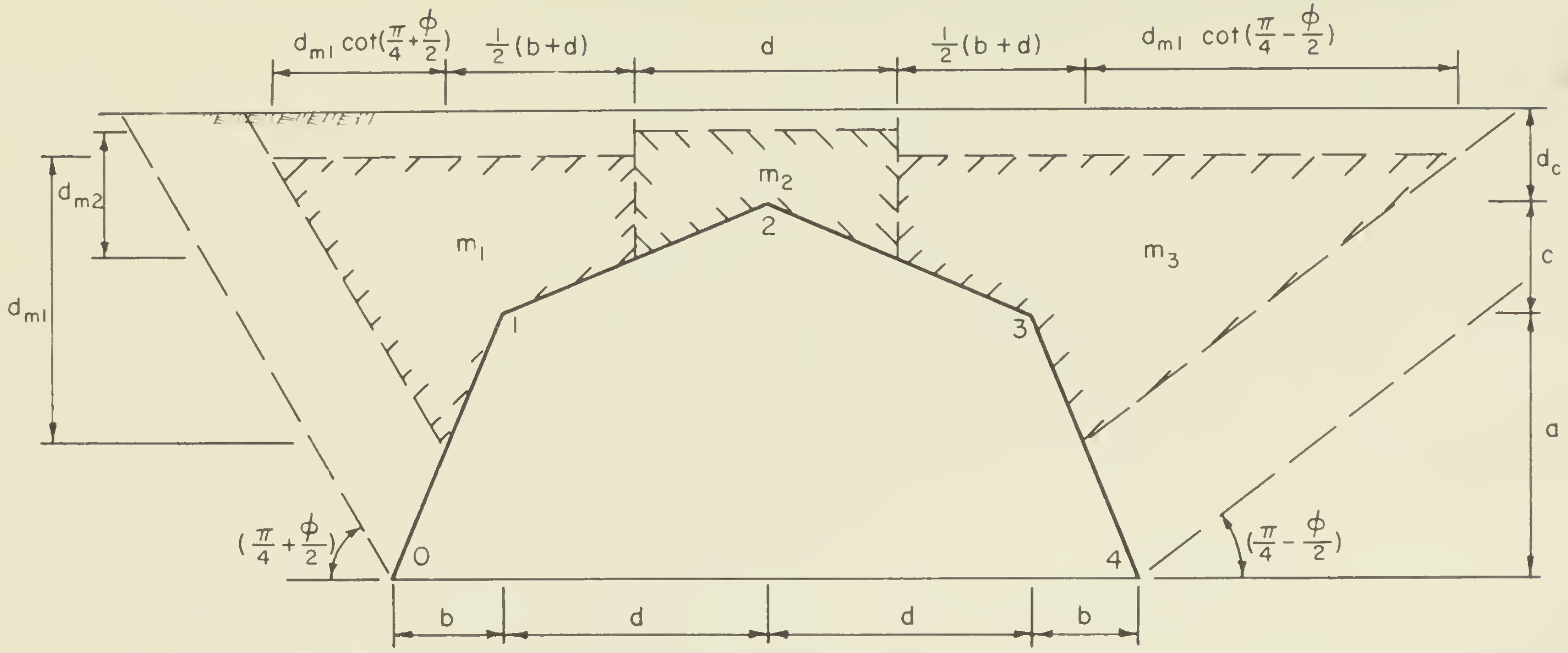
$d_{m1} \cot(\frac{\pi}{4}+\frac{\phi}{2})$
$\frac{1}{2}(b+d)$
d
$\frac{1}{2}(b+d)$
$d_{m1} \cot(\frac{\pi}{4}-\frac{\phi}{2})$
d_{m2}
d_{m1}
m_1
m_2
m_3
0
1
2
3
4
d_c
c
a
$(\frac{\pi}{4}+\frac{\phi}{2})$
$(\frac{\pi}{4}-\frac{\phi}{2})$
b
d
d
b

Figure 5.1. Masses of Soil Associated with Horizontal Components of Inertial Forces at Joints

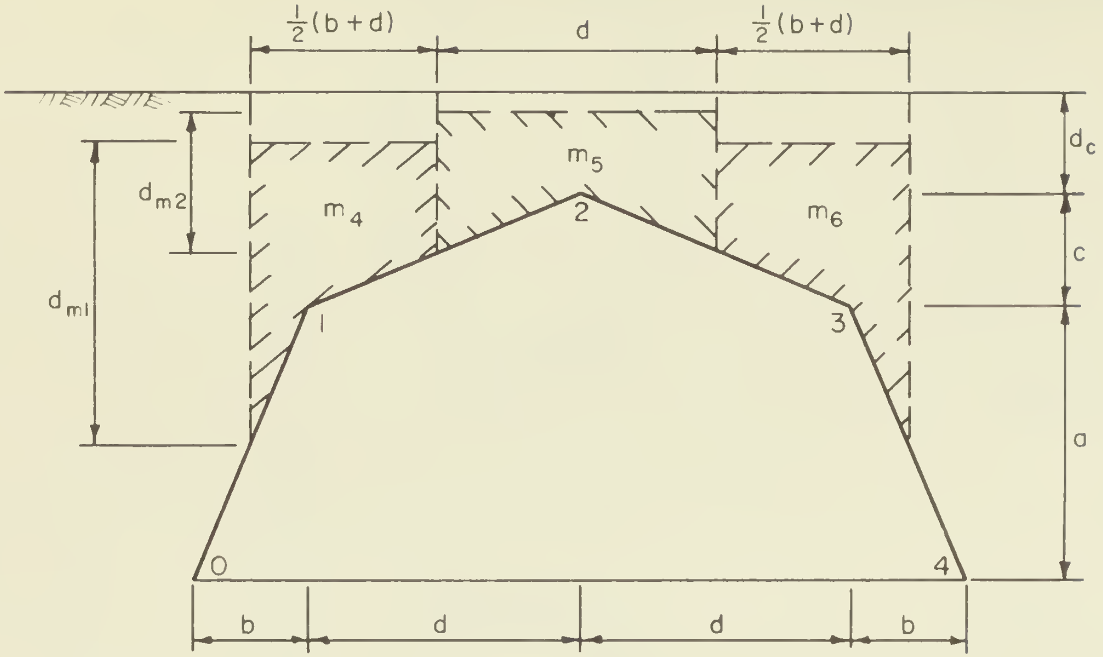

Figure 5.2. Masses of Soil Associated with Vertical Components of Inertial Forces at Joints

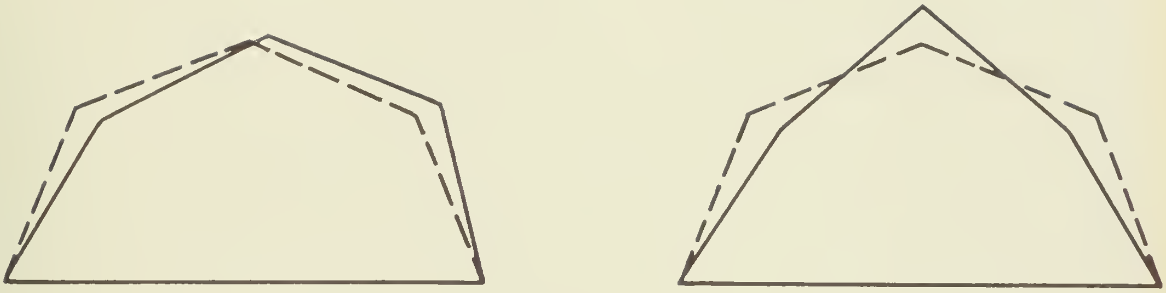

1. Asymmetric-Right

2. Symmetric-In

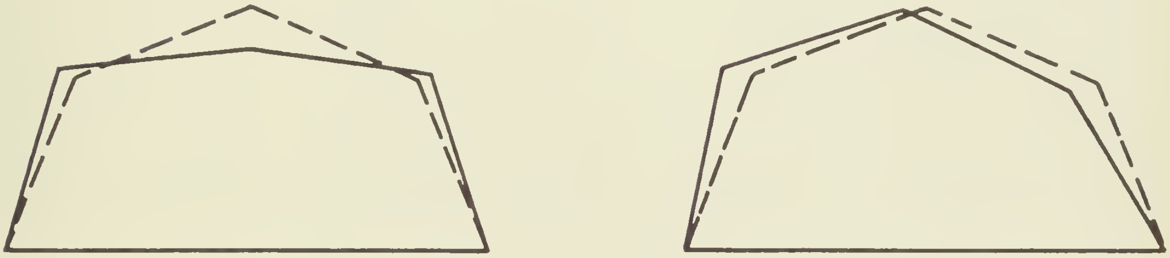

3. Symmetric-Out

4. Asymmetric-Left

Figure 5.3. Motions of Model

CHAPTER VI

BLAST PRESSURE LOADING

It is the purpose of this chapter to define the loading on the dynamic model in terms of the geometry of the arch-soil "structure" and the shock wave (blast overpressure) resulting from the explosion of a nuclear weapon. The majority of the blast parameters are taken from references (16) and (17). The shape of the overpressure decay curve behind the shock front is taken from reference (20). The assumptions made in selecting these parameters are discussed in Section 2.4.

In defining the load on a buried structure the shape and characteristics of the blast wave in soil are of obvious importance. Studies of the forces transmitted through the soil cover are being made by several groups at the present time. A summary of much of the significant work which had been done on this problem, together with a convenient numerical technique for solving the one-dimensional problem of stress wave transmission through soil, is contained in reference (18). From these studies it appears that there is little or no significant attenuation in the vertical, free-field overpressures within the relatively shallow depths considered in this thesis. The results of a study of the configuration of the shock front in soil are presented herein as Appendix B.

For derivations in this chapter the blast loading is considered to be transmitted by the soil directly to the arch without modification. This is consistent with the approach used in Chapters IV and V in deriving expressions for the deformation and inertial resistances of the soil surrounding the arch. The assumption is made that the ground surface is flat in the vicinity of the arch so that dynamic pressures and reflection phenomena due to surface irregularities need not be considered.

While the model and the methods of dynamic analysis used in this thesis are suitable for studying blast overpressure loadings due to shock waves approaching the structure from any direction, the expressions developed in this chapter are derived on the basis of a shock wave approaching from the side of the arch, i.e. with the direction of travel of the shock wave normal to the longitudinal axis of the arch. This geometry produces maximum asymmetry in the arch loading and thus should lead to maximum lateral response of the arch.

The assumption that nuclear blast waves may be approximated using the idealized curves of references (16), (17) and (20) is basic to all of the derivations in this chapter. A convenient, but as will be seen not altogether essential, assumption is made that the seismic velocity of the soil is practically constant between ground zero and the point of interest, i.e. the location of the structure.

6.1 Definition of Loading Regions

The arch itself may receive load at all points on its periphery during passage of the shock wave. However, in defining the load on the replacement model used for the dynamic analysis load is brought in only at the joints. These joint loadings are simply concentrations of the distributed loading sensed by the arch itself. The load concentrations are obtained by defining regions in the vicinity of each joint which will tend to bring load to that joint. Then the average blast overpressures acting on these regions are concentrated and applied to the model at the joints. It is more convenient here to deal with the horizontal and vertical components of the load at each joint than with the resultant forces themselves, just as was the case with the inertial forces considered in Chapter V.

In the following sections regions tending to bring load to each joint, i.e. "loading regions," are defined for various shock wave-soil combinations. In general, for shallow-buried structures such as are considered in this study, the configuration of the shock front in the soil may be considered as a plane perpendicular to the direction of travel of the shock front. It is oriented, in the plane of the arch, at an angle with respect to the shock front in air which is dependent upon the relative values of the seismic velocity of the soil and the velocity of the shock wave in air at the point of interest (cf. Appendix B). Since in this study the abutments are assumed immovable (cf. Section 1.2), loading regions tending to bring load primarily to the abutments are neglected.

The three cases considered below are for:

(1) A vertical shock front in the soil,

(2) A shock front in the soil which is inclined at an angle less than the inclination of the upper bars of the model, and

(3) A shock front in the soil which is inclined at an angle greater than the inclination of the upper bars and less than the inclination of the lower bars of the model.

A series of problems (cf. Chapter VIII and Appendices C and D), which was solved using various angles of inclination for the shock front and holding the remaining variables constant, indicated that the lateral response of the model was not particularly sensitive to variations in this angle. Thus, the assumption of a constant seismic velocity in the soil between ground zero and the location of the structure, while convenient in defining the inclination of the shock front in the soil, is not too significant here. Therefore, the case of a shock front in soil inclined at an angle between the vertical and the inclination of the lower bars of the model is omitted. Also omitted is

the case of a horizontal shock front in soil. While this may be readily handled by the techniques developed herein, it is outside the scope of this study (cf. Section 2.4).

6.1.1 Case I - Vertical Shock Front in Soil

From the results of the study presented in Appendix B it can be seen that a nearly vertical shock front in the soil results when the velocity of the shock front in air at the point of interest and the seismic velocity of the soil are nearly equal. This case is illustrated in Figure 6.1.

Since the configuration of the shock front in soil has been assumed as a plane perpendicular to the plane of the arch, it will, in general, strike the arch at some point of tangency or at an abutment. The problem of the shock wave enveloping the arch itself can be handled quite readily (cf. reference (21)). However, for the purposes of this study it is more convenient and not significantly less accurate to consider instead the shock wave as enveloping the replacement model.

In interpreting Figure 6.1 consider the shock front in air as moving along the ground surface from left to right while the shock front in soil, as an extension of the shock front in air, moves through the soil. Prior to the arrival of the shock front at point Oa', the shock wave is assumed to have no influence on the structure. As the shock front moves from Oa' to Ob, the shock wave engulfs the "passive" soil failure wedge corresponding to outward displacement of the windward haunch, joint 1 (cf. Section 4.2). The average overpressure acting at the ground surface between points Oa' and Ob is thus $\bar{p}'_{s1}$. As the shock front moves from point Oa to point Ob, the shock wave engulfs the "active" soil failure wedge corresponding to inward displacement of the windward haunch, joint 1 (cf. Section 4.1). The average overpressure acting between points Oa and Ob is thus $\bar{p}_{s1}$.

As the shock front moves from point 0 to point 1a, the shock wave is assumed to load the left abutment, joint 0; therefore, this region is not considered in the arch loading. The shock front then moves from the midpoint of bar 1, point 1a, to the midpoint of bar 2, point 1b, and in so doing is assumed to load joint 1. The average overpressure acting between points 1a and 1b is designated $\bar{p}_1$.

As the shock front moves on from point 1b, the shock wave starts to load joint 2; therefore, for convenience, point 1b is also labeled point 2a. Now the shock wave may be assumed to load joint 2 as the shock front moves from point 2a to point 2b. The average overpressure acting between points 2a and 2b is designated $\bar{p}_2$.

It may be noted here that the horizontal component of the loading between points 2a and 2 tends to act to the right at joint 2, while the horizontal component of the loading between points 2 and 2b tends to act to the left. For this reason it is convenient to designate the average overpressure acting between points 2a and 2 as $\bar{p}_{2a}$ and that acting between points 2 and 2b as $\bar{p}_{2b}$.

As the shock front moves on from point 2b, it starts to load joint 3. Accordingly, it is convenient to label point 2b also as point 3a. Now, the average overpressure acting between points 3a and 3b is assumed to load joint 3 and is designated $\bar{p}_3$.

The average overpressure acting between points 3b and 4 is assumed to load the right abutment, joint 4, and is therefore neglected.

As the shock front moves from point 4a to point 4b, the shock wave engulfs the "active" soil failure wedge corresponding to the inward displacement of the leeward haunch, joint 3. The average overpressure acting between points 4a and 4b is thus $\bar{p}_{s3}$.

As the shock front moves from point 4a to point 4b', the shock wave engulfs the "passive" soil failure wedge corresponding to the outward displacement of the leeward haunch, joint 3. The average overpressure acting between points 4a and 4b' is thus $\bar{p}'_{s3}$.

For purposes of calculating the "rib-shortening" correction derived in Section 3.5, the average overpressure acting on the entire arch is needed. This is taken as the average overpressure acting between points 0 and 4 and is designated $\bar{p}_a$. For convenience in this case point 0 is also labeled "aa" and point 4 is also labeled "ab."

Note in the foregoing description that no actual "loading" of the arch takes place until the shock front reaches point 1a. It is assumed that no movement of the arch occurs prior to this time. Therefore, the time of arrival of the shock front at point 1a is taken as zero time for this case. This assumption is consistent with the derivation of the "deformation" resistence of the soil in Chapter IV. It is not unreasonable when one considers the high velocity of the shock wave, the relatively small dimensions of the arch-soil "structure," the inertia of the soil loaded prior to this time and the relatively small displacements of the structure during the early part of the loading history.

In the derivation of expressions for the load concentrations on the model (cf. Section 6.2) it is convenient to use the times at which the shock front arrives at the windward and leeward boundaries of the various loading regions. Zero time for this case has already been chosen at point 1a. This is expressed algebraically by Equation (6.1.1).

$$t_{1a} = 0 \qquad (6.1.1)$$

The remaining time parameters are given by Equations (6.1.2), expressed in terms of the velocity of the shock front in air, U, and the geometry of the arch-soil "structure" as shown in Figure 6.1.

$$\begin{aligned}
t_{0a'} &= -\left(b + 2d_o \cot\left[\frac{\pi}{4} - \frac{\varphi}{2}\right]\right)/2U \\
t_{0a} &= -\left(b + 2d_o \cot\left[\frac{\pi}{4} + \frac{\varphi}{2}\right]\right)/2U \\
t_{0b} &= -(b - 2bd_o/a)/2U \\
t_{1b} &= (b + d)/2U \\
t_{2a} &= t_{1b} \\
t_{2} &= (b + 2d)/2U \\
t_{2b} &= (b + 3d)/2U \\
t_{3a} &= t_{2b} \\
t_{3b} &= (b + 2d)/U \\
t_{4a} &= (-b + 2B - 2bd_o/a)/2U \\
t_{4b} &= \left(-b + 2B + 2d_o \cot\left[\frac{\pi}{4} + \frac{\varphi}{2}\right]\right)/2U \\
t_{4b'} &= \left(-b + 2B + 2d_o \cot\left[\frac{\pi}{4} - \frac{\varphi}{2}\right]\right)/2U \\
t_{aa} &= -b/2U \\
t_{ab} &= (-b + 2B)/2U
\end{aligned} \tag{6.1.2}$$

where, in general: t_{ja} = time of arrival of the shock front at the windward boundary of loading region j

t_{jb} = time of arrival of the shock front at the leeward boundary of loading region j.

6.1.2 Case II - Shock Front in Soil Inclined at Angle Less Than Inclination of Upper Bars of Model

The results of the study presented in Appendix B indicate that for seismic velocities less than the velocity of the shock wave in air at the point of interest, the shock front in soil will be inclined at an angle to the shock wave in air. The expressions derived in this section are for the

case where the inclination of the shock wave in soil with respect to the horizontal, η, is less than the angle of inclination of the upper bars of the model, i.e.:

$$\eta < \arctan \frac{c}{d} \tag{6.1.3}$$

This case is illustrated in Figure 6.2. Note that in this case the shock front in soil first strikes the model at the crown. Therefore, for this case the time of arrival of the shock wave at the crown is taken as zero time.

$$t_2 = 0 \tag{6.1.4}$$

The considerations in selecting this time as the reference are the same as for the preceding case (cf. Section 6.1.1).

The loading regions shown in Figure 6.2 are defined in an analogous manner to those for the vertical shock front in soil and therefore are not described in detail here. However, there are several differences worthy of note, viz:

1. The "active" and "passive" soil failure wedges are not fully enveloped by the shock wave until the shock front in soil reaches the corresponding abutment.

2. On the windward side of the model the shock front strikes the midpoint of the upper bar before reaching the midpoint of the lower bar. However, the midpoints of the bars are not relabeled. This introduces an inconsistency in the notation, but not a serious one, since the order in which the boundaries of a "loading region" are reached by the shock front is obvious in any set of computations.

3. The crown, joint 2, is enveloped by the shock wave from the top downward instead of from left to right as was the case in the preceding section. Here also the notation is not changed.

4. The average overpressure acting on the arch for this case is taken as the average overpressure acting between points 2 and 4. This corresponds to the envelopement of the model by the shock wave as the shock front travels from the crown to the leeward abutment. For convenience, points 2 and 4 are also labeled "aa" and "ab."

The time parameters defining the times of arrival of the shock front at the boundaries of the loading regions are given in Equations (6.1.5). These may be written readily by referring to Figure 6.2.

$$
\begin{aligned}
t_{0a'} &= - d_c/C_s' - (B + 2d_o \cot \left[\frac{\pi}{4} - \frac{\varphi}{2}\right])/2U \\
t_{0a} &= - d_c/C_s' - (B + 2d_o \cot \left[\frac{\pi}{4} + \frac{\varphi}{2}\right])/2U \\
t_{0b} &= (a + c)/C_s' - B/2U \\
t_{1a} &= (a + 2c)/2C_s' - (b + 2d)/2U \\
t_{1b} &= c/2C_s' - d/2U \\
t_{2a} &= t_{1b} \\
t_{2b} &= c/2C_s' + d/2U \\
t_{3a} &= t_{2b} \\
t_{3b} &= (a + 2c)/2C_s' + (b + 2d)/2U \\
t_{4a} &= - d_c/C_s' + (B - 2bd_o/a)/2U \\
t_{4b} &= (a + c)/C_s' + B/2U \\
t_{4b'} &= t_{4b} \\
t_{aa} &= t_2 \\
t_{ab} &= t_{4b}
\end{aligned}
\tag{6.1.5}
$$

Equations (6.1.5) are written in terms of the apparent vertical component of the velocity of the shock front in soil, C'_s. If the inclination of the shock front in soil, η, with respect to the horizontal is obtained from Appendix B, Equation (B.3), C'_s may be obtained from Equation (6.1.6).

$$C'_s = U \tan \eta \tag{6.1.6}$$

6.1.3 Case III - Shock Front in Soil Inclined at Angle Intermediate Between Inclinations of Upper and Lower Bars of Model

The expressions derived in this section are for the case where the inclination of the shock front in the soil is greater than the inclination of the upper bars of the model and less than the inclination of the lower bars of the model, i.e.:

$$\arctan \frac{c}{d} < \eta < \arctan \frac{a}{b} \tag{6.1.7}$$

This is illustrated in Figure 6.3. Note that the shock front strikes the windward haunch first. Therefore, the time of arrival of the shock front at the windward haunch is taken as zero time for this case.

$$t_1 = 0 \tag{6.1.8}$$

The considerations for the selection of t_1 as the reference time are the same as those listed in Section 6.1.1 for the selection of the reference time for the vertical shock front in soil.

The loading regions shown in Figure 6.3 are defined in the same fashion as those in the preceding sections. However, several differences do exist for this case, viz:

1. The windward haunch is assumed to be loaded as the shock front moves from the haunch to the midpoint of either the upper or lower adjoining bar depending upon which occurs later. In other words, the shock front may arrive at point 1a either before or after it strikes point 1b. The order of arrival depends upon the relative geometries of the shock front and the model.

2. The soil failure wedges on the leeward side of the model are assumed to be loaded as the shock front moves from point 4a to either the leeward abutment or the intersection of the failure plane and the ground surface, whichever occurs later. The order of arrival depends upon the relative geometries of the shock front and the model just as in the case of the windward haunch discussed in the preceding paragraph.

3. The average overpressure acting on the arch in this case is taken as the average overpressure acting between points 1 and 4. For convenience these points are also labeled for this case as "aa" and "ab". This corresponds to the envelopment of the model by the shock wave as the shock front travels from the windward haunch to the leeward abutment.

The time parameters defining the times of arrival of the shock front at the boundaries of the loading regions are given by Equations (6.1.9). These may be written readily by referring to Figure 6.3.

$$
\begin{aligned}
t_{0a'} &= -(c + d_c)/C_s' - (b + d_o \cot\left[\frac{\pi}{4} - \frac{\varphi}{2}\right])/U \\
t_{0a} &= -(c + d_c)/C_s' - (b + d_o \cot\left[\frac{\pi}{4} + \frac{\varphi}{2}\right])/U \\
t_{0b} &= a/C_s' - b/U \\
{}^{*}t_{1a} &= a/2C_s' - b/2U \\
{}^{*}t_{1b} &= -c/2C_s' + d/2U \\
t_{2a} &= t_{1b} \\
t_{2} &= -c/C_s' + d/U \\
t_{2b} &= -c/2C_s' + 3d/2U \\
t_{3a} &= t_{2b} \\
t_{3b} &= a/2C_s' + (4d + b)/2U
\end{aligned}
\qquad (6.1.9)
$$

---

* Use either t_{1a} or t_{1b}, whichever is larger.

$$t_{4a} = -(c + d_c)/C'_s + (-b + B - bd_o/a)/U$$

$$^{*}(t_{4b})_1 = -(c + d_c)/C'_s + \left(-b + B + d_o \cot\left[\frac{\pi}{4} + \frac{\varphi}{2}\right]\right)/U$$

$$^{*}(t_{4b})_2 = a/C'_s + (-b + B)/U$$

$$^{**}(t_{4b'})_1 = -(c + d_c)/C'_s + \left(-b + B + d_o \cot\left[\frac{\pi}{4} - \frac{\varphi}{2}\right]\right)/U$$

$$^{**}(t_{4b'})_2 = (t_{4b})_2$$

$$t_{aa} = t_1$$

$$t_{ab} = (t_{4b})_2$$

Equations (6.1.9) are written in terms of the apparent vertical component of the velocity of the shock front in soil, C'_s. If the inclination of the shock front in soil, η, with respect to the horizontal is obtained from Appendix B, Equation (B.3), then C'_s may be obtained from Equation (6.1.6).

6.2 Load Concentrations on Model

The load concentrations on the model are derived in this section by considering the average overpressure acting at the ground surface on the loading regions defined in Section 6.1. The approach used is illustrated in Figure 6.4. The overpressure is assumed to have no effect upon the region until time t_{ja}, the time of arrival of the shock front at the windward boundary, ja, of the region, j. The average overpressure acting on the region, $\bar{p}_j$, is then assumed to build up linearly as the shock front traverses the region from the windward boundary, ja, to the leeward boundary, jb. At times greater than the time of arrival of the shock front at the leeward boundary, t_{jb}, the

---

* Use either $(t_{4b})_1$ or $(t_{4b})_2$, whichever is larger.

** Use either $(t_{4b'})_1$ or $(t_{4b'})_2$, whichever is larger.

average overpressure acting on the region is assumed to have a value equal to the instantaneous value of the overpressure at the center of the region. This approach is essentially the same as is used in reference (16) in defining the loading of flat surfaces oriented parallel to the direction of travel of the shock wave. Various techniques involving the integration of the overpressure-time pulse followed by an averaging of the impulse over the region of interest were studied and found to offer little or no advantage over the simpler approach described above.

In general, the average overpressure acting on a loading region is expressed by Equations (6.2.1)

$$\begin{aligned}
t \leq t_{ja}: &\qquad \bar{p}_j(t) = 0 \\
t_{ja} \leq t \leq t_{jb}: &\qquad \bar{p}_j(t) = p\left(\frac{t_{jb}-t_{ja}}{2}\right)\left[\frac{t - t_{ja}}{t_{jb}-t_{ja}}\right] \\
t_{jb} \leq t \leq \frac{1}{2}(t_{ja}+t_{jb})+t_d: &\qquad \bar{p}_j(t) = p\left(t - \frac{t_{ja}+t_{jb}}{2}\right) \qquad (6.2.1) \\
\frac{1}{2}(t_{ja}+t_{jb})+t_d \leq t &\qquad : \bar{p}_j(t) = 0
\end{aligned}$$

where $\bar{p}_j(t)$ = average overpressure acting on region j at any time, t (cf. Figure 6.4)

$p(t)$ = variation of overpressure behind the shock front with time (cf. reference (20))

t = time

t_{ja} = time of arrival of the shock front at the windward boundary of region j

t_{jb} = time of arrival of the shock front at the leeward boundary of region, j.

It has been pointed out earlier, in the cases of the inclined shock fronts, that because the reference points on the model are labeled from left to right, inconsistencies in the notation exist when the shock front approaches a region from a different direction. This occurs, for example, in Case II where the

shock front strikes point 1b before arriving at point 1a (cf. Figure 6.2). This type of situation may be handled readily using Equations (6.2.1) by considering the earlier time as t_{ja} and the later time as t_{jb} irrespective of the designation of the corresponding points on the model.

Expressions for the concentrated loads acting at the joints of the model may now be written in terms of the average overpressures acting on the corresponding loading regions, Equations (6.2.1). Here the assumption is used that the overpressure acting at the ground surface is transmitted vertically downward by the soil as a vertical overpressure in the soil.(18) Further, it is assumed that the horizontal overpressure in the soil, p_h, bears a constant relationship, K_{pr}, to the vertical overpressure, p_v.(15,17,19)

$$K_{pr} = p_h/p_v \tag{6.2.2}$$

Note that the following expressions, Equations (6.2.3), are for the horizontal and vertical components of the load concentrations at the joints rather than for the resultant loads themselves. This is simply for convenience in derivation and for use later in determining the equivalent loads on the system (cf. Section 6.3). Referring to Figures 3.2 and 6.1, 6.2 or 6.3, one may write:

$$\begin{aligned}
H_1 &= -\tfrac{1}{2} K_{pr}\bar{p}_1(a+c) \\
H_2 &= -\tfrac{1}{2} K_{pr}(\bar{p}_{2a}-\bar{p}_{2b})c \\
H_3 &= +\tfrac{1}{2} K_{pr}\bar{p}_3(a+c) \\
H_4 &= +\tfrac{1}{2} \bar{p}_1(b+d) \\
H_5 &= +\ \bar{p}_2 d \\
H_6 &= +\tfrac{1}{2} \bar{p}_3(b+d)
\end{aligned} \tag{6.2.3}$$

Note that since the overpressure acts downward, it is considered negative in accordance with the sign convention used herein (cf. Section 1.2).

6.3 Development of Equivalent Load

The concentrated loads acting at the joints of the model must be combined in order to obtain their resultant effect upon the two-degree-of-freedom system. The "Load Relationships" derived in Section 3.2.1, Equations (3.2.5), express the resultant loads in terms of the equivalent horizontal loads at the haunches. This is in agreement with the choice of the horizontal displacement components of the haunches as the independent variables for the dynamic analysis.

While Equations (6.2.3) and (3.2.5) may be used successively to obtain the equivalent load on the system, it is more convenient to combine them and express the equivalent loads in terms of the average overpressures acting on the various loading regions. Equations (6.3.1) are obtained by substituting Equations (6.2.3) into Equations (3.2.5).

$$\begin{aligned} \bar{H}_1 &= -\frac{1}{2}\bar{p}_1\left[K_{pr}(a+c) + (b/a)(b+d)\right] - \frac{1}{4}(\bar{p}_{2a}-\bar{p}_{2b})cK_{pr}(1-bc/ad) \\ &\quad + \frac{1}{2}\bar{p}_2 d(d/c - b/a) \\ \bar{H}_3 &= -\frac{1}{4}(\bar{p}_{2a}-\bar{p}_{2b})cK_{pr}(1 - bc/ad) \\ &\quad - \frac{1}{2}\bar{p}_2 d(d/c - b/a) + \frac{1}{2}\bar{p}_3\left[K_{pr}(a+c) + (b/a)(b+d)\right] \end{aligned} \qquad (6.3.1)$$

The notation in the preceding equations may be simplified as shown in Equations (6.3.2).

$$\begin{aligned} \bar{H}_1 &= -J_1\bar{p}_1 - J_2(\bar{p}_{2a} - \bar{p}_{2b}) + J_3\bar{p}_2 \\ \bar{H}_3 &= \qquad\quad - J_2(\bar{p}_{2a} - \bar{p}_{2b}) - J_3\bar{p}_2 + J_1\bar{p}_3 \end{aligned} \qquad (6.3.2)$$

where $J_1 = \frac{1}{2}K_{pr}(a+c) + \frac{1}{2}(b/a)(b+d)$

$J_2 = \frac{1}{4}cK_{pr}(1-bc/ad)$

$J_3 = \frac{1}{2}d(d/c-b/a)$

Note that the dimensions of J_1, J_2, and J_3 must be in agreement with the units in which the overpressure is expressed.

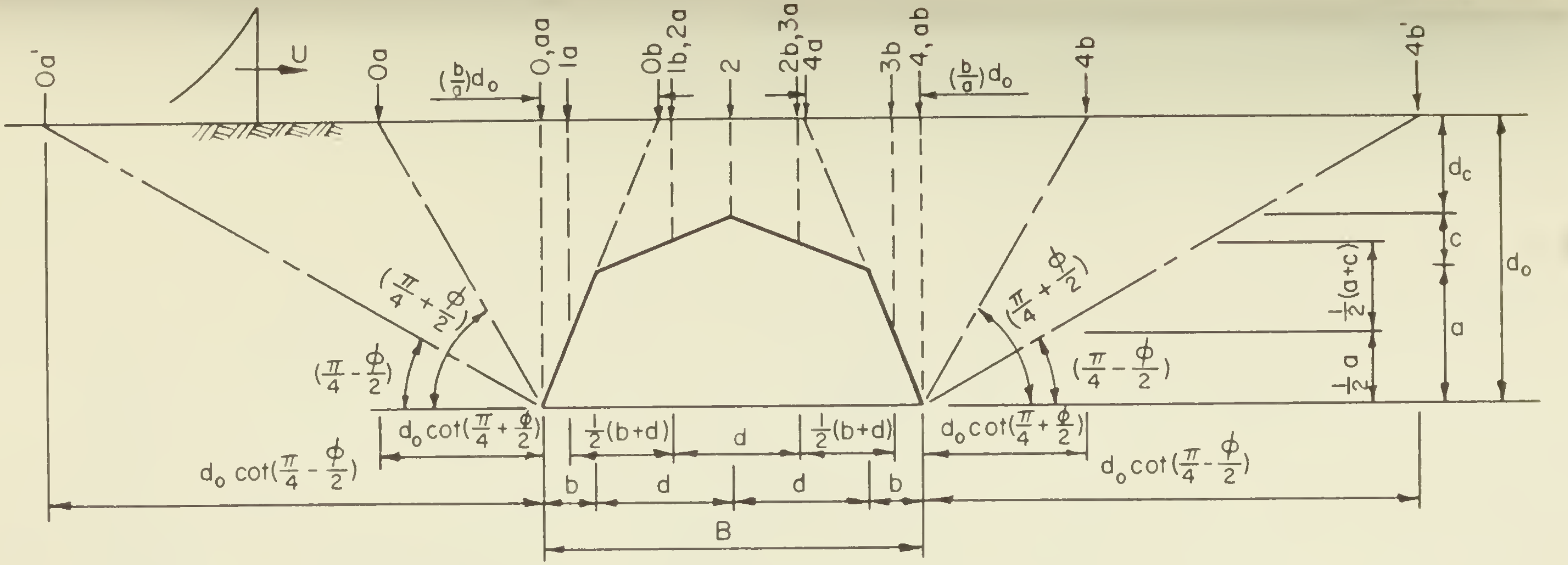
0a'
U
0a
$(\frac{b}{a})d_o$
0,aa
1a
0b
1b,2a
2
2b,3a
4a
3b
4,ab
$(\frac{b}{a})d_o$
4b
4b'
d_c
c
d_o
$\frac{1}{2}(a+c)$
a
$\frac{1}{2}a$
$(\frac{\pi}{4}+\frac{\phi}{2})$
$(\frac{\pi}{4}-\frac{\phi}{2})$
$(\frac{\pi}{4}+\frac{\phi}{2})$
$(\frac{\pi}{4}-\frac{\phi}{2})$
$d_o\cot(\frac{\pi}{4}+\frac{\phi}{2})$
$\frac{1}{2}(b+d)$
d
$\frac{1}{2}(b+d)$
$d_o\cot(\frac{\pi}{4}+\frac{\phi}{2})$
$d_o\cot(\frac{\pi}{4}-\frac{\phi}{2})$
$d_o\cot(\frac{\pi}{4}-\frac{\phi}{2})$
b
d
d
b
B

Figure 6.1. Loading Regions for Case I

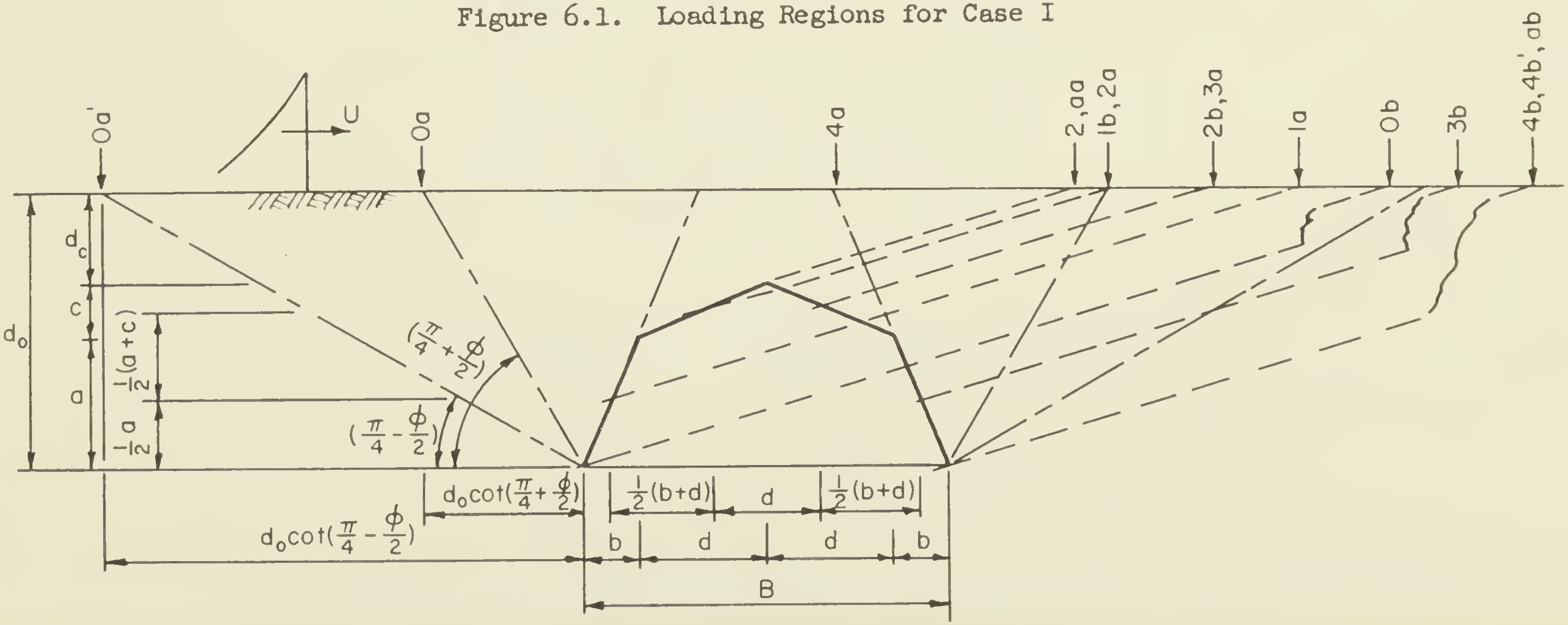
0a'
U
0a
4a
2,aa
1b,2a
2b,3a
1a
0b
3b
4b,4b',ab
d_c
c
d_o
a
$\frac{1}{2}(a+c)$
$\frac{1}{2}a$
$(\frac{\pi}{4}+\frac{\phi}{2})$
$(\frac{\pi}{4}-\frac{\phi}{2})$
$d_o\cot(\frac{\pi}{4}+\frac{\phi}{2})$
$d_o\cot(\frac{\pi}{4}-\frac{\phi}{2})$
$\frac{1}{2}(b+d)$
d
$\frac{1}{2}(b+d)$
b
d
d
b
B

Figure 6.2. Loading Regions for Case II

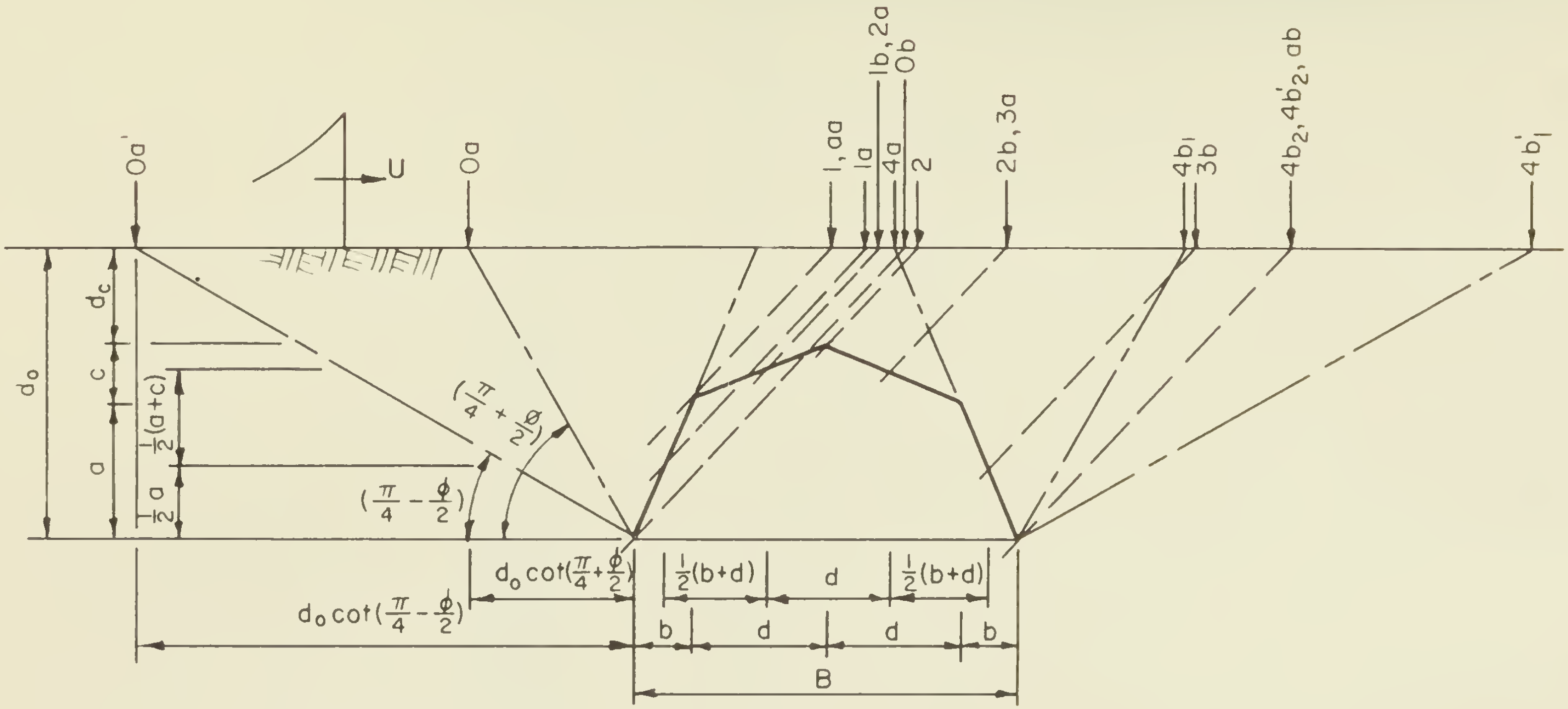

0a'
U
0a
1, aa
1a
1b, 2a
4a
0b
2
2b, 3a
4b1
3b
4b2, 4b'2, ab
4b'1
d_o
d_c
c
a
$\frac{1}{2}(a+c)$
$\frac{1}{2}a$
$(\frac{\pi}{4}+\frac{\phi}{2})$
$(\frac{\pi}{4}-\frac{\phi}{2})$
$d_o \cot(\frac{\pi}{4}+\frac{\phi}{2})$
$d_o \cot(\frac{\pi}{4}-\frac{\phi}{2})$
$\frac{1}{2}(b+d)$
d
$\frac{1}{2}(b+d)$
b
d
d
b
B

Figure 6.3. Loading Regions for Case III

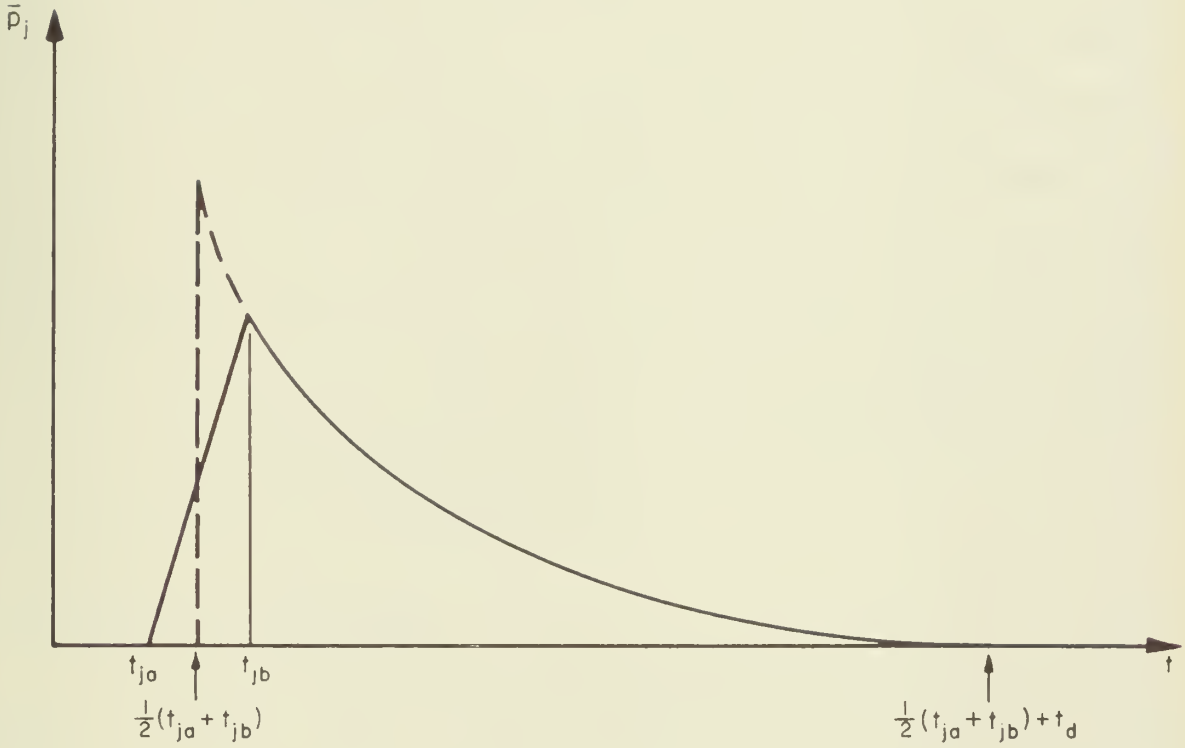

Figure 6.4. Generalized Overpressure-Time Diagram for Typical Loading Region

CHAPTER VII

EQUATIONS OF MOTION

Now that expressions for the equivalent forces, masses and resistances of the two-degree-of-freedom system have been derived, it is possible to develop the equations of motion for the system in terms of these quantities. While a simplified notation is used throughout this chapter, the expressions may be expanded readily by inserting the proper expressions from Chapters III through VI. As an aid in visualizing the two-degree-of-freedom system, the equivalent masses, resistances and loads are considered to exist and act at the haunches, i.e. at joints 1 and 3 of the model. This is only a physical analogy, but it is convenient in comparing the expressions derived in this chapter with those of the preceding chapters.

7.1 Development of Equations

The forces acting on one of the two equivalent masses are shown in Figure 7.1 in general terms. A general expression for the equations of motion may be obtained by applying d'Alembert's Principle and equating the sum of the horizontal forces acting on the mass to zero. The result is given in Equation (7.1.1).

$$\bar{m}_{j,m}\ddot{h}_j + Q_j + \bar{Q}_{sj} = \bar{H}_j \tag{7.1.1}$$

where $\bar{m}_{j,m}$ = equivalent mass of j

$\ddot{h}_j$ = acceleration of mass j

Q_j = equivalent deformation resistance of the arch at j

$\bar{Q}_{sj}$ = equivalent deformation resistance of the soil at j

$\bar{H}_j$ = equivalent load acting on mass j.

Since each of the equivalent masses is actually a function of both of the independent accelerations (cf. Equations (5.2.6)), the two equations

of motion as expressed by Equations (7.1.1) are not in a convenient form for integration. However, since Equations (5.2.6) are linear in the acceleration terms, the equations of motion may be rewritten explicitly for the independent acceleration components as shown in the following derivation.

Equations (7.1.2) are obtained by substituting Equations (5.2.6) into Equations (7.1.1).

$$\begin{aligned} \mu_{1,m}\ddot{h}_1 - \nu_{1,m}\ddot{h}_3 &= \bar{H}_1 - Q_1 - \bar{Q}_{s1} \\ -\nu_{3,m}\ddot{h}_1 + \mu_{3,m}\ddot{h}_3 &= \bar{H}_3 - Q_3 - \bar{Q}_{s3} \end{aligned} \qquad (7.1.2)$$

Solving Equations (7.1.2) simultaneously for $\ddot{h}_1$ and $\ddot{h}_3$ gives Equations (7.1.3).

$$\begin{aligned} \ddot{h}_1 &= \frac{\mu_{3,m}}{\mu_{1,m}\mu_{3,m}-\nu_{1,m}\nu_{3,m}}(\bar{H}_1-Q_1-\bar{Q}_{s1}) + \frac{\nu_{1,m}}{\mu_{1,m}\mu_{3,m}-\nu_{1,m}\nu_{3,m}}(\bar{H}_3-Q_3-\bar{Q}_{s3}) \\ \ddot{h}_3 &= \frac{\nu_{3,m}}{\mu_{1,m}\mu_{3,m}-\nu_{1,m}\nu_{3,m}}(\bar{H}_1-Q_1-\bar{Q}_{s1}) + \frac{\mu_{1,m}}{\mu_{1,m}\mu_{3,m}-\nu_{1,m}\nu_{3,m}}(\bar{H}_3-Q_3-\bar{Q}_{s3}) \end{aligned} \qquad (7.1.3)$$

The notation of Equations (7.1.3) may be simplified as shown in Equations (7.1.4).

$$\begin{aligned} \ddot{h}_1 &= F_{1,m}(\bar{H}_1-Q_1-\bar{Q}_{s1}) + G_{1,m}(\bar{H}_3- Q_3-\bar{Q}_{s3}) \\ \ddot{h}_3 &= F_{3,m}(\bar{H}_1-Q_1-\bar{Q}_{s1}) + G_{3,m}(\bar{H}_3- Q_3-\bar{Q}_{s3}) \end{aligned} \qquad (7.1.4)$$

where $F_{1,m} = \dfrac{\mu_{3,m}}{\mu_{1,m}\mu_{3,m}-\nu_{1,m}\nu_{3,m}}$

$$G_{1,m} = \frac{\nu_{1,m}}{\mu_{1,m}\mu_{3,m}-\nu_{1,m}\nu_{3,m}}$$

$$F_{3,m} = \frac{\nu_{3,m}}{\mu_{1,m}\mu_{3,m}-\nu_{1,m}\nu_{3,m}}$$

$$G_{3,m} = \frac{\mu_{1,m}}{\mu_{1,m}\mu_{3,m}-\nu_{1,m}\nu_{3,m}}$$

m = index denoting the motion of the system as defined in Section 5.2. m = 1,2,3,4.

Equations (7.1.4) may now be integrated simultaneously in order to obtain the velocities and displacements of the system at any time under a given set of dynamic loads.

7.2 Natural Periods of Vibration

The natural periods of vibration of any system are highly significant parameters in predicting the response of that system to dynamic loads. The natural periods of the model which is used in this study for the dynamic analysis may be found quite readily from the equations of motion derived in the preceding section.

Before proceeding with the derivation of expressions for the natural periods of vibration of the model, however, it is convenient to express the resistance of the arch, Equations (3.4.7), in a slightly different form. Equations (3.4.7) express the equivalent resistance of the arch in terms of the resisting moments developed at the hinges of the model. While this is convenient for use in an elasto-plastic analysis, it is inconvenient for the purpose of finding the natural periods of vibration corresponding to the initial, elastic response of the system.

The elastic resistance of the model may be expressed in terms of the independent displacement coordinates by substituting Equations (3.2.11) and (3.3.1) into Equations (3.4.7).

$$\begin{aligned} Q_1 &= K_B(A_1h_1-A_3h_3)(q_a+q_bh_1-q_bh_3) - K_B(-A_2h_1+A_2h_3)(q_c+q_dh_1-q_bh_3) \\ Q_3 &= K_B(-A_3h_1+A_1h_3)(q_a+q_bh_1-q_bh_3) + K_B(-A_2h_1+A_2h_3)(q_c+q_bh_1-q_dh_3) \end{aligned} \qquad (7.2.1)$$

Equations (7.2.1) may be simplified by limiting consideration to small displacements such that the products of the displacements are small with respect to the remaining terms and may be neglected. The simplified expressions are given as Equations (7.2.2).

$$
\begin{aligned}
Q_1 &= (A_1q_a+A_2q_c)K_Bh_1 - (A_3q_a+A_2q_c)K_Bh_3 \\
Q_3 &= -(A_3q_a+A_2q_c)K_Bh_1 + (A_1q_a+A_2q_c)K_Bh_3
\end{aligned}
\qquad (7.2.2)
$$

The notation in Equations (7.2.2) may be simplified as shown in Equations (7.2.3).

$$
\begin{aligned}
Q_1 &= \tau_1h_1 - \tau_3h_3 \\
Q_3 &= -\tau_3h_1 + \tau_1h_3
\end{aligned}
\qquad (7.2.3)
$$

where

$$
\begin{aligned}
\tau_1 &= (A_1q_a + A_2q_c)K_B \\
&= (K_B/2L^2)(5+a/c+b/d+2c/a+bc/ad) \\
\tau_3 &= (A_3q_a+A_2q_c)K_B \\
&= (K_B/2L^2)(3 + a/c - b/d - bc/ad)
\end{aligned}
$$

The discussion will now proceed with the derivation of expressions for the natural periods of vibration of the system. One may write the equations of motion for the system in free vibration, Equations (7.2.4), directly from the general equations of motion for the system, Equations (7.1.1), by eliminating the loading terms.

$$\bar{m}_{j,m}\ddot{h}_j + Q_j + \bar{Q}_{sj} = 0 \qquad (7.2.4)$$

If a sinusoidally varying time function is assumed for the motions of the system, the accelerations, $\ddot{h}_j$, and displacements, h_j, of the system are related as shown in Equations (7.2.5).

$$\ddot{h}_j = -\omega_m^2 h_j \qquad (7.2.5)$$

where ω_m = circular natural frequency of the system for the particular motion being studied (cf. Section 5.2).

Equations (7.2.4) may be rewritten in expanded form by inserting Equations (5.2.6) and (7.2.5). The result is given as Equations (7.2.6).

$$\begin{aligned} -\mu_{1,m}\omega_m^2 h_1 + \nu_{1,m}\omega_m^2 h_3 + Q_1 + \bar{Q}_{s1} &= 0 \\ \nu_{3,m}\omega_m^2 h_1 - \mu_{3,m}\omega_m^2 h_3 + Q_3 + \bar{Q}_{s3} &= 0 \end{aligned} \tag{7.2.6}$$

Substituting Equations (4.4.14) and (7.2.3) into Equations (7.2.6) gives:

$$\begin{aligned} \mu_{1,m}\omega_m^2 h_1 - \nu_{1,m}\omega_m^2 h_3 - \tau_1 h_1 + \tau_3 h_3 - (\bar{K}_{s1}/a)h_1 &= 0 \\ -\nu_{3,m}\omega_m^2 h_1 + \mu_{3,m}\omega_m^2 h_3 + \tau_3 h_1 - \tau_1 h_3 - (\bar{K}_{s3}/a)h_3 &= 0 \end{aligned} \tag{7.2.7}$$

Note that Equation (4.4.15) must be used in lieu of Equation (4.4.14) for either of Equations (7.2.7) when the motion being considered is such that the haunch is displaced outward against the soil rather than inward into the arch. This qualification also applies to the remainder of this derivation. Rewriting and rearranging Equations (7.2.7) gives:

$$\begin{aligned} (\mu_{1,m}\omega_m^2 - \tau_1 - \bar{K}_{s1}/a)h_1 + (-\nu_{1,m}\omega_m^2 + \tau_3)h_3 &= 0 \\ (-\nu_{3,m}\omega_m^2 + \tau_3)h_1 + (\mu_{3,m}\omega_m^2 - \tau_1 - \bar{K}_{s3}/a)h_3 &= 0 \end{aligned} \tag{7.2.8}$$

Equations (7.2.8) yield solutions different from zero only if their determinant vanishes. This permits Equation (7.2.9), the frequency equation, to be written in terms of the circular natural frequencies of the system.

$$\begin{aligned} &\left[\mu_{1,m}\mu_{3,m} - \nu_{1,m}\nu_{3,m}\right]\omega_m^4 - \Big[\mu_{1,m}(\tau_1 + \bar{K}_{s3}/a) \\ &\quad + \mu_{3,m}(\tau_1 + \bar{K}_{s1}/a) - \tau_3(\nu_{1,m} + \nu_{3,m})\Big]\omega_m^2 \\ &\quad + \left[(-\tau_1 - \bar{K}_{s1}/a)(-\tau_1 - \bar{K}_{s3}/a) - (\tau_3)^2\right] = 0 \end{aligned} \tag{7.2.9}$$

The circular natural frequency for any one of the four motions of the system (cf. Section 5.2) may be obtained by substituting the proper values of $\mu_{1,m}$, $\nu_{1,m}$, $\mu_{3,m}$, and $\nu_{3,m}$ (cf. Equation (5.2.6)) and the proper expressions for soil stiffness, i.e. either $\bar{K}_{sj}$ or $\bar{K}'_{sj}$ (cf. Equations (4.4.14) and (4.4.15)),

into Equation (7.2.9) and solving for ω_m. Note that since both $\bar{K}_{sj}$ and $\bar{K}'_{sj}$ are functions of the overpressure restraining the soil, the circular natural frequency, hence the natural period of vibration, of the system will vary as the shock wave passes over the structure. In general, solution of Equation (7.2.9) yields two values of ω_m^2. The proper value may be selected by substituting the values, in turn, into Equations (7.2.8) and noting the relationship between the displacements h_1 and h_3. The proper value is indicated when the relationship between h_1 and h_3 agrees with the system motion being studied.

Once the proper circular natural frequency has been found, it may be substituted into Equation (7.2.10) and the natural period of vibration of the system, T_m, obtained for the particular system motion and overpressure conditions being studied.

$$T_m = \frac{2\pi}{\omega_m} \tag{7.2.10}$$

While there is no real advantage in solving Equation (7.2.9) in general terms, a simplified expression for the circular natural frequency can be written for those special cases in which the stiffness and mass parameters are symmetrical. In this study this condition exists, for example, for the "Symmetric-In" and "Symmetric-Out" motions with no overpressure restraining movement of the soil. Equation (7.2.11) is obtained by setting $\mu_{1,m} = \mu_{3,m} = \mu_m$, $\nu_{1,m} = \nu_{3,m} = \nu_m$ and $\bar{K}_{s1} = \bar{K}_{s3} = \bar{K}_s$ in Equation (7.2.9) and solving for the value of ω_m corresponding to symmetrical response.

$$\omega_m = \sqrt{\frac{\tau_1 + \tau_3 + \bar{K}_s/a}{\mu_m + \nu_m}} \tag{7.2.11}$$

Note that $\bar{K}'_s/a$ may be used in place of $\bar{K}_s/a$ in Equation (7.2.11) if the motion being studied so indicates.

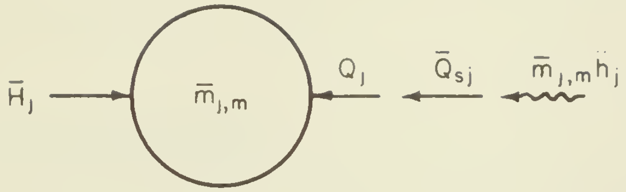

Figure 7.1. Forces Acting on Typical Equivalent Mass

CHAPTER VIII

NUMERICAL STUDIES

This chapter covers the basis of the numerical studies made in connection with this thesis. The range of variables included in the studies is given together with a description of the blast wave properties used. The numerical examples are described and, finally, a set of sample calculations is included. The results of these studies are presented in tabular and in graphical form in Appendices C and D.

8.1 Range of Variables Studied

The quantitative investigations made in connection with this thesis are designed to illustrate the behavior of shallow-buried, two-hinged arches subjected to nuclear blast loading. Two different arches are used, one a semicircular, reinforced concrete arch, 16'8" in diameter, and the other a corrugated metal arch in the form of a segment of a circle with a rise of 11' 8 1/2" and a span of 25' 1 1/4". The concrete arch has a uniform thickness of 8" and is reinforced with No. 4 bars running circumferentially on 10" centers at mid-thickness. Intermediate grade reinforcing steel is used with an assumed yield strength of 50 ksi under dynamic load. The elastic modulus of the steel is taken as 30,000 ksi. The average strength of the concrete as measured by the standard 6" x 12" test cylinder is taken as 3.5 ksi at 28 days. Substituting this value for the concrete cylinder strength into the appropriate expressions of reference (22) yields a corresponding elastic modulus for the concrete of 3,820 ksi. The corrugated metal arch is 10 gauge with an elastic modulus of 30,000 ksi and an assumed yield strength of 30 ksi under dynamic loading.

The arches are studied at depths of cover over the crown varying from zero to one-half of the arch span. Intermediate depths of cover of one-eighth and one-quarter of the span are used.

The soil cover is taken as a granular, cohesionless material with a unit weight of 120 pcf, an angle of internal friction of 30° and a hydrostatic pressure ratio of horizontal to vertical soil pressures in the "at rest" state of stress of 0.5. The friction angle between the soil and the arch is assumed as two-thirds of the angle of internal friction of the soil, or 20°. The seismic velocity of the soil is assumed as 3,000 feet per second for the majority of the numerical work; however, a series of problems is included varying the seismic velocity from 1,000 feet per second to 3,000 feet per second in order to study the significance of this parameter.

The blast loading is assumed to result from a contact surface burst of a one-megaton nuclear weapon. Overpressures ranging from 50 psi to 1,000 psi are considered. The shock wave properties are discussed in Section 8.2.

Approximate calculations based upon reference (16) indicate that the overpressures selected occur outside of the crater and therefore are in agreement with the loading assumptions discussed in Section 2.4. Structures located at the higher overpressures will probably be inside the fireball and will also be subjected to heavy doses of nuclear radiation. Again, as discussed in Section 2.4, these effects must be considered in any actual design; however, they will have little or no effect upon the structural response of the arch.

The majority of the numerical solutions are computed assuming a ratio of horizontal to vertical overpressure in the soil of one-fourth. In addition a series of problems is included in which this ratio is varied from one-fourth to one.

8.2 Shock Wave Properties

The shock wave parameters used in this study are taken from references (16), (17) and (20). A summary of the more significant parameters is presented in Table 8.1. There is some disagreement among authorities$^{(17,20)}$ on the duration of the positive phase of the shock wave in the higher overpressure regions. The differences in the values given are not great, however, when one considers the actual variation in all shock wave parameters to be expected in the field. Further, small differences in positive phase duration are not significant in this study because of the rapid response of the arch (cf. Appendix D). However, the rapid response of the arch does make the system quite sensitive to the initial shape of the blast wave. Therefore, while the positive phase duration for the 1000-psi shock wave may be taken as the same as that for a 100-psi shock wave without significantly affecting the results, the initial shape of the two shock waves must be defined carefully. This latter aspect of the problem is discussed in detail in the following paragraphs.

The results of a study of the configuration of the shock front in soil are presented in Appendix B.

The decay with time of the overpressure behind the shock front is discussed in reference (20). Later studies of shock wave characteristics are available but are not used here because of their security classification. Reference (20) gives the following approximate expressions for the variation with time of the overpressure at a point behind the shock front during the passage of the positive phase of the shock wave.

$$0 \leq t' \leq t_d: \qquad p(t')/p_{so} = (1 - t'/t_d)\, e^{-\alpha(t'/t_d)} \qquad (8.2.1)$$

$$45 \text{ psi} < p_{so} < 700 \text{ psi}: \qquad \alpha = a_1 + \frac{b_1}{1+c_1(t'/t_d)} \qquad (8.2.2)$$

where t' = elapsed time at the reference point after the shock front has passed

$p(t')$ = overpressure at the reference point at time t'

p_{so} = peak value of the overpressure as the shock front passes the reference point

t_d = duration of the positive phase of the shock wave at the reference point

e = natural logarithmic base = 2.71828...

$$a_1 \begin{cases} = -0.231 + 0.388(p_{so}/P_o) - 0.0332(p_{so}/P_o)^2; & p_{so} \leq 150 \text{ psi} \\ = 0; & p_{so} > 150 \text{ psi} \end{cases}$$

$$b_1 \begin{cases} = (p_{so}/P_o)[0.88 + 0.072(p_{so}/P_o)]; & p_{so} < 150 \text{ psi} \\ = (p_{so}/P_o)[1.67 - 0.011(p_{so}/P_o)]; & p_{so} > 150 \text{ psi} \end{cases}$$

$c_1 = 8.71 + 0.1843(p_{so}/P_o) - 104/[(p_{so}/P_o) + 10]$

P_o = ambient atmospheric pressure (taken as 14.7 psi for numerical work in this study).

The overpressure-time relationship for 50 psi is obtained by substituting p_{so} = 50 psi and t_d = 1.60 seconds (cf. Table 8.1) into Equations (8.2.1) and (8.2.2). The resulting expression is given as Equation (8.2.3).

$$p(t')/50 = (1-t'/160)\, e^{-[0.705+3.83/(1+t')]t'/1.60} \qquad (8.2.3)$$

The computer program used in this study for the solution of the numerical examples (cf. Section 8.3) approximates the "actual" overpressure-time curves with a series of straight-line segments. These line segments may be obtained for the 50-psi shock wave by plotting Equation (8.2.3) and selecting a series of straight-line segments which approximate the curve to a reasonable degree over the time interval of interest. The coordinates of the endpoints of the lines selected are given in Table 8.2.

The overpressure-time relationship for 100 psi may be obtained by substituting p_{so} = 100 psi and t_d = 1.48 seconds (cf. Table 8.1) into Equations (8.2.1) and (8.2.2). The resulting expression is given as Equation (8.2.4).

$$p(t')/100 = (1-t'/1.48)\, e^{-[0.872 + \frac{9.32}{1+3.78(t'/1.48)}] \frac{t}{1.48}} \qquad (8.2.4)$$

Proceeding as in the case of the 50-psi shock wave gives the lines defined by the overpressure-time coordinates listed in Table 8.3 as an approximation to the overpressure-time curve.

Since the 1,000-psi shock wave falls outside the range in which Equations (8.2.1) and (8.2.2) apply, the overpressure-time relationship for this shock wave may be obtained by interpolating in the curves of references (20) and (23). This was done and a series of straight-line segments selected which approximate the "actual" overpressure-time curve reasonably well. The line segments selected are defined by the overpressure-time coordinates listed in Table 8.4.

8.3 Description of Numerical Examples

The properties of the arches selected for the numerical examples are given in Section 8.1. Table 8.5 indicates the variations in parameters applied to each of these arches.

The lower value of overpressure to which the reinforced concrete arch is subjected is well below the level which should cause buckling or general yielding of the arch due to thrust in the arch rib (cf. Section 8.4). The higher value of 1,000 psi is selected to magnify any tendencies of the arch to respond laterally. It is not intended to be below buckling or general yielding limitations. As pointed out in Chapter IX, however, the arch rib contributes relatively little to the lateral resistance of the arch-soil "structure" as compared with the soil contribution. Therefore, the 1,000-psi results are indicative of the response of an arch with a sufficiently large cross section that buckling and general yielding are no longer critical.

The 50-psi loading on the corrugated metal arch is reasonably close to the overpressure causing general yielding due to thrust in the arch rib for the assumed soil and loading conditions. In fact, the case of zero depth of cover over the crown could very well be ruled out of any practical consideration on this basis alone; however, it is included in this study for comparison purposes. The 100-psi and 1,000-psi loadings are used to give a comparison with the corresponding loadings on the reinforced concrete arch.

Further, the observation made above in the case of the reinforced concrete arch, regarding the relative contributions of the arch and the soil to the lateral resistance of the system, is even more applicable here. Therefore, it may be stated that if the arch is strengthened sufficiently to withstand the thrusts developed in the arch rib, the response results of the 100-psi and 1,000-psi studies should be indicative of the response of the strengthened structure.

Integration of the equations of motion for each of the numerical examples was done on the Illiac, the high-speed digital computer at the University of Illinois. Structural Research Laboratory Code 462(24) was adapted to perform this integration.

Tabular comparisons of the results obtained from the examples listed in Table 8.5 are presented in Appendix C. Response curves and configuration diagrams for the arch at various critical times are presented in Appendix D.

8.4 Sample Calculations

Calculations are presented here for the reinforced concrete arch with a depth of cover over the crown equal to one-fourth of the arch span. The arch and soil cover are shown in Figure 8.1. The arch is subjected to a 100-psi shock wave from the explosion of a one megaton nuclear weapon as a contact surface burst. The seismic velocity of the soil is assumed as 3,000 feet per second and the horizontal overpressure induced in the soil by the shock wave is assumed to be one-fourth of the vertical overpressure. In general, the calculations are based on a one-foot width parallel to the longitudinal axis of the arch (cf. Section 2.1).

8.4.1 Calculation of Parameters and Coefficients

The horizontal displacements of the haunches, h_1 and h_3, are chosen as the independent displacements. The remaining displacements are related to them by Equations (3.2.7).

$$h_2 = \frac{1}{2}(1-bc/ad)(h_1+h_3)$$

$$= \frac{1}{2}[1-(2.440)^2/(5.893)^2][h_1+h_3]$$

$$h_2 = 0.4143(h_1+h_3) \qquad (8.4.1)$$

$$h_4 = -(b/a)h_1$$

$$= -(2.440/5.893)h_1$$

$$h_4 = -0.4141\ h_1 \qquad (8.4.2)$$

$$h_5 = \frac{1}{2}(d/c-b/a)(h_1-h_3)$$

$$= \frac{1}{2}(5.893/2.440 - 2.440/5.893)(h_1-h_3)$$

$$h_5 = 1.0006(h_1-h_3) \qquad (8.4.3)$$

$$h_6 = (b/a)h_3$$

$$= (2.440/5.893)h_3$$

$$h_6 = 0.4141\ h_3 \qquad (8.4.4)$$

The total rotations of the joints are related to the independent displacements by Equations (3.2.11).

$$A_1 = \frac{1}{2}(2/a+1/c+b/ad)$$

$$= \frac{1}{2}[2/5.893 + 1/2.440 + 2.440/(5.893)^2]$$

$$= 0.4098\ ft^{-1}$$

$$A_2 = 1/c$$

$$= 1/2.440$$

$$= 0.4098\ ft^{-1}$$

$$A_3 = \frac{1}{2}\,(1/c - b/ad)$$

$$= \frac{1}{2}\,[1/2.440 - 2.440/(5.893)^2]$$

$$= 0.1698 \text{ ft}^{-1}$$

$$\psi_1 = A_1h_1 - A_3h_3$$

$$\psi_1 = 0.4098\ h_1 - 0.1698\ h_3 \tag{8.4.5}$$

$$\psi_2 = -A_2h_1 + A_2h_3$$

$$\psi_2 = -\ 0.4098\ h_1 + 0.4098\ h_3 \tag{8.4.6}$$

$$\psi_3 = A_3h_1 - A_1h_3$$

$$\psi_3 = 0.1698\ h_1 - 0.4098\ h_3 \tag{8.4.7}$$

The general form of the moment-rotation relationship for the model hinges is shown in Figure 8.2. The dimensions on this figure may be found using Equation (3.3.1). The material properties for the arch are listed in Section 8.1. Figure 8.3 is a sketch of the cross section of the arch rib. Now, in the derivation which follows, neglect direct stress in the arch rib and let:

h_a = thickness of the concrete arch rib

d_a = effective depth of the concrete arch rib

b_a = width of the arch rib parallel to the longitudinal axis of the arch

j = ratio of the distance, jd_a, between the resultants of the compressive and tensile stresses to the effective depth, d_a

k = ratio of the distance, kd_a, between the extreme fiber and the neutral axis to the effective depth, d_a

I_g = gross moment of inertia of the arch rib cross section

I_t = transformed moment of inertia of the arch rib cross section

I_j = average moment of inertia of the arch rib cross section

A_s = area of reinforcing steel in a one-foot width of arch

f'_c = 28-day strength of a standard 6" x 12" concrete test cylinder

f_{dy} = yield strength of the reinforcing steel under dynamic loading

E_s = modulus of elasticity of the reinforcing steel

E_j = modulus of elasticity of the concrete in the arch

n = modular ratio for steel and concrete.

From reference (22):

$$n = 5 + 10{,}000/f'_c$$

$$= 5 + 10{,}000/3{,}500$$

$$= 7.86$$

Then:

$$E_j = E_s/n$$

$$= 30 \times 10^6/7.86$$

$$= 3.82 \times 10^6 \text{ psi}$$

$$M_y = A_s f_{dy} jd_a$$

$$= 0.24(50)(7/8)(4)(1/12)$$

$$= 3.50 \text{ ft-kips}$$

$$I_g = b_a(h_a)^3/12$$

$$= 12(8)^3/12$$

$$= 512 \text{ in}^4$$

$$I_t = b_a(kd_a)^3/3 + nA_s d_a^2(1-k)^2$$

$$= \frac{12}{3}\,[(3/8)(4)]^3 + 7.86(0.24)(4)^2(1-3/8)^2$$

$$= 25.3 \text{ in}^4$$

$$I_j = \frac{1}{2}(I_g + I_t)$$

$$= \frac{1}{2}(512 + 25.3)$$

$$= 268.6 \text{ in}^4$$

$$K_B = E_j I_j / L_j$$

$$= (3.82 \times 10^6)(268.6)/(6.378)(12)$$

$$= 1117.2 \text{ ft-kips/radian}$$

$$\psi_y = M_y / K_B$$

$$= 3.50/1117.2$$

$$= 0.003133 \text{ radians}$$

The relationships shown in Figure 8.2 are expressed algebraically in Equations (8.4.8)

$$\begin{aligned} 0 \le \psi_j \le \psi_y &: \quad M_j = K_B \psi_j \\ \psi_y \le \psi_j &: \quad M_j = M_y \end{aligned} \qquad (8.4.8)$$

Note that the value of ψ_y must be adjusted for any "permanent set" in the hinge as the structure responds. Also, Equations (8.4.8) are valid for rotation in either direction. For convenience, the inequalities at the left of Equations (8.4.8) are shown for the positive direction of rotation only.

The equivalent arch resistance may be found using Equations (3.4.7).

$$q_a = (1/L^2)(a+c)$$

$$= [1/(6.378)^2][5.893 + 2.440]$$

$$= 0.2049 \text{ ft}^{-1}$$

$$q_b = (1/2L^2)(d/c - b/a)$$

$$= [1/2(6.378)^2][5.893/2.440 - 2.440/5.893]$$

$$= 0.0246 \text{ ft}^{-2}$$

$$q_c = c/L^2$$

$$= 2.440/(6.378)^2$$

$$= 0.0600\ \text{ft}^{-1}$$

$$q_d = (1/2L^2)(d/c+b/a)$$

$$= [1/2(6.378)^2][5.893/2.440 + 2.440/5.893]$$

$$= 0.0348\ \text{ft}^{-2}$$

$$Q_1 = M_1(q_a+q_b h_1-q_b h_3) - M_2(q_c+q_d h_1-q_b h_3)$$

$$Q_3 = - M_3(q_a+q_b h_1-q_b h_3) + M_2(q_c+q_b h_1-q_d h_3)$$

$$Q_1 = M_1(0.2049 + 0.0246\ h_1 - 0.0246\ h_3)$$

$$- M_2(0.0600 + 0.0348\ h_1 - 0.0246\ h_3)$$

$$Q_3 = - M_3(0.2049 + 0.0246\ h_1 - 0.0246\ h_3)$$

$$+ M_2(0.0600 + 0.0246\ h_1 - 0.0348\ h_3) \qquad (8.4.9)$$

From the results of the study presented in Appendix A one may conclude that the hydrostatic pressure ratios for soil pressures corresponding to the fully active and the fully passive states of stress in the soil may be calculated to a reasonable degree of approximation using the Coulomb formulas (cf. reference (14)).

$$K_A = \frac{\cos^2(\varphi-\omega)}{\cos^2\omega\ \cos(\delta+\omega)\left[1 + \sqrt{\dfrac{\sin(\delta+\varphi)\sin(\varphi-i)}{\cos(\delta+\omega)\cos(\omega-i)}}\right]^2} \qquad (8.4.10)$$

where K_A = hydrostatic pressure ratio corresponding to the "Active State of Plastic Equilibrium" in the soil (cf. Section 2.2)

φ = angle of internal friction of the soil

ω = angle of inclination with respect to the vertical of the lower bars of the model

δ = effective friction angle between the arch and the soil

i = slope of the ground surface with respect to the horizontal

$$K_A = \frac{\cos^2(30^\circ - 22^\circ 29.6')}{\cos^2(22^\circ 29.6')\cos(20^\circ+22^\circ 29.6')\left[1 + \sqrt{\dfrac{\sin(20^\circ+30^\circ)\sin 30^\circ}{\cos(20^\circ+22^\circ 29.6')\cos(22^\circ 29.6')}}\right]^2}$$

$$K_A = 0.510$$

$$K_P = \frac{\cos^2(\varphi+\omega)}{\cos^2\omega\,\cos(\omega-\delta)\left[1 - \sqrt{\dfrac{\sin(\varphi+\delta)\sin(\varphi+i)}{\cos(\omega-\delta)\cos(\omega-i)}}\right]^2} \qquad (8.4.11)$$

where K_P = hydrostatic pressure ratio corresponding to the "Passive State of Plastic Equilibrium" in the soil (cf. Section 2.2).

$$K_P = \frac{\cos^2(30^\circ+22^\circ 29.6')}{\cos^2(22^\circ 29.6')\cos(22^\circ 29.6'-20^\circ)\left[1 - \sqrt{\dfrac{\sin(30^\circ+20^\circ)\sin 30^\circ}{\cos(22^\circ 29.6'-20^\circ)\cos(22^\circ 29.6')}}\right]^2}$$

$$= 3.433$$

The soil pressure ratios corresponding to the directions of P'_A and P'_P for an "at rest" state of stress in the soil (cf. Section 2.2) may be found using Equations (4.1.11) and (4.2.11).

$$K_{OA} = \sqrt{1+k_o^2}\cos[(\omega+\delta)-\arctan(1/k_o)]$$

$$= \sqrt{1+(0.5)^2}\cos[(22^\circ 29.6'+20^\circ)-\arctan(1/0.5)]$$

$$= 1.051^*$$

$$K_{OP} = \sqrt{1+k_o^2}\cos[\arctan(1/k_o) - (\omega-\delta)]$$

$$= \sqrt{1+(0.5)^2}\cos[\arctan(1/0.5) - (22^\circ 29.6'-20^\circ)]$$

$$= 0.543$$

The deformation corresponding to full development of the "active" state of stress in the soil is taken as an inward rotation of the lower bar

---

* An error of 1.3% in K_{OA} is introduced at this point. It was found to cause a change in the calculated response of less than 1%.

of the model, $\xi_{\ell y}$, of 0.001 radian (cf. Section 4.4). The deformation corresponding to full development of the "passive" state of stress in the soil is then taken as an outward rotation of the lower bar of the model, $\xi'_{\ell y}$, as given by Equation (4.4.8).

$$\xi'_{\ell y} = \xi_{\ell y}\left(\frac{K_P - K_{OP}}{K_{OA} - K_A}\right)$$

$$= 0.001\left(\frac{3.433 - 0.543}{1.051 - 0.510}\right)$$

$$= 0.005342 \text{ radian}$$

While $\xi'_{\ell y}$ is not known to this degree of precision, it is convenient to retain a sufficient number of significant figures that calculation of the slope of the "elastic" line in the soil resistance-deformation relationship (cf. Figure 4.12) will give the same result for the build-up of both the "active" and the "passive" states of stress in the soil at a given overpressure level as assumed in Section 4.4.

Expressions for the soil "stiffness" may now be obtained from Equations (4.4.10) and (4.4.12).

$$k' = \frac{\gamma_s d_o^3}{6a\ \xi_{\ell y}}(K_{OA}-K_A)[\cos(\omega+\delta)+(b/a)\sin(\omega+\delta)]$$

$$= \frac{0.120(12.500)^3(1.051-0.510)}{6(5.893)(0.001)}[\cos(22^\circ 29.6'+20^\circ)$$

$$+ \left(\frac{2.440}{5.893}\right)\sin(22^\circ 29.6'+20^\circ)]$$

$$= 3647 \text{ kips/radian}$$

$$k'' = (3/\gamma_s d_o)k'$$

$$= [3(3647)/(0.120)(12.500)][0.144]$$

$$= 1050 \text{ kips/radian-psi}$$

$$\bar{K}_{sj} = k' - k''\bar{p}_{sj}$$

$$\bar{K}_{sj} = 3647 - 1050\ \bar{p}_{sj} \tag{8.4.12}$$

$$\bar{K}'_{sj} = k' - k''\bar{p}'_{sj}$$

$$\bar{K}'_{sj} = 3647 - 1050\ \bar{p}'_{sj} \tag{8.4.13}$$

Alternatively, the soil stiffness may be expressed using Equations (4.4.14) and (4.4.15).

$$\bar{K}_{sj}/a = (k'-k''\ \bar{p}_{sj})/a$$

$$= (3647-1050\ \bar{p}_{sj})/5.893$$

$$\bar{K}_{sj}/a = 618.9 - 178.2\ \bar{p}_{sj} \tag{8.4.14}$$

$$\bar{K}'_{sj}/a = (k'-k''\ \bar{p}'_{sj})/a$$

$$\bar{K}'_{sj}/a = 618.9 - 178.2\ \bar{p}'_{sj} \tag{8.4.15}$$

The soil resistance-deformation diagram for this problem is shown in Figure 8.4.

The mass concentrations corresponding to the horizontal and vertical components of the inertial forces acting at the joints of the model are given by Equations (5.1.13). The geometry of the arch-soil "structure" is shown in Figure 8.1. The geometry of the soil masses assumed to move with the arch is shown in Figures 5.1 and 5.2. The limiting vertical dimensions of the soil masses at the haunches are determined using Equations (5.1.3) and (5.1.4).

$$d_{ml} = [(a/2)+c+d_c] \leq (b+d)$$

$$[(\frac{5.893}{2}) + 2.440 + 4.167] \overset{?}{\leq} (2.440+5.893)$$

$$9.554 > 8.333$$

$\therefore$ use : $d_{m1} = 8.333$ ft

$$d_{m2} = [(c/2)+d_c] \leq 2d$$

$$[(2.440/2) + 4.167] \overset{?}{\leq} 2(5.893)$$

$$5.387 < 11.786$$

$\therefore$ use: $d_{m2} = 5.387$ ft.

$$(m_1)_{in} = \frac{\gamma_s}{2g}\left[d_{m1}(\frac{b}{2})+(d_{m1}-\frac{a}{2})(\frac{b+d}{2}) + (d_{m1}-\frac{a+c}{2})(\frac{d}{2})+d_{m1}^2 \cot(\frac{\pi}{4}+\frac{\varphi}{2})\right]$$

$$+ \gamma_a h_a L/g$$

$$= \frac{0.120}{2(32.2)}\left[8.333(\frac{2.440}{2}) + (8.333 - \frac{5.893}{2})(\frac{2.440 + 5.893}{2})\right.$$

$$\left. + (8.333 - \frac{5.893 + 2.440}{2})(\frac{5.893}{2}) + (8.333)^2 \cot 60^\circ\right]$$

$$+ \frac{0.150(8)(6.378)}{12(32.2)}$$

$$= 0.1782 \text{ k-sec}^2/\text{ft}$$

$$(m_1)_{out} = \frac{\gamma_s}{2g}\left[d_{m1}(\frac{b}{2})+(d_{m1}-\frac{a}{2})(\frac{b+d}{2}) + (d_{m1}-\frac{a+c}{2})(\frac{d}{2}) + d_{m1}^2 \cot(\frac{\pi}{4}-\frac{\varphi}{2})\right]$$

$$+ \gamma_a h_a L/g$$

$$= \frac{0.120}{2(32.2)}\left[8.333(\frac{2.440}{2}) + (8.333- \frac{5.893}{2})(\frac{2.440 + 5.893}{2})\right.$$

$$\left. + (8.333 - \frac{5.893 + 2.440}{2})(\frac{5.893}{2}) + (8.333)^2 \cot 30^\circ\right]$$

$$+ \frac{0.150(8)(6.378)}{12(32.2)}$$

$$= 0.3276 \text{ k-sec}^2/\text{ft}$$

$$m_2 = \frac{\gamma_s d}{g} (d_{m2} - \frac{c}{4}) + \frac{\gamma_a h_a L}{g}$$

$$= \frac{0.120(5.893)}{32.2} (5.387 - \frac{2.440}{4}) + \frac{0.150(8)(6.378)}{12(32.2)}$$

$$= 0.1247 \text{ k-sec}^2/\text{ft}$$

$$(m_3)_{in} = (m_1)_{in}$$

$$= 0.1782 \text{ k-sec}^2/\text{ft}$$

$$(m_3)_{out} = (m_1)_{out}$$

$$= 0.3276 \text{ k-sec}^2/\text{ft}$$

$$m_4 = \frac{\gamma_s}{2g} \left[d_{m1}(\frac{b}{2}) + (d_{m1} - \frac{a}{2})(\frac{b+d}{2}) + (d_{m1} - \frac{a+c}{2})(\frac{d}{2}) \right] + \frac{\gamma_a h_a L}{g}$$

$$= \frac{0.120}{2(32.2)} \left[8.333(\frac{2.440}{2}) + (8.333 - \frac{5.893}{2})(\frac{2.440 + 5.893}{2}) \right.$$

$$\left. + (8.333 - \frac{5.893 + 2.440}{2})(\frac{5.893}{2}) \right] + \frac{0.150(8)(6.378)}{12(32.2)}$$

$$= 0.1035 \text{ k-sec}^2/\text{ft}$$

$$m_5 = m_2$$

$$= 0.1247 \text{ k-sec}^2/\text{ft}$$

$$m_6 = m_4$$

$$= 0.1035 \text{ k-sec}^2/\text{ft}$$

The equivalent masses for the two-degree-of-freedom system can now be found using the mass concentrations calculated above and Equations (5.2.6). The calculations for these parameters can be shortened considerably by noting that $(m_1)_{in} = (m_3)_{in}$, $(m_1)_{out} = (m_3)_{out}$, $m_4 = m_6$ and $\nu_{1,m} = \nu_{3,m}$.

$$\mu_{1,m}\Big|_{m\,=\,1,2} = (m_1)_{in} + \frac{m_2}{4}(1 - \frac{bc}{ad})^2 + m_4(\frac{b}{a})^2 + \frac{m_5}{4}(\frac{d}{c} - \frac{b}{a})^2$$

$$= 0.1782 + \frac{0.1247}{4}\left[1 - \frac{(2.440)^2}{(5.893)^2}\right] + 0.1035(\frac{2.440}{5.893})^2$$

$$+ \frac{0.1247}{4}(\frac{5.893}{2.440} - \frac{2.440}{5.893})^2$$

$$= 0.3422 \text{ k-sec}^2/\text{ft}$$

$$\mu_{1,m}\Big|_{m\,=\,3,4} = (m_1)_{out} + \frac{m_2}{4}(1 - \frac{bc}{ad})^2 + m_4(\frac{b}{a})^2 + \frac{m_5}{4}(\frac{d}{c} - \frac{b}{a})^2$$

$$= 0.3276 + \frac{0.1247}{4}\left[1 - \frac{(2.440)^2}{(5.893)^2}\right] + 0.1035(\frac{2.440}{5.893})^2$$

$$+ \frac{0.1247}{4}(\frac{5.893}{2.440} - \frac{2.440}{5.893})^2$$

$$= 0.4916 \text{ k-sec}^2/\text{ft}$$

$$\nu_{1,m}\Big|_{m\,=\,1,2,3,4} = -\frac{m_2}{4}(1 - \frac{bc}{ad})^2 + \frac{m_5}{4}(\frac{d}{c} - \frac{b}{a})^2$$

$$= -\frac{0.1247}{4}\left[1 - \frac{(2.440)^2}{(5.893)^2}\right] + \frac{0.1247}{4}(\frac{5.893}{2.440} - \frac{2.440}{5.893})^2$$

$$= 0.1034 \text{ k-sec}^2/\text{ft}$$

$$\mu_{3,m}\Big|_{m\,=\,1,3} = \mu_{1,m}\Big|_{m\,=\,3,4}$$

$$= 0.4916 \text{ k-sec}^2/\text{ft}$$

$$\mu_{3,m}\Big|_{m\,=\,2,4} = \mu_{1,m}\Big|_{m\,=\,1,2}$$

$$= 0.3422 \text{ k-sec}^2/\text{ft}$$

$$\nu_{3,m}\Big|_{m\,=\,1,2,3,4} = \nu_{1,m}\Big|_{m\,=\,1,2,3,4}$$

$$= 0.1034 \text{ k-sec}^2/\text{ft}$$

The equivalent masses for the four motions of the system (cf. Figure 5.3) may now be written.

Asymmetric-Right:
$$\bar{m}_{1,1} = 0.3422-0.1034\ \ddot{h}_3/\ddot{h}_1$$
$$\bar{m}_{3,1} = 0.4916-0.1034\ \ddot{h}_1/\ddot{h}_3 \qquad (8.4.16)$$

Symmetric-In:
$$\bar{m}_{1,2} = 0.3422-0.1034\ \ddot{h}_3/\ddot{h}_1$$
$$\bar{m}_{3,2} = 0.3422-0.1034\ \ddot{h}_1/\ddot{h}_3 \qquad (8.4.17)$$

Symmetric-Out:
$$\bar{m}_{1,3} = 0.4916-0.1034\ \ddot{h}_3/\ddot{h}_1$$
$$\bar{m}_{3,3} = 0.4916-0.1034\ \ddot{h}_1/\ddot{h}_3 \qquad (8.4.18)$$

Asymmetric-Left:
$$\bar{m}_{1,4} = 0.4916-0.1034\ \ddot{h}_3/\ddot{h}_1$$
$$\bar{m}_{3,4} = 0.3422-0.1034\ \ddot{h}_1/\ddot{h}_3 \qquad (8.4.19)$$

The equivalent loads on the two-degree-of-freedom system are given by Equations (6.3.2).

$$J_1 = \frac{1}{2} K_{pr}(a+c) + \frac{1}{2}(b/a)(b+d)$$
$$= 0.144 \left[\frac{1}{2}(\frac{1}{4})(5.893 + 2.440) + \frac{1}{2}(\frac{2.440}{5.893})(2.440 + 5.893)\right]$$
$$= 0.3985 \text{ k/psi}$$

$$J_2 = \frac{1}{4} cK_{pr}(1 - \frac{bc}{ad})$$
$$= \frac{1}{4}(2.440)(\frac{1}{4})(0.144)[1 - (2.440)^2/(5.893)^2]$$
$$= 0.0182 \text{ k/psi}$$

$$J_3 = \frac{1}{2} d(d/c - b/a)$$
$$= \frac{5.893}{2} (5.893/2.440 - 2.440/5.893)(0.144)$$
$$= 0.8491 \text{ k/psi}$$

$$\bar{H}_1 = - J_1\bar{p}_1 - J_2(\bar{p}_{2a} - \bar{p}_{2b}) + J_3\bar{p}_2$$

$$\bar{H}_3 = - J_2(\bar{p}_{2a} - \bar{p}_{2b}) - J_3\bar{p}_2 + J_1\bar{p}_3$$

$$\begin{aligned} \bar{H}_1 &= - 0.3985\ \bar{p}_1 - 0.0182(\bar{p}_{2a} - \bar{p}_{2b}) + 0.8491\ \bar{p}_2 \\ \bar{H}_3 &= - 0.0182\ (\bar{p}_{2a} - \bar{p}_{2b}) - 0.8491\ \bar{p}_2 + 0.3985\ \bar{p}_3 \end{aligned} \qquad (8.4.20)$$

Since Equations (8.4.12) through (8.4.15) for equivalent soil stiffnesses and Equations (8.4.20) for equivalent loads are written in terms of the average overpressures acting on the loading regions defined in Section 6.1, it is necessary to find these overpressures using Equations (6.2.1) and the proper set of time parameters from Section 6.1. Table 8.1 gives the velocity of the shock front at the 100-psi overpressure level as 2,950 feet per second. This is approximately equal to the assumed value of 3,000 feet per second for the seismic velocity of the soil. From the results of the study presented in Appendix B, one may assume, for the depth considered in this example, that the shock front in soil is essentially vertical and a continuation of the shock front in air. This corresponds to Case I, Section 6.1.1. The time parameters for this case are given by Equations (6.1.1) and (6.1.2).

$$\begin{aligned} t_{oa'} &= - (b+2d_o\cot\left[\frac{\pi}{4} - \frac{\varphi}{2}\right])/2U \\ &= - [2.440+2(12.500)\cot 30^\circ]/2(2950) \\ &= - 0.0078 \text{ seconds} \end{aligned}$$

$$\begin{aligned} \bar{t}_{o'} &= \frac{1}{2}(t_{oa'} + t_{ob}) \\ &= \frac{1}{2}(-0.0078+0.0013) \\ &= - 0.0032 \text{ seconds} \end{aligned}$$

$$t_{ob} = -(b-2bd_o/a)/2U$$

$$= -[2.440-2(2.440)(12.500)/5.893]/2(2950)$$

$$= +0.0013 \text{ seconds}$$

$$t_{oa} = -(b+2d_o\cot[\frac{\pi}{4}+\frac{\varphi}{2}])/2U$$

$$= -[2.440+2(12.500)\cot 60^{\circ}]/2(2950)$$

$$= -0.0029 \text{ seconds}$$

$$\bar{t}_o = \frac{1}{2}(t_{oa}+t_{ob})$$

$$= \frac{1}{2}(-0.0029+0.0013)$$

$$= -0.0008 \text{ seconds}$$

$$t_{1a} = 0$$

$$\bar{t}_1 = \frac{1}{2}(t_{1a}+t_{1b})$$

$$= \frac{1}{2}(0+0.0014)$$

$$= +0.0007 \text{ seconds}$$

$$t_{1b} = (b+d)/2U$$

$$= (2.440+5.893)/2(2950)$$

$$= +0.0014 \text{ seconds}$$

$$t_{2a} = t_{1b}$$

$$= +0.0014 \text{ seconds}$$

$$\bar{t}_2 = \frac{1}{2}(t_{2a}+t_{2b})$$

$$= \frac{1}{2}(+0.0014+0.0034)$$

$$= +0.0024 \text{ seconds}$$

$t_{2b} = (b+3d)/2U$

$= [2.440+3(5.893)]/2(2950)$

$= +\ 0.0034$ seconds

$\bar{t}_{2a} = \frac{1}{2}\,(t_{2a} + t_2)$

$= \frac{1}{2}\,(+0.0014+0.0024)$

$= +\ 0.0019$ seconds

$t_2 = (b+2d)/2U$

$= [2.440+2(5.893)]/2(2950)$

$= +\ 0.0024$ seconds

$\bar{t}_{2b} = \frac{1}{2}\,(t_2 + t_{2b})$

$= \frac{1}{2}\,(+0.0024+0.0034)$

$= +\ 0.0029$ seconds

$t_{3a} = t_{2b}$

$= +0.0034$ seconds

$\bar{t}_3 = \frac{1}{2}\,(t_{3a} + t_{3b})$

$= \frac{1}{2}\,(+0.0034+0.0048)$

$= +\ 0.0041$ seconds

$t_{3b} = (b+2d)/U$

$= [2.440+2(5.893)]/2950$

$= +\ 0.0048$ seconds

$t_{4a} = (-b+2B-2bd_o/a)/2U$

$= [-2.440+2(16.667)-2(2.440)(12.500)/5.893]/2(2950)$

$= +\ 0.0035$ seconds

$$\bar{t}_4 = \frac{1}{2}\,(t_{4a} + t_{4b})$$

$$= \frac{1}{2}\,(+0.0035+0.0077)$$

$$= +\ 0.0056 \text{ seconds}$$

$$t_{4b} = (-b+2B+2d_o\cot\,[\tfrac{\pi}{4} - \tfrac{\varphi}{2}])/2U$$

$$= [-2.440+2(16.667)+2(12.500)\cot\,60^\circ]/2(2950)$$

$$= +\ 0.0077 \text{ seconds}$$

$$\bar{t}_{4'} = \frac{1}{2}\,(t_{4a} + t_{4b'})$$

$$= \frac{1}{2}\,(+0.0035+0.0126)$$

$$= +\ 0.0080 \text{ seconds}$$

$$t_{4b'} = (-b+2B+2d_o\ \cot\,[\tfrac{\pi}{4} - \tfrac{\varphi}{2}])/2U$$

$$= [-2.440+2(16.667)+2(12.500)\cot\,30^\circ]/2(2950)$$

$$= +\ 0.0126 \text{ seconds}$$

$$t_{aa} = -\ b/2U$$

$$= -\ 2.440/2(2950)$$

$$= -\ 0.0004 \text{ seconds}$$

$$\bar{t}_a = \frac{1}{2}\,(t_{aa} + t_{ab})$$

$$= \frac{1}{2}\,(-0.0004+0.0052)$$

$$= +\ 0.0024 \text{ seconds}$$

$$t_{ab} = (-b+2B)/2U$$

$$= [-2.440+2(16.667)]/2(2950)$$

$$= +\ 0.0052 \text{ seconds}$$

The solution of Equations (6.2.1) may be presented conveniently in tabular form as shown in Table 8.6. Since the integration of the equations of motion is to be performed on the Illiac, each of the overpressure-time functions is approximated by a series of straight-line segments. Therefore, the overpressure-time coordinates given in Table 8.3 are used for the general overpressure-time function, p(t'), with the exception that the maximum value of each overpressure, i.e. $(\bar{p}_j)_{max} = p(\frac{t_{jb}-t_{ja}}{2})$, is taken directly from the p(t') vs. t' curve itself. This is easily done and improves the approximation slightly. Thus, Table 8.6 contains the coordinates of the end points of the series of straight-line segments used to approximate the average overpressure acting on each of the loading regions.

The equations of motion may be written using Equations (7.1.4).

$$F_{1,m} = \frac{\mu_{3,m}}{\mu_{1,m}\mu_{3,m}-\nu_{1,m}\nu_{3,m}}$$

$$F_{1,1} = \frac{0.4916}{(0.3422)(0.4916)-(0.1034)^2}$$

$$= 3.1213 \text{ ft/k-sec}^2$$

$$G_{1,m} = \frac{\nu_{1,m}}{\mu_{1,m}\mu_{3,m}-\nu_{1,m}\nu_{3,m}}$$

$$G_{1,1} = \frac{0.1034}{(0.3422)(0.4916)-(0.1034)^2}$$

$$= 0.6565 \text{ ft/k-sec}^2$$

$$F_{3,m} = \frac{\nu_{3,m}}{\mu_{1,m}\mu_{3,m}-\nu_{1,m}\nu_{3,m}}$$

$$F_{3,1} = \frac{0.1034}{(0.3422)(0.4916)-(0.1034)^2}$$

$$= 0.6565 \text{ ft/k-sec}^2$$

$$G_{3,m} = \frac{\mu_{1,m}}{\mu_{1,m}\mu_{3,m} - \nu_{1,m}\nu_{3,m}}$$

$$G_{3,1} = \frac{0.3422}{(0.3422)(0.4916)-(0.1034)^2}$$

$$= 2.1727 \text{ ft/k-sec}^2$$

The remainder of the coefficients are calculated in the same manner. Inserting the coefficients into the equations of motion for the four motions of the system (cf. Figure 5.3) gives:

Asymmetric-Right:

$$\begin{aligned} \ddot{h}_1 &= 3.1213(\bar{H}_1 - Q_1 - \bar{Q}_{s1}) + 0.6565(\bar{H}_3 - Q_3 - \bar{Q}_{s3}) \\ \ddot{h}_3 &= 0.6565(\bar{H}_1 - Q_1 - \bar{Q}_{s1}) + 2.1727(\bar{H}_3 - Q_3 - \bar{Q}_{s3}) \end{aligned} \qquad (8.4.21)$$

Symmetric-In:

$$\begin{aligned} \ddot{h}_1 &= 3.2159(\bar{H}_1 - Q_1 - \bar{Q}_{s1}) + 0.9717(\bar{H}_3 - Q_3 - \bar{Q}_{s3}) \\ \ddot{h}_3 &= 0.9717(\bar{H}_1 - Q_1 - \bar{Q}_{s1}) + 3.2159(\bar{H}_3 - Q_3 - \bar{Q}_{s3}) \end{aligned} \qquad (8.4.22)$$

Symmetric-Out:

$$\begin{aligned} \ddot{h}_1 &= 2.1283(\bar{H}_1 - Q_1 - \bar{Q}_{s1}) + 0.4477(H_3 - Q_3 - \bar{Q}_{s3}) \\ \ddot{h}_3 &= 0.4477(\bar{H}_1 - Q_1 - \bar{Q}_{s1}) + 2.1283(\bar{H}_3 - Q_3 - \bar{Q}_{s3}) \end{aligned} \qquad (8.4.23)$$

Asymmetric-Left:

$$\begin{aligned} \ddot{h}_1 &= 2.1727(\bar{H}_1 - Q_1 - \bar{Q}_{s1}) + 0.6565(\bar{H}_3 - Q_3 - \bar{Q}_{s3}) \\ \ddot{h}_3 &= 0.6565(\bar{H}_1 - Q_1 - \bar{Q}_{s1}) + 3.1213(\bar{H}_3 - Q_3 - \bar{Q}_{s3}) \end{aligned} \qquad (8.4.24)$$

8.4.2 Investigation of General Yielding and Buckling of Arch Rib

Before proceeding with the integration of the equations of motion, it is advisable to investigate the effects of the thrust in the arch rib. The average overpressure acting on the arch is given in Table 8.6 as $\bar{p}_a$.

The thrust in the arch, T, caused by this average overpressure is given approximately by Equation (3.5.1), which is repeated here for convenience as Equation (8.4.25).

$$T \approx \frac{1}{2} \bar{p}'_a B \qquad (8.4.25)$$

where $\bar{p}'_a$ = effective uniform radial overpressure acting on the arch

B = span of the arch

Since the value of K_{pr} being used in this problem is one-fourth, the radial overpressure acting on the arch will vary from 25% of $\bar{p}_a$ at the abutments to 100% of $\bar{p}_a$ at the crown. Thus, because the arch is semi-circular, this gives an average radial overpressure on the arch of 62.5% of the vertical overpressure. However, this neglects the thrust induced in the arch as the sides are forced outward against the soil during lateral response. Therefore, some higher proportion of the vertical overpressure is appropriate. For the approximate calculation here, $\bar{p}'_a$ is taken as three-fourths of $\bar{p}_a$.

A measure of the capacity of the arch rib cross section to carry thrust loads may be obtained from Equation (8.4.26).

$$T_y = 0.85 f'_c A_c + f_{dy} A_s \qquad (8.4.26)$$

where T_y = thrust corresponding to general yielding of the arch rib

f'_c = 28-day strength of a standard 6"x12" concrete test cylinder

A_c = area of concrete in the arch rib cross section

A_s = area of steel in the arch rib cross section

f_{dy} = dynamic yield strength of the reinforcing steel

Equation (8.4.26) neglects bending moment in the arch rib and is therefore approximate; however, because the mode of response being considered here is essentially a breathing mode, and further because of the high degree of soil restraint, bending in the arch rib is not of prime importance in this

investigation. Substituting values into Equation (8.4.26) gives:

$$T_y = 0.85(3.5)(96.00-0.24) + 50(0.24)$$

$$= 297 \text{ kips}$$

The average overpressure, $\bar{p}_a$, corresponding to general yielding of the arch rib may now be found using Equation (8.4.25).

$$(\bar{p}_a)_{max} = \frac{(\bar{p}'_a)_{max}}{0.75}$$

$$= \frac{2T_y}{0.75B}$$

$$= \frac{2(297)(1000)}{0.75(16.667)(144)}$$

$$= 330 \text{ psi}$$

Since 330 psi is greater than the maximum value of $\bar{p}_a$ in Table 8.6, i.e. $\bar{p}_a = -97.7$ psi, the arch should not fail by general yielding.

A qualification should be made here regarding the use of an "average" radial overpressure in this case. Since the crown is subjected to an overpressure level greater than the "average" value, local yielding may occur which could lead to general failure of the arch. This is particularly true when the depth of cover over the crown is zero or very small.

In considering the elastic stability of the arch rib, one must keep in mind that buckling is not instantaneous. For the higher yield nuclear weapons, however, the duration of the positive phase of the shock wave is quite long when compared with the characteristic response time of the structure so that buckling is a possibility which should be investigated. If one assumes that the arch rib may be approximated by a bar pinned at the crown and at the abutment and restrained by the soil, the elastic stability of the arch rib may be investigated using Equation (8.4.27).(25)

$$T_{cr} = \frac{\pi^2 EI}{\ell^2}\left(m^2 + \frac{\beta_k \ell^4}{m^2\pi^4 EI}\right)$$

$$T_{cr} = \frac{4EI}{R^2}\left(m^2 + \frac{\beta_k R^4}{16m^2 EI}\right) \qquad (8.4.27)$$

where T_{cr} = thrust corresponding to buckling of the arch rib into a simple sine curve

E = modulus of elasticity of the arch material

I = moment of inertia of the arch rib cross section

ℓ = developed length of one-half of the arch

m = number of half sine loops in the buckled configuration

β_k = soil stiffness, here assumed to act in both directions

R = radius of the arch.

Equation (8.4.28) may be obtained from Equation (8.4.27) by equating the critical thrust values for which the number of half-waves changes from m to m+1.

$$m^2(m+1)^2 = \frac{\beta_k R^4}{16EI} \qquad (8.4.28)$$

The minimum soil stiffness corresponding to the maximum thrust in the arch is obtained by noting that the maximum value of $\bar{p}_a$ in Table 8.6 occurs at t = 0.0052 seconds. While the configuration of the arch at t = 0.0052 seconds is not yet known, a "lower bound" for the soil stiffness may be obtained by using the minimum soil restraining pressure acting at this time. From Table 8.6 it appears that $\bar{p}'_{s3}$ has an absolute magnitude, i.e. 18 psi, less than all of the other soil restraining pressures at t = 0.0052 seconds.

$$-\bar{p}'_{s3} = \left(\frac{0.0052-0.0035}{0.0126-0.0035}\right)(96.4)$$

$$\bar{p}'_{s3} = -18 \text{ psi}$$

The soil stiffness is now determined using Equation (8.4.15).

$$\bar{K}'_{sj}/a = 618.9 - 178.2\ \bar{p}'_{sj}$$

$$\bar{K}'_{s3}/a = 618.9 - 178.2(-18)$$

$$= 3827\ \text{k/ft}^2$$

$$\beta_k = 3827/0.144$$

$$= 26{,}600\ \text{psi}$$

The number of half sine loops corresponding to these conditions is obtained from Equation (8.4.28).

$$m^2(m+1)^2 = \frac{\beta_k R^4}{16EI}$$

$$= \frac{26{,}600(100)^4}{16(3.82\text{x}10^6)(268.6)}$$

$$= 162.03$$

$$m(m+1) = 12.729$$

$$m = 3.103$$

The critical thrust may now be found from Equation (8.4.27) by substituting the integral value of m which gives the lowest value of T_{cr}. The value m = 4 gives the minimum value in this case. (Note: Differentiating Equation (8.4.27) with respect to m, setting $dT_{cr}/dm = 0$, and solving for m gives m = 3.568).

$$T_{cr} = \frac{4EI}{R^2}\left(m^2 + \frac{\beta_k R^4}{16m^2 EI}\right)$$

$$= \frac{4(3.82\text{x}10^6)(268.6)}{(100)^2(1000)}\left(16 + \frac{162.03}{16}\right)$$

$$= 10{,}723\ \text{kips}$$

The average overpressure, $\bar{p}_a$, corresponding to buckling of the arch may now be found using Equation (8.4.25).

$$(\bar{p}_a)_{cr} = \frac{2T_{cr}}{0.75B}$$

$$= \frac{2(10723)}{0.75(16.667)(144)}$$

$$= 11{,}900 \text{ psi}$$

This approach, although approximate, indicates that the arch should not buckle elastically prior to general yielding of the arch rib itself. Note that this is an "elastic" analysis so that the actual buckling of the arch in this case is associated with general yielding of the arch rib as described in the first part of Section 8.4.2.

8.4.3 Integration

Since it has now been determined that neither buckling nor general yeilding of the arch rib should occur under the given loading, it is possible to proceed with the integration of the equations of motion. The results shown in Appendices C and D were obtained using a digital computer (cf. Section 8.3). Two of the problems were also integrated by hand in order to check the computer solutions.

A cycle of integration is given below to illustrate the operations involved. The numerical integration formulas used are those derived by Professor N. M. Newmark and presented in references (4), (5), (6) and (7). Equations (8.4.29) are expressions for the velocity and displacement of mass j at the end of time interval Δt in terms of the acceleration at the end of the interval and the acceleration, velocity and displacement at the beginning of the interval.

$$\dot{h}_{j,n+1} = \dot{h}_{j,n} + \frac{\Delta t}{2}(\ddot{h}_{j,n} + \ddot{h}_{j,n+1})$$

$$h_{j,n+1} = h_{j,n} + \dot{h}_{j,n}(\Delta t) + (\tfrac{1}{2} - \beta')\ddot{h}_{j,n}(\Delta t)^2 + \beta' \ddot{h}_{j,n+1}(\Delta t)^2 \qquad (8.4.29)$$

where $\ddot{h}_{j,n}$, $\dot{h}_{j,n}$, $h_{j,n}$ = acceleration, velocity and displacement, respectively, of mass j at time $t = t_n$

$\ddot{h}_{j,n+1}$, $\dot{h}_{j,n+1}$, $h_{j,n+1}$ = acceleration, velocity and displacement, respectively, of mass j at time $t = t_{n+1}$

Δt = time interval = $t_{n+1} - t_n$

β' = parameter introduced to indicate how much of the acceleration at the end of the time interval enters into the relations for the displacement at the end of the time interval.

Since it is desired to use a linear approximation to the acceleration curve within each time interval, the value $\beta' = 1/6$ is used in Equations (8.4.29).

$$\dot{h}_{j,n+1} = \dot{h}_{j,n} + \frac{\Delta t}{2}(\ddot{h}_{j,n} + \ddot{h}_{j,n+1})$$

$$h_{j,n+1} = h_{j,n} + \dot{h}_{j,n}(\Delta t) + (1/3)\ddot{h}_{j,n}(\Delta t)^2 + (1/6)\ddot{h}_{j,n+1}(\Delta t)^2 \qquad (8.4.30)$$

In the following illustrative example a time interval, Δt, of 0.0001 seconds is used. This time interval was actually used for the computer solutions in order to detect the rapid changes in the loading as the shock wave traverses the structure. Solutions were also obtained using time intervals of 0.001 seconds for several of the problems which had more slowly varying load-time functions in order to check the significance of round-off error. These solutions were nearly identical with the solutions obtained using Δt = 0.0001 seconds.

For illustrative purposes it is preferable to consider a time interval other than the first. Therefore, for this example three time intervals have already been integrated, so that at time t_n = 0.0003 seconds,

the displacements, velocities and accelerations of the equivalent masses are:

$$h_{1,n} = +0.397\text{x}10^{-6} \text{ ft} \qquad h_{3,n} = +0.084\text{x}10^{-6} \text{ ft}$$

$$\dot{h}_{1,n} = +3.927\text{x}10^{-3} \text{ ft/sec} \qquad \dot{h}_{3,n} = +0.835\text{x}10^{-3} \text{ ft/sec}$$

$$\ddot{h}_{1,n} = +26.474 \text{ ft/sec}^2 \qquad \ddot{h}_{3,n} = +5.568 \text{ ft/sec}^2$$

Assume values of the accelerations at the end of the interval, i.e. at time $t_{n+1} = 0.0004$ seconds, as follows:

$$\ddot{h}_{1,n+1} = +35.279 \text{ ft/sec}^2 \qquad \ddot{h}_{3,n+1} = +7.420 \text{ ft/sec}^2$$

The velocities at $t_{n+1} = 0.0004$ seconds may be found using the first of Equations (8.4.30).

$$\dot{h}_{1,n+1} = (+3.972\text{x}10^{-3}) + \frac{1}{2}(+26.474+35.279)(10^{-4})$$

$$= +7.060\text{x}10^{-3} \text{ ft/sec}$$

$$\dot{h}_{3,n+1} = +1.485\text{x}10^{-3} \text{ ft/sec}$$

The displacements at $t_{n+1} = 0.0004$ seconds may be calculated using the second of Equations (8.4.30).

$$h_{1,n+1} = (+0.397\text{x}10^{-6})+(+3.972\text{x}10^{-3})(10^{-4})$$

$$+(1/3)(26.474)(10^{-8})+(1/6)(35.279)(10^{-8})$$

$$= +0.941\text{x}10^{-6} \text{ ft}$$

$$h_{3,n+1} = +0.198\text{x}10^{-6} \text{ ft}$$

The rotations of each joint are found using Equations (8.4.5), (8.4.6) and (8.4.7).

$$\psi_1 = 0.4098\, h_1 - 0.1698\, h_3$$

$$= [0.4098(0.941) - 0.1698(0.198)][10^{-6}]$$

$$= +0.352\text{x}10^{-6} \text{ radians}$$

$$\psi_2 = -0.305\text{x}10^{-6} \text{ radians}$$

$$\psi_3 = +0.079\text{x}10^{-6} \text{ radians}$$

The resisting moments at each hinge are found from Equations (8.4.8).

$$\begin{aligned} M_1 &= \psi_1 K_B \\ &= (+0.352\text{x}10^{-6})(1117.2) \\ &= +0.393\text{x}10^{-3} \text{ ft-kips} \end{aligned}$$

$$M_2 = -0.340\text{x}10^{-3} \text{ ft kips}$$

$$M_3 = +0.088\text{x}10^{-3} \text{ ft kips}$$

The equivalent lateral resistance of the arch is now found from Equations (8.4.9).

$$\begin{aligned} Q_1 &= M_1(0.2049+0.0246\ h_1-0.0246\ h_3)-\ M_2(0.0600+0.0348\ h_1 \\ &\quad -0.0246\ h_3) \\ &= [+0.393\text{x}10^{-3}][0.2049+0.0246(+0.941\text{x}10^{-6}) \\ &\quad -0.0246(+0.198\text{x}10^{-6})] - [-0.340\text{x}10^{-3}][0.0600 \\ &\quad +0.0348(+0.941\text{x}10^{-6})-0.0246(+0.198\text{x}10^{-6})] \\ &= +0.101\text{x}10^{-3} \text{ kips} \end{aligned}$$

$$Q_3 = -0.038\text{x}10^{-3} \text{ kips}$$

The displacement $h_{1,n+1} = +0.941\text{x}10^{-6}$ ft indicates that the windward haunch, joint 1, is displaced inward into the arch. From Table 8.6 the average overpressure acting on the "active" soil failure wedge adjacent to joint 1, $\bar{p}_{s1}$, at $t_{n+1} = 0.0004$ seconds is 77.2 psi.

$$\begin{aligned} -\ \bar{p}_{s1} &= 67.9 + \frac{0.0004}{0.0013}(98.3 - 67.9) \\ &= 77.2 \text{ psi} \end{aligned}$$

The soil stiffness corresponding to this condition is given by Equation (8.4.12).

$$\bar{K}_{sj} = 3647 - 1050\ \bar{p}_{sj}$$

$$\bar{K}_{s1} = 3647 - 1050(-77.2)$$

$$= 84{,}710 \text{ kips/radian}$$

The displacement $h_{3,n+1} = +0.198\text{x}10^{-3}$ ft indicates that the leeward haunch, joint 3, is displaced outward against the soil. From Table 8.6 the average overpressure acting on the "passive" soil failure wedge adjacent to joint 3, $\bar{p}'_{s3}$, at $t_{n+1} = 0.0004$ seconds is zero because the shock front has not yet arrived at point 4a (cf. Figure 6.1). The soil stiffness corresponding to this condition is given by Equation (8.4.13).

$$\bar{K}'_{sj} = 3647 - 1050\ \bar{p}'_{sj}$$

$$\bar{K}'_{s3} = 3647 - 1050(0)$$

$$= 3647 \text{ kips/radian}$$

The rotations of the windward and leeward pressure surfaces are obtained using Equations (4.4.13).

$$\xi_1 = h_1/a$$

$$= \frac{+0.941\text{x}10^{-6}}{5.893}$$

$$= +0.160\text{x}10^{-6} \text{ radians}$$

$$\xi_3 = h_3/a$$

$$= \frac{+0.198\text{x}10^{-6}}{5.893}$$

$$= +0.034\text{x}10^{-6} \text{ radians}$$

Since these rotations are less than the yield values calculated previously,

i.e., $\xi_{ly} = 0.001$ radians and $\xi'_{ly} = 0.005342$ radians, and no "permanent set" has yet occurred in the soil, the equivalent soil resistances may be calculated as follows:

$$\bar{Q}_{s1} = \bar{K}_{s1}\,\xi_1$$

$$= 84{,}710(+0.160\text{x}10^{-6})$$

$$= +13.55\text{x}10^{-3} \text{ kips}$$

$$\bar{Q}_{s3} = \bar{K}'_{s3}\,\xi_3$$

$$= 3{,}647(+0.034\text{x}10^{-6})$$

$$= +0.124\text{x}10^{-3} \text{ kips}$$

The equivalent loads on the system may be determined from Equations (8.4.20). The average overpressures loading the structure at $t_{n+1} = 0.0004$ seconds are given in Table 8.6.

$$-\bar{p}_1 = \left(\frac{0.0004}{0.0014}\right)(99.4) = 28.4 \text{ psi}$$

$$\bar{p}_2 = 0$$

$$\bar{p}_3 = 0$$

$$\bar{p}_{2a} = 0$$

$$\bar{p}_{2b} = 0$$

$$\bar{H}_1 = -0.3985\,\bar{p}_1 - 0.0182(\bar{p}_{2a} - \bar{p}_{2b}) + 0.8491\,\bar{p}_2$$

$$= -0.3985(-28.4)$$

$$= +11.32 \text{ kips}$$

$$\bar{H}_3 = 0$$

The fact that both of the velocities, $\dot{h}_{1,n+1}$ and $\dot{h}_{3,n+1}$, at time $t_{n+1} = 0.0004$ seconds are positive indicates that both haunches are moving

toward the right. Thus, the motion of the structure is "Asymmetric-Right" (cf. Figure 5.3) and the equations of motion for the system at this time are given by Equations (8.4.21). By substituting the effective load and resistance parameters calculated in this section into Equations (8.4.21), it is now possible to check the assumed values of the accelerations at time $t_{n+1} = 0.0004$ seconds.

$$\begin{aligned}\ddot{h}_{1,n+1} &= 3.1213(\bar{H}_1-Q_1-\bar{Q}_{s1})+0.6565(\bar{H}_3-Q_3-\bar{Q}_{s3}) \\ &= 3.1213\,[11.32-(+0.101\text{x}10^{-3})-(+13.55\text{x}10^{-3})] \\ &\quad +0.6565[0-(-0.038\text{x}10^{-3})-(+0.124\text{x}10^{-3})] \\ &= +35.29\ \text{ft/sec}^2\end{aligned}$$

$$\ddot{h}_{3,n+1} = +7.42\ \text{ft/sec}^2$$

Since these values are essentially the same as the assumed values, i.e. $\ddot{h}_{1,n+1} = +35.279$ ft/sec^2 and $\ddot{h}_{3,n+1} = +7.420$ ft/sec^2, additional trials are not required and the velocities and displacements at t = 0.0004 seconds which were calculated above are correct. Thus, the integration may now proceed to the next time interval. The results of the solution of this problem up to t = 0.09 seconds are given in Figure D.3.

8.4.4 Rib Shortening

The effect of rib shortening is illustrated in Figures D.24, D.25 and D.26. Expressions for the "rib-shortening" corrections are obtained using Equations (3.5.8). In the following derivations an average uniform radial pressure on the arch equal to 75% of the vertical overpressure in the soil is assumed (cf. Section 8.4.2).

$$\delta h_1 = -\frac{1}{2}\,\bar{p}'_a \left[\frac{BL^2c}{AE(ad-bc)}\right]$$

$$= -\frac{1}{2}\,\bar{p}'_a \left[\frac{16.667(6.378)^2(2.440)(12)}{8(3.82\text{x}10^6)(5.893^2-2.440^2)}\right]$$

$$= -11.29\text{x}10^{-6}\,\bar{p}'_a$$

$$\delta h_1 = -8.47\text{x}10^{-6}\,\bar{p}_a \tag{8.4.31}$$

$$\delta h_2 = 0 \tag{8.4.32}$$

$$\delta h_3 = -\,\delta h_1$$

$$\delta h_3 = +8.47\text{x}10^{-6}\,\bar{p}_a \tag{8.4.33}$$

$$\delta h_4 = \frac{1}{2}\,\bar{p}'_a \left[\frac{BL^2d}{AE(ad-bc)}\right]$$

$$= \frac{1}{2}\,\bar{p}'_a \left[\frac{16.667(6.378)^2(5.893)(12)}{8(3.82\text{x}10^6)(5.893^2-2.440^2)}\right]$$

$$= 27.26\text{x}10^{-6}\,\bar{p}'_a$$

$$\delta h_4 = 20.45\text{x}10^{-6}\,\bar{p}_a \tag{8.4.34}$$

$$\delta h_5 = \frac{1}{2}\,\bar{p}'_a \left(\frac{BL^2}{cAE}\right)$$

$$= \frac{1}{2}\,\bar{p}'_a \left[\frac{16.667(6.378)^2(12)}{2.440(8)(3.82\text{x}10^6)}\right]$$

$$= 54.55\text{x}10^{-6}\,\bar{p}'_a$$

$$\delta h_5 = 40.92\text{x}10^{-6}\,\bar{p}_a \tag{8.4.35}$$

$$\delta h_6 = \delta h_4$$

$$\delta h_6 = 20.45\text{x}10^{-6}\,\bar{p}_a \tag{8.4.36}$$

The parameters required to plot Figure D.25 are calculated below in order to illustrate the operations involved. The time selected for this computation corresponds to the first maximum downward displacement of the crown. From Figure D.3, this occurs at t = 0.0198 seconds. The displacement components at this time may be calculated using the data plotted in Figure D.3 and Equations (8.4.1) through (8.4.4).

$$h_1 = -5.8\text{x}10^{-3} \text{ ft}$$

$$\begin{aligned} h_2 &= +0.4143(h_1+h_3) \\ &= +0.4143(-5.8+5.0)(10^{-3}) \\ &= -0.4\text{x}10^{-3} \text{ ft} \end{aligned}$$

$$h_3 = +5.0\text{x}10^{-3} \text{ ft}$$

$$\begin{aligned} h_4 &= -0.4141\ h_1 \\ &= -0.4141(-5.8\text{x}10^{-3}) \\ &= +2.4\text{x}10^{-3} \text{ ft} \end{aligned}$$

$$h_5 = -10.8\text{x}10^{-3} \text{ ft}$$

$$\begin{aligned} h_6 &= +0.4141\ h_3 \\ &= +0.4141(+5.0\text{x}10^{-3}) \\ &= +2.1\text{x}10^{-3} \text{ ft} \end{aligned}$$

The average overpressure acting on the arch at t = 0.0198 seconds may be obtained either from Table 8.6 or from a plot of $\overline{p}_a(t)$ vs. t. For this example a value of $\overline{p}_a = -88.1$ psi was obtained from a plot of $\overline{p}_a(t)$ vs. t. This value is now substituted into Equations (8.4.31) through (8.4.36) in order to obtain the "rib-shortening" corrections at t = 0.0198 seconds.

$$\delta h_1 = -8.47\text{x}10^{-6}\ \bar{p}_a$$
$$= -8.47\text{x}10^{-6}(-88.1)$$
$$= +0.7\text{x}10^{-3}\ \text{ft}$$

$$\delta h_2 = 0$$

$$\delta h_3 = -\ \delta h_1$$
$$= -0.7\text{x}10^{-3}\ \text{ft}$$

$$\delta h_4 = +20.45\text{x}10^{-6}\ \bar{p}_a$$
$$= +20.45\text{x}10^{-6}(-88.1)$$
$$= -1.8\text{x}10^{-3}\ \text{ft}$$

$$\delta h_5 = +40.92\text{x}10^{-6}\ \bar{p}_a$$
$$= +40.92\text{x}10^{-6}(-88.1)$$
$$= -3.6\text{x}10^{-3}\ \text{ft}$$

$$\delta h_6 = \delta h_4$$
$$= -1.8\text{x}10^{-3}\ \text{ft}$$

The net displacement components, $\bar{h}_j$, of the joints of the model may now be obtained by adding algebraically the "rib-shortening" corrections to the displacement components calculated above.

$$\bar{h}_j = h_j + \delta h_j \tag{8.4.37}$$

$$\bar{h}_1 = (-5.8+0.7)(10^{-3})$$
$$= -5.1\text{x}10^{-3}\ \text{ft}$$

$$\bar{h}_2 = (-0.4+0)(10^{-3})$$
$$= -0.4\text{x}10^{-3}\ \text{ft}$$

$$\bar{h}_3 = (+5.0-0.7)(10^{-3})$$
$$= +4.3\text{x}10^{-3} \text{ ft}$$

$$\bar{h}_4 = (+2.4-1.8)(10^{-3})$$
$$= +0.6\text{x}10^{-3} \text{ ft}$$

$$\bar{h}_5 = (-10.8-3.6)(10^{-3})$$
$$= -14.4\text{x}10^{-3} \text{ ft}$$

$$\bar{h}_6 = (+2.1-1.8)(10^{-3})$$
$$= +0.3\text{x}10^{-3} \text{ ft}$$

The resultant displacements of each joint, Δ_j, may be obtained as the square root of the sum of the squares of the net horizontal and vertical displacement components at that joint.

$$\Delta_j = \sqrt{(\bar{h}_j)^2 + (\bar{h}_{j+3})^2} \tag{8.4.38}$$

$$\Delta_1 = 5.1\text{x}10^{-3} \text{ ft}$$
$$\Delta_2 = 14.4\text{x}10^{-3} \text{ ft}$$
$$\Delta_3 = 4.3\text{x}10^{-3} \text{ ft}$$

8.4.5 Calculation of Natural Periods of Vibration

As an illustration of the calculation of the natural periods of vibration of the system, the natural period of vibration is calculated below for the structure as it approaches its first maximum response at the leeward haunch. Because the "stiffness" of the soil varies with the overpressure restraining the soil wedges (cf. Section 4.4), the time selected for this example is the time corresponding to maximum soil "stiffness" up to this instant.

From Figure D.3 one determines that the motion of the structure is "Symmetric-Out" (cf. Figure 5.3) as the system approaches its first maximum displacement at the leeward haunch and that this maximum occurs at $t = 0.0173$ seconds. Thus, the haunches are displaced outward and a "passive" state of stress is developing in the soil on both sides of the arch. From Table 8.6, or from plots of the overpressure-time functions, the maximum soil restraining pressures acting on the "passive" soil failure wedges during the interval between $t = 0$ and $t = 0.0173$ seconds are found to occur at $t = 0.0126$ seconds when $\bar{p}'_{s1} = -89.0$ psi (obtained from plot) and $\bar{p}'_{s3} = -96.4$ psi.

The soil stiffnesses corresponding to these restraining pressures are obtained from Equations (8.4.15).

$$\bar{K}'_{sj}/a = 618.9 - 178.2\ \bar{p}'_{sj}$$

$$\bar{K}'_{s1}/a = 618.9 - 178.2(-89.0)$$

$$= 16{,}480 \text{ k/ft}$$

$$\bar{K}'_{s3}/a = 618.9 - 178.2(-96.4)$$

$$= 17{,}800 \text{ k/ft}$$

The arch stiffness parameters required for substitution into the frequency equation may be found by referring to Equation (7.2.3).

$$\tau_1 = \frac{K_B}{2L^2}\,(5+a/c+b/d+2c/a+bc/ad)$$

$$= \frac{1117.2}{2(6.378)^2}\left[5 + \frac{5.893}{2.440} + \frac{2.440}{5.893} + \frac{2(2.440)}{5.893} + \frac{(2.440)^2}{(5.893)^2}\right]$$

$$= 121.2 \text{ k/ft}$$

$$
\begin{aligned}
\tau_2 &= \frac{K_B}{2L^2}(3 + a/c - b/d - bc/ad) \\
&= \frac{1117.2}{2(6.378)^2}\left[3 + \frac{5.893}{2.440} - \frac{2.440}{5.893} - \frac{(2.440)^2}{(5.893)^2}\right] \\
&= 66.3 \text{ k/ft}
\end{aligned}
$$

The equivalent mass parameters for the "Symmetric-Out" motion are those appearing in Equation (8.4.18).

$$\mu_{1,3} = \mu_{3,3} = 0.4916 \text{ k-sec}^2/\text{ft}$$

$$\nu_{1,3} = \nu_{3,3} = 0.1034 \text{ k-sec}^2/\text{ft}$$

The parameters obtained above may now be substituted into Equation (7.2.9) and the resulting equation solved for ω_m^2 .

$$
\begin{aligned}
&\left[\mu_{1,m}\mu_{3,m} - \nu_{1,m}\nu_{3,m}\right]\omega_m^4 - \left[\mu_{1,m}(\tau_1 + \bar{K}'_{s3}/a)\right. \\
&\left. + \mu_{3,m}(\tau_1 + \bar{K}'_{s1}/a) - \tau_3(\nu_{1,m} + \nu_{3,m})\right]\omega_m^2 \\
&+ \left[(\tau_1 + \bar{K}'_{s1}/a)(\tau_1 + \bar{K}'_{s3}/a) - (\tau_3)^2\right] \\
&= 0
\end{aligned}
$$

$$
\begin{aligned}
&[(0.4916)^2 - (0.1034)^2]\ \omega_m^4 - [0.4916(121+17{,}800) \\
&\ + 0.4916(121+16{,}480) - 66.3(0.1034+0.1034)]\ \omega_m^2 \\
&\ + [(121+16{,}480)(121+17{,}800) - (66.3)^2] \\
&\ = 0
\end{aligned}
$$

$$0.2310\ \omega_m^4 - 16{,}960\ \omega_m^2 + 279.4\text{x}10^6 = 0$$

$$\omega_{3,1}^2 = 29{,}000 \text{ rad}^2/\text{sec}^2$$

$$\omega_{3,2}^2 = 44{,}400 \text{ rad}^2/\text{sec}^2$$

The value of ω_m^2 corresponding to "Symmetric-Out" motion may be found by substituting $\omega_{3,1}^2$ and $\omega_{3,2}^2$, in turn, into either of Equations (7.2.8).

$$(\mu_{1,m}\omega_m^2 - \tau_1 - \bar{K}'_{s1}/a)h_1 + (-\nu_{1,m}\,\omega_m^2 + \tau_3)h_3 = 0$$

For $\omega_{3,1}^2 = 29{,}000$ rad^2/sec^2:

$$[0.4916(29{,}000)-121-16{,}480]h_1+[-0.1034(29{,}000)+66.3]h_3 = 0$$

$$h_3 = -0.80\ h_1$$

Since h_1 and h_3 are of opposite signs, the haunches are displaced in opposite directions and the configuration is "symmetric". (Substitution of $\omega_{3,2}^2 =$ 44,400 rad^2/sec^2 into Equations (7.2.8) gives $h_3 = +1.16\ h_1$, indicating that both haunches are displaced in the same direction and that the configuration is therefore "asymmetric").

The correct value of ω_m^2 is thus 29,000 rad^2/sec^2 from which $\omega_m = 170.3$ rad/sec. This value may now be substituted into Equation (7.2.10) in order to find the natural period of vibration of the system at this particular time in this particular motion.

$$T_m = 2\pi/\omega_m$$

$$T_3 = 2\pi/170.3$$

$$= 0.037 \text{ seconds}$$

TABLE 8.1

SHOCK WAVE PROPERTIES

Peak Side-on Overpressure	psi	1000	100	50
Distance from 1 MT Contact Surface Burst	yds	480	1100	1500
Duration of Positive Phase	sec	1.48	1.48	1.60
Velocity of Shock Front in Air	fps	8700	2950	2240

TABLE 8.2

OVERPRESSURE-TIME COORDINATES FOR 50-psi SHOCK WAVE

t'	sec	0	0.065	0.20	0.40	0.80
p(t')	psi	50	40	26.5	15.5	5.0

TABLE 8.3

OVERPRESSURE-TIME COORDINATES FOR 100-psi SHOCK WAVE

t'	sec	0	0.070	0.205	0.395	0.702
p(t')	psi	100	60	31.5	16	6

TABLE 8.4

OVERPRESSURE-TIME COORDINATES FOR 1000-psi SHOCK WAVE

t'	sec	0	0.01	0.04	0.12	0.40
p(t')	psi	1000	600	250	100	25

TABLE 8.5

SUMMARY OF NUMERICAL EXAMPLES

Depth of Cover Over Crown	Reinforced Concrete Arch		Corrugated Metal Arch		
	100 psi	1000 psi	50 psi	100 psi	1000 psi
0	(1)	(1)	(1)	(1)	(1)
$\frac{1}{8}$ (Span)	(1)	(1)	(1)	(1)	-
$\frac{1}{4}$ (Span)	(1),(3)	(1)	(1)	(1),(2)	(1)
$\frac{1}{2}$ (Span)	(1)	(1)	(1)	(1)	-

Notes: (1) $K_{pr} = 1/4$, $C_s = 3000$ fps

(2) $K_{pr} = 1/4, 1/2, 3/4, 1$

(3) $C_s = 1000, 2400, 3000$ fps

TABLE 8.6

OVERPRESSURE-TIME RELATIONSHIPS

oading Region	Parameter		Coordinates					
1a-1b	$t=t'+0.0007$	sec	0	0.0014	0.0707	0.2057	0.3957	
	t'	sec	-	0.0007	0.0700	0.2050	0.3950	
	$-\bar{p}_1$	psi	0	99.4	60	31.5	16	
2a-2b	$t=t'+0.0024$	sec	0	0.0014	0.0034	0.0724	0.2074	0.3974
	t'	sec	-	--	0.0010	0.0700	0.2050	0.3950
	$-\bar{p}_2$	psi	0	0	99.2	60	31.5	16
3a-3b	$t=t'+0.0041$	sec	0	0.0034	0.0048	0.0741	0.2091	0.3991
	t'	sec	-	--	0.0007	0.0700	0.2050	0.3950
	$-\bar{p}_3$	psi	0	0	99.4	60	31.5	16
2a-2	$t=t'+0.0019$	sec	0	0.0014	0.0024	0.0719	0.2069	0.3969
	t'	sec	-	--	0.0005	0.0700	0.2050	0.3950
	$-\bar{p}_{2a}$	psi	0	0	99.6	60	31.5	16
2-2b	$t=t'+0.0029$	sec	0	0.0024	0.0034	0.0729	0.2079	0.3979
	t'	sec	-	--	0.0005	0.0700	0.2050	0.3950
	$-\bar{p}_{2b}$	psi	0	0	99.6	60	31.5	16
0a-0b	$t=t'-0.0008$	sec	0	0.0013	0.0692	0.2042	0.3942	
	t'	sec	0.0008	0.0021	0.0700	0.2050	0.3950	
	$-\bar{p}_{s1}$	psi	67.9	98.3	60	31.5	16	
0a'-0b	$t=t'-0.0032$	sec	0	0.0013	0.0668	0.2018	0.3918	
	t'	sec	-	0.0045	0.0700	0.2050	0.3950	
	$-\bar{p}'_{s1}$	psi	82.6	96.4	60	31.5	16	
4a-4b	$t=t'+0.0056$	sec	0	0.0035	0.0077	0.0756	0.2106	0.4006
	t'	sec	-	--	0.0021	0.0700	0.2050	0.3950
	$-\bar{p}_{s3}$	psi	0	0	98.3	60	31.5	16
4a-4b'	$t=t'+0.0080$	sec	0	0.0035	0.0126	0.0780	0.2130	0.4030
	t'	sec	-	--	0.0046	0.0700	0.2050	0.3950
	$-\bar{p}'_{s3}$	psi	0	0	96.4	60	31.5	16
aa-ab	$t=t'+0.0024$	sec	0	0.0052	0.0724	0.2074	0.3974	
	t'	sec	-	0.0028	0.0700	0.2050	0.3950	
	$-\bar{p}_a$	psi	7	97.7	60	31.5	16	

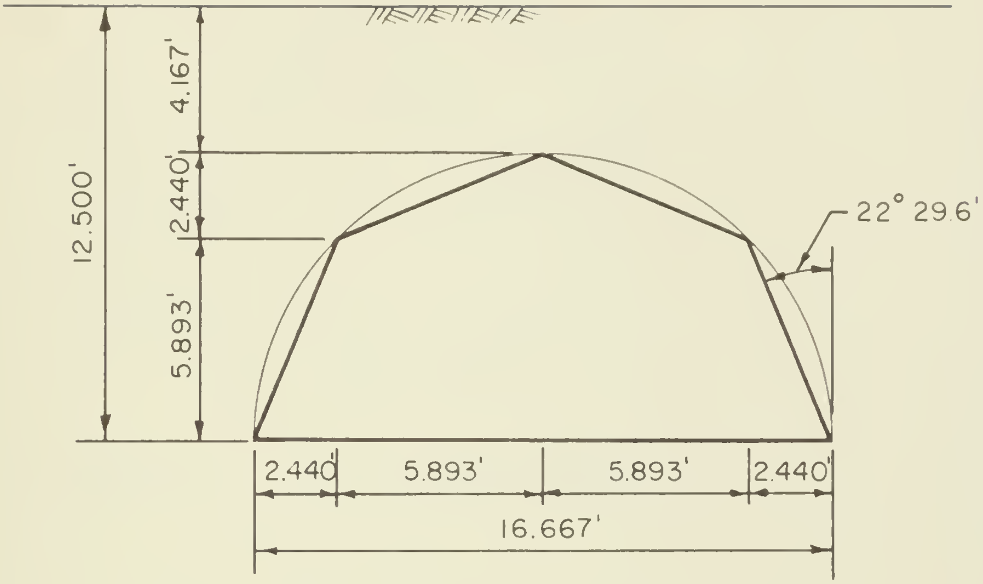

Figure 8.1. Reinforced Concrete Arch, $d_c = B/4$

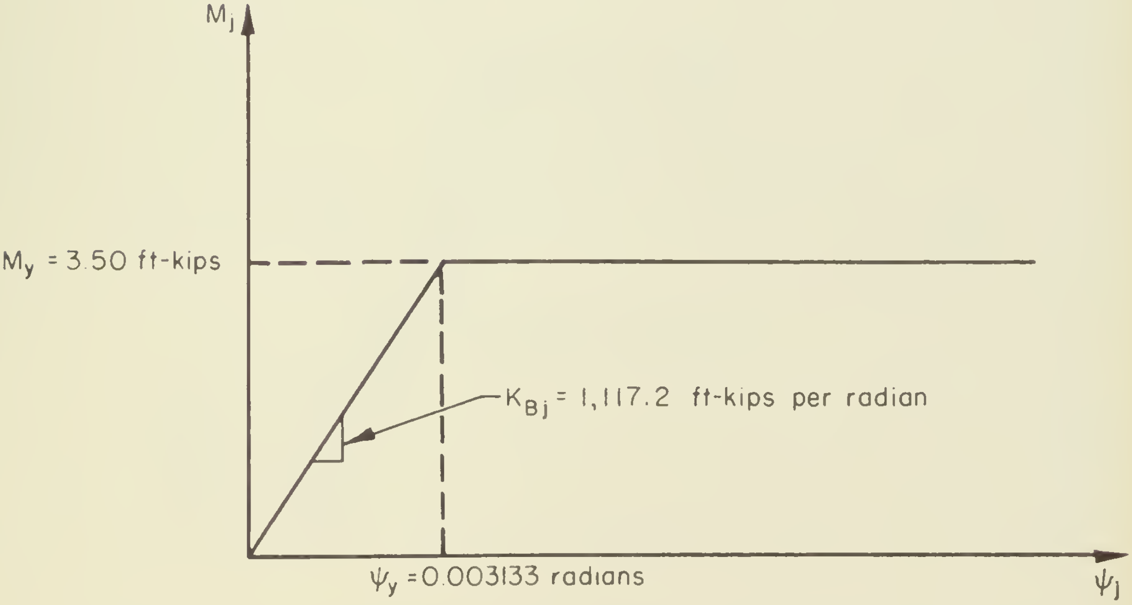

Figure 8.2. Moment-Rotation Diagram for Joints of Model

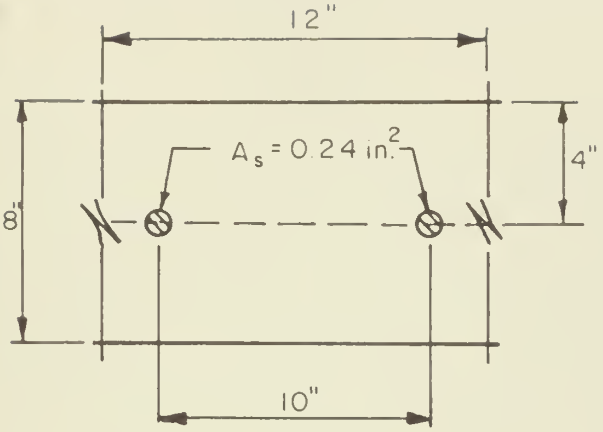

Figure 8.3. Arch Rib Cross Section

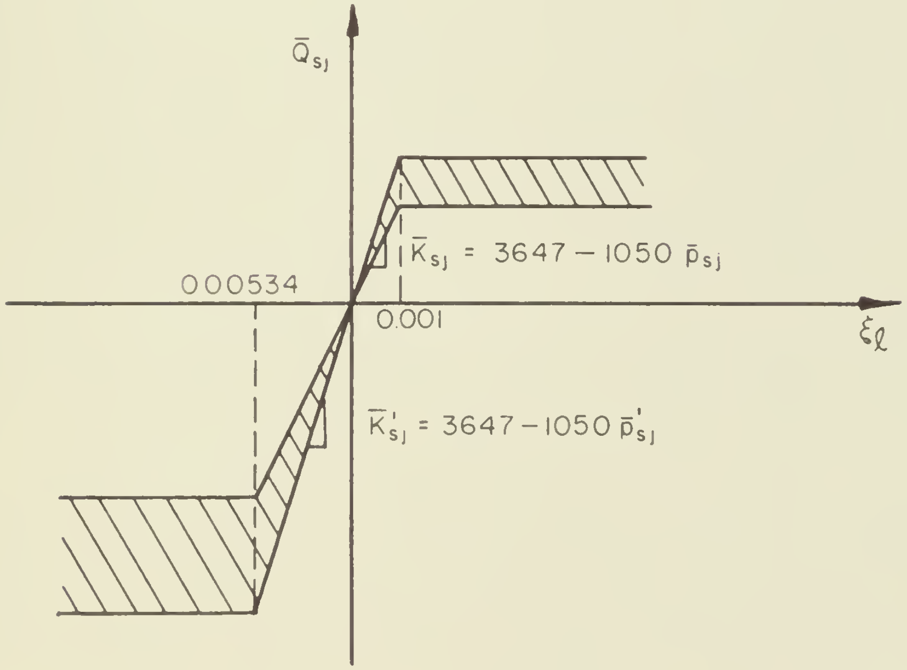

Figure 8.4. Equivalent Soil Resistance-Displacement Diagram

CHAPTER IX

SUMMARY

The results of the numerical investigation performed in connection with this thesis are summarized in this chapter. Included also are a listing of the conclusions which have been drawn on the basis of this investigation and some recommendations for further study. The numerical examples are described in Chapter VIII and the results presented in tabular and in graphical form in Appendices C and D. In general, the results give an informative picture of the lateral response of shallow-buried arches to nuclear blast loadings under a variety of conditions.

9.1 Discussion

In interpreting the results of the numerical investigation as presented in the appendices, one should keep in mind that the relative values of the response are more significant than their absolute values. The relative values permit comparison of arch behavior as geometry and loading parameters are varied. The absolute values are somewhat misleading because of their dependence upon the assumptions made in the dynamic analysis. In general, the calculated displacements are smaller than the displacements which one would expect in an actual structure. This is true first because of the replacement of the actual structure having continuous flexibility with a dynamic model having only two degrees of freedom, and second because of the idealized soil conditions assumed to exist before and during response. For example, any lack of compaction in the backfill surrounding an actual arch will be manifested directly as increased deformation of the arch because of the relatively large influence of the resistance mobilized in the soil on the

response of the arch. This is discussed in detail below. Further, displacements of an actual structure will be affected by differences between the actual blast wave characteristics and those of the idealized blast wave used in these calculations. This effect could lead to either greater or smaller values of displacement.

Another factor influencing the numerical results is the absence of any damping factor in the equations of motion. While damping is not considered to have a significant effect upon the magnitude of the lateral response during the initial portion of the response history, it will reduce later maxima in all cases short of failure. For this reason, the comparisons made in Appendix C are based on "initial", or first, maximum values at each joint.

A comparison of the natural periods of vibration of the structures is presented in Tables C.1 and C.2. In general, as the depth of cover is increased, the natural period of vibration of the structure is decreased. This indicates that the "stiffness" of the soil tends to be more significant than the additional mass which the soil adds to the vibrating system. At first glance the natural periods corresponding to zero depth of cover at the crown appear to be out of sequence. This is because the change in mass from the "no cover" to the "$d_c = 0$" condition is much greater than the changes in mass between any two of the succeeding cover geometries listed. In fact, because of the limitations imposed on the dimensions of the soil masses by Equations (5.1.3) and (5.1.4), the change in mass with increasing depth of cover eventually becomes zero. On the other hand, the stiffness of the structure continues to increase with depth becoming, relatively, quite large for the case of a soil depth at the crown equal to one-half of the arch span.

It should be pointed out here that because of the nature of the assumptions upon which the dynamic model is based, the natural periods of vibration given in Tables C.1 and C.2 for the "Asymmetric" modes are closer to the periods of the actual system than the periods for the "Symmetric" modes. The symmetric modes are influenced to a significant extent by the extensional as well as the flexural characteristics of the arch while the asymmetric modes are almost entirely flexural, or "bending", modes.

Table C.2 contains the natural periods of the systems as they approach their first maximum response at the leeward haunch. Aside from a relatively small initial inward movement of the windward haunch and upward movement of the crown in certain cases, this is the first maximum reached by the system (cf. Appendix D). In all of the cases studied the system motion is "Symmetric-Out" (cf. Figure 5.3) as the system approaches this maximum. Since the natural period is a function, in part, of the soil stiffness (cf. Equations (7.2.9) and (7.2.10)), and the soil stiffness in turn is a function, in part, of the overpressure restraining the soil failure wedges (cf. Equations (4.4.10) and (4.4.12)), it is necessary to specify the particular time at which the natural period is to be calculated so that the overpressure acting on the soil failure wedges may be found. The time selected in each case is the time corresponding to maximum restraint of the "passive" soil failure wedges as the system approaches its first maximum response at the leeward haunch.

In Table C.2 it is interesting to note that, as in Table C.1, the natural period tends to decrease with increasing depth of cover. Also, the natural period decreases with increasing overpressure. This results from the fact that the overpressure acts to increase the soil stiffness but has no effect upon the mass of the system.

In Tables C.3, C.4, and C.5 the first maximum values of response are compared. The tendency of the arch to move initially inward at the windward haunch and upward at the crown in certain cases (cf. Appendix D) has not been considered in selecting "first" maxima. As can be seen from the response curves in Appendix D, the sequence of response is, in general:

1. The response reaches a maximum (outward) value at the leeward haunch.
2. The response reaches a maximum (downward) value at the crown.
3. The response reaches a maximum (outward) value at the windward haunch.

In all cases as the depth of earth cover is increased, the magnitude of response is decreased. In general, as the overpressure is increased, the magnitude of response is increased. However, this increase in the magnitude of response is not as great as might be expected. This is caused by the increase in soil resistance with increasing overpressure level. An exception to this occurs in the case of the corrugated metal arch with no soil cover at the crown. Here an increase in the overpressure loading from 50 psi to 100 psi results in a reduction in the magnitude of the response. This is due to the fact that the mass remains constant with a change in overpressure while both the loading and resistance parameters vary with overpressure level. Increasing the overpressure level to 1000 psi overcomes the "mass effect" and the magnitude of the response increases as expected.

It should be noted here that comparing first maximum in those cases having no soil cover at the crown is somewhat misleading. Examination of the response curves in Appendix D reveals that the second maxima tend to become very large for certain combinations of structure geometry and loading (cf. Figures D.7, D.15 and D.22). For these cases, the overpressure is not sufficient to hold the structure down and the crown "pops up."

Another point of interest may be illustrated using the data presented in Figures C.3, C.4 and C.5. This concerns the relative contributions of the arch and the soil to the lateral deformation resistance of the system. Consider, for example, the reinforced concrete arch with a depth of soil cover at the crown equal to one-fourth of the arch span and subjected to a 100-psi shock wave. Now consider the configuration of the structure at the time of its first maximum response at the leeward haunch, i.e. at $t = 0.0173$ seconds. From Table C.5 the horizontal displacement of the leeward haunch, h_3, at this time is +0.0054 feet. From Figure D.3, the horizontal displacement of the windward haunch, h_1, at this time is -0.0048 feet. Proceeding as in the sample calculations of Section 8.4 gives corresponding values of the equivalent arch and soil resistances as:

$$Q_1 = -0.87 \text{ kips} \qquad \overline{Q}_{s1} = -77.09 \text{ kips}$$

$$Q_3 = +0.91 \text{ kips} \qquad \overline{Q}_{s3} = +93.47 \text{ kips}$$

This illustrates the fact that the arch contribution to the lateral response of the system is relatively small as compared with the soil contribution. This also indicates that the larger displacements obtained in the case of the corrugated metal arch may be due more to the larger span of the corrugated metal arch rather than to the smaller resistance of the steel arch rib as compared with the concrete arch rib.

The data contained in Table C.6 show the effect of varying the ratio, K_{pr}, of the horizontal to vertical overpressures induced in the soil by the shock wave in air (cf. Figures D.17 through D.20). In general, as K_{pr} is increased, the magnitude of the response is decreased. Exceptions to this are the initial inward movement of the windward haunch and the accompanying upward movement of the crown. These movements are magnified by increasing K_{pr}.

The effect of the angle of inclination of the shock front in the soil was studied and the results of the study presented in Table C.7 (cf. Figures D.3, D.4 and D.5). Since the angle of inclination of the shock front in soil, η, is a function of the relative values of the velocity of the shock wave in air, U, and the seismic velocity of the soil, C_s, (cf. Appendix B), varying η for a constant U has the same effect as a corresponding variation in C_s (cf. Equations (B.3)). Table C.7 lists the maxima for the solutions in chronological order. In general, increasing the angle of inclination of the shock front in soil with respect to the horizontal accentuates the initial inward movement of the windward haunch (and accompanying upward movement of the crown) but has no significant effect on the magnitudes of the other maxima.

Response curves for all of the cases studied are presented in Appendix D, Figures D.1 through D.23. The figures are arranged with those for the reinforced concrete arch first followed by those for the corrugated metal arch. The figures are grouped by overpressure level and are ordered within each group by increasing depth of cover. The solutions for $p_{so} = 50$ psi and $p_{so} = 100$ psi are plotted for the first 90 milliseconds after the shock wave reaches the structure, those for $p_{so} = 1000$ psi for 18 milliseconds. The curves include the first maximum response at each joint in all cases.

Configuration diagrams, Figures D.24 through D.30, are presented for two of the solutions. These diagrams are arranged chronologically and illustrate the configuration of the structure at each of the first maxima (neglecting the small initial movements of the windward haunch and the crown as before). In addition, for purposes of comparison, Figure D.30 shows the configuration of the corrugated metal arch at the time of the second maximum response at the windward haunch.

The configuration diagrams are drawn first neglecting and then including rib shortening. The effect of rib shortening is seen to be a general inward and downward movement of the structure. While rib shortening might seem to cause the arch to move away from the soil and thus invalidate some of the assumptions upon which the lateral response analysis is based, test results have indicated(17) that the soil will deform also and that the deformations of the soil are of the same order as those of the arch. Further, the blast loading is transmitted to the arch by the soil so that any movement of the arch away from the soil tends to decrease the load on the arch, thus counteracting the tendency for the arch and the soil to move apart. Finally, the blast wave in air tends to push the soil down around the arch by the very nature of its action.

9.2 Conclusions

The numerical results discussed in the preceding section lead to the general conclusion that well compacted soil surrounding a shallow-buried, underground arch contributes the major portion of the resistance of the arch to lateral deformation when subjected to the blast load resulting from a nuclear explosion.

If consideration is limited to those cases where the depth of cover is sufficient to prevent the crown from moving upward out of the ground, e.g. $d_c \geq B/8$, and the arch rib cross section is sufficient to withstand the thrust developed in the arch without general yielding or buckling, it may be concluded that the arch will successfully withstand the applied loading. Further, if the following parameters are varied individually in turn, it may be concluded that:

1. As the depth of cover is increased, the magnitude of the response will decrease.

2. As the overpressure level is increased, the magnitude of the response will increase.

3. As the ratio of horizontal to vertical overpressure induced in the soil by the shock wave in air is increased, the magnitudes of the initial movements of the windward haunch inward and the crown upward will increase; however, the later magnitudes of the lateral response will decrease.

4. As the angle of inclination with respect to the horizontal of the shock front in soil is increased, the magnitudes of the initial movements of the windward haunch inward and the crown upward will increase; however, the angle of inclination of the shock front in soil has no significant effect upon the magnitude of the later response.

5. As the span of the arch is increased, the magnitude of the response will increase.

6. The maximum response of the arch will occur at the crown, principally in the vertical direction.

In general, it may be concluded that the natural periods of vibration of the bending modes of the arch will be decreased by:

1. Increasing the depth of soil cover, and
2. Increasing the overpressure level.

9.3 Recommendations

While the present study enables one to make certain predictions regarding the relative behavior of shallow-buried arches under various combinations of geometry and nuclear blast loading conditions, it is limited by the assumptions which are made in writing and solving the equations of motion for the system. This study might logically be extended in one or more of the following areas.

There appears to be a significant lack of knowledge regarding the interaction between the structure and the soil. While classical earth pressure theory gives an indication of the resistance offered by the soil, this aspect of the problem could well be investigated in detail. For example, there is a notable lack of experimental data relating to the amount of deformation required to develop the passive state of plastic equilibrium.

A soil resistance-deformation relationship somewhat more in agreement with existing experimental data might be obtained by considering a more rapid shift in the direction of the deformation resistance offered by the soil as the system "rebounds." This approach is unattractive from a computational standpoint but may bear further investigation.

A logical extension of this study is a consideration of more than two degrees of freedom for the dynamic system. This would give a closer approximation to the actual structure and would permit simultaneous consideration of extensional and bending modes of response. It might also permit footing motions to be considered.

The determination of the overpressure causing elastic buckling of the arch rib is an interesting problem. While the calculations in Chapter VIII indicate that this condition is not critical, they are approximate. A closer estimate of the critical overpressure would be helpful.

A closer approximation to actual response values might be obtained by considering the rise time of the pressure pulse in the soil. This is difficult to define at depths of interest in this problem using existing information. In fact, the entire problem of the transmission of the shock wave through the soil merits careful study.

A closer approximation to the later maxima of the displacement-time relationships may be obtained by including a damping term in the equations of motion. Since this term would appear to be most significant in those

cases with little or no soil cover, it should be kept in mind that depths of soil cover approaching zero at the crown may be unattractive from a practical standpoint. This is due to the fact that blast resistance is only part of the over-all problem of providing protection against the effects of nuclear weapons. Thermal and nuclear radiation effects will also be significant at overpressure levels of interest in this problem.

LIST OF REFERENCES

1. Albright, G. H., Evaluation ... Shelters, Project 3.3, Operation Plumbbob, ITR-1422, U.S. Atomic Energy Commission Technical Information Service Extension, Oak Ridge, Tennessee, November, 1957 (CONFIDENTIAL - FORMERLY RESTRICTED DATA).

2. Flathau, W. J., Breckenridge, R. A., and Wiehle, C. K., Blast ... Structures, Project 3.1, Operation Plumbbob, ITR-1420, U.S. Atomic Energy Commission Technical Information Service Extension, Oak Ridge, Tennessee, November 1957 (CONFIDENTIAL - FORMERLY RESTRICTED DATA).

3. Albright, G. H., Rush, P. J., LeDoux, J. C., True, V., and White, C. R., Response ... Region, Project 3.2, Operation Hardtack, ITR-1626-1, U.S. Atomic Energy Commission Technical Information Service Extension, Oak Ridge, Tennessee, September, 1958 (SECRET - FORMERLY RESTRICTED DATA).

4. Newmark, N. M., "A Method of Computation for Structural Dynamics," Proceedings, ASCE, Vol. 85, No. EM 3, July, 1959, pp. 67-94.

5. Newmark, N. M., "Computation of Dynamic Structural Response in the Range Approaching Failure," Proceedings of the Symposium on Earthquake and Blast Effects on Structures, Earthquake Engineering Research Institute and University of California at Los Angeles, Los Angeles, California, June, 1952, pp. 114-129.

6. Newmark, N. M., "Analysis and Design of Structures to Resist Atomic Blast," Bulletin of the Virginia Polytechnic Institute, Engineering Experiment Station Series No. 106, Vol. 49, No. 3, Part 2, Blacksburg, Virginia, January, 1956, pp. 49-77.

7. Tung, T. P., and Newmark, N. M., A Review of Numerical Integration Methods for Dynamic Response of Structures, Report to Office of Naval Research, U. S. Navy, Contract N6ori-071(06), University of Illinois Civil Engineering Studies, Structural Research Series No. 69, Urbana, Illinois, March, 1954.

8. Eppink, R. T., Response of Arches Under Dynamic Loads, Ph.D. Thesis, Department of Civil Engineering, University of Illinois, Urbana, Illinois, 1960.

9. Terzaghi, K., and Peck, R. B., Soil Mechanics in Engineering Practice, John Wiley and Sons, New York, 1948.

10. Terzaghi, K., "Large Retaining-Wall Tests," Engineering News-Record, February 1, 22, March 8, 29, April 19, 1934.

11. Taylor, D. W., Fundamentals of Soil Mechanics, John Wiley and Sons, New York, 1948.

12. Peck, R. B., Hanson, W. E., and Thornburn, T. H., Foundation Engineering, John Wiley and Sons, New York, 1953.

13. Lee, T. U., Earth Pressure Against Spill-Through Abutments, Ph.D. Thesis, Department of Civil Engineering, University of Illinois, Urbana, Illinois, 1951.

14. Huntington, W. C., Earth Pressures and Retaining Walls, John Wiley and Sons, New York, 1957.

15. Merritt, J. L., and Newmark, N. M., Design of Underground Structures to Resist Nuclear Blast, Report to Chief of Engineers, U.S. Army, Contract DA-49-129-eng-312, University of Illinois, Civil Engineering Studies, Structural Research Series No. 149, Urbana, Illinois, April, 1958.

16. The Effects of Nuclear Weapons, U.S. Department of Defense and U.S. Atomic Energy Commission, U.S. Government Printing Office, Washington, D.C., June, 1957.

17. Anderson, F. E., Jr., "Blast Phenomena from a Nuclear Burst," Proceedings, ASCE, Vol. 84, No. ST7, November, 1958, pp. 1836-1 to 1836-8.

18. Smith, R. H., and Newmark, N. M., Numerical Integration for One-Dimensional Stress Waves, Report to Office of Naval Research, U.S. Navy, Contract Nonr 1834(03), University of Illinois Civil Engineering Studies, Structural Research Series No. 162, Urbana, Illinois, August, 1958.

19. Newmark, N. M., Hansen, R. J., Holley, M. J., and Biggs, J. M., Protective Construction Review Guide (Unclassified Extracts), Report to Office of the Secretary of Defense, U.S. Department of Defense, Contract SD-52, University of Illinois and Massachusetts Institute of Technology, January, 1959.

20. Brode, H. L., "Numerical Solutions of Spherical Blast Waves," Journal of Applied Physics, Vol. 26, No. 6, June, 1955, pp. 766-775.

21. Walls, W. A., The Influence of Blast and Earth Pressure Loading on the Dynamic Response of Flexible Underground Two-Hinged Arches, Ph.D. Thesis, Department of Civil Engineering, University of Illinois, Urbana, Illinois, 1960.

22. Jensen, V. P., "Ultimate Strength of Reinforced Concrete Beams as Related to the Plasticity Ratio of Concrete," University of Illinois Bulletin, Engineering Experiment Station Bulletin Series No. 345, Vol. 40, No. 44, Urbana, Illinois, June, 1943.

23. Brode, H. L., Numerical Solutions of Spherical Blast Waves, P-571-AEC (Supplement), The RAND Corporation, Santa Monica, California, July, 1955.

24. Structural Research Laboratory Programs, Structural Research Laboratory, Department of Civil Engineering, University of Illinois, Vol. 2, No. 462, Urbana, Illinois, October, 1956.

25. Timoshenko, S. P., and Gere, J. M., Theory of Elastic Stability, McGraw-Hill Book Company, New York, 1961.

APPENDIX A

HYDROSTATIC PRESSURE RATIOS IN SOIL SUBJECTED TO NUCLEAR BLAST LOADING

This study is an investigation of the effect of blast overpressure on calculated values of the hydrostatic pressure ratios in soil corresponding to the "Active State of Plastic Equilibrium" and the "Passive State of Plastic Equilibrium." The calculations are based upon classical earth pressure theory using the Coulomb assumptions to describe conditions in the soil failure wedges (cf. Section 2.2). A perfectly homogeneous, cohesionless soil is assumed with the blast overpressure considered as a surcharge loading.

Two solutions for each of the hydrostatic pressure ratios are compared, one obtained using the "Trial Wedge" method and the other obtained using an algebraic expression of Coulomb's method. The example chosen for these calculations is a semicircular arch, 16' 8" in diameter, with a depth of cover over the crown equal to one-fourth of the arch span. This structure is illustrated in Figure A.1. The blast loading is taken as the 100-psi shock wave resulting from a one-megaton nuclear explosion at the ground surface. The pressure surfaces are defined based on the dynamic model as described in Chapter IV. The soil is assumed to have a unit weight of 120 pounds per cubic foot and an angle of internal friction of 30 degrees. The effective friction angle between the arch and the soil is taken as two-thirds of the angle of internal friction of the soil, or 20 degrees.

The geometry and soil conditions of this problem are the same as those of the illustrative example discussed in Section 8.4. Thus, the average overpressure acting on the failure wedges may be obtained from Table 8.6. For the purposes of this study, the maximum value of the average

overpressure restraining the "passive" soil failure wedge is used, i.e. $\bar{p}'_{sj} = -96.4$ psi. While the average overpressure restraining the "active" soil failure wedge has a somewhat higher maximum value, i.e. $\bar{p}_{sj} = -98.3$ psi, it is considered at a later time when it has decayed to a value of 96.4 psi so that both sets of calculations may be made for the same restraining pressure. This is slightly more convenient. Actually, since this investigation deals principally with the effect of "large" surcharge loadings on calculated values of the hydrostatic pressure ratios corresponding to plastic equilibrium in soil, any reasonable value of the restraining pressure may be used.

Coulomb's formula for the hydrostatic pressure ratio corresponding to the "Active State of Plastic Equilibrium," K_A, as derived in reference (14), is given below as Equation (A.1).

$$K_A = \frac{\cos^2(\varphi-\omega)}{\cos^2 \omega \cos(\delta+\omega)\left[1+\sqrt{\frac{\sin(\delta+\varphi)\sin(\varphi-i)}{\cos(\delta+\omega)\cos(\omega-i)}}\right]^2} \qquad \text{(A.1)}$$

where φ = angle of internal friction of the soil

ω = angle of inclination with respect to the vertical of the lower bars of the model

δ = effective friction angle between the arch and the soil

i = slope of the ground surface with respect to the horizontal.

Substituting the soil properties listed above and the geometry shown in Figure A.1 into Equation (A.1) gives $K_A = 0.510$.

$$K_A = \frac{\cos^2(30^\circ-22^\circ 29.6')}{\cos^2(22^\circ 29.6')\cos(20^\circ+22^\circ 29.6')\left[1+\sqrt{\frac{\sin(20^\circ+30^\circ)\sin 30^\circ}{\cos(20^\circ+22^\circ 29.6')\cos(22^\circ 29.6')}}\right]^2}$$

$$= 0.510$$

Coulomb's formula for the hydrostatic pressure ratio corresponding to the "Passive State of Plastic Equilibrium," K_P, as derived in reference (14), is given below as Equation (A.2).

$$K_P = \frac{\cos^2(\varphi+\omega)}{\cos^2 \omega \cos(\omega-\delta) \left[1 - \sqrt{\frac{\sin(\varphi+\delta)\sin(\varphi+i)}{\cos(\omega-\delta)\cos(\omega-i)}}\right]^2} \qquad (A.2)$$

Substituting values into Equation (A.2) gives $K_P = 3.433$.

$$K_P = \frac{\cos^2(30^\circ+22^\circ 29.6')}{\cos^2(22^\circ 29.6')\cos(22^\circ 29.6'-20^\circ) \left[1 - \sqrt{\frac{\sin(30^\circ+20^\circ)\sin 30^\circ}{\cos(22^\circ 29.6'-20^\circ)\cos(22^\circ 29.6')}}\right]^2}$$

$$= 3.433$$

The results of the graphical solutions for the resultant forces on the pressure surface using the "Trial Wedge" method are given in Table A.1. The corresponding hydrostatic pressure ratios are calculated below.

No overpressure acting:

$$K_A = \frac{P_A}{\frac{1}{2}\gamma_s d_o^2}$$

where P_A = resultant force acting on the pressure surface for an "active" state of stress in the soil

$$= \frac{4,800}{\frac{1}{2}(120)(12.500)^2}$$

$$K_A = \frac{4,800}{9,375}$$

$$= 0.512$$

$$K_P = \frac{P_P}{\frac{1}{2}\gamma_s d_o^2}$$

where P_P = resultant force acting on the pressure surface for a "passive" state of stress in the soil.

$$= \frac{31,050}{9,375}$$

$$= 3.312$$

With overpressure acting:

$$K_A = \frac{P_A}{\frac{1}{2}\gamma_s d_o^2 + \bar{p}_{sj} d_o}$$

$$= \frac{92,500}{9,375+96.4(12.500)(144)}$$

$$= 0.506$$

$$K_P = \frac{P_P}{\frac{1}{2}\gamma_s d_o^2 + \bar{p}'_{sj} d_o}$$

$$= \frac{619,000}{182,900}$$

$$= 3.384$$

The inclination of the failure surfaces with respect to the horizontal are presented in Table A.2. The inclinations obtained from the "Trial Wedge" solutions are compared with the assumed inclinations of $(\frac{\pi}{4} + \frac{\varphi}{2})$ for the "active" failure surface and $(\frac{\pi}{4} - \frac{\varphi}{2})$ for the "passive" failure surface for the numerical work in this thesis.

From the comparative results presented in Table A.1, it may be concluded that the overpressure loadings have a negligible effect upon the hydrostatic pressure ratios in the soil. Further, both the "Trial Wedge" method and Equations (A.1) and (A.2) give essentially the same values of

K_A and K_P. Finally, in Table A.2 it may be seen that the assumed inclinations of the failure surfaces in the soil are in reasonable agreement with the inclinations obtained from the "Trial Wedge" solutions.

TABLE A.1

HYDROSTATIC PRESSURE RATIOS IN SOIL AS COMPUTED BY "TRIAL WEDGE" METHOD AND COULOMB FORMULAS

	State of Stress in Soil	Trial Wedge		Formula
		Without Blast	With Blast	
Resultant Force on Pressure Surface, kips	Active, P_A	4.80	92.5	
	Passive, P_P	31.05	619	
Hydrostatic Pressure Ratio	Active, K_A	0.512	0.506	0.510
	Passive, K_P	3.312	3.384	3.433

TABLE A.2

INCLINATION WITH RESPECT TO HORIZONTAL OF FAILURE SURFACES IN SOIL

State of Stress in Soil	Trial Wedge Solution		Assumed Value
	Without Blast	With Blast	
Active	64°	64°	$(\frac{\pi}{4} + \frac{\varphi}{2}) = 60^\circ$
Passive	26°	26°	$(\frac{\pi}{4} - \frac{\varphi}{2}) = 30^\circ$

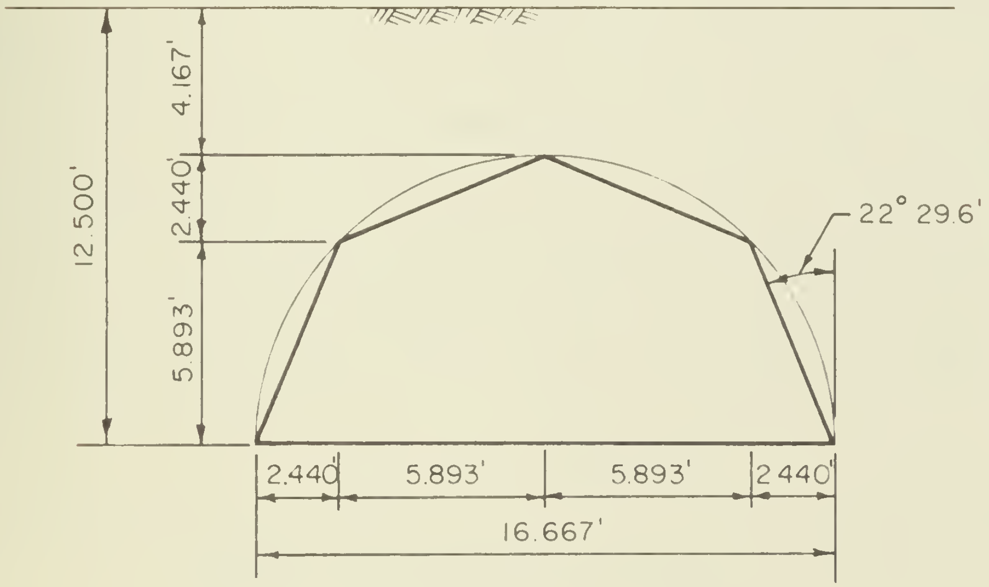

Figure A.1. Semicircular Arch, B = 16'8", d_c = B/4

APPENDIX B

SHAPE OF SHOCK FRONT IN SOIL

The object of this study is the determination of the configuration of the shock front of the air-induced shock wave in soil. Primary interest is limited to those depths below the ground surface associated with the shallow-buried arches studied in this thesis. Knowledge of the shock front configuration is needed in order to define the loading on the arch during its envelopment by the shock wave (cf. Chapter VI).

The approach used in this study is outlined below. Essentially, a point of interest is selected and the location of the shock front of the air-induced shock wave in soil determined for the time after the explosion corresponding to the time of arrival of the shock wave in air at this point of interest. It is assumed that the shock wave in air travels with velocity, U, which is a continuously varying function of the peak overpressure and ambient atmospheric conditions as expressed by Equation (B.1).(16)

$$U = c_o \sqrt{1 + 6p_{so}/7P_o} \tag{B.1}$$

where c_o = ambient sound velocity in air ahead of the shock front (assumed as 1130 feet per second)

p_{so} = peak air overpressure at the shock front

P_o = ambient atmospheric pressure ahead of the shock front (assumed as 14.7 psi).

The shock wave in soil is assumed to travel at the seismic velocity of the soil, C_s. This study considers a semi-infinite, homogeneous, soil mass with no surface irregularities and with a constant seismic velocity. Further, the seismic velocity of the soil is assumed not to vary with depth, direction or with the overpressure level in the shock wave.

The shock wave tends to travel symmetrically outward from Ground Zero as a roughly spherical segment of ever-increasing radius. Therefore, this problem may be considered in two dimensions and the shock front assumed to extend indefinitely in the third dimension. At distances from Ground Zero which are of interest in this problem, the radius of curvature of the shock front in air is quite large, so that this assumption does not lead to significant error.

The calculations in this appendix are based upon a one-megaton, contact surface burst. The pressure-distance relationship is taken from reference (17) The point of interest is selected at a distance from Ground Zero such that the peak value of the overpressure at the shock front is 100 psi. Seismic velocities of 1,000, 2,000, 3,000 and 6,000 feet per second are considered.

The procedure followed in the calculations may be divided into six steps as follows:

1. Select the point of interest.

2. Select a series of check points, 1, 2, 3,...n, between the point of interest and Ground Zero. Plot these points to scale along a horizontal line representing the ground surface.

3. Calculate the time interval, Δt_n, required for the shock wave in air to travel between each of the check points and the point of interest.

4. Calculate the distance traveled by the shock front in soil, d_{sn}, at the seismic velocity of the soil, C_s, during each time interval found in Step 3.

$$d_{sn} = (\Delta t)_n C_s \tag{B.2}$$

5. Using each check point, n, selected in Step 2 as a center, swing a semicircular arc in the "soil" with a radius equal to the value of d_{sn} calculated for that check point in Step 4.

6. A curve tangent to the arcs drawn in Step 5 is thus an approximation of the shock front in soil at the instant the shock front reaches the point of interest selected in Step 1.

The results of this study are presented in Figures B.1 through B.4.

While this study is quite limited, it may be concluded tentatively that for the relatively shallow depths considered in this thesis, the shock front in soil may be considered as a plane perpendicular to the direction of travel of the shock wave and inclined at an angle, η, with respect to the horizontal as given by Equations (B.3). These equations may be written with the aid of Figure B.5.

$$\begin{aligned} C_s/U &\leq 1: &\quad \eta &= \arcsin C_s/U \\ C_s/U &\geq 1: &\quad \eta &= \pi/2 \end{aligned} \tag{B.3}$$

where C_s = seismic velocity of the soil

U = velocity of the shock wave in air at the point of interest.

While the shock front in soil at depths close to the ground surface for $C_s/U > 1$ remains essentially vertical, the fact that it tends to "run ahead" of the shock front in air may tend to increase the "rise time" of the overpressure-time function in the soil at a particular point of interest. Since an increase in the rise time tends to reduce the dynamic response of a system to a given impulse, this effect is not considered in the numerical work of this thesis (cf. Section 2.4).

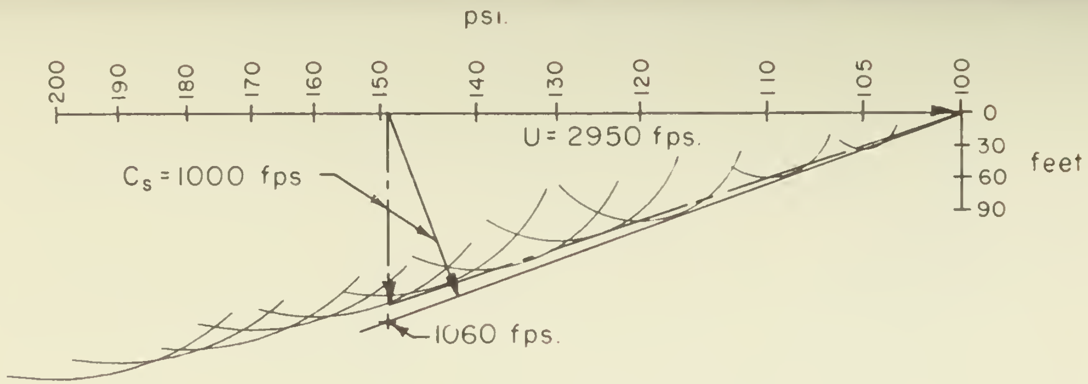

Figure B.1. Shock Front in Soil: p_{so} = 100 psi, C_s = 1,000 fps

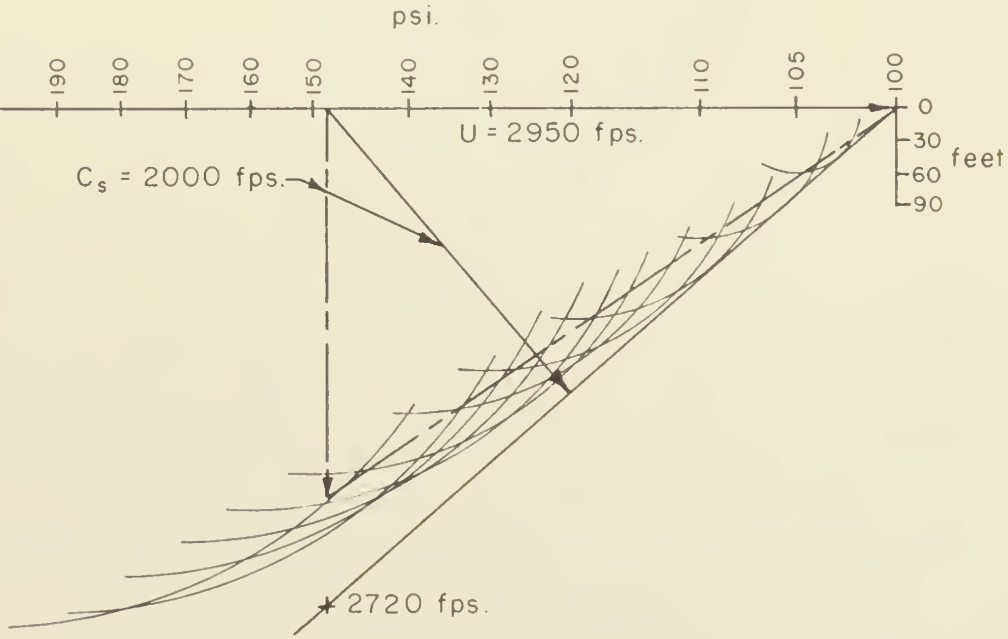

Figure B.2. Shock Front in Soil: p_{so} = 100 psi, C_s = 2,000 fps

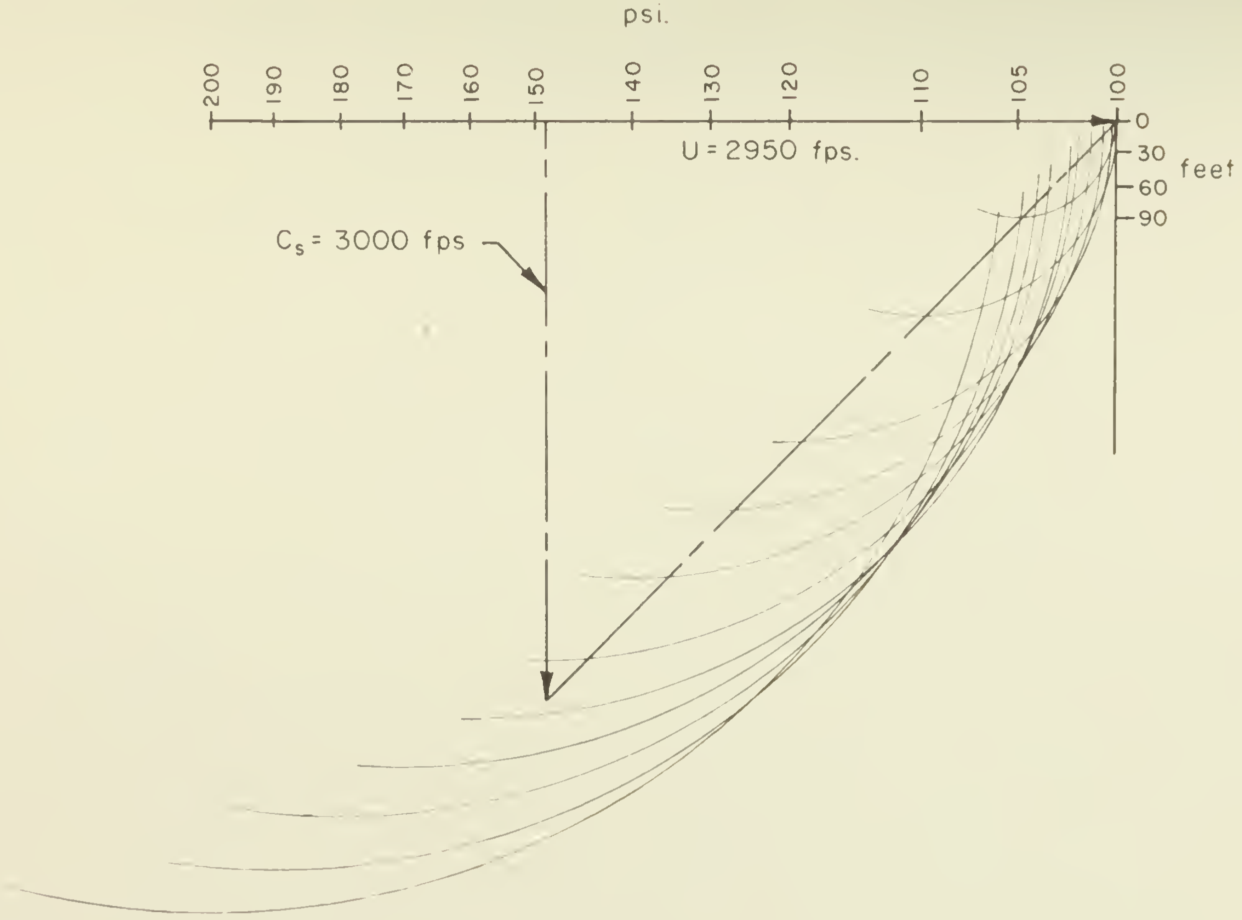

Figure B.3. Shock Front in Soil: p_{so} = 100 psi, C_s = 3,000 fps

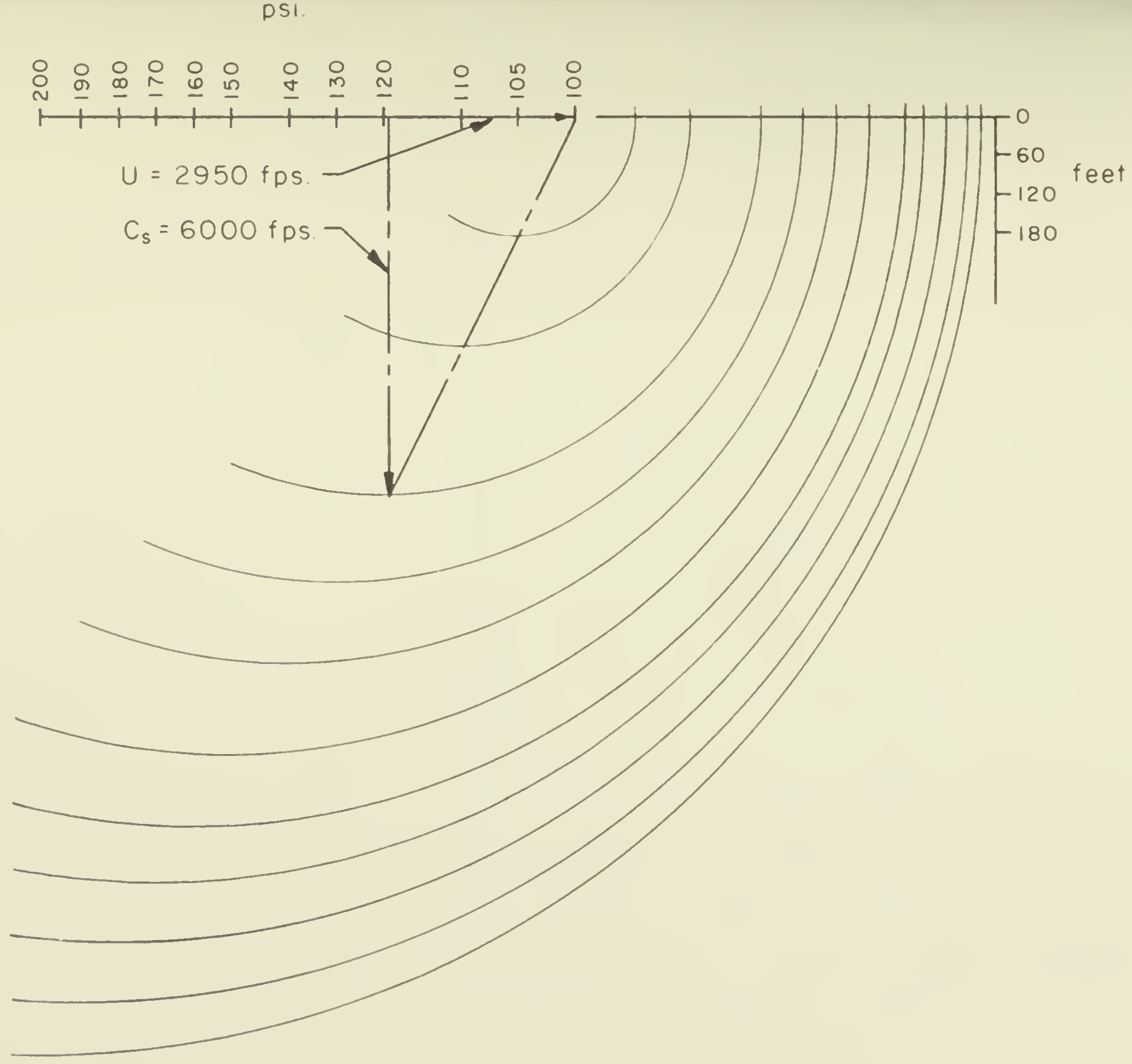

Figure B.4. Shock Front in Soil: p_{so} = 100 psi, C_s = 6,000 fps

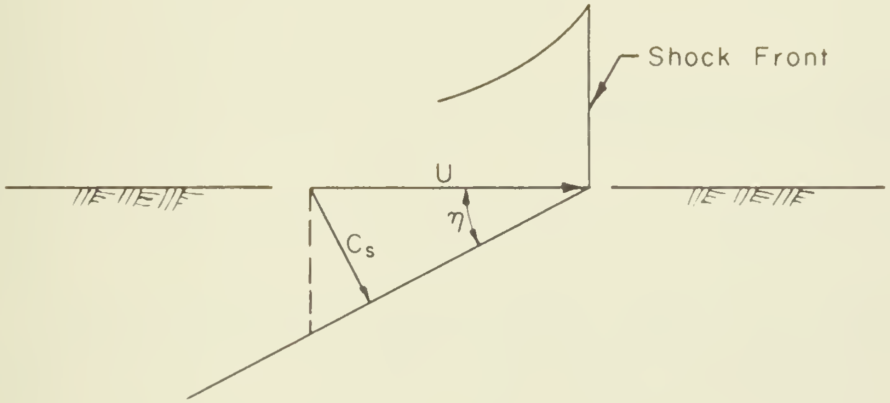

Figure B.5. Inclination of Shock Front in Soil

APPENDIX C

TABULAR COMPARISONS OF NUMERICAL RESULTS

This appendix contains a series of tables in which comparisons are made of the various numerical solutions. In general, quantities are expressed as follows:

Displacements, h_j, in feet

Overpressures, p, in psi

Cover depth at crown, d_c, in proportion of arch span, B

Time, t, in seconds

Natural periods of vibration, T_m, in seconds.

The sign convention used in these tables is the same as that stated in Section 1.2, i.e. displacements to the right and upward are considered positive. The shock wave is considered to engulf the structure from left to right.

A summary of the numerical examples considered is contained in Table 8.5.

TABLE C.1

NATURAL PERIODS OF VIBRATION WITH NO OVERPRESSURE ACTING ON SOIL FAILURE WEDGES

(seconds)

Soil Cover	Reinforced Concrete Arch			Corrugated Metal Arch		
	Asymmetric	Symmetric		Asymmetric	Symmetric	
		In	Out		In	Out
None	0.147	0.115	0.115	0.484	0.389	0.389
d_c = 0	0.163	0.156	0.133	0.175	0.234	0.189
= B/8	0.144	0.179	0.153	0.183	0.255	0.214
= B/4	0.129	0.172	0.148	0.162	0.233	0.199
= B/2	0.092	0.136	0.123	0.111	0.173	0.154

TABLE C.2

NATURAL PERIODS OF VIBRATION AT FIRST MAXIMUM RESPONSE OF LEEWARD HAUNCH

(seconds)

(Motion: "Symmetric-Out" in all cases)

Depth of Cover Over Crown	Reinforced Concrete Arch		Corrugated Metal Arch		
	100 psi	1000 psi	50 psi	100 psi	1000 psi
0	0.034	0.012	0.060	0.043	0.015
B/8	0.038	0.013	0.073	0.045	(1)
B/4	0.037	0.015	0.073	0.054	0.019
B/2	0.032	0.011	0.062	0.046	(1)

(1) Not calculated.

TABLE C.3

FIRST MAXIMUM RESPONSE AT WINDWARD HAUNCH

(Neglect small initial inward movement)

Cover Depth at Crown	Parameter(1)	Reinforced Concrete Arch (Span = 16'8")		Corrugated Metal Arch (Span = 25' 1 1/4")		
		100 psi	1000 psi	50 psi	100 psi	1000 psi
0	h_1	-0.0135	-0.0137	-0.0191	-0.0138	-0.0199
	t	0.0214	0.0068	0.0383	0.0254	0.0087
B/8	h_1	-0.0087	-0.0092	-0.0121	-0.0132	(2)
	t	0.0236	0.0075	0.0450	0.0336	
B/4	h_1	-0.0063	-0.0068	-0.0084	-0.0093	-0.0101
	t	0.0229	0.0074	0.0450	0.0337	0.0110
B/2	h_1	-0.0040	-0.0043	-0.0051	-0.0057	(2)
	t	0.0204	0.0065	0.0393	0.0296	

(1) h_1 = horizontal displacement of windward haunch, in feet.
t = time corresponding to h_1, in seconds.

(2) Not computed.

TABLE C.4

FIRST MAXIMUM RESPONSE AT CROWN

(Neglect small initial upward movement)

Cover Depth at Crown	Parameter(1)	Reinforced Concrete Arch (Span = 16'8")		Corrugated Metal Arch (Span = 25' 1 1/4")		
		100 psi	1000 psi	50 psi	100 psi	1000 psi
0	h_5	-0.0237	-0.0281	-0.0344	-0.0275	-0.0441
	t	0.0186	0.0053	0.0325	0.0213	0.0069
B/8	h_5	-0.0151	-0.0173	-0.0205	-0.0218	(2)
	t	0.0205	0.0060	0.0390	0.0285	
B/4	h_5	-0.0108	-0.0123	-0.0141	-0.0151	-0.0171
	t	0.0198	0.0060	0.0388	0.0285	0.0085
B/2	h_5	-0.0069	-0.0073	-0.0085	-0.0095	(2)
	t	0.0174	0.0053	0.0339	0.0252	

(1) h_5 = vertical displacement of crown, in feet.
t = time corresponding to h_5, in seconds

(2) Not computed.

TABLE C.5

FIRST MAXIMUM RESPONSE AT LEEWARD HAUNCH

Cover Depth at Crown	Parameter(1)	Reinforced Concrete Arch (Span = 16'8")		Corrugated Metal Arch (Span = 25' 1 1/4")		
		100 psi	1000 psi	50 psi	100 psi	1000 psi
0	h_3	+0.0119	+0.0163	+0.0181	+0.0162	+0.0268
	t	0.0165	0.0050	0.0293	0.0195	0.0065
B/8	h_3	+0.0075	+0.0094	+0.0102	+0.0108	(2)
	t	0.0181	0.0055	0.0341	0.0247	
B/4	h_3	+0.0054	+0.0066	+0.0070	+0.0076	+0.0092
	t	0.0173	0.0053	0.0337	0.0246	0.0075
B/2	h_3	+0.0037	+0.0039	+0.0044	+0.0049	(2)
	t	0.0154	0.0045	0.0295	0.0220	

(1) h_3 = horizontal displacement of leeward haunch, in feet.
t = time corresponding to h_3, in seconds.

(2) Not computed.

TABLE C.6

EFFECT OF HORIZONTAL-TO-VERTICAL OVERPRESSURE RATIO ON LATERAL RESPONSE(1)

(First maximum values)

Parameter(2)	K_{pr}			
	1/4	1/2	3/4	1
$(+h_1)_{max}$	0.0007	0.0013	0.0022	0.0034
Time	0.0068	0.0086	0.0104	0.0121
$(+h_3)_{max}$	0.0076	0.0057	0.0043	0.0034
Time	0.0246	0.0221	0.0192	0.0164
$(-h_5)_{max}$	-0.0151	-0.0106	-0.0060	-0.0016
Time	0.0285	0.0279	0.0268	0.0238
$(-h_1)_{max}$	-0.0093	-0.0076	-0.0059	-0.0044
Time	0.0337	0.0340	0.0342	0.0342

(1) Based on Corrugated Metal Arch, p_{so} = 100 psi, d_c = B/4.

(2) h_1 = horizontal movement of windward haunch, in feet

h_3 = horizontal movement of leeward haunch, in feet

h_5 = vertical movement of crown, in feet

Time, in seconds

TABLE C.7

EFFECT OF INCLINATION OF SHOCK FRONT IN SOIL ON LATERAL RESPONSE(1)

(First maximum values(2))

Inclination of Shock Front in Soil	90°00'	54°22'	18°44'
Seismic Velocity in Soil	3000 fps	2400 fps	1000 fps
$(+h_5)_{max}$	+0.0001	+0.0001	(3)
Time	0.0031	0.0022	
$(+h_1)_{max}$	+0.0004	+0.0002	(4)
Time	0.0045	0.0036	
$(+h_3)_{max}$	+0.0054	+0.0052	+0.0061
Time	0.0173	0.0163	0.0157
$(-h_5)_{max}$	-0.0108	-0.0105	-0.0112
Time	0.0198	0.0189	0.0174
$(-h_1)_{max}$	-0.0063	-0.0062	-0.0058
Time	0.0229	0.0220	0.0210

(1) Based on Reinforced Concrete Arch, $d_c = B/4$, $p_{so} = 100$ psi

(2) h_1 = horizontal movement of windward haunch, in feet

h_3 = horizontal movement of leeward haunch, in feet

h_5 = vertical movement of crown, in feet.

(3) No initial upward movement of crown.

(4) No initial inward movement of windward haunch.

APPENDIX D

GRAPHICAL PRESENTATION OF NUMERICAL RESULTS

The results of the numerical work done in connection with this thesis are presented in this appendix in graphical form. Displacement-time "response" curves are included for each of the problems solved. Three curves are plotted for each problem as follows:

h_1 = horizontal displacement of the windward haunch
h_3 = horizontal displacement of the leeward haunch
h_5 = vertical displacement of the crown

The sign convention used in this appendix is the same as that stated in Section 1.2, i.e. displacements to the right and upward are considered positive. In addition to the response curves, the configuration of the dynamic model is illustrated for two of the problems at several significant times in their response histories.

The problems are described in Chapter VIII and summarized in Figure 8.5. A set of sample calculations for one of the problems is presented in Section 8.4. The significance of the results is discussed in Chapter IX.

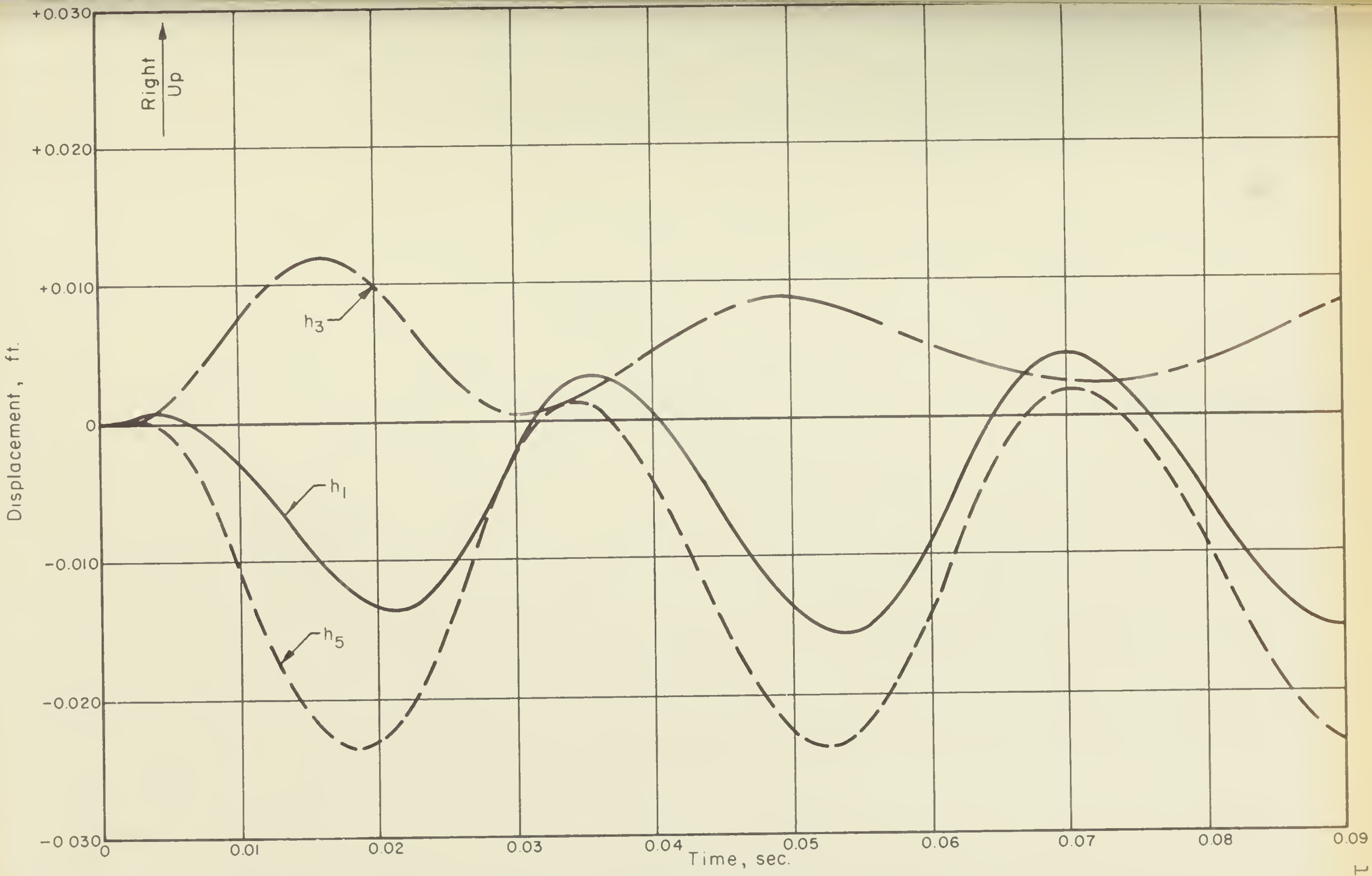

Figure D.1. Response Curves for Reinforced Concrete Arch: p_{so} = 100 psi, d_c = 0

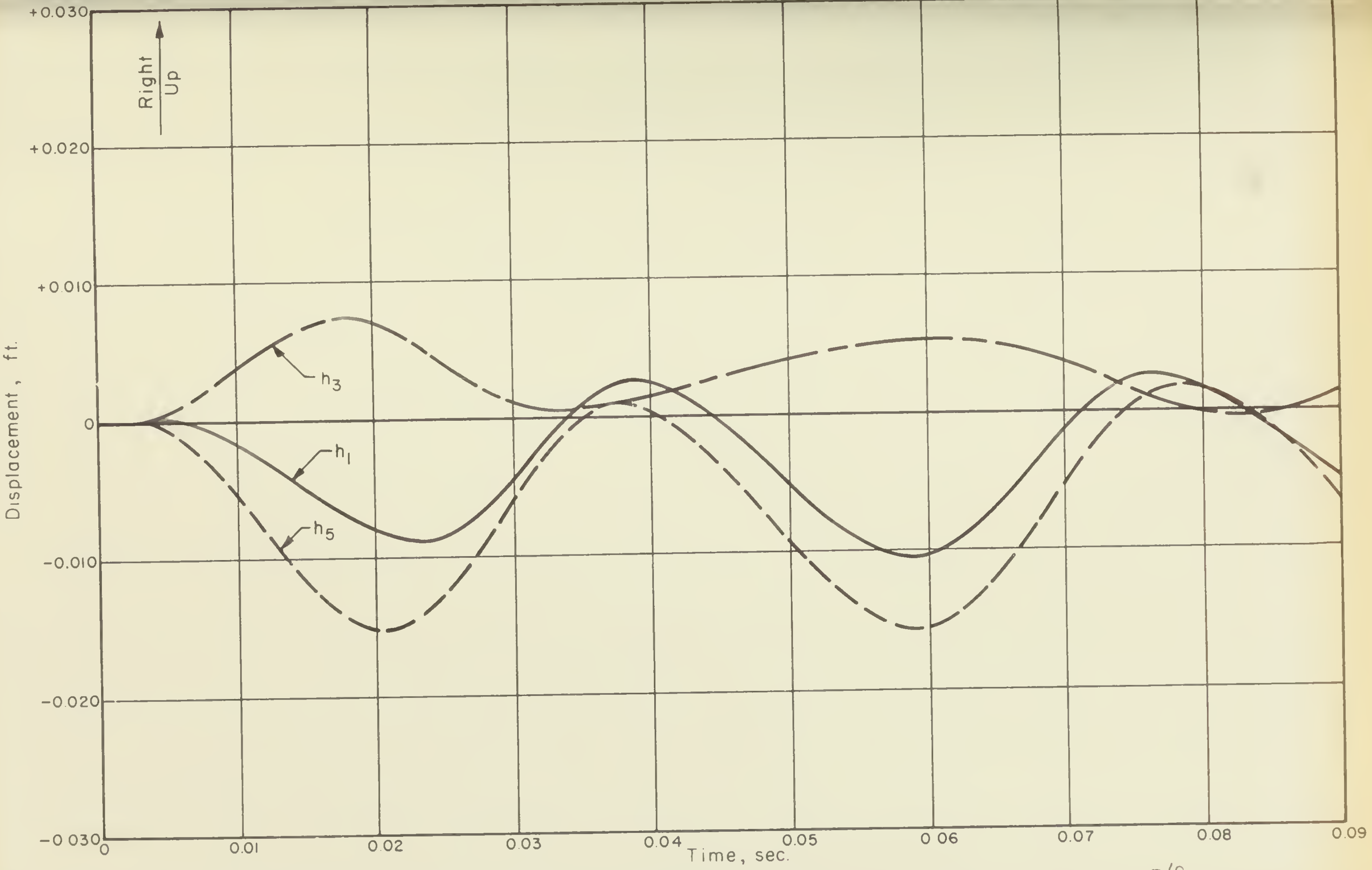

Figure D.2. Response Curves for Reinforced Concrete Arch: p_{so} = 100 psi, d_c = B/8

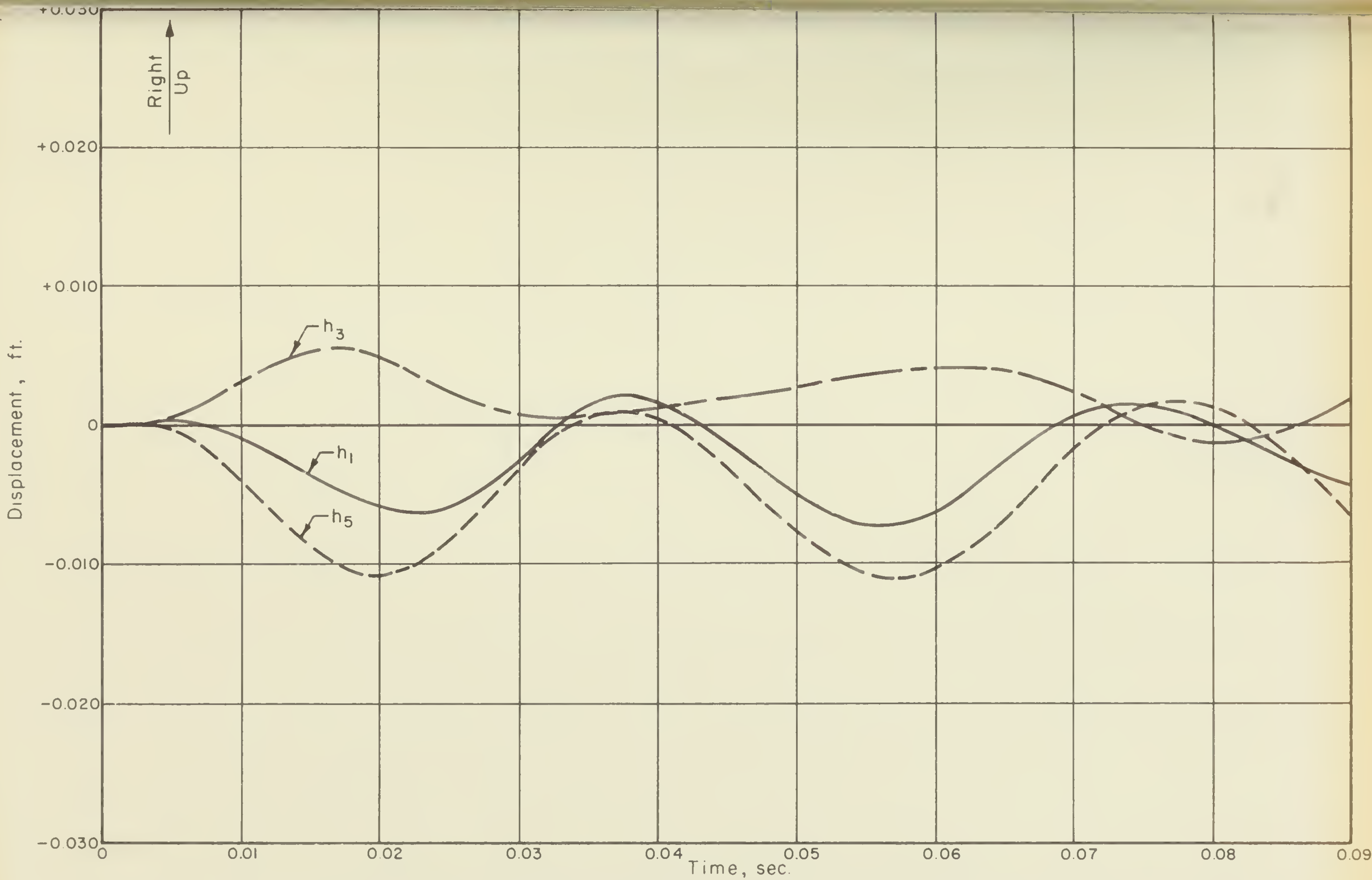

Figure D.3. Response Curves for Reinforced Concrete Arch: p_{so} = 100 psi, d_c = B/4, C_s = 3,000 fps

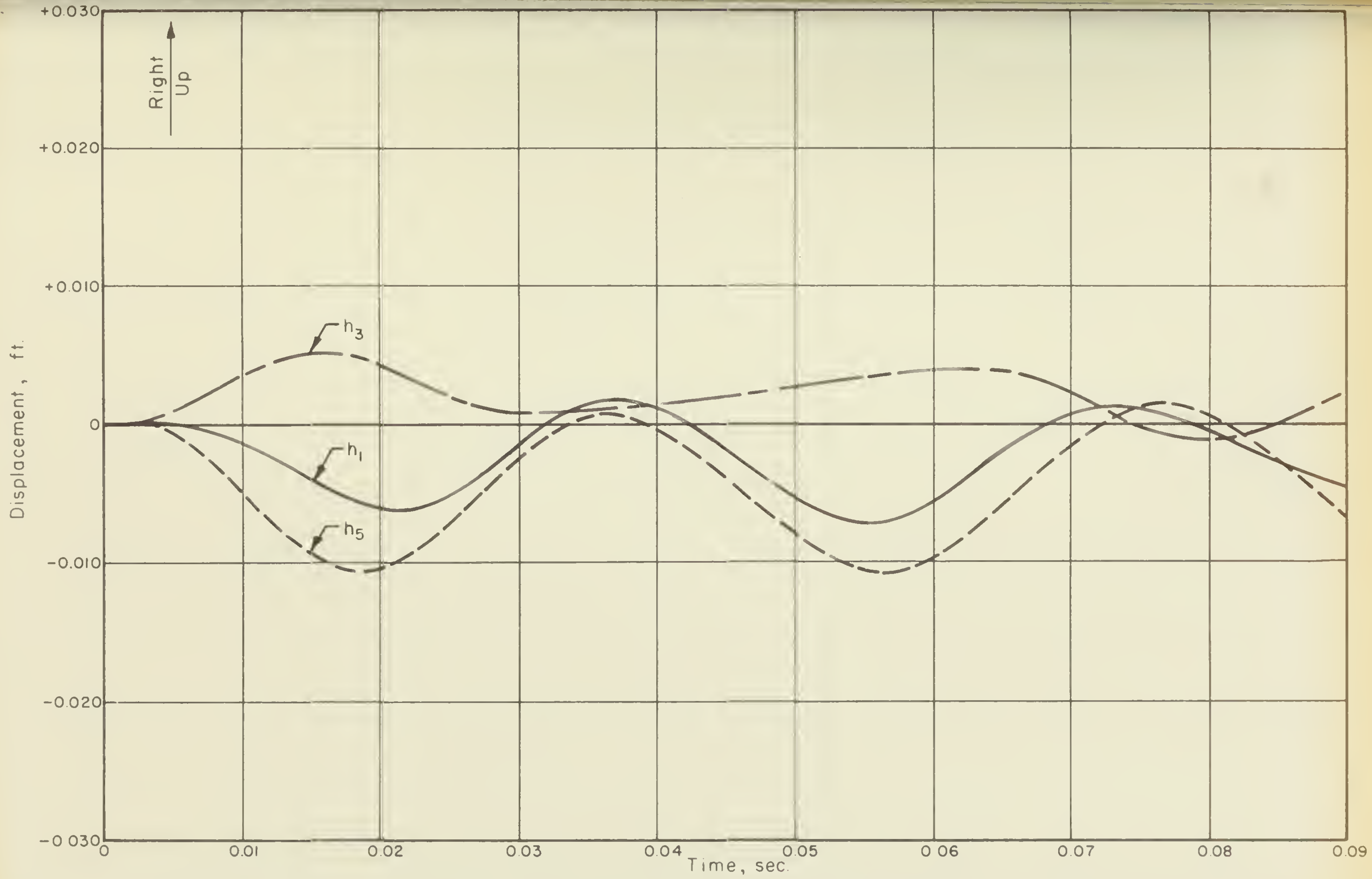

Figure D.4. Response Curves for Reinforced Concrete Arch: $p_{so} = 100$ psi, $d_c = B/4$, $C_s = 2,400$ fps

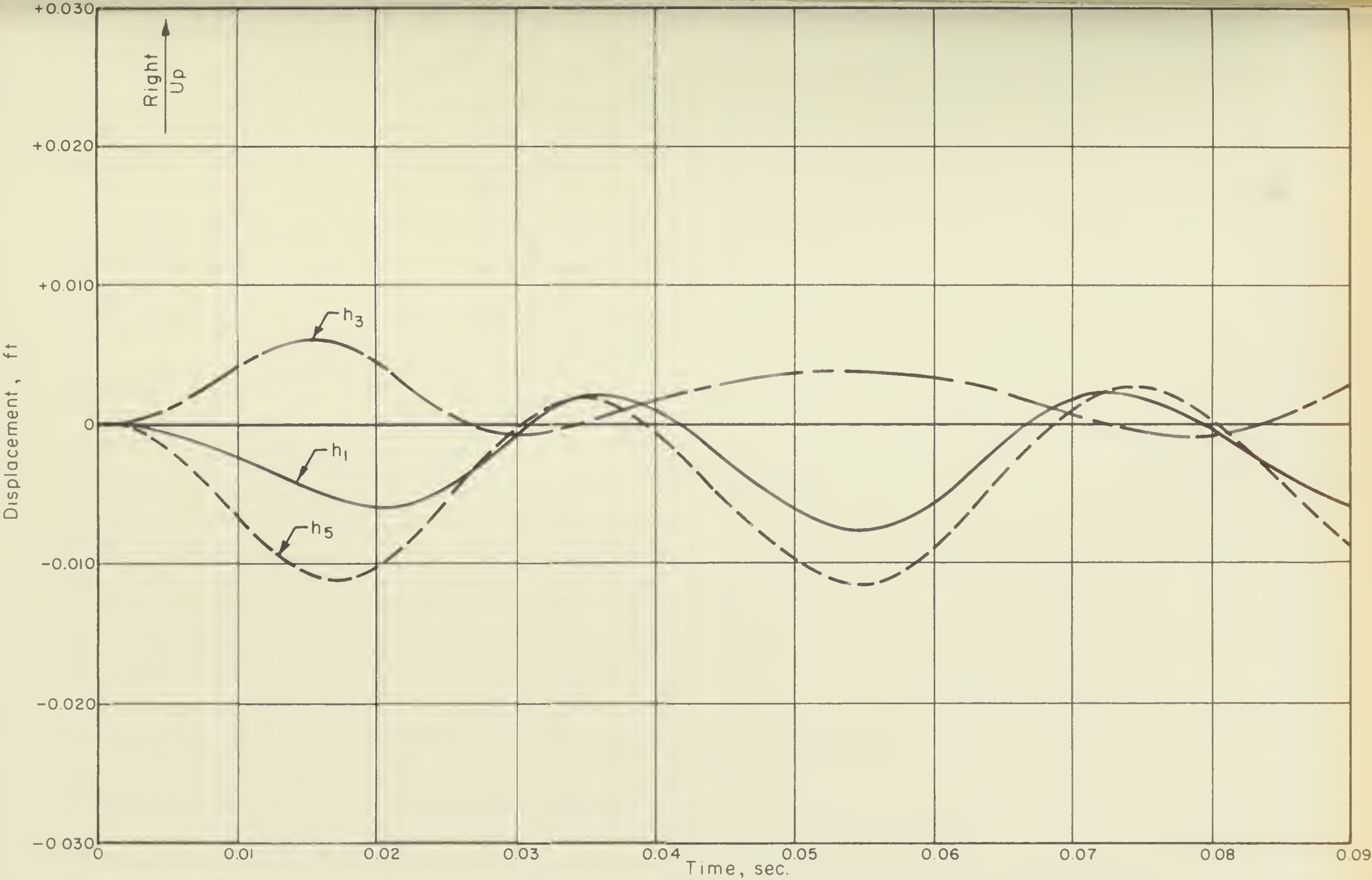

Figure D.5. Response Curves for Reinforced Concrete Arch: p_{so} = 100 psi, d_c = B/4, C_s = 1,000 fps

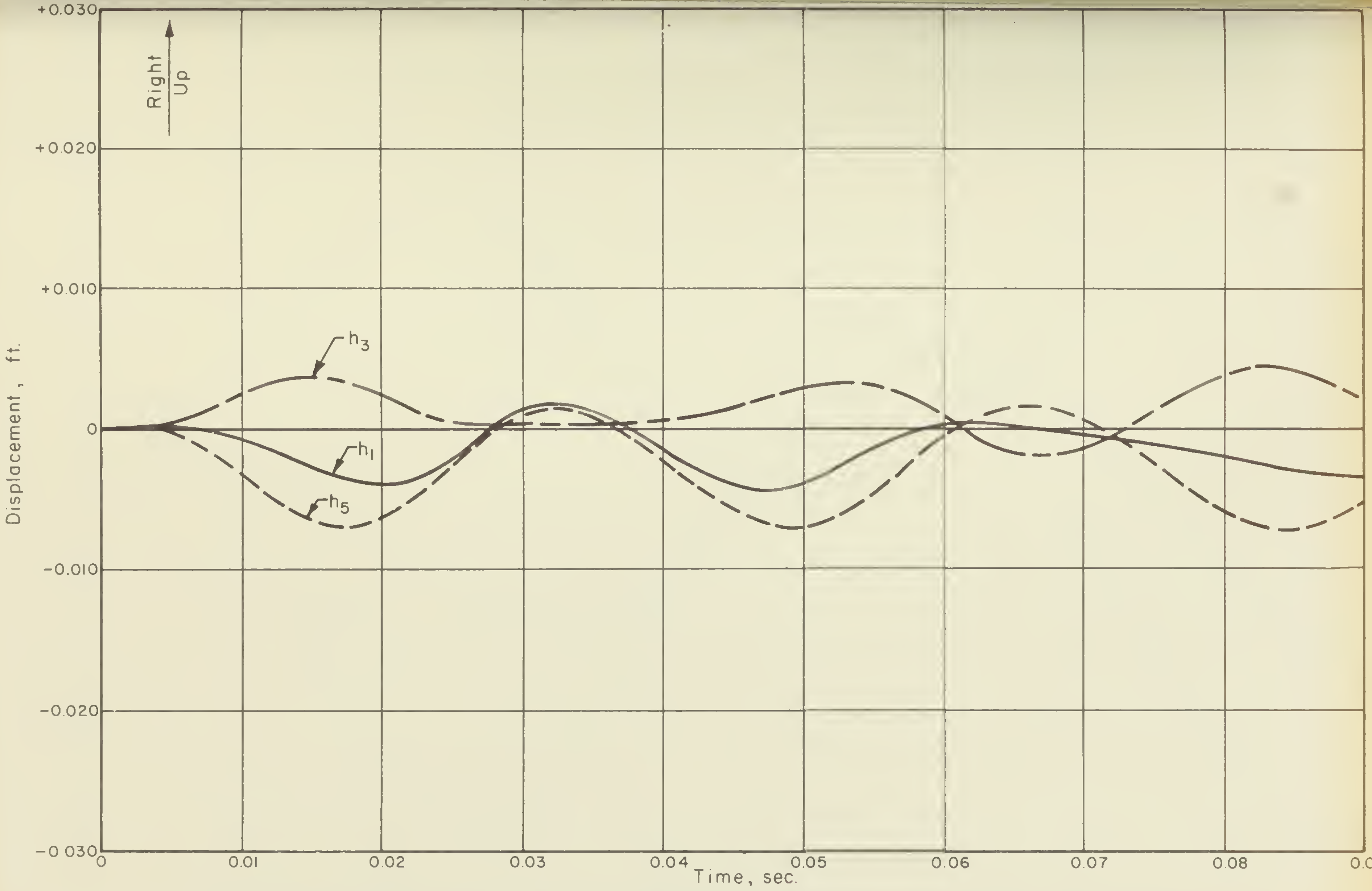

Figure D.6. Response Curves for Reinforced Concrete Arch: p_{so} = 100 psi, d_c = B/2

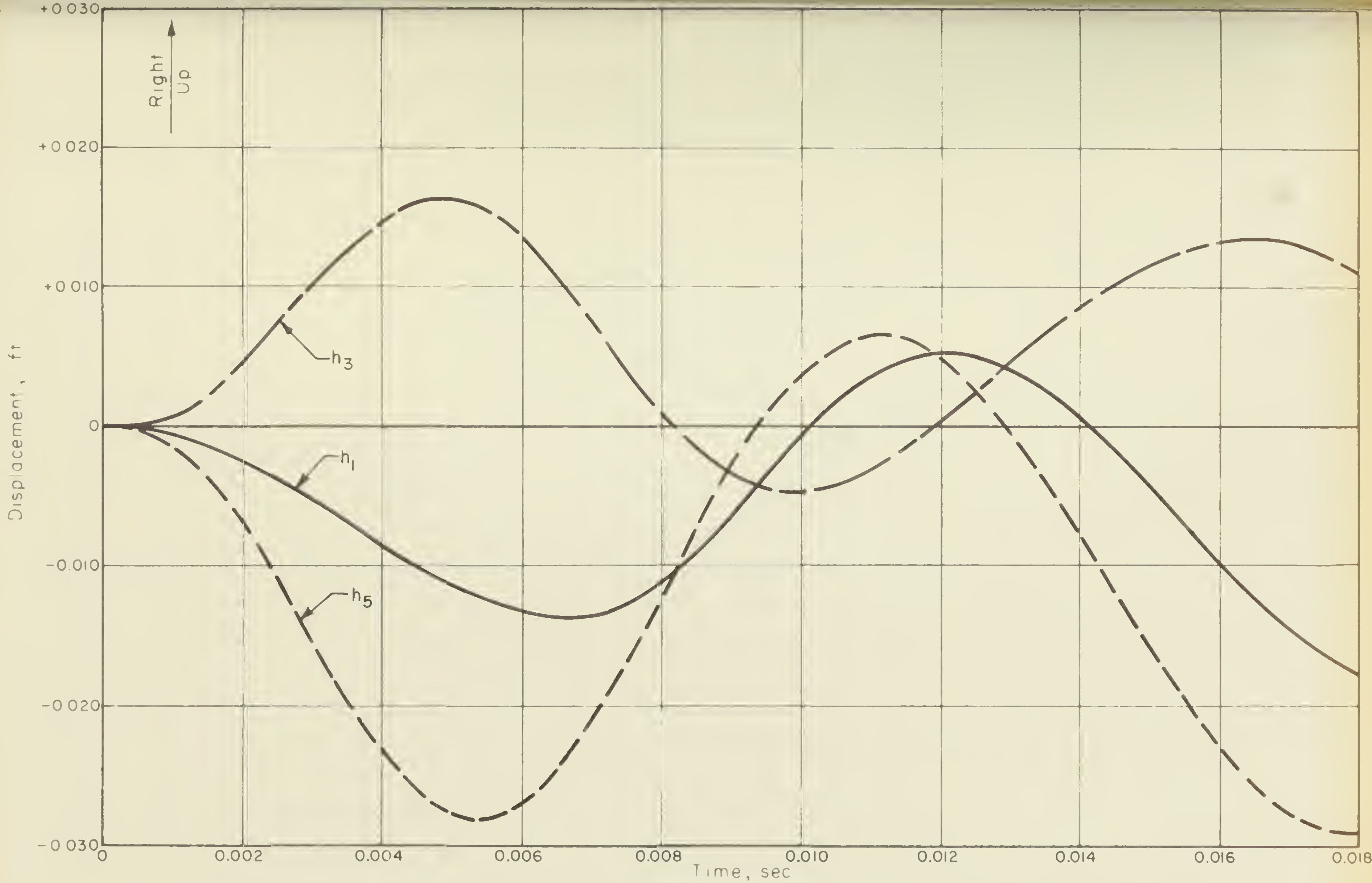

Figure D.7. Response Curves for Reinforced Concrete Arch: p_{so} = 1,000 psi, d_c = 0

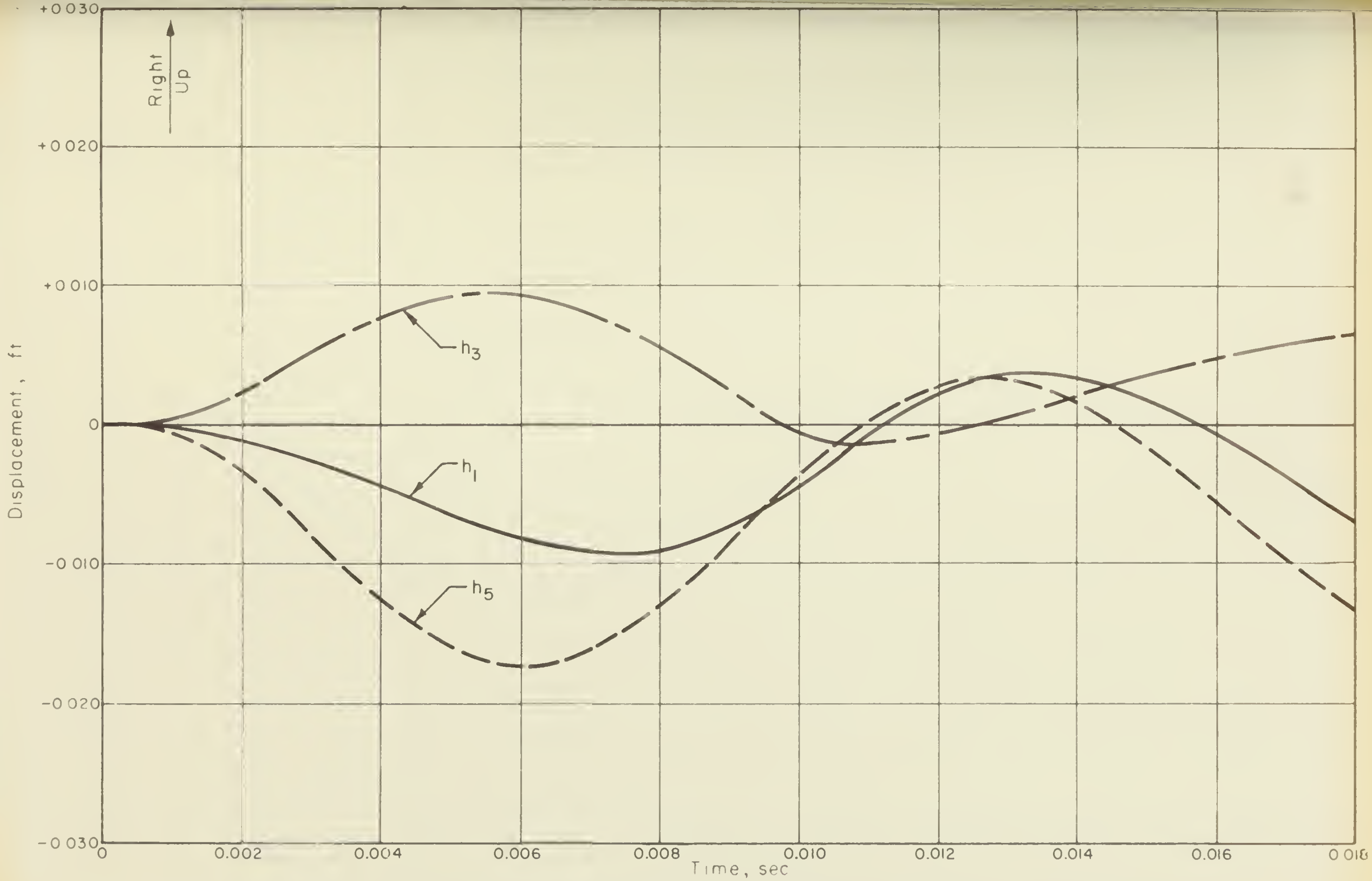

Figure D.8. Response Curves for Reinforced Concrete Arch: p_{so} = 1,000 psi, d_c = B/8

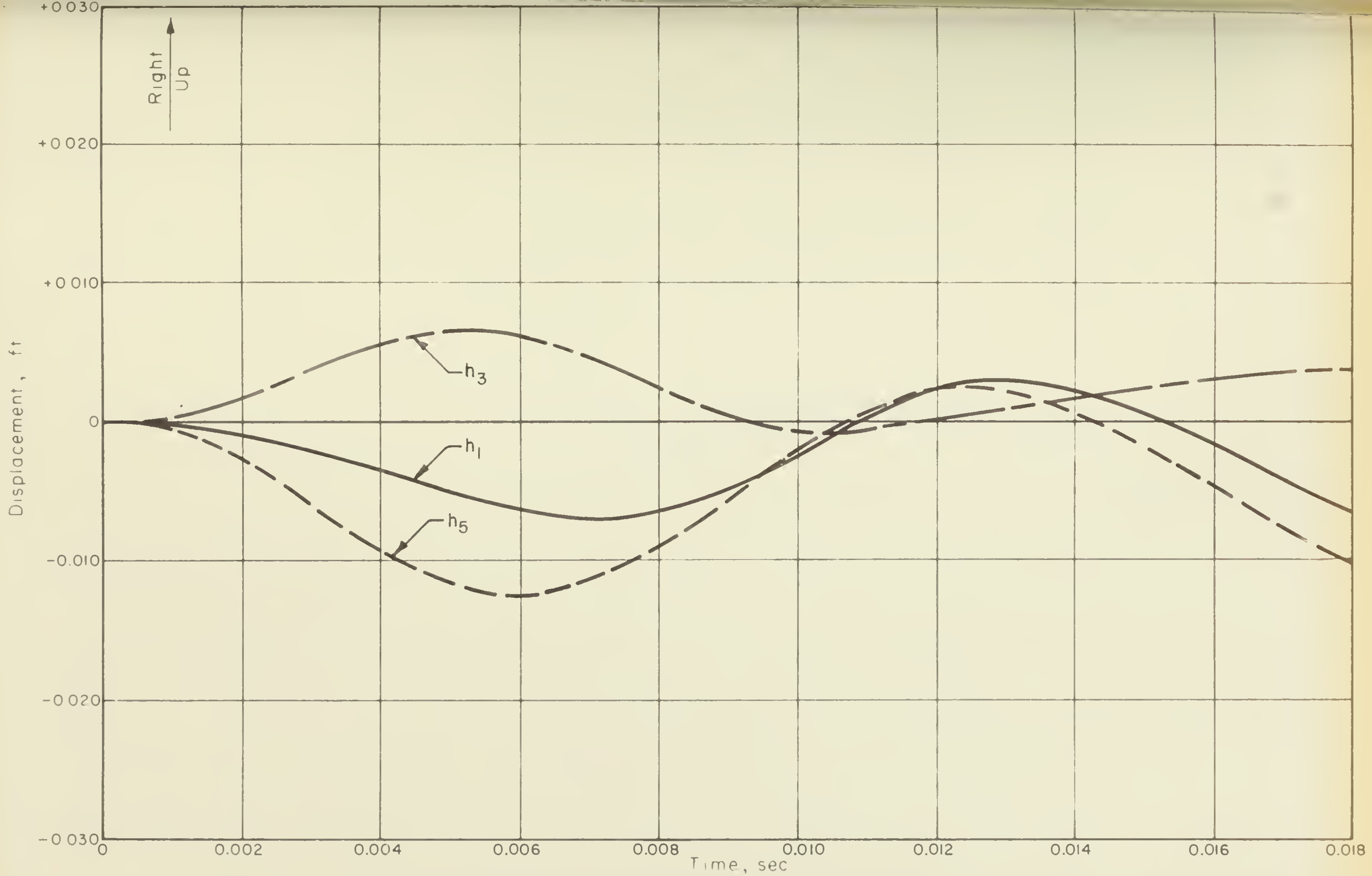

Figure D.9. Response Curves for Reinforced Concrete Arch: p_{so} = 1,000 psi, d_c = B/4

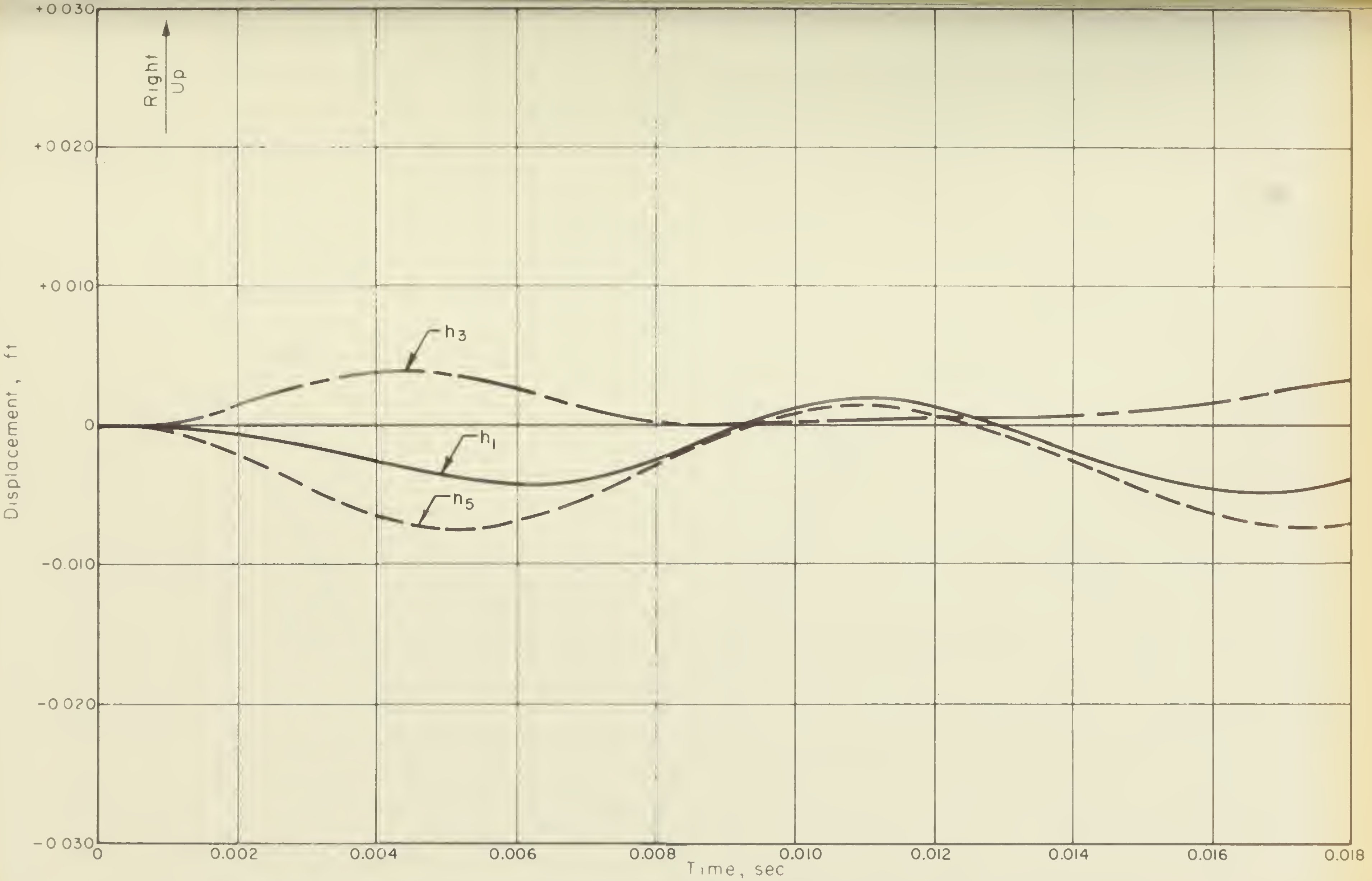

Figure D.10. Response Curves for Reinforced Concrete Arch: p_{so} = 1,000 psi, d_c = B/2

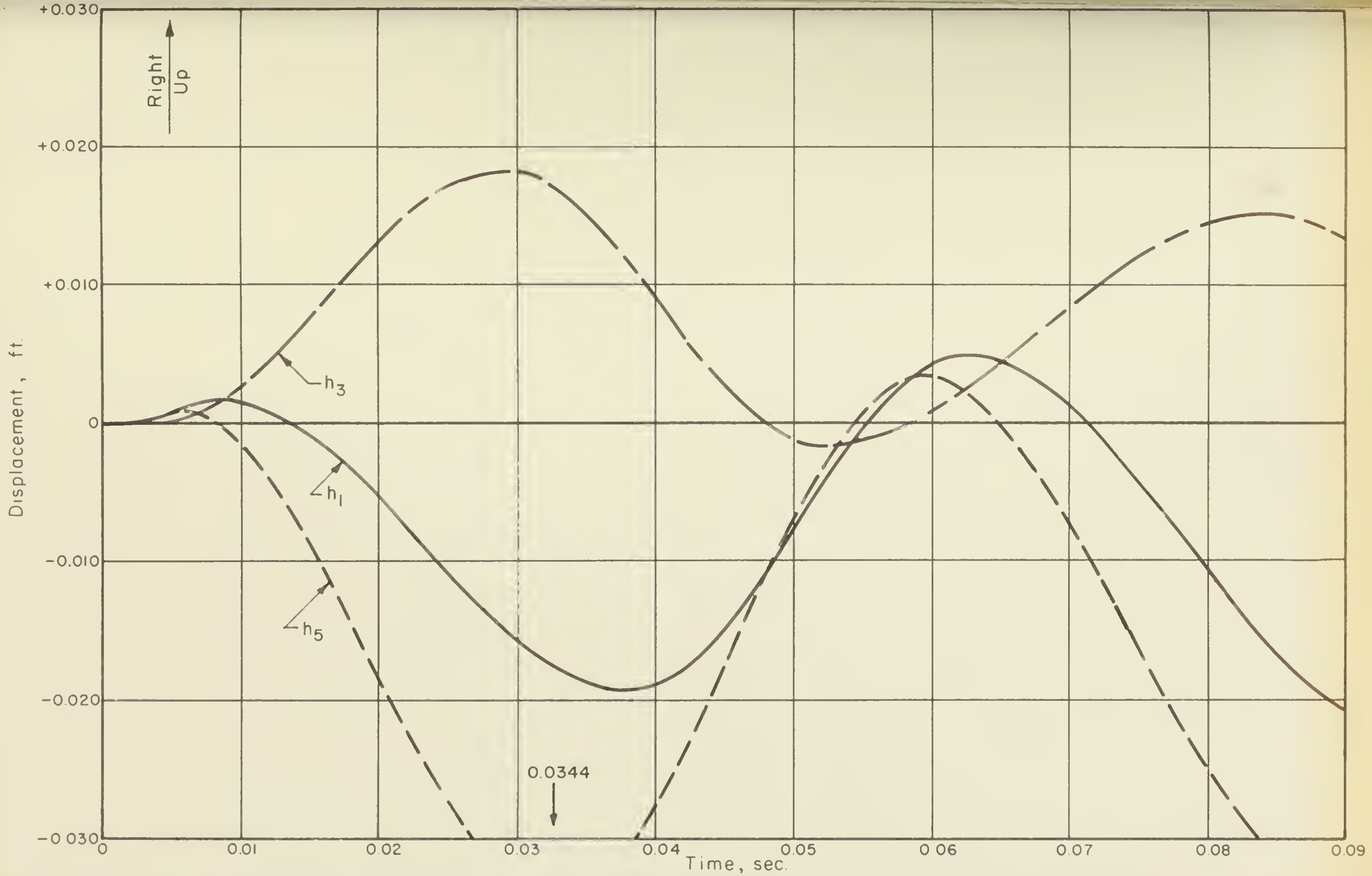

Figure D.11. Response Curves for Corrugated Metal Arch: p_{so} = 50 psi, d_c = 0

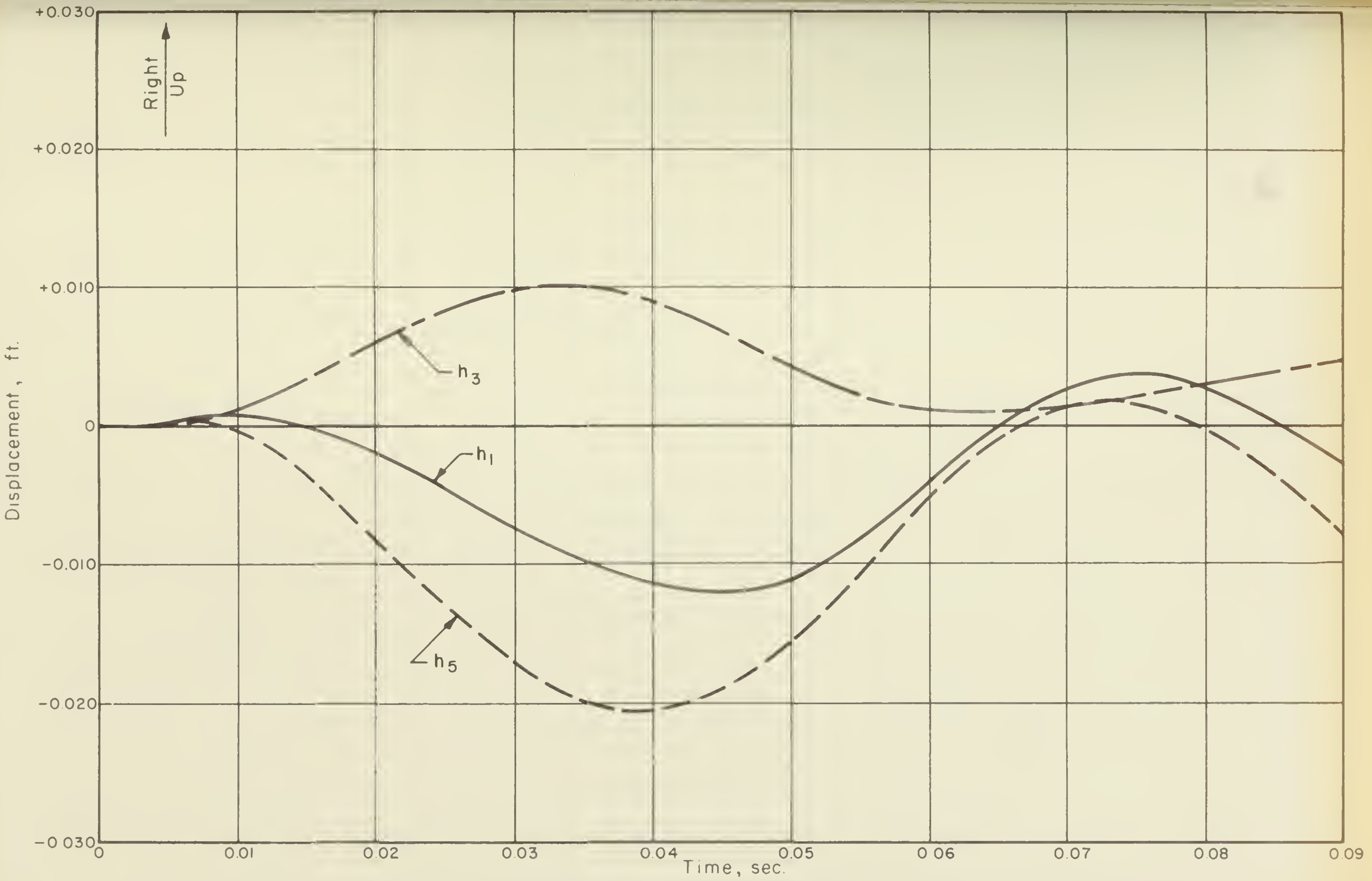

Figure D.12. Response Curves for Corrugated Metal Arch: p_{so} = 50 psi, d_c = B/8

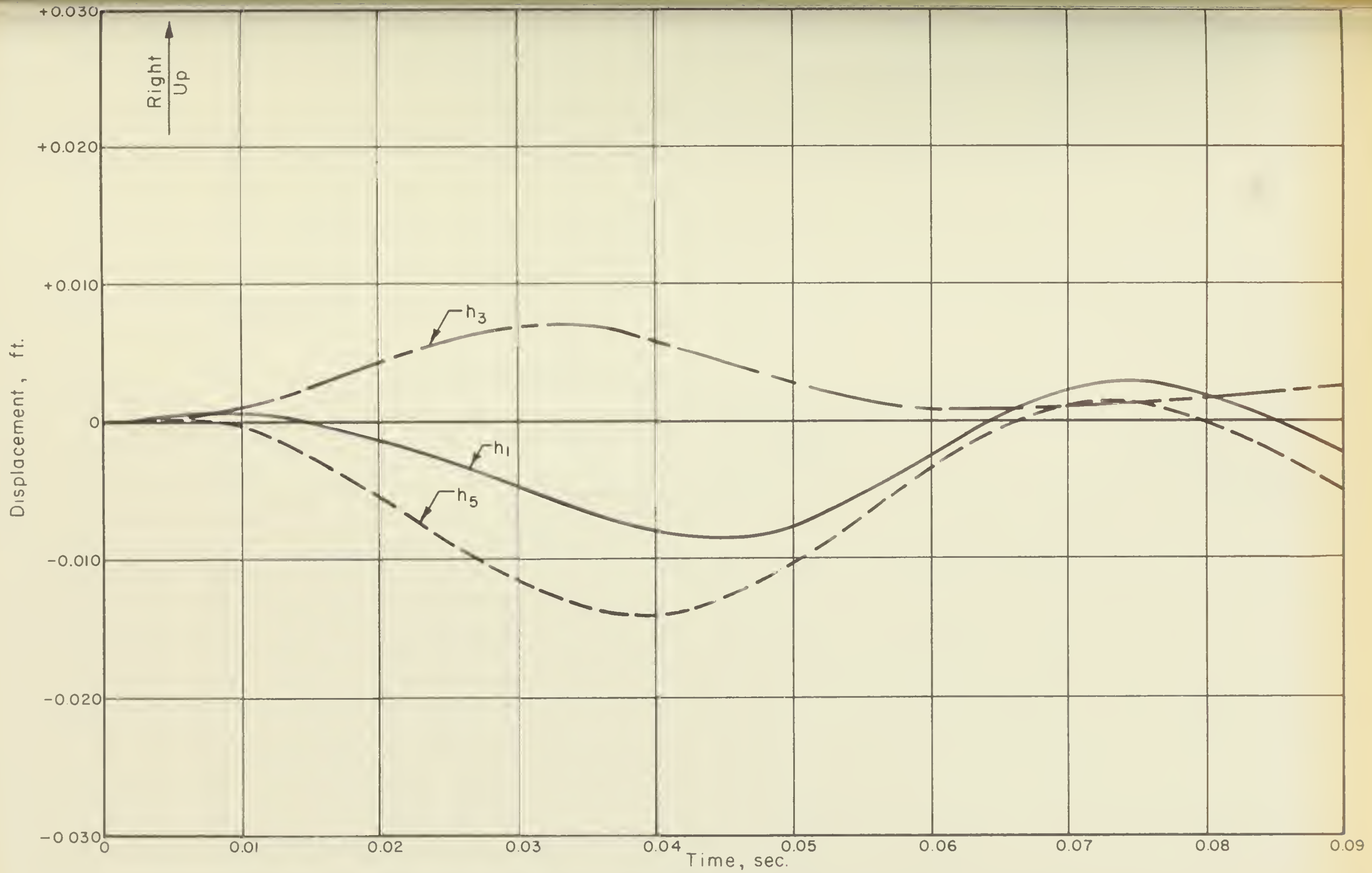

Figure D.13. Response Curves for Corrugated Metal Arch: p_{so} = 50 psi, d_c = B/4

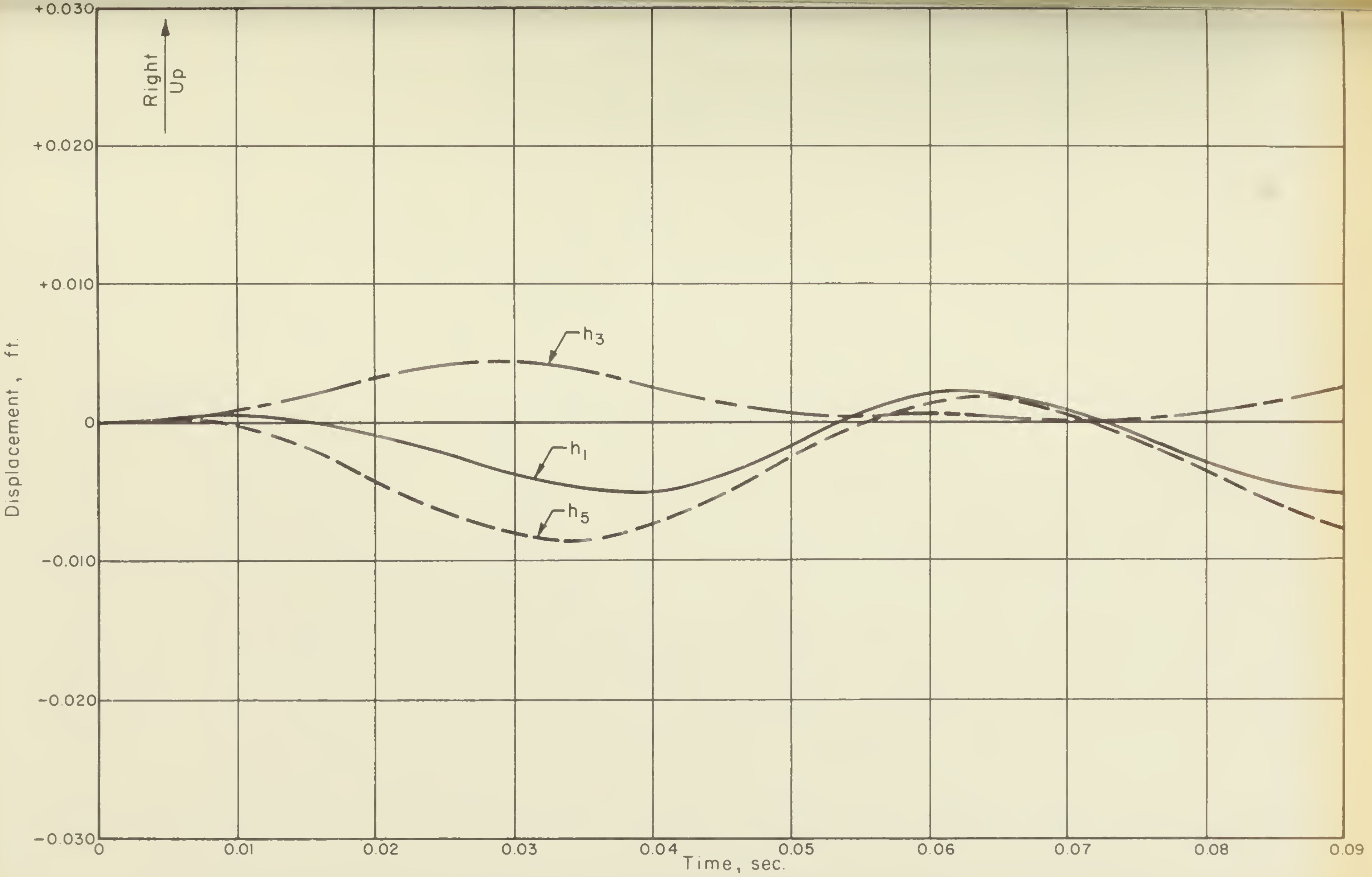

Figure D.14. Response Curves for Corrugated Metal Arch: p_{so} = 50 psi, d_c = B/2

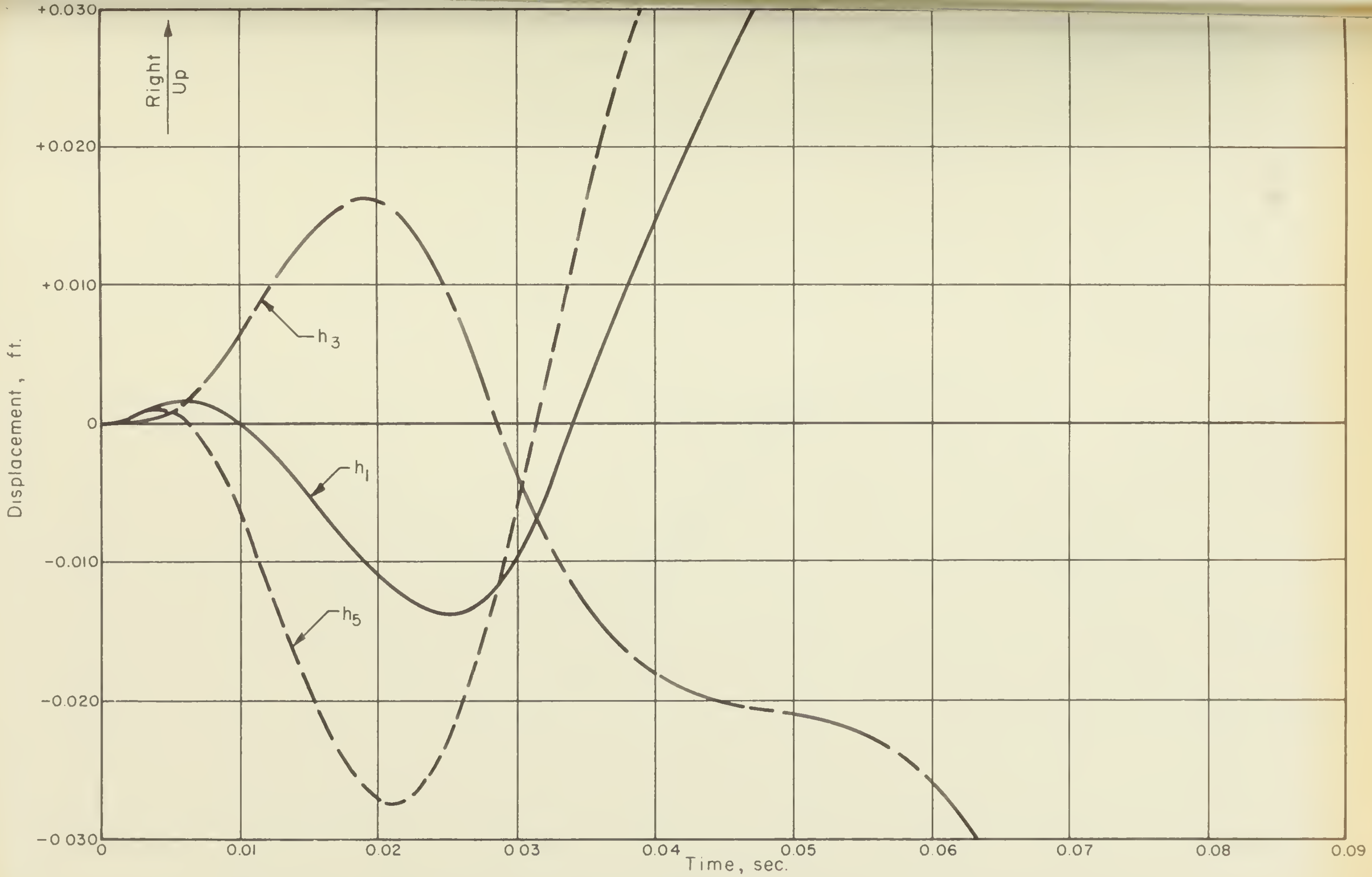

Figure D.15. Response Curves for Corrugated Metal Arch: p_{so} = 100 psi, d_c = 0

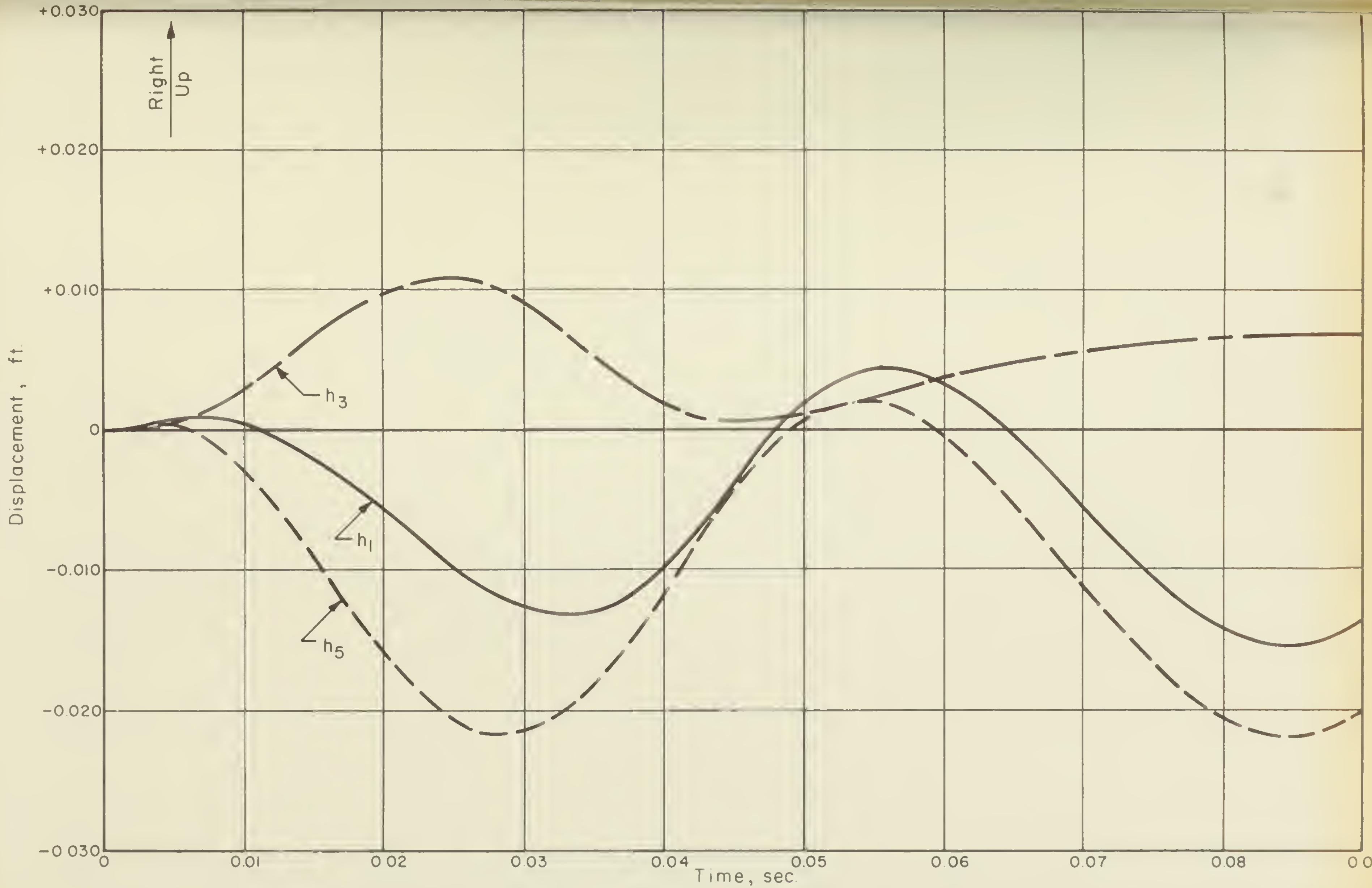

Figure D.16. Response Curves for Corrugated Metal Arch: p_{so} = 100 psi, d_c = B/8

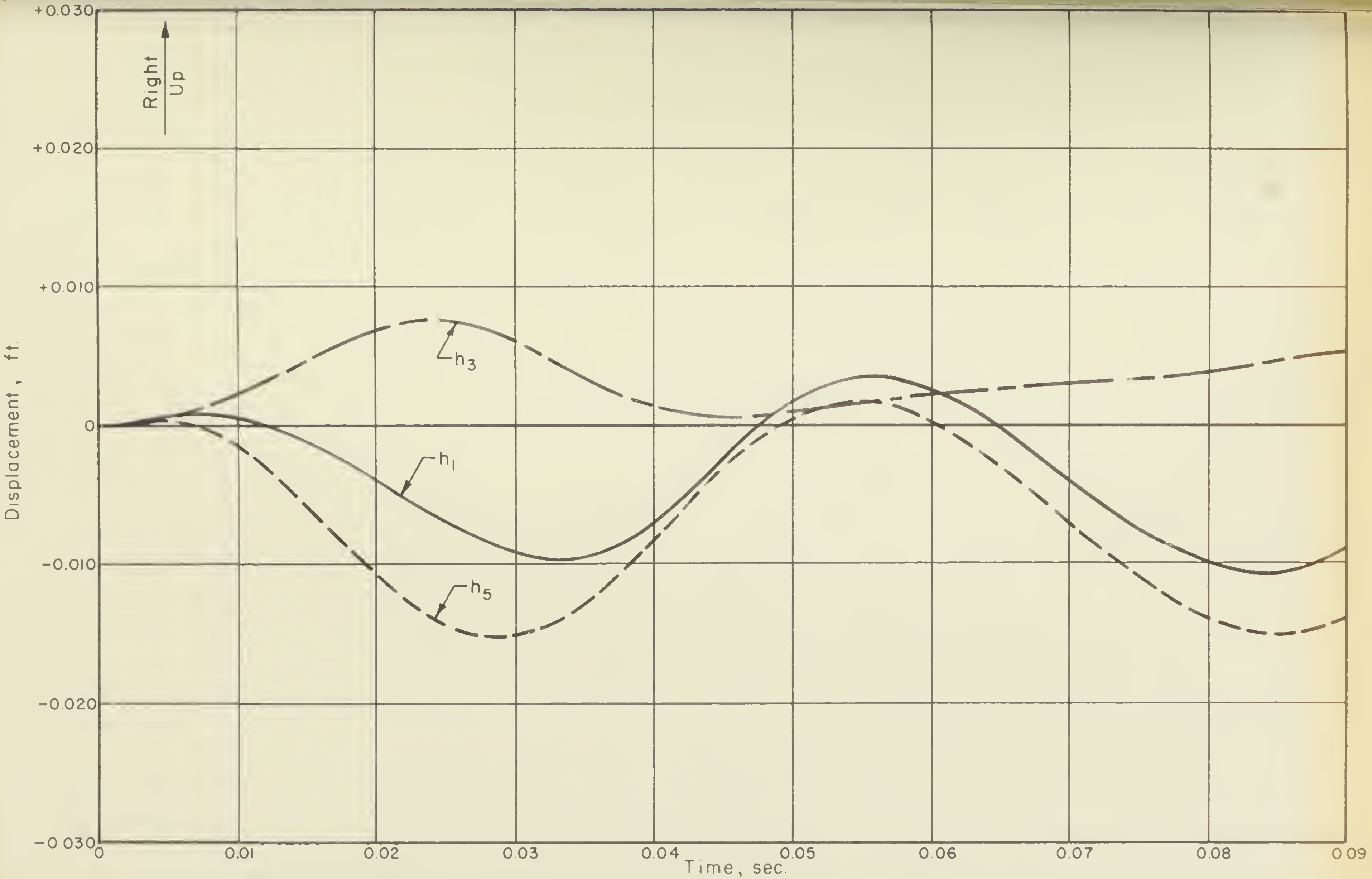

Figure D.17. Response Curves for Corrugated Metal Arch: p_{so} = 100 psi, d_c = B/4, K_{pr} = 1/4

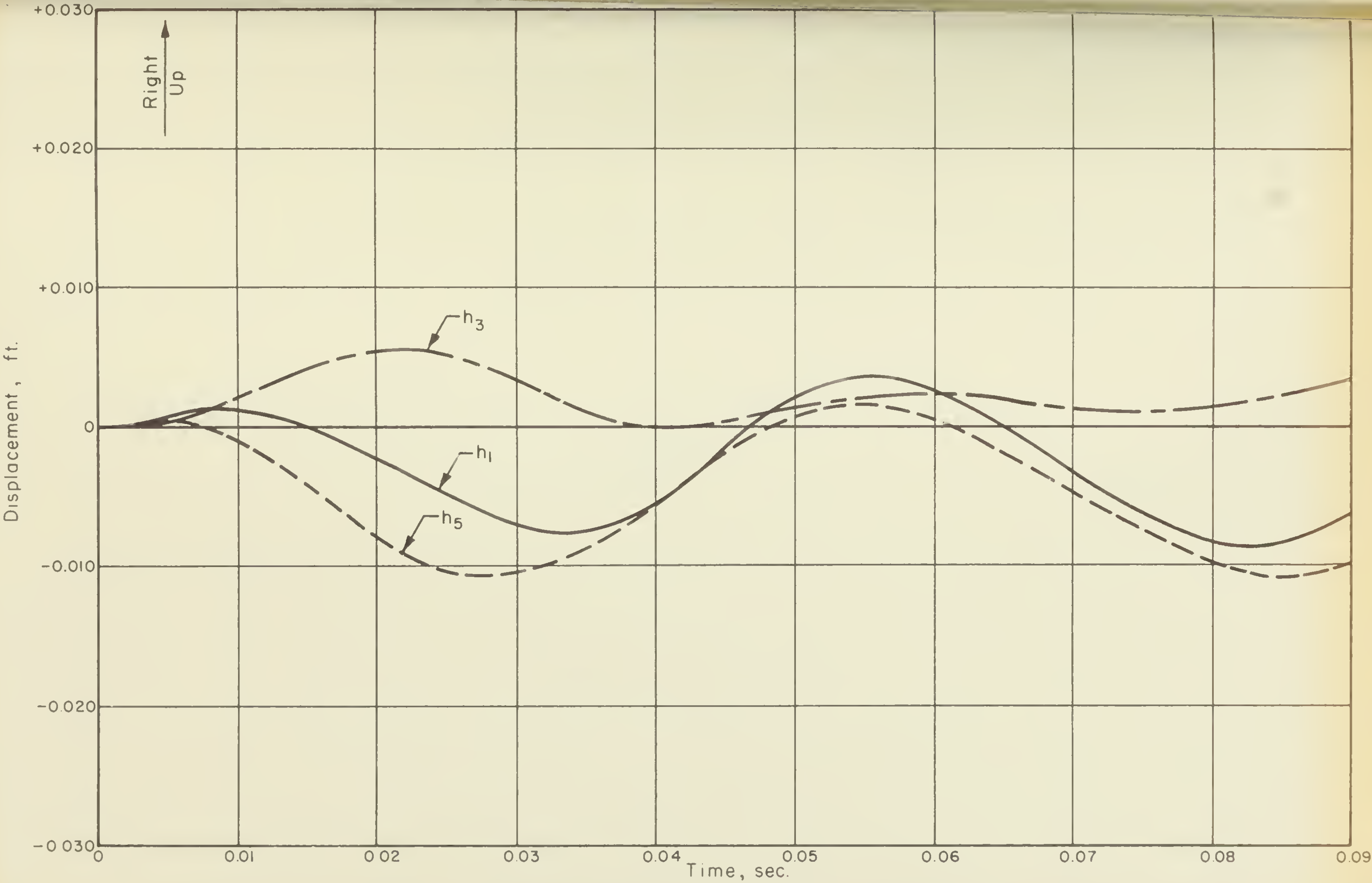

Figure D.18. Response Curves for Corrugated Metal Arch: $p_{so} = 100$ psi, $d_c = B/4$, $K_{pr} = 1/2$

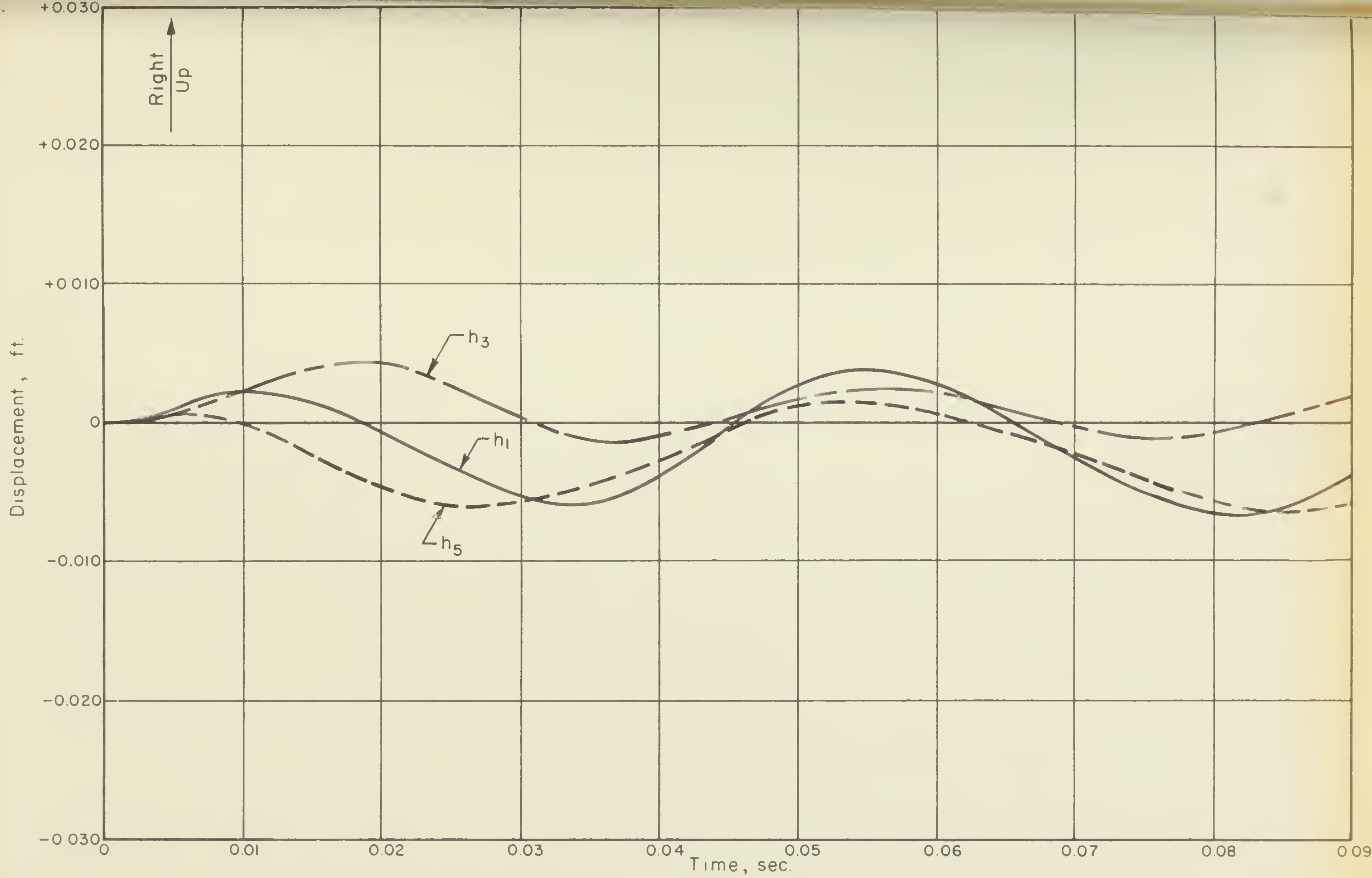

Figure D.19. Response Curves for Corrugated Metal Arch: $p_{so} = 100$ psi, $d_c = B/4$, $K_{pr} = 3/4$

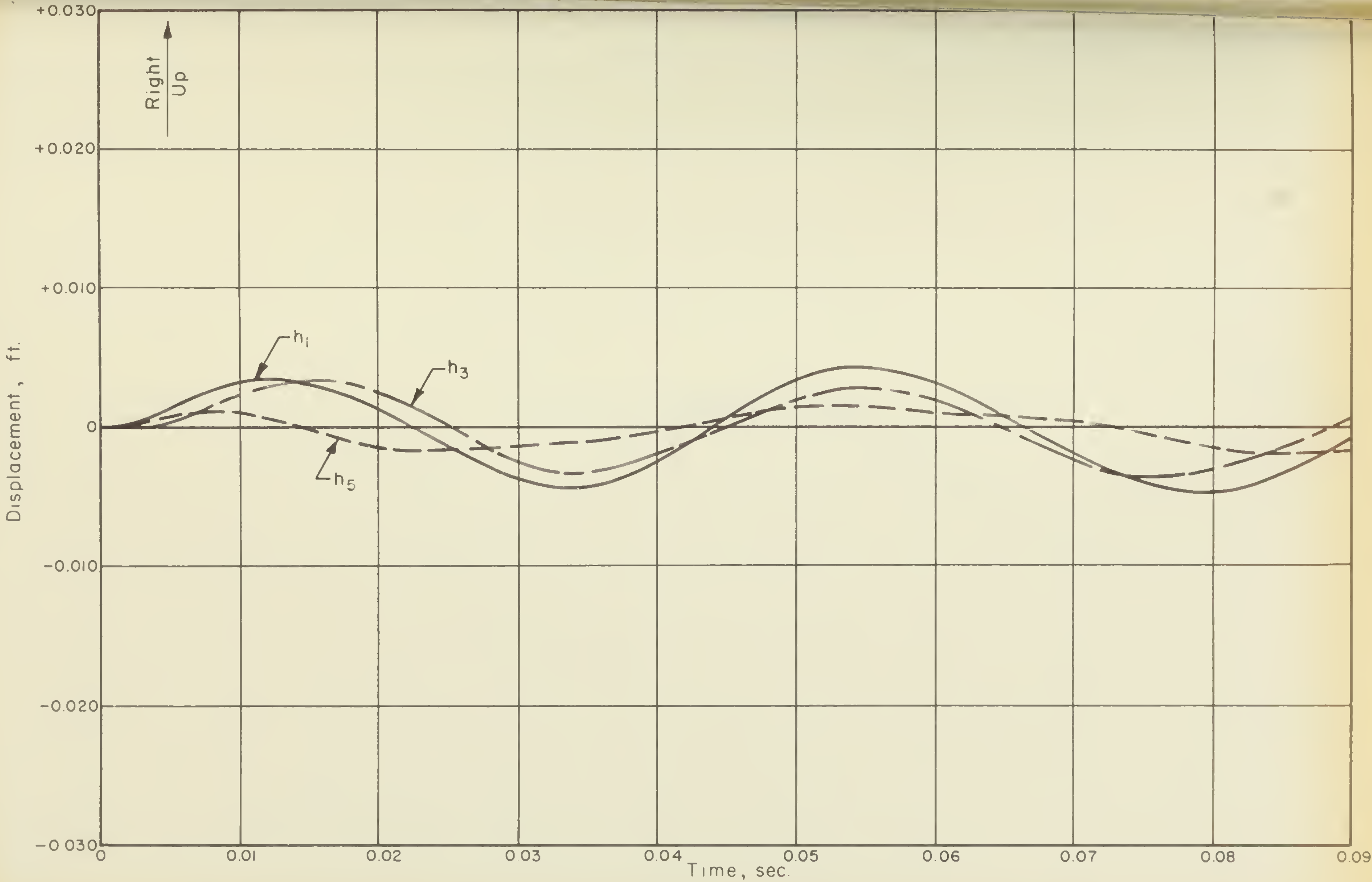

Figure D.20. Response Curves for Corrugated Metal Arch: p_{so} = 100 psi, d_c = B/4, K_{pr} = 1

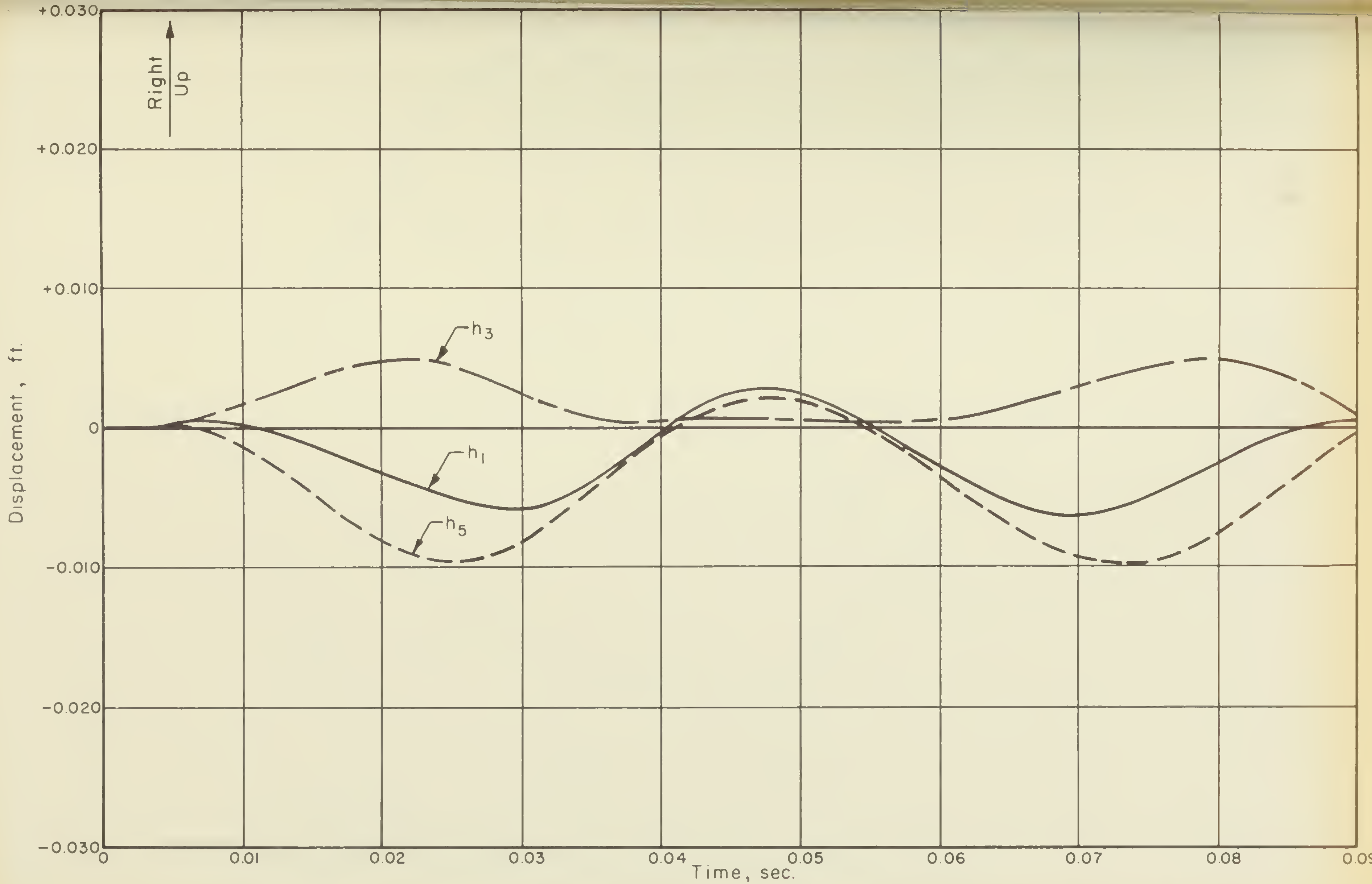

Figure D.21. Response Curves for Corrugated Metal Arch: p_{so} = 100 psi, d_c = B/2

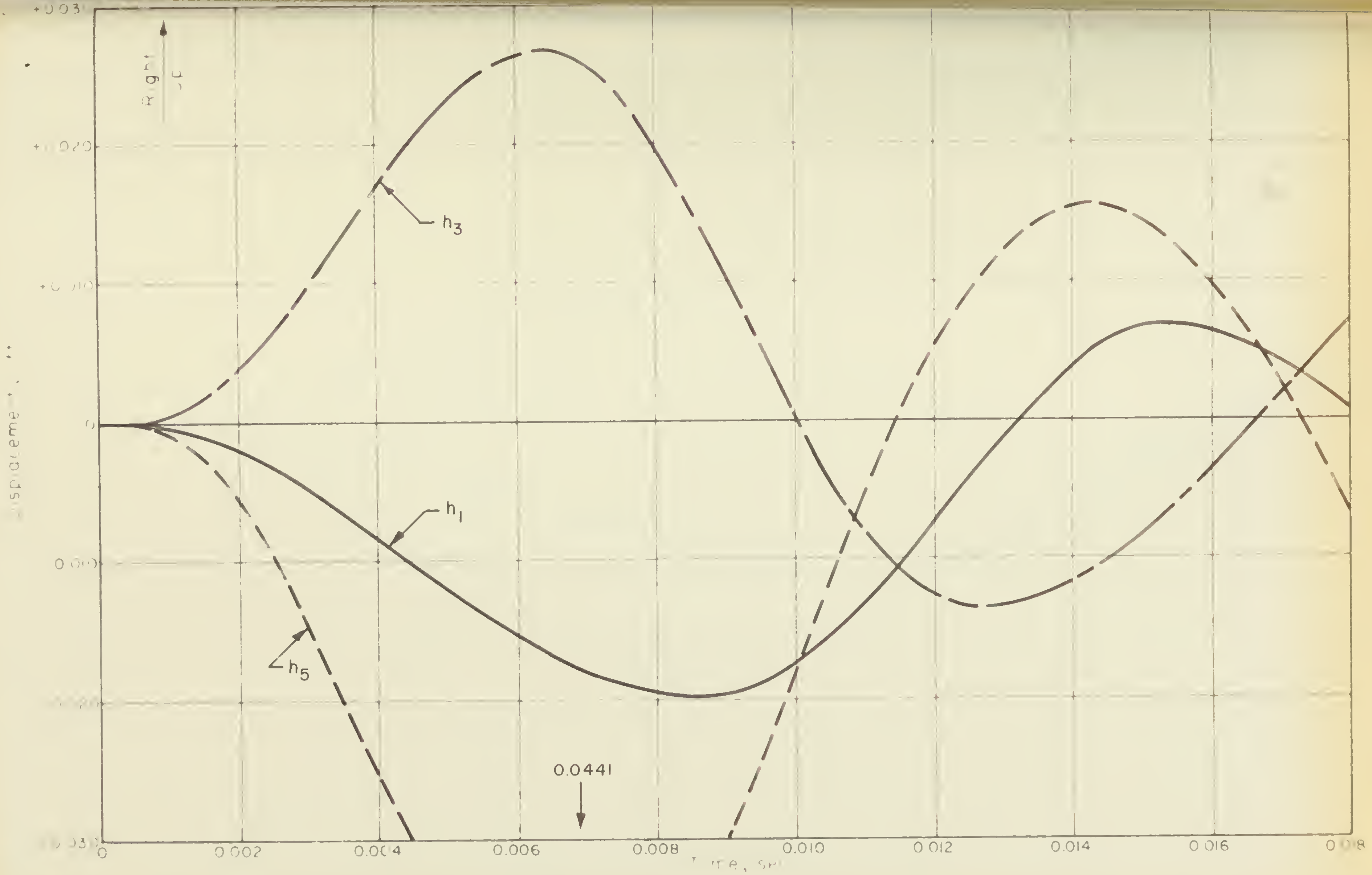

Figure D.22. Response Curves for Corrugated Metal Arch: p_{so} = 1,000 psi, d_c = 0

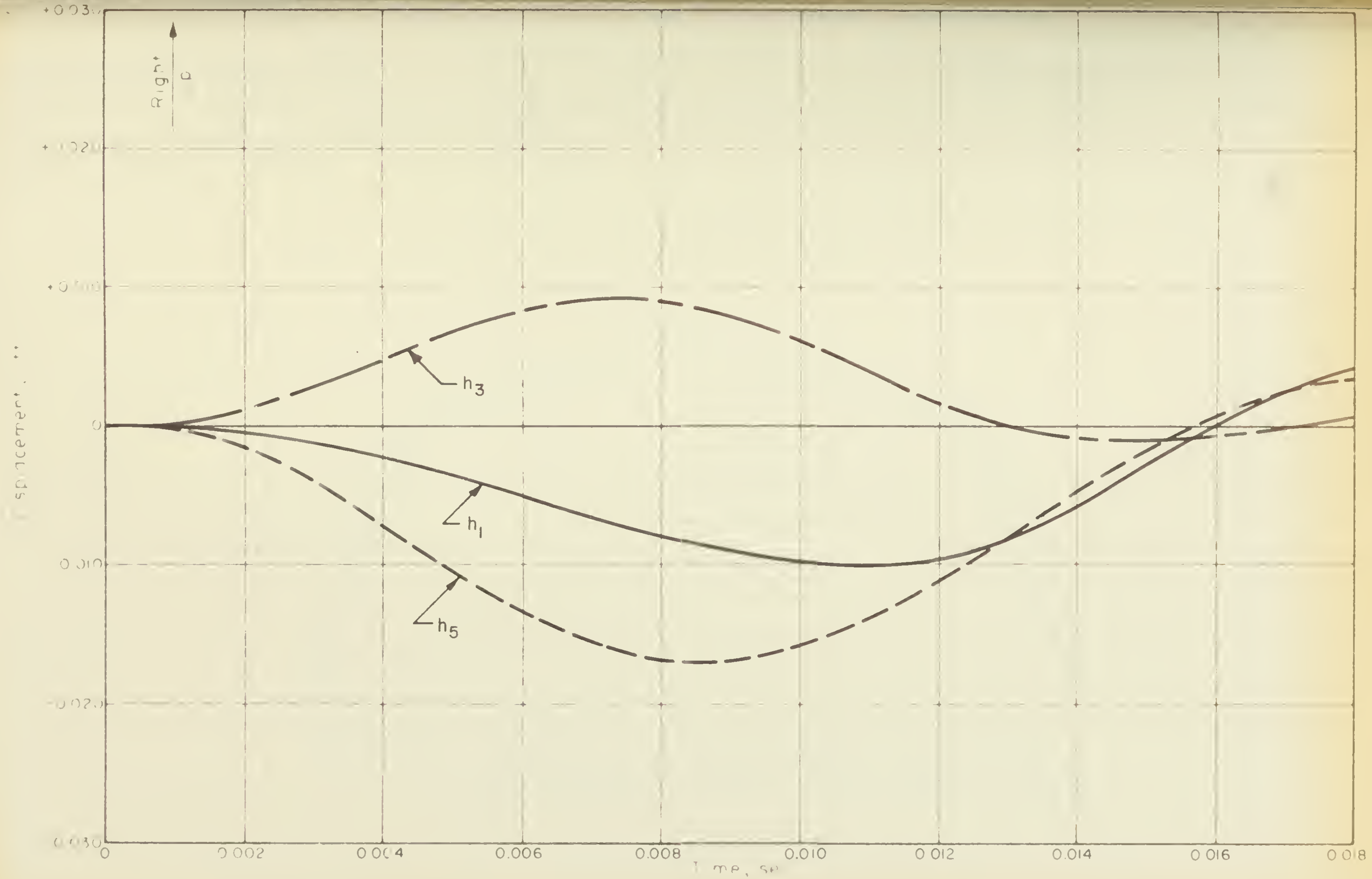

Figure D.23. Response Curves for Corrugated Metal Arch: p_{so} = 1,000 psi, d_c = B/4

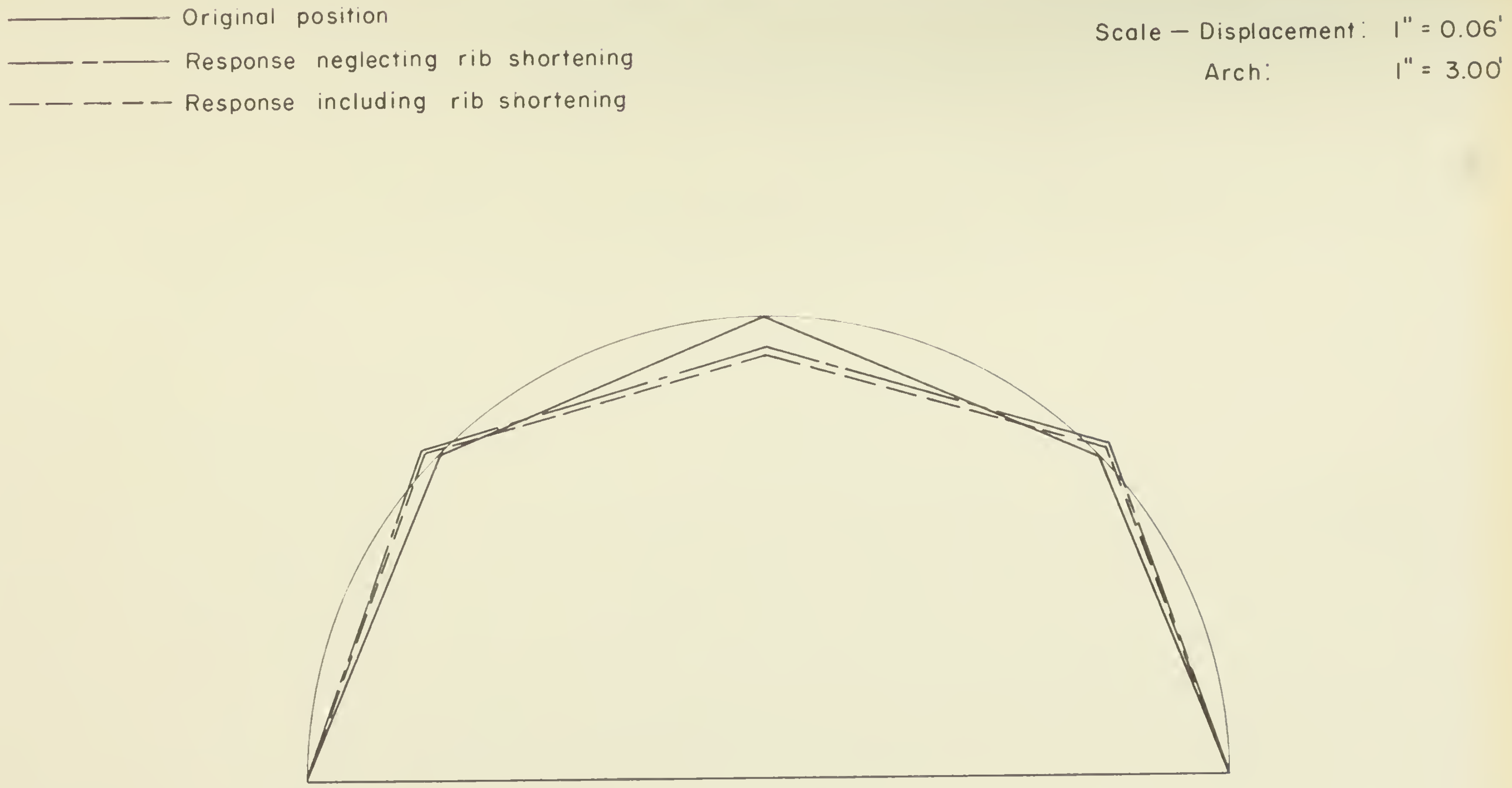
Original position
Response neglecting rib shortening
Response including rib shortening
Scale — Displacement: 1" = 0.06'
Arch: 1" = 3.00'

Figure D.24. Configuration Diagram for Reinforced Concrete Arch: p_{so} = 100 psi, d_c = B/4, t = 0.0173 seconds, $(+h_3)_{max}$

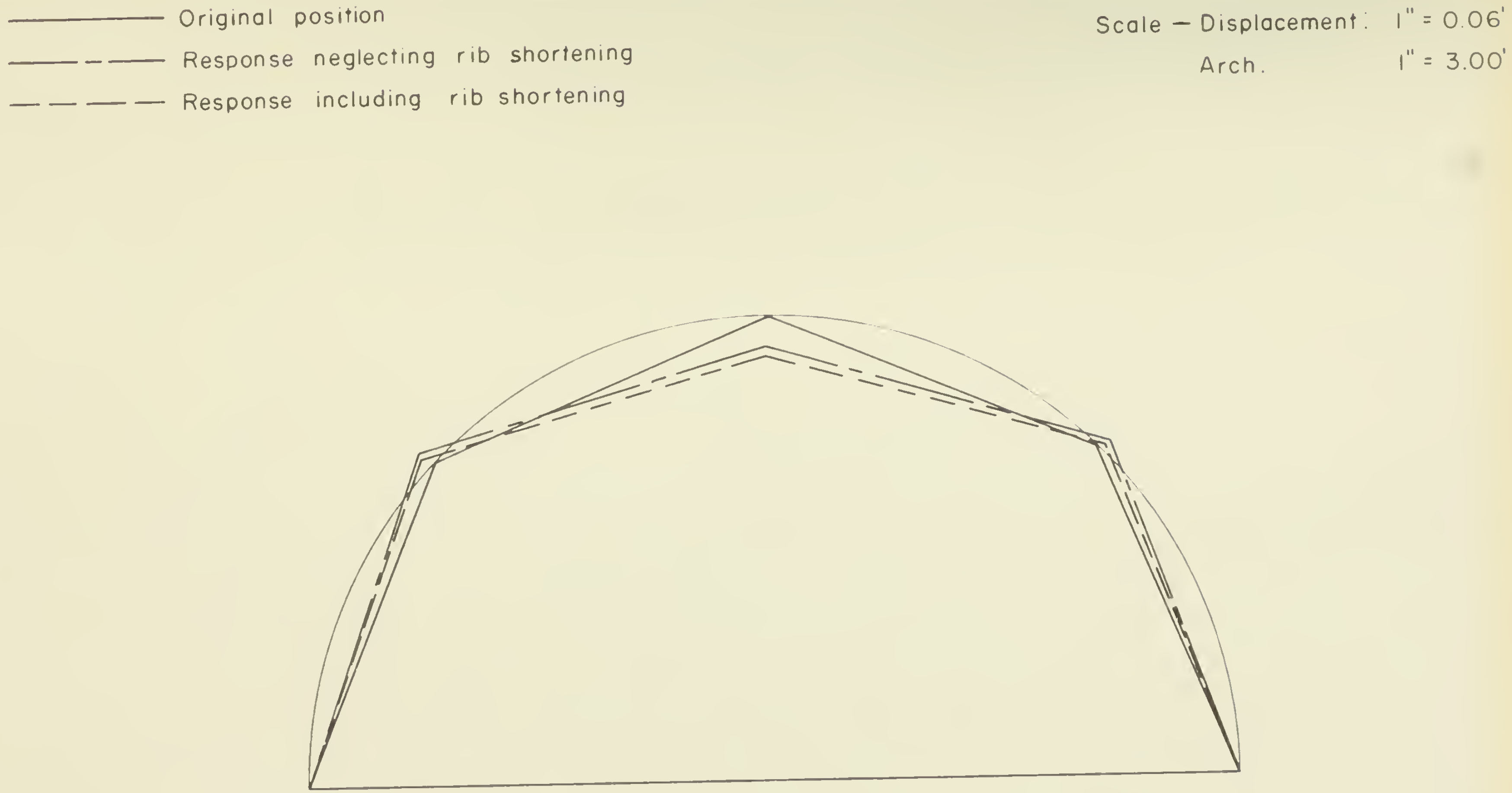
Original position
Response neglecting rib shortening
Response including rib shortening
Scale — Displacement: 1" = 0.06'
Arch. 1" = 3.00'

Figure D.25. Configuration Diagram for Reinforced Concrete Arch: $p_{so} = 100$ psi, $d_c = B/4$, $t = 0.0198$ seconds, $(-h_5)_{max}$

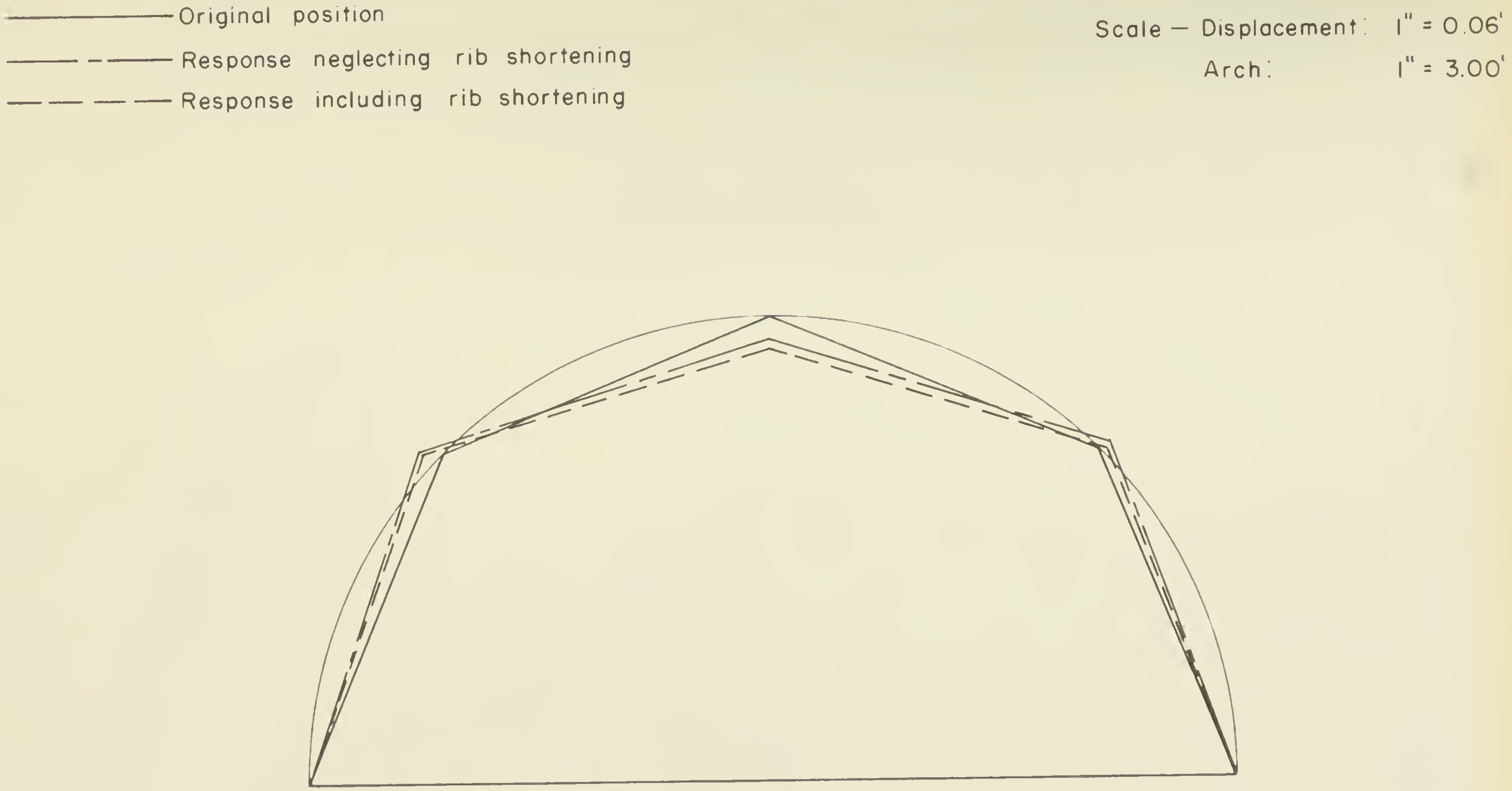
Original position
Response neglecting rib shortening
Response including rib shortening
Scale — Displacement: 1" = 0.06'
Arch: 1" = 3.00'

Figure D.26. Configuration Diagram for Reinforced Concrete Arch: $p_{so} = 100$ psi, $d_c = B/4$, $t = 0.0229$ seconds, $(-h_1)_{max}$

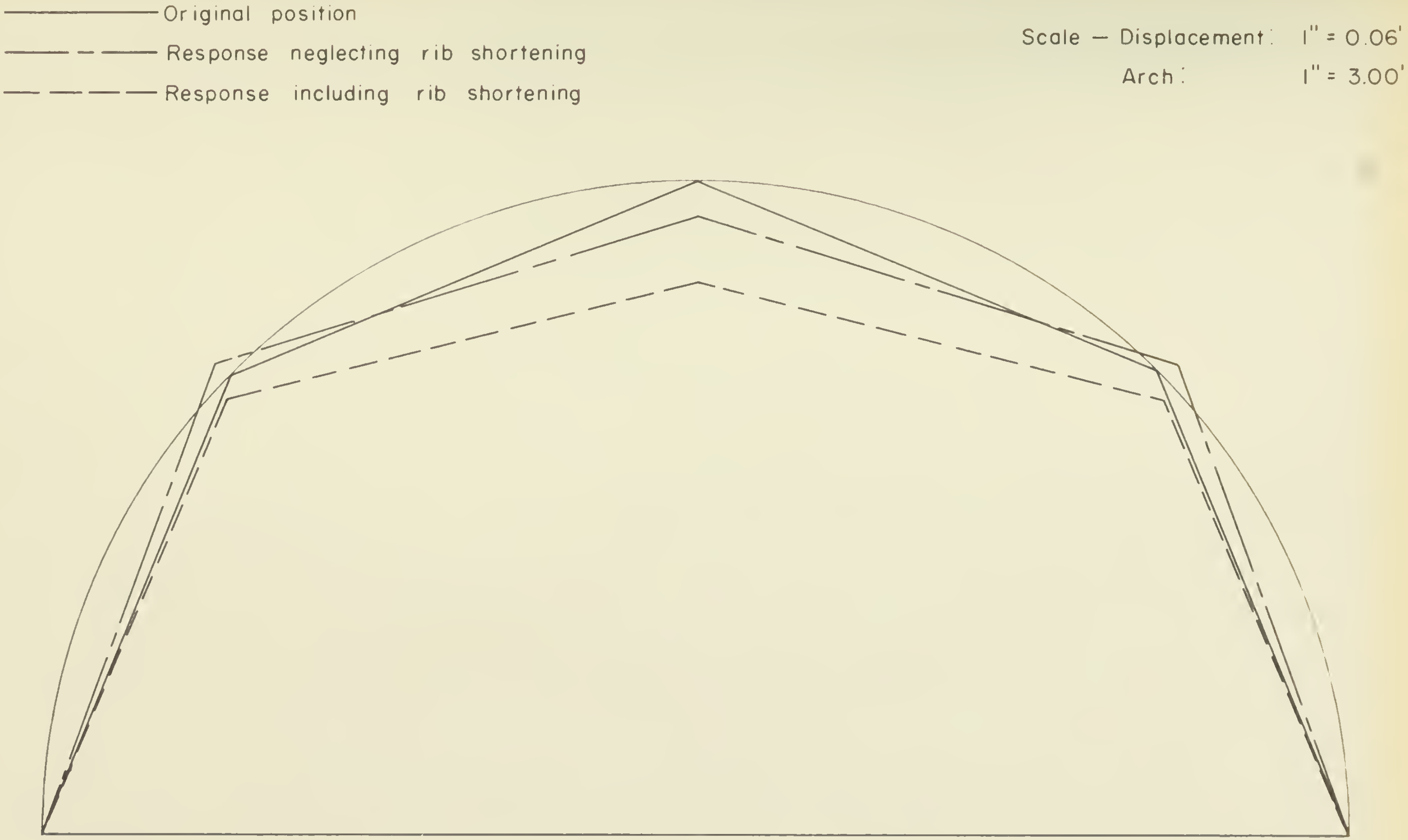
Original position
Response neglecting rib shortening
Response including rib shortening
Scale — Displacement: 1" = 0.06'
Arch: 1" = 3.00'

Figure D.27. Configuration Diagram for Corrugated Metal Arch: $p_{so} = 50$ psi, $d_c = B/4$, $t = 0.0337$ sec., $(+h_3)_{max}$

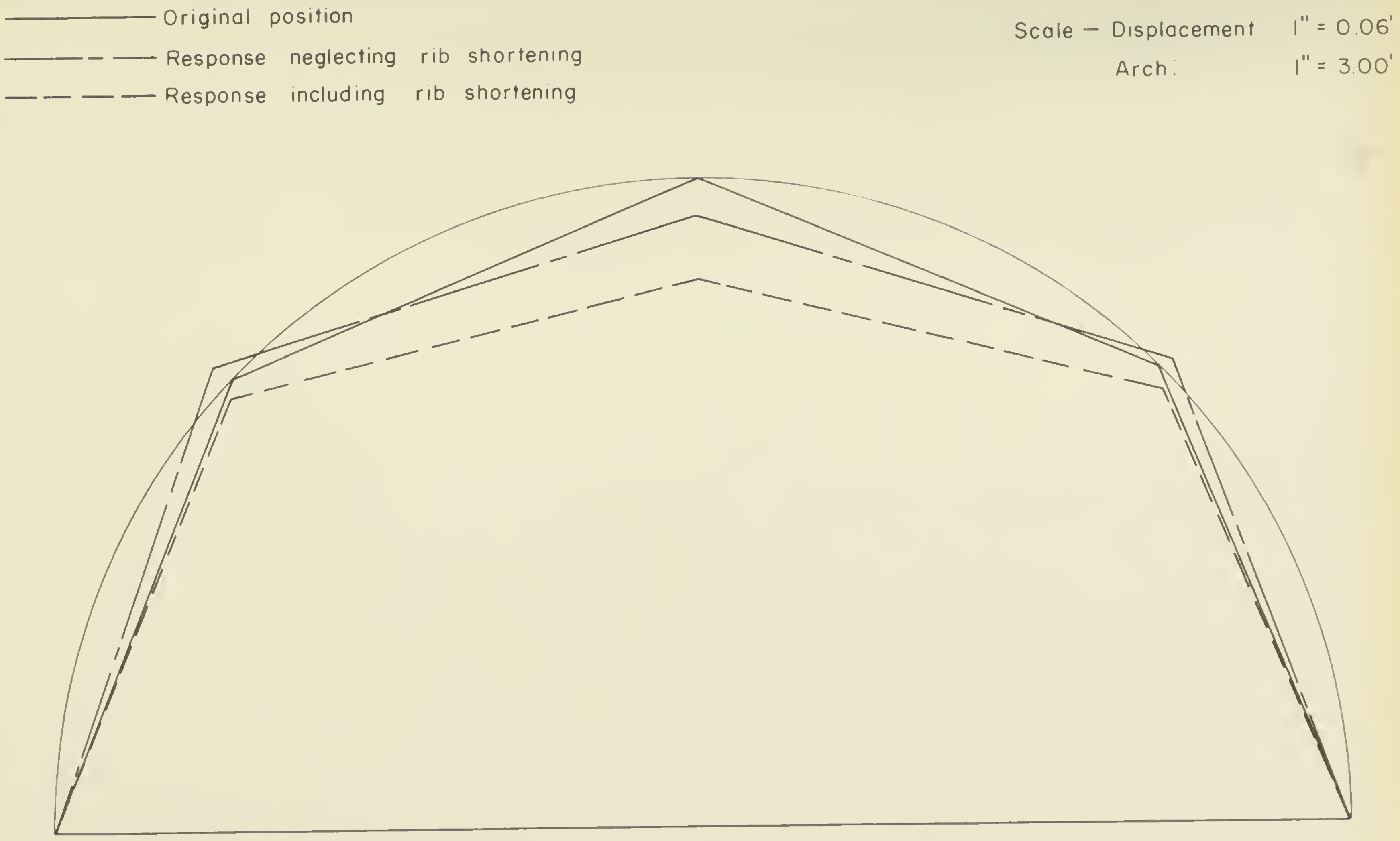
Original position
Response neglecting rib shortening
Response including rib shortening
Scale — Displacement 1" = 0.06'
Arch: 1" = 3.00'

Figure D.28. Configuration Diagram for Corrugated Metal Arch: p_{so} = 50 psi, d_c = B/4, t = 0.0388 sec., $(-h_5)_{max}$

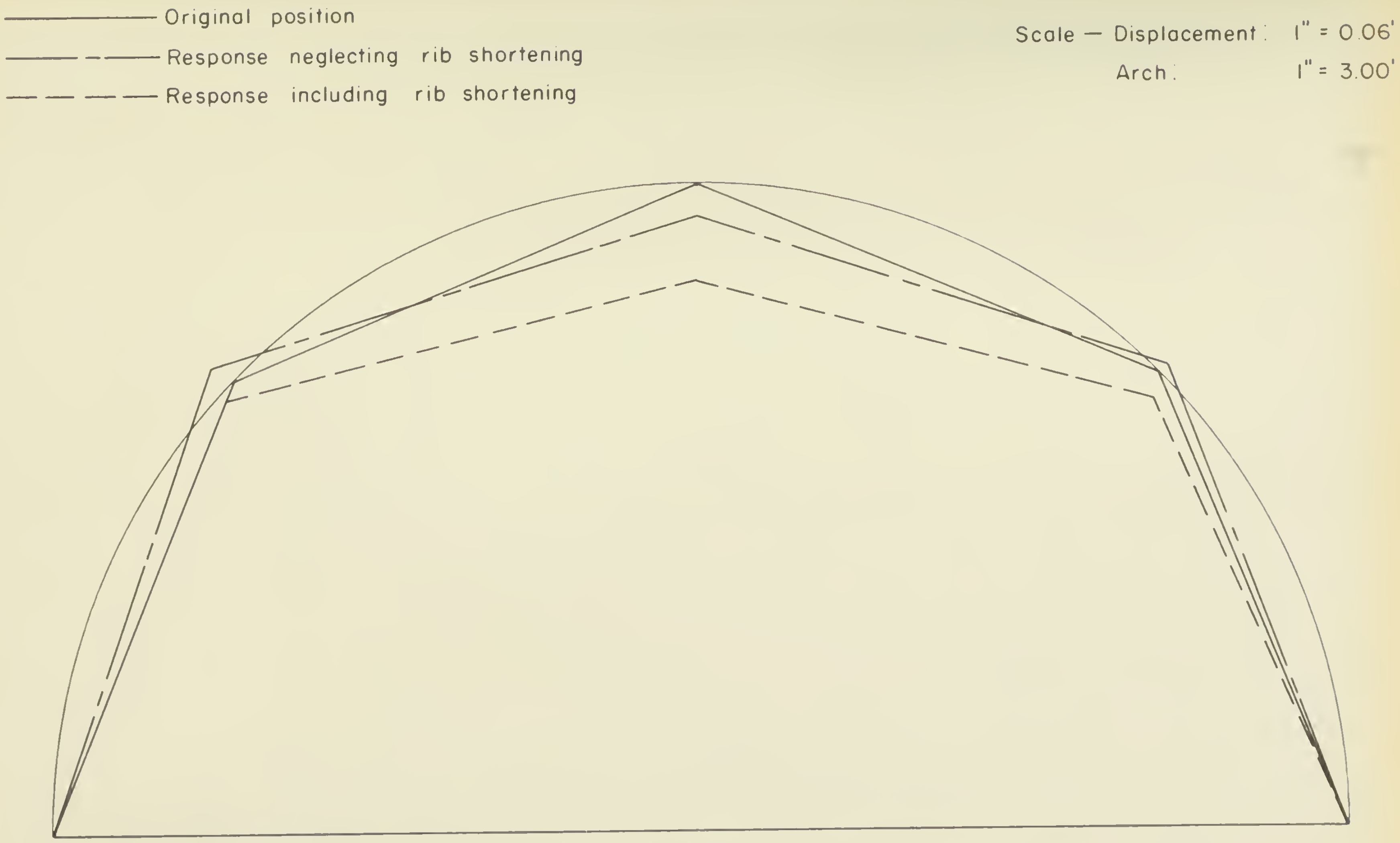
Original position
Response neglecting rib shortening
Response including rib shortening
Scale — Displacement: 1" = 0.06'
Arch: 1" = 3.00'

Figure D.29. Configuration Diagram for Corrugated Metal Arch: $p_{so} = 50$ psi, $d_c = B/4$, $t = 0.0450$ sec., $(-h_1)_{max}$

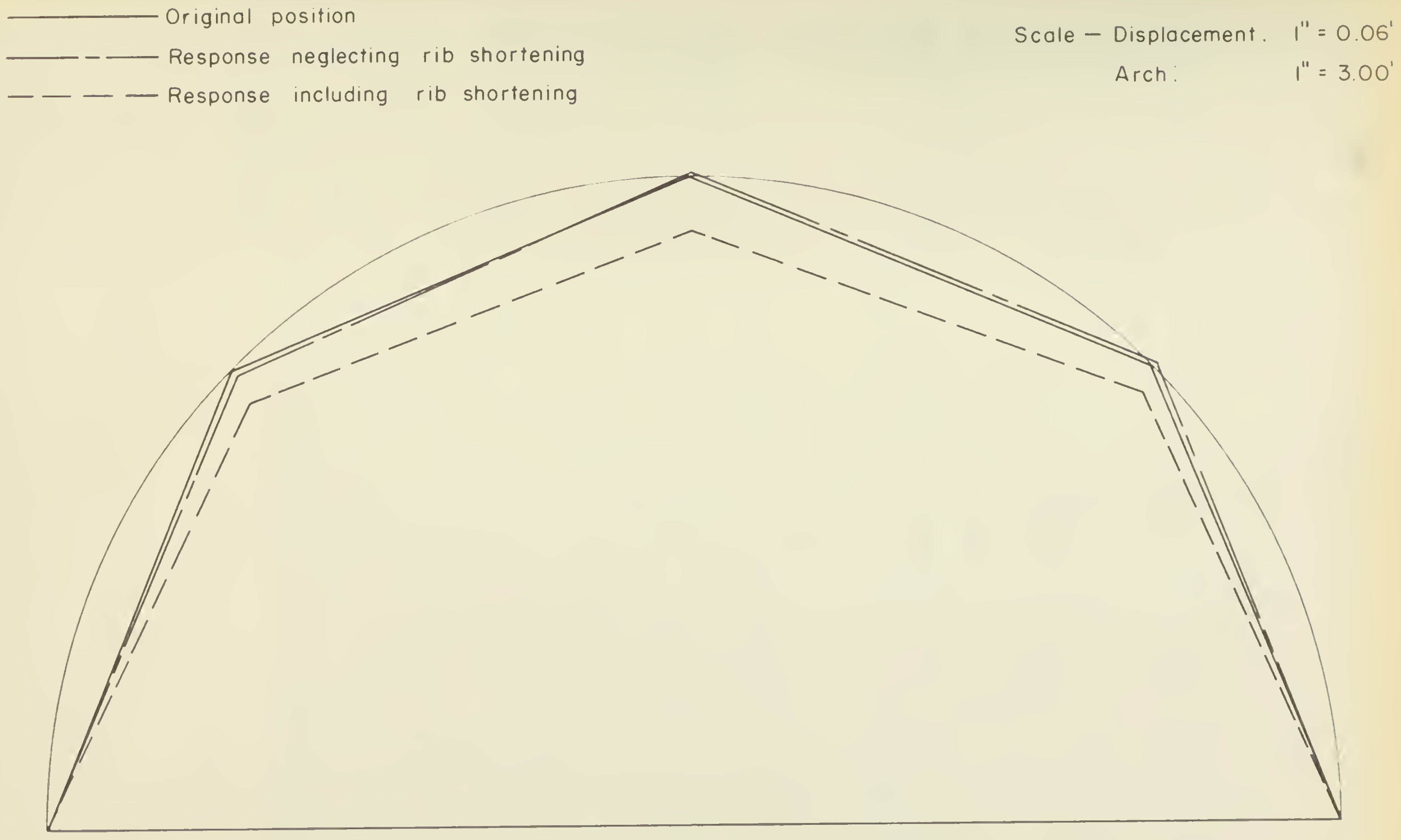
Original position
Response neglecting rib shortening
Response including rib shortening
Scale — Displacement. 1" = 0.06'
Arch: 1" = 3.00'

Figure D.30. Configuration Diagram for Corrugated Metal Arch: $p_{so} = 50$ psi, $d_c = B/4$, $t = 0.0750$ sec., $(+h_1)_{max}$

VITA

Caryll Robbins Whipple was born October 12, 1927, in Altoona, Pennsylvania. He was graduated from the Altoona Senior High School in 1945 and entered The Pennsylvania State University that year. The following year he entered the United States Naval Academy at Annapolis, Maryland, and was graduated in 1950 with the degree of Bachelor of Science. After serving in various capacities as a junior officer aboard the aircraft carrier USS FRANKLIN D. ROOSEVELT, he attended the Rensselaer Polytechnic Institute, Troy, New York, and received the degree of Bachelor of Civil Engineering in 1953.

He served as an assistant to the District Public Works Officer, Third Naval District, New York, New York, and as a project planning officer and later as a resident officer in charge of construction with the Officer in Charge of Construction, U.S. Navy Bureau of Yards and Docks Contracts, Madrid, Spain. He entered the University of Illinois in June, 1956, and was awarded the degree of Master of Science in Civil Engineering in 1957.

During the period from September, 1957, until July, 1960, he was a Professor of Atomic Defense and Disaster Control Engineering at the U.S. Naval Civil Engineer Corps Officers' School, Port Hueneme, California. He holds the rank of Lieutenant Commander in the Civil Engineer Corps of the United States Navy.

thesW53
The dynamic response of shallow-buried a
3 2768 001 95048 8
DUDLEY KNOX LIBRARY